Electrochemical Society

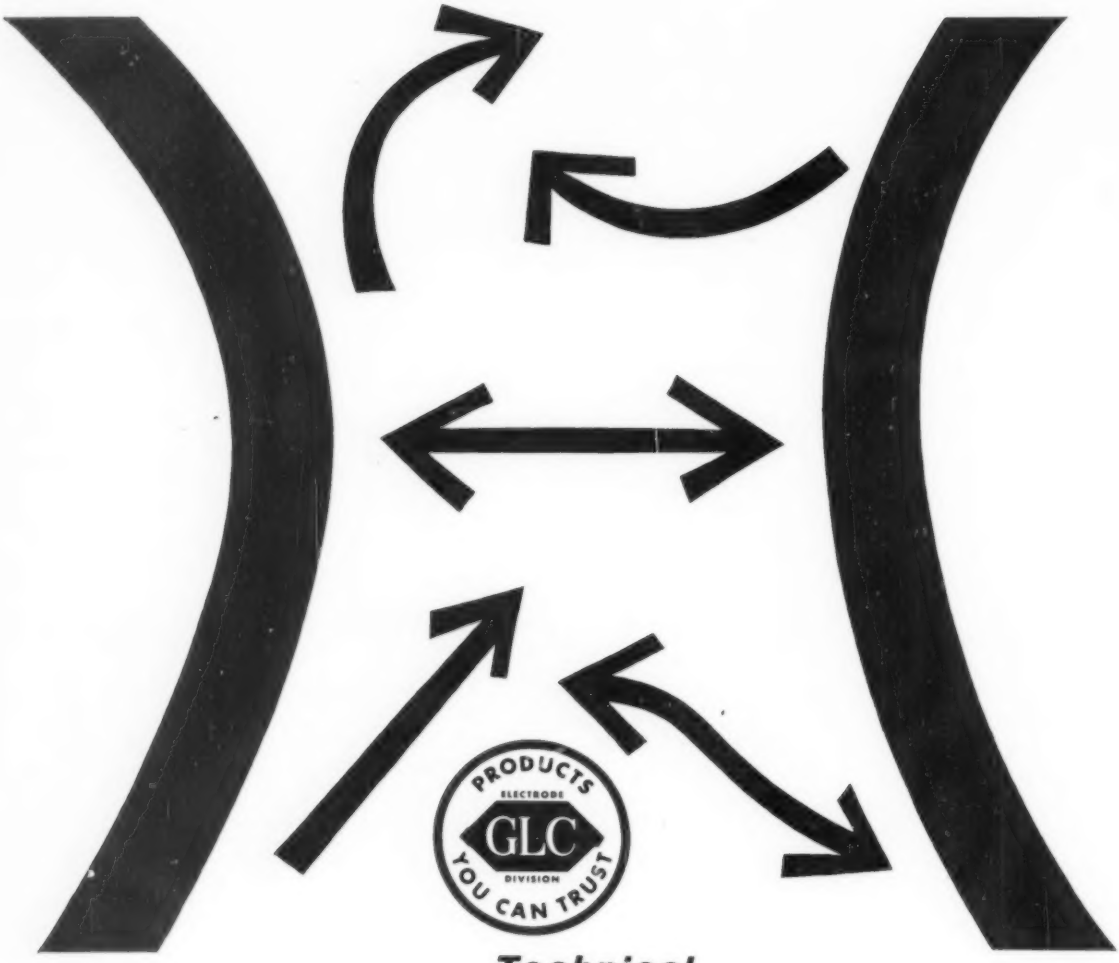

Technical

Exchanges

with

Customers . . . now provide conclusive proof that custom-made anodes materially lower electrolytic cell operating costs. May we show you the evidence?

GREAT LAKES CARBON CORPORATION

18 EAST 48TH STREET, NEW YORK 17, N. Y. OFFICES IN PRINCIPAL CITIES

EDITORIAL STAFF

H. H. Uhlig, Chairman, Publication Committee

Cecil V. King, Editor

Norman Hackerman, Technical Editor

Ruth G. Sterns, Managing Editor

U. B. Thomas, News Editor

H. W. Salzberg, Book Review Editor

Natalie Michalski, Assistant Editor

DIVISIONAL EDITORS

W. C. Vosburgh, Battery

Milton Stern, Corrosion, I

R. T. Foley, Corrosion, II

T. D. Callinan, Electric Insulation

Seymour Senderoff, Electrodeposition

H. C. Froelich, Electronics

Ernest Paskell, Electronics—Semiconductors

Sherlock Swann, Jr., Electro-Organic, I

Stanley Wawzonek, Electro-Organic, II

John M. Blocher, Jr., Electrothermics and Metallurgy, I

A. U. Seybolt, Electrothermics and Metallurgy, II

N. J. Johnson, Industrial Electrolytic

C. W. Tobias, Theoretical Electrochemistry, I

A. J. deBethune, Theoretical Electrochemistry, II

ADVERTISING OFFICE

ECS
1860 Broadway, New York 23, N. Y.

ECS OFFICERS

W. C. Gardiner, President
Olin Mathieson Chemical Corp., Niagara Falls, N. Y.

R. A. Schaefer, Vice-President
The Bunting Brass and Bronze Co., Toledo, Ohio

Henry B. Linford, Vice-President
Columbia University, New York, N. Y.

F. L. LaQue, Vice-President
International Nickel Co., Inc., New York, N. Y.

Lyle I. Gilbertson, Treasurer
Air Reduction Co., Murray Hill, N. J.

I. E. Campbell, Secretary
National Steel Corp., Weirton, W. Va.

Robert K. Shannon, Executive Secretary
National Headquarters, The ECS, 1860 Broadway, New York 23, N. Y.

Manuscripts submitted to the Journal should be sent, in triplicate, to the Editorial Office at 1860 Broadway, New York 23, N. Y. They should conform to the Instructions to Authors, last published in the August 1959 issue, pp. 232C-233C. Manuscripts so submitted become the property of The Electrochemical Society and may not be published elsewhere, in whole or in part, unless permission is requested and granted by the Editor.

Inquiries re positive microfilm copies of volumes should be addressed to University Microfilms, Inc., 313 N. First St., Ann Arbor, Mich.

Journal of the

Electrochemical Society

DECEMBER 1959 **VOL. 106 • NO. 12**

CONTENTS

Editorial

The Training of a Teacher 303C

Technical Papers

A Study of the Zinc-Noble Metal Couple in Alkaline Solutions. *T. P. Dirkse and E. G. Vrieland* 997

The Anodic Dissolution and Electrolytic Polishing of Metals. *J. K. Higgins* 999

An Investigation of Chemical Variables Affecting the Formation of Films on Copper in Aqueous Solutions. *W. H. Davenport, V. F. Nole, and W. D. Robertson* 1005

The Formation of Porous Oxides on Metals. *D. W. Aylmore, S. J. Gregg, and W. B. Jepson* 1010

Galvanic Relationships between Aluminum Alloys and Magnesium Alloys. *M. R. Bothwell*
I. Galvanic Couples 1014
II. Aluminum Claddings on Magnesium 1019

Electrical Conduction in Liquid Dielectrics under Pulse Conditions. *K. A. Macfadyen and G. C. Helliwell* 1022

Luminescence of Copper-Activated Calcium and Strontium Orthophosphates. *W. L. Wanmaker and C. Bakker* 1027

Copper and Tin-Activated Halophosphate Phosphors. *B. E. Hunt and A. H. McKeag* 1032

Electrical Properties of High-Purity Silicon Made from Silicon Tetraiodide. *L. V. McCarty* 1036

Rare Earth Compound Semiconductors. *J. F. Miller, F. J. Reid, and R. C. Himes* 1043

Diffusion of Cerium and Zirconium in Molten Uranium. *T. Smith* 1046

Diffusion-Exchange of Exchange Ions and Nonexchange Electrolyte in Ion-Exchange Membrane Systems. *M. A. Peterson and H. P. Gregor* 1051

Technical Notes

A Method for Evaluating Battery Grade Manganese Dioxide. *F. Kornfeil* 1062

A Study of Stripping Anodized Coatings from an Aluminum Alloy. *W. Beck, J. Danovich, and S. J. Ketcham* 1063

The Gudden-Pohl Effect of ZnS:Cu. *Y. Kotera and K. Naraoka* 1066

Diffusion of Oxygen in Hafnium. *J. P. Pemsler* 1067

Technical Feature

The Fuel Cell and the Carnot Cycle. *H. A. Liebhafsky* 1068

Discussion Section **1072-1084**

Current Affairs **307C-317C**

Published monthly by The Electrochemical Society, Inc., from Manchester, N. H., **Executive Offices, Editorial Office** and **Circulation Dept.,** and **Advertising Office** at 1860 Broadway, New York 23, N. Y., combining the JOURNAL and TRANSACTIONS OF THE ELECTROCHEMICAL SOCIETY. Statements and opinions given in articles and papers in the JOURNAL OF THE ELECTROCHEMICAL SOCIETY are those of the contributors, and The Electrochemical Society assumes no responsibility for them. Nondeductible subscription to members $5.00; subscription to nonmembers $18.00. Single copies $1.25 to members, $1.75 to nonmembers.

Copyright 1959 by The Electrochemical Society, Inc.

Entered as second-class matter at the Post Office at Manchester, N. H., under the act of August 24, 1912.

Four 2000kw units make up the 8000kw installation recently completed by Perkin for a major chemical company. Other power capacities – up to 100,000 amperes and 500 volts dc – can be obtained easily by connecting units in parallel or series to meet voltage and current requirements. Simple design permits side-by-side grouping of cabinets.

PERKIN SILICON RECTIFIERS CUT YEARLY MAINTENANCE TO MINUTES

Recent installation delivers 8000kw, 625v, has 94-97% efficiency

You save from the moment you order all-static silicon rectifier equipment from Perkin. Compared with conventional mercury-arc rectifiers and other conversion equipment, Perkin units cost less initially, cost less to install, and cost less to operate. They do their job more dependably, more quietly . . . at about two-thirds the weight and in less than one-half the space.

The key to this important advance in dc power conversion is the all-metal silicon rectifier diode. This rugged, non-aging semiconductor device eliminates the need for filament power, tubes, excitation, ignition systems, elaborate cooling systems – in fact, removes all the usual reasons for supervision and repair. It makes possible equipment that you can trust completely in unattended locations.

Downtime and overhauls are a thing of the past. You can measure yearly maintenance in minutes instead of days! And thanks to the reliability and stability of silicon, the high efficiency of your Perkin equipment lasts around the clock, through the years.

PERKIN

One of a series

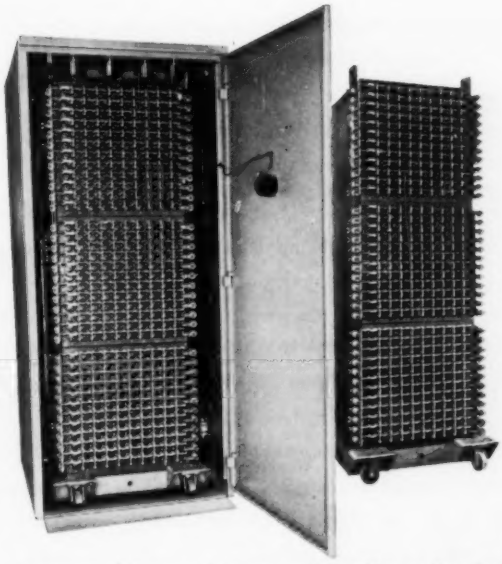

"Draw-out" feature lets you roll rectifier unit out of cabinet for immediate access to all internal components. Units move easily, install anywhere—need no special foundations or pumping facilities, create no noise or vibration problems.

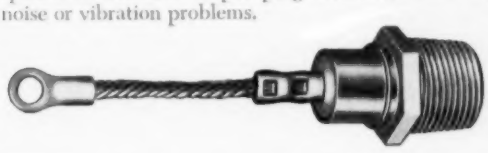

Non-aging, high-temperature silicon diodes keep equipment efficiency high through the years. Elements are hermetically sealed, bond is metal-to-glass. No organic binders or potting compounds are used.

PERKIN
ENGINEERING CORPORATION

345 Kansas St., El Segundo, Calif. • ORegon 8-7215

EASTERN AREA ENGINEERING OFFICE:
P.O. Box 388, Paoli, Penna. • NI 4-6278

NEW ENGLAND AREA OFFICE:
46 Amesbury, Lawrence, Mass. • MUrdock 3-3252

Representatives in Principal Cities

PERKIN SILICON RECTIFIER EQUIPMENT...

is short circuit-proof, has coordinated protection of diode fuse, output fuse and input breaker. Overload protection meets NEMA standards.

Conservative design of Perkin industrial rectifier units assures uninterrupted operation even if one rectifier element or more should fail. Should any *one* rectifier element in a string fail, the fuse does *not* burn out, and the entire rectifier unit will continue to operate. Should *several* rectifier elements in a string fail, the fuse *will* burn out to protect the remaining rectifier elements in that string, and still the entire rectifier unit will continue to operate.

Forced balance of voltage and current prevents overloading of elements, eliminates need for matching silicon junction replacements.

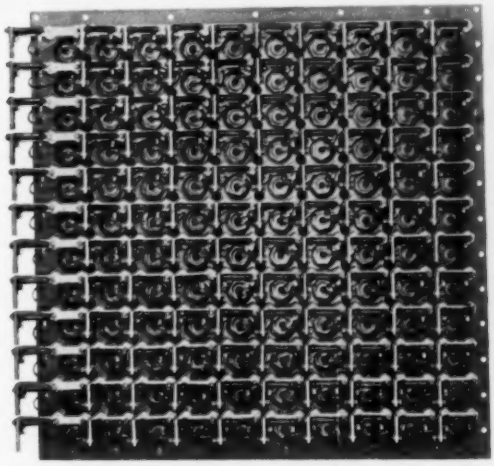

Perkin also offers a full line of standard industrial silicon rectifier units starting at 25kw. Moderate prices, prompt delivery.

Write on your letterhead for detailed technical information, indicating your specifications, or for a copy of our latest technical article, "Industrial Semiconductor Rectifiers."

One of a series

The revealing face of an iron crystal

A single crystal is an ideal system for studying the solid state. Physicists at the General Motors Research Laboratories have turned to whisker-like growths of nearly perfect single iron crystals to investigate three intriguing phenomena: magnetic domains, dislocation defects, and—more recently—high temperature oxidation.

In this latest study, the two crystallographically different surfaces found on iron whiskers are being used to examine the anisotropy or axial-dependent nature of the oxidation process. In early stages of oxidation, the oxide patterns that form on clean surfaces have been found to be strongly dependent upon the orientation of the underlying crystal. In later stages of oxidation, tiny oxide "cilia" actually grow on the surface of the iron whisker. But these new whiskery forms of oxidation are no longer related to the crystal's surface arrangement. The next step in this program involves correlating the oxidation behavior with lattice structure defects such as vacancies and dislocations.

This type of solid state research is revealing the atomic processes underlying strength, magnetic characteristics, and corrosion resistance of metals. At GM Research, we believe the solution to practical problems is increasingly dependent on fundamental information such as this. And each solution enables us to continue to provide "More and better things for more people."

GENERAL MOTORS RESEARCH LABORATORIES

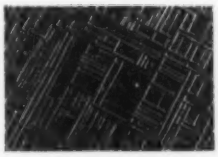

Early Oxidation
(750x)

Oxide Whiskers
(12,000x)

Reduction of Oxide Products
(2500x)

Editorial

The Training of a Teacher

In recent years, and especially since the ascent of Sputniks I and II, we have seen severe criticism of our secondary school system, while many proposals have been advanced for improving the curriculum and the teaching. In particular, how can the study of science be stimulated, and how can students with potential scientific ability be singled out, kept interested, and pushed on through college and into scientific careers? There is even now a shortage of well-trained science teachers, and it is not at all likely that the supply of new teachers will keep pace with the growing number of students.

In his presidential address to the American Chemical Society last September, Dr. John C. Bailar, Jr., pointed out that in Switzerland the majority of science teachers at the level of our high schools have doctoral degrees in science. By contrast, only a minority of our high school chemistry teachers have completed a college major in chemistry, and many of them have had no more than one year of college chemistry. As Dr. Bailar said, possession of the Ph.D. degree does not guarantee a good teacher, but he added that it does ensure an adequate knowledge of the subject.

Now, Ph.D.'s and science majors could no doubt be obtained in increasing numbers to teach in high schools, by raising salaries to the level paid by industry; that is up to the School Board, and the people at the polls. But we doubt whether an American Ph.D. degree is at all desirable for a high school chemistry teacher, with the exception of special cases. If first-year college chemistry does not provide proper factual and background material for a prospective high school teacher, perhaps something is wrong with the course. We do not mean that every student, after a year of college chemistry, should be able to teach the subject in high school; but that the School Board should choose on the basis of personality, enthusiasm, and ability to work with young people, rather than knowledge of thermodynamics, quantum theory, and reaction mechanism. The capable man will soon remedy his deficiencies.

In fact, much is done today to help the high school science teacher add to his knowledge. There are In-Service Institutes, summer and refresher courses which cost him nothing except time and interest. Many films are available, including a complete high school chemistry course. The A.A.A.S., with financial assistance from NSF, has enough books in its traveling science library to circulate among 1700 high schools this year. These aids are well worth exploring and expanding and being made available to all. An aid which many a teacher would gratefully appreciate would be relief from lunchroom duty, hall-policing, and other extra-curricular activities, along with interest and cooperation from his superiors in his plans, preparation, and study.

All too frequently, there are slips in bringing proper talent to the right place at the right time. One young man of our acquaintance, who has a Master's degree in chemistry, is teaching biology this year. Another chemistry major, with two years of graduate work and some teaching experience, is teaching high school mathematics. The School Board has its troubles too.

—CVK

SARGENT

Laboratory Recorders

Designed For Your Specific Laboratory Needs

Model MR

The Model "MR" Recorder

Here is the ultimate in recorders designed exclusively for almost all measurements commonly made in the chemical laboratory. This instrument measures current and voltage and all other quantities which can be transposed into potential or current signals.

The Model "MR" features: 31 Potentiometric Ranges; 9 Chart Speeds, or 27 Chart Speeds with the Sargent Multi-range Attachment; and it is designed for laboratory bench operation.

S-72150 Sargent Recorder (Pat. Pend.) $1725.00

S-72151 Sargent Recorder with Multi-Range Attachment, 27 Chart Speeds $1775.00

For complete specifications write for Bulletin R

Model SR

The Model "SR" Recorder

Sargent offers the Model SR to fill the need for a low cost recorder that features: maximum accuracy at a minimum cost; 250 mm width chart; fast balancing speed of 1 second; high sensitivity, high gain amplifier; and square cornering at 10,000 to 50,000 ohms input. This instrument provides the minimum required flexibility at the lowest possible cost.

S-72180 Sargent Recorder (Pat. Pend.) $675.00

For complete specifications write for Bulletin SR

Designed and Manufactured by E. H. Sargent & Co.

SARGENT SCIENTIFIC LABORATORY INSTRUMENTS • APPARATUS • SUPPLIES • CHEMICALS

E. H. SARGENT & CO., 4647 W. FOSTER, CHICAGO 30, ILLINOIS
DETROIT 4, MICH. • DALLAS 35, TEXAS • BIRMINGHAM 4, ALA. • SPRINGFIELD, N. J.

how do you look at ANODES?

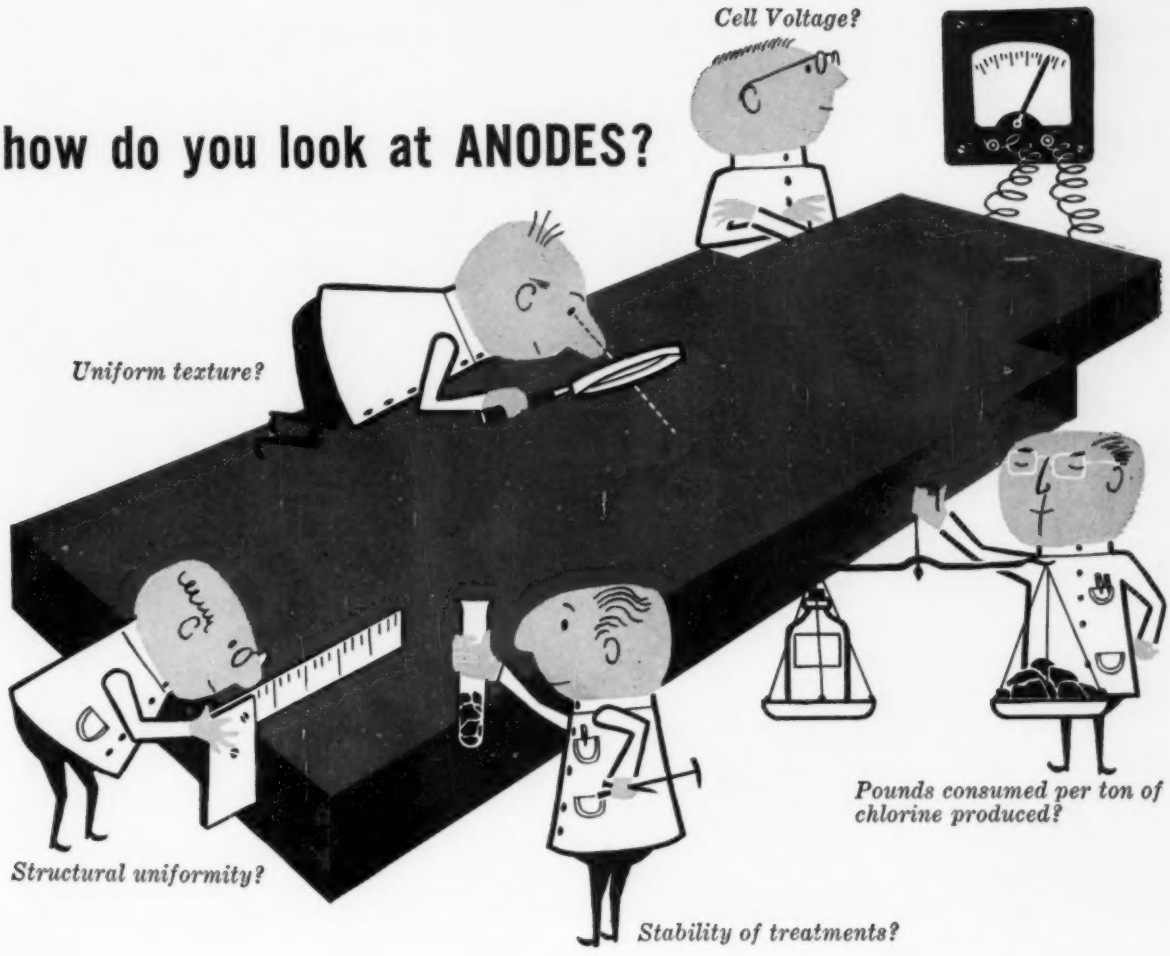

Judged by Cell Maintenance Costs Alone,

the highly stable impregnants used in Stackpole GraphAnode reduce diaphragm clogging to a bare minimum. The graphite is consumed slowly and evenly. Because GraphAnode anodes present uniform, low-porosity surfaces to the electrolyte, the graphite does not slough off to clog the diaphragm or to contaminate the cell.

Judged by Anode Cost and Performance,

Stackpole GraphAnode proves second to none whether you figure in terms of anode life, or in tons of chlorine produced per pound of graphite consumed. You get maximum anode life . . . and with the added advantage of low cell voltages. Stackpole engineers stand ready to offer a convincing demonstration on your equipment.

Stackpole Carbon Company, St. Marys, Pa.

STACKPOLE
GraphAnode®

ELECTROCHEMICAL ANODES FOR DIAPHRAGM, MERCURY, MANGANESE DIOXIDE, & SODIUM CHLORATE CELLS. OTHER TYPES FOR CATHODIC PICKLING, ALUMINUM ANODIZING, AND OTHER USES.

CATHODIC PROTECTION ANODES • FLUXING & DE-GASSING TUBES • SALT BATH RECTIFICATION RODS • ROCKET NOZZLES • RISER RODS • GRAPHITE BEARINGS & SEAL RINGS • ELECTRODES & HEATING ELEMENTS • WELDING CARBONS • VOLTAGE REGULATOR DISCS • "CERAMAGNET"® CERAMIC MAGNETS • ELECTRICAL CONTACTS • BRUSHES for all rotating electrical equipment • and many other carbon, graphite and electronic components.

Operator making a routine quality control test of type and resistivity on silicon characterization crystal.

Round-the-clock operations at new Du Pont plant assure you of ample supplies of Hyperpure Silicon

Du Pont's new Brevard, N. C., HYPERPURE Silicon plant—with a 70,000 lbs./yr. capacity—is now operating at high production rate to assure you of a prompt supply of high-purity silicon in the form, grade and quantity you need. Du Pont is uniquely qualified to serve you because of its experience as pioneer producer of semiconductor grades of silicon. This experience includes installing the first full-scale commercial silicon plant in the world and frequent expansion of productive facilities since then.

Single crystals of Du Pont HYPERPURE Silicon are now available in a wide range of resistivities, thanks to Du Pont's new research and manufacturing techniques. Each has a specially prepared "spec. sheet."

Here's more news: Du Pont recently completed a $3,000,000 Technical Service Laboratory specifically designed, equipped and staffed to handle customer problems. Here, highly trained Du Pont Technical Specialists are available to discuss any difficulties in crystal growing or manufacture you may encounter.

Du Pont HYPERPURE Silicon is also available in densified cut rods . . . and rods specially designed for float-zone refining in Grades 1, 2 and 3, with carefully controlled purity levels. As an additional service, Du Pont offers doping material at no additional cost.

Free booklet is available upon request. It describes the manufacture, properties and uses of HYPERPURE Silicon. E. I. du Pont de Nemours & Co. (Inc.), Pigments Dept., Silicon Development Group, Wilmington 98, Delaware.

HYPERPURE SILICON

DU PONT
REG. U.S. PAT. OFF.

BETTER THINGS FOR BETTER LIVING
. . . THROUGH CHEMISTRY

A Study of the Zinc-Noble Metal Couple in Alkaline Solutions

Thedford P. Dirkse and Edwin G. Vrieland

Department of Chemistry, Calvin College, Grand Rapids, Michigan

ABSTRACT

A metal-like coating is formed frequently on copper or silver leads which are attached to the zinc electrodes in commercial zinc-alkaline cells. This coating is zinc or a zinc-rich alloy. The conditions under which this coating is formed have been studied, and several possible mechanisms for its formation are presented and discussed.

It is generally known to those in the battery industry that when silver or copper is coupled with zinc in an alkaline solution, a zinc-like deposit is formed on the noble metal (1). However, so far as is known, no satisfactory explanation has been given for this phenomenon. For that reason, a study of this reaction was undertaken.

Experimental

Thin metal strips about 1 x 5 cm were used, and coupling was accomplished by twisting the ends of the strips together or by wrapping a zinc strip or screen around the noble metal. In some of the runs the entire couple was completely immersed in the KOH solution while at other times a part of the couple was exposed to the air. Nickel, silver, copper, platinum, and lead served as the noble metals, but most of the work was done with Ag and Cu. All runs were carried out at room temperature in 35% KOH. C.P. reagents were used without further purification.

At first there was some difficulty in obtaining a coating on the Ag or Cu. Various anions usually found in commercial KOH, such as Cl^-, $CO_3^=$,$SO_4^=$, HO_2^-, were added to the electrolyte, but had no effect on the formation of the coating. Amalgamating the zinc electrode also failed to influence the formation of this deposit. However, addition of ZnO to the KOH solutions hastened the formation of this coating considerably. Coatings were formed on Ag, Cu, Pb, and Pt, but not on Ni.

The nature of the coating was checked by several methods. The deposit was very thin and, except for Ag, produced no detectable alteration in the x-ray pattern of the noble metal. With Ag, the coating gave two faint lines that could be attributed to a solid solution of Ag in Zn, and one line that is also found in the Zn pattern. The coating produced in 24 hr weighed only about half a milligram. It was removed from the noble metal by treatment with HCl or dilute HNO_3. Ordinary chemical analysis of this solution gave no certain indication of Zn due to the small amount of deposit. Analysis with a Todd Spectranal, however, did give definite evidence for the presence of Zn.

The potential of the coated Cu and Ag in these solutions was within 25 mv of that of pure Zn. This substantiates the suggestion that this coating is Zn or a Zn-rich alloy or solid solution.

When Ni was used as the noble metal it appeared as if a coating was formed on the Ni, but repeated attempts at analysis failed to produce any substantial evidence for Zn. In one experiment three cells were set up under identical conditions using, respectively, Ag, Cu, and Ni as the noble metals in KOH-ZnO solutions which had been deoxygenated. A coating seemed to form on all three electrodes but later, when they were rinsed, the Ni appeared shiny whereas the other two coatings were not affected. These latter coatings did contain Zn, but no certain evidence for Zn could be obtained from the Ni specimen.

There was also evidence that dissolved oxygen tends to hinder the coating process. The coating appeared to form more quickly in solutions which had been deoxygenated.

Discussion

The above results show that Zn is deposited on Cu, Ag, Pb, and Pt when these metals are coupled with Zn in strong KOH solutions containing dissolved ZnO. No such deposit is formed when Ni is coupled with Zn. Any mechanism for this process, then, must allow for a difference between Ni and these other metals. A few possibilities are considered below.

1. The possibility that this phenomenon is due to mere adsorption was ruled out by the fact that strips of Ag and Cu received no coating when they were immersed for 24 hr in a KOH solution containing dissolved ZnO.

2. A more likely explanation involves an electrochemical mechanism, i.e., the potential of reaction [1]

$$Zn + 4\,OH^- \rightarrow Zn(OH)_4^= + 2e \qquad [1]$$

which is the reaction at the Zn electrode, is sufficient to bring about reaction [2]

$$Zn(OH)_4^= + Ag + 2e \rightarrow Zn(Ag) + 4\,OH^- \qquad [2]$$

One requirement of this mechanism is that the energy or potential necessary to reduce Zn onto Ag or Cu is less than that needed to reduce it onto Zn. This is not a case of the simultaneous deposition of Zn and the noble metal (2). The noble metal was always coupled to the Zn and it is difficult to see how any noble metal ions could go into solution. Further, Straumanis and Fang (2) noted the formation of Cu-Zn, Ag-Zn, and Ni-Zn alloys. In our

work Ni definitely did not form an alloy with Zn. Yet Ni and Zn form much the same type of alloy system as do Ag-Zn and Cu-Zn. It is possible that a thin oxide film on the Ni prevents the formation of the Ni-Zn alloy here. However, H_2 is always evolved from the noble metal in such a couple and this could reduce the oxide film. Furthermore, a slight Zn deposit was formed on stainless steel (which also possibly has a thin oxide film) when it was used as the noble metal and coupled with Zn.

It has been shown that there is, in some instances, an undervoltage associated with the deposition of small amounts of metal (3). It was suggested that this undervoltage is dependent on the closeness of approach of the lattice parameters of the noble metal and the deposited metal. Using the data in reference (3) the nearest neighbor in Ag is 2.88Å; in Zn, 2.66Å; in Cu, 2.55Å; in Ni, 2.49Å; in Pb, 3.49Å; and in Pt, 2.77Å. The mismatch then is +31.9% for Pb; +8.3% for Ag; +4.1% for Pt; −4.1% for Cu; and −6.4% for Ni, where + indicates that the parameters are larger for the noble metal than for Zn. These values suggest that Cu and Ni should behave similarly. In both of these metals the atoms are closer together than in Zn. The small difference between Cu and Ni would hardly seem sufficient to account for the fact that Zn deposits readily on Cu but not on Ni. If an undervoltage phenomenon is responsible for this Zn coating, then the extent of the mismatch is not the controlling factor. If it were, then no coating should have been formed on Pb.

The phenomenon of undervoltage is associated with the deposition of thin metallic films such as are deposited on the noble metal of the zinc-noble-metal couple. That only thin films are produced argues for the fact that certain sites on the noble-metal surface are responsible for this undervoltage, and hence the x-ray diffraction pattern of the noble metal is but slightly altered, if at all, by the deposition of the zinc. If, for example, the active sites were submicroscopic pits on the surface, the Zn atoms could fit easily into such pits on Ag, Pb, and Pt, but would do so with difficulty on Ni. In considering the possibility of an undervoltage phenomenon here, it should also be noted that the work in reference (3) was carried out in acid solutions and the shift of potential did depend in part on the pH. The solutions used in this work were approximately 8M KOH. In such solutions the Zn^{++} concentration is only about 10^{-15}M. Any undervoltage associated with this process must be rather small because the Zn-noble metal couple had a potential only about 15 to 25 mv more anodic than that of Zn.

3. Another possible mechanism involves a chemical in addition to an electrochemical reaction at the noble metal surface. When Zn and the noble metal are coupled in KOH solutions, hydrogen gas is evolved at the noble metal, reaction [3].

$$2H_2O + 2e \rightarrow H_2 + 2\,OH^- \qquad [3]$$

The deposition of Zn at the noble metal then can be due to the reduction of the zinc-containing ions or $Zn(OH)_2$ by H_2, Eq. [4].

$$H_2 + Zn(OH)_2 \rightarrow Zn + 2H_2O \qquad [4]$$

However, the reaction does not proceed with molecular hydrogen. Hydrogen gas was bubbled for several hours over a Ag electrode in KOH-ZnO electrolyte, but no Zn was deposited or produced. This suggests that the reduction is accomplished with atomic hydrogen.

At such an electrode surface there is a competition between reactions [5] and [6].

$$2H + Zn(OH)_2 \rightarrow Zn + 2H_2O \qquad [5]$$

$$2H \rightarrow H_2 \qquad [6]$$

Whether or not Zn is deposited at a noble metal electrode in a Zn-noble metal couple will depend on the relative rates of reactions [5] and [6]. According to Bonhoeffer (4) the efficiency of different metals in causing the combination of hydrogen atoms is almost exactly in the reverse order to their overvoltage values, i.e., the higher the hydrogen overvoltage the slower the rate of reaction [6]. It is difficult to find comparable hydrogen overvoltage data for strongly alkaline solutions. However, it has been suggested (5) that the relative overvoltage values are the same in alkaline as in acid solutions. If this is true, then the hydrogen overvoltages vary in the following order: Pb>Cu=Ag>Ni>Pt (5, p. 420). This order is not to be accepted without question. When Zn was coupled with these metals, gas was evolved most copiously at Pb which would indicate a lower overvoltage value. This would favor reaction [6] rather than [5]. But, since Zn was deposited on Pb and Pt, it would seem then that it should also have been deposited on Ni.

It is possible that a third competing reaction enters in. This reaction involves the dissolving of Zn from the coating deposited on the noble metal. It has been noted that a coating that appeared to form on Ni disappeared during rinsing. Furthermore, when a coated Cu strip was placed in water, the Zn redissolved within a day or two. To check this further, Ag-Zn and Cu-Zn couples were allowed to stand in KOH-ZnO solutions for a week. Then the Zn strip was removed from each couple. After standing for a few days the coating began to disappear from the Cu but not from the Ag. After a week the Cu was clean but the Ag was still coated.

When Zn is deposited on a noble metal, a Zn-noble metal couple is formed and reactions [1] and [3] can take place on the coated metal. This, of course, opposes the deposition of Zn on the noble metal. This opposing process appears to occur most readily on Ni, to some extent on Cu, and hardly at all on Ag.

A likely explanation for this concerns the lattice parameters of these metals. As has been noted earlier, Ni has the smallest "nearest neighbor" distance, less than that of Zn. Consequently, Zn is deposited merely on the surface of the Ni and is not held there tenaciously. The "nearest neighbor" distance for Cu is larger than that for Ni but still it is smaller than that for Zn. Zinc, therefore, deposits with less difficulty on Cu than on Ni, is held more firmly, and shows less tendency to reenter the elec-

trolyte. With Ag, Pb, and Pt, the Zn fits easily into pits on the surface and, consequently, is held rather firmly there, perhaps forming solid solutions in which the activity of the Zn atoms is less than one. This reduces the tendency of Zn to reenter the solution.

An attempt was made to verify the suggestion that the Zn is produced by the reduction of $Zn(OH)_2$ or $Zn(OH)_4^=$ with atomic hydrogen. A strip of Ag was placed in KOH-ZnO electrolyte and the potential on this strip was gradually increased until bubbles of gas just became visible on the surface of the metal. The potential of the Ag was then about 20 mv more anodic than that of Zn. The Ag electrode was held at this potential for about 6 hr. Small amounts of H_2 were formed during this interval and, at the same time, a deposit of Zn formed on the surface of the Ag. When the Ag was more anodic than this, no visible deposit was formed.

In summary, it is suggested that the Zn coating formed on the noble metal in a Zn-noble metal couple placed in KOH-ZnO electrolyte results from the reduction of the dissolved Zn species by atomic hydrogen. Whether the Zn coating persists depends on how well the deposited Zn atoms fit into the lattice of the noble metal. The more easily the Zn atoms are accommodated the more likely a solid solution will be formed thereby reducing the activity of the deposited Zn atoms. This reduced activity lessens the tendency of the deposited Zn to redissolve.

The mechanism suggested above is intended to deal only with the first layer or film of Zn deposited on the noble metal. However, very little additional deposit of Zn takes place. The deposition in such a Zn-noble metal couple seems to stop after several hours and the evolution of H_2 practically ceases then also.

Acknowledgment

The authors acknowledge with thanks the helpful comments of S. Eidensohn and W. S. Herbert and the courtesy of the Electric Storage Battery Company in furnishing the materials used in this work.

Manuscript received June 17, 1959.

Any discussion of this paper will appear in a Discussion Section to be published in the June 1960 JOURNAL.

REFERENCES

1. J. M. Booe, *This Journal*, **99**, 197C (1952).
2. M. E. Straumanis and C. C. Fang, *ibid.*, **98**, 9 (1951).
3. R. C. De Geiso and L. B. Rogers, *ibid.*, **106**, 433 (1959).
4. K. F. Bonhoeffer, *Z. physik. Chem.*, **113**, 199 (1924).
5. G. Kortüm, J. O'M. Bockris, "Textbook of Electrochemistry," Vol. II, p. 423, Elsevier Publishing Co., Houston (1951).

The Anodic Dissolution and Electrolytic Polishing of Metals

J. K. Higgins

Metallurgy Division, Atomic Energy Research Establishment, Harwell, Didcot, Berks, England

ABSTRACT

An experimental study has been made, using the potentiostat technique, of the anodic dissolution and electrolytic polishing of nickel in hydrochloric acid. The effect of experimental conditions on the potential/current density curves and the value of the limiting current density has been investigated. Results have been interpreted on the basis of a simple diffusion mechanism, and complications arising from the thick salt films found in the more concentrated solutions have been considered. Some results showing the connection between polishing and passivity have been collected for copper anodes in potassium cyanide solutions containing potassium hydroxide.

Theories of the anodic dissolution of metals under conditions such that electrolytic polishing occurs have been referred largely to the case of copper in phosphoric acid (1). Some authors have emphasized the role played by salt and oxide films during polishing (2, 3). In order to extend the theory to include another metal besides copper the anodic behavior of nickel in hydrochloric acid was studied. Results confirm the general theory and provide clear evidence of the occurrence and importance of salt films during electrolysis. The system was studied by constructing potential/current density (C.D.) curves under various experimental conditions. The potentiostat technique (4) was used in which the anode potential is set at any arbitrary value, the current being controlled by the potentiostat to maintain this value. In order to investigate the relationship between electrolytic polishing and passivity some data on the anodic dissolution of copper in potassium cyanide were obtained under conditions favorable to oxide film formation, in strongly alkaline solution.

Experimental Technique

The electrolytic cell consisted of a 400-ml squat beaker containing 250 cc of electrolyte in all cases. The anodes of projected area 0.15 cm^2 were made by drawing wire (S.W.G. 16) to the appropriate length through a rubber bung in one end of a glass tube and filing the end of the wire flat. The glass tube fitted with the rubber bung and wire anode was mounted vertically, exposing about 2.5 mm of the wire to the electrolyte. The cathode was a Pt spiral of area 1 cm^2 in a tube whose end was closed with a filter paper plug. A Zn/0.1M — $ZnSO_4$ reference electrode was connected to the working electrode by means of a Luggin capillary, and was chosen be-

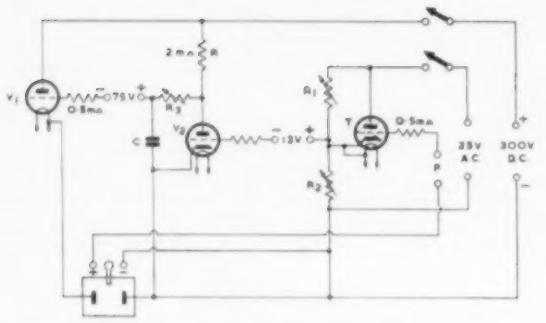

Fig. 1. Potentiostat A. $\overline{V_1}$, Osram triode PX25; $\overline{V_2}$, Brimar pentode 8 Al strapped as triode; T, Osram thyratron GTIC; C, 8 μF electrolytic condenser; R, 20,000 ohms; R_1, 100,000 ohms; R_2, 1000 ohms.

cause its potential always would be more negative than any it might be required to maintain. The potential of the electrode remained constant at −0.80 v on the hydrogen scale for about 4 weeks. All the anode potentials quoted are expressed on the standard hydrogen scale, the values being obtained by subtracting 0.8 v from the cell voltage of the combination anode (or working electrode)/reference electrode. The electrolyte was usually maintained at 20° ± 0.5°C.

The circuit diagram of the first electronic potentiostat is shown in Fig. 1 and is due to Hickling (4). Upon the application of 300 v d.c. the condenser C charges up through the resistance R, opposes the 75-v negative bias applied to the grid of the triode valve V_1 and thus allows a progressively increasing current to flow through V_1 and the cell. However, C can discharge through V_2 when its negative grid bias of 13 v is opposed by a voltage across V_2; this voltage is developed when the thyratron T fires. T is set 50 times a second by the 25-v a-c supply; it is adjusted to its critical tripping voltage by the automatic biasing potentiometer R_1-R_2. Into the grid circuit of the thyratron are placed the potentiometer P (connected to make the grid more negative) and the working/reference electrode combination in opposition. When the voltage of the electrode combination is greater than that set upon P, then the thyratron will fire, the current through V_1 will drop momentarily and will be connected to maintain the potential of the working electrode at this point indefinitely. The 300, 75, and 13 v d.c. supplied were obtained from suitable rectifying circuits. The potentiostat could deliver 0.1 amp; its control circuit was sensitive to ± 0.01 v; the current taken from the reference electrode was less than 1 μamp.

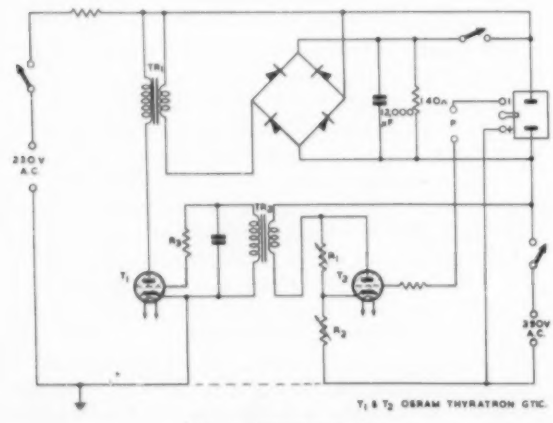

Fig. 2. Potentiostat B

The circuit of the second potentiostat, also due to Hickling, is shown in Fig. 2. The thyratron T_2 is included in a circuit similar to that used in the first potentiostat. When the voltage between the working/reference electrode combination is greater than that set on the potentiometer P, then T_2 fires and induces a voltage across the secondary of TR_2, 180° out of phase due to the condenser; this voltage being applied to the grid of T_1, this valve does not fire.

When the voltage of the working/reference electrode combination is less than that across P then T_2 does not fire, the biasing voltage on T_1 is absent, T_1 fires and induces a voltage across the secondary of TR_1 which is rectified, smoothed, and fed to the electrolytic cell. The current through the cell is thus controlled to maintain the potential of the working electrode indefinitely. In practice it was found that the negative bias on T_1 was not sufficient to withhold any one pulse of electricity, and consequently a 140-ohm resistance was connected across the output to by-pass some of the current. The output current is not limited by having to pass through a triode valve, and an output of several amperes could be obtained with the instrument at low output voltages; but as the output voltage increased the current fell off considerably. The two potentiostats are called A and B, respectively.

Experimental Results

Nickel in Hydrochloric Acid

Potential/C.D. graphs were obtained for nickel anodes in hydrochloric acid of concentration from 0.1*N* to 10.0*N*. The anode potential was increased in steps of 0.2 v, the current becoming constant after a few seconds, when it was read off. The current stabilized to a constant value almost immediately as the anode potential was reduced in steps of 0.2 v to give the descending curve. In Fig. 3A and B are given the curves obtained in 9*N* HCl.

The C.D. was undetectable in Fig. 3A until an anode potential of + 0.15 v was reached, when it rose rapidly for a small increase in potential, attaining a high value of about 0.40 amp/cm². As the potential was increased by a further small amount then the C.D. fell, and remained substantially constant with further increase in potential, the limiting C.D. region, until chlorine gas was evolved at about 2.5 v and the C.D. rose. The descending curve followed the ascending curve closely except that the high peak at C on the ascending curve did not recur. Before the limiting C.D. region was reached the anode was etched to a gray matt surface, while in the limiting C.D. region a thick green film formed, the anode being seen to be brightened underneath on removal from the electrolyte.

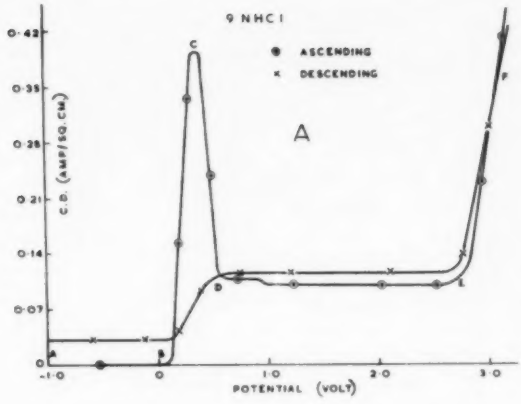

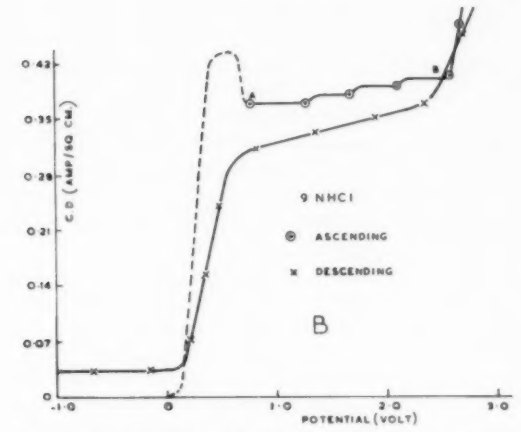

Fig. 3. A and B. Nickel in 9N HCl : Anode C.D. vs. Anode Potential.

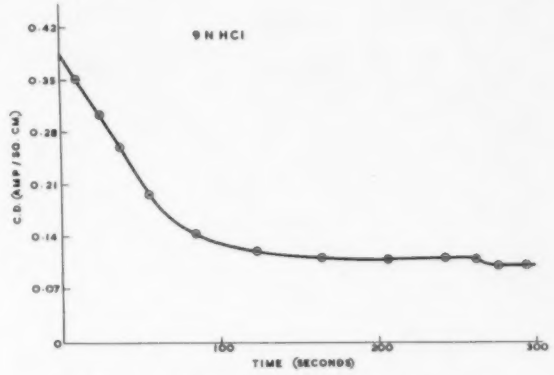

Fig. 4. Nickel in HCl : Limiting C. D. vs. Time

In order to remove the thick green film formed in the limiting C.D. region the following technique was adopted: the anode potential was increased in steps of 0.2 v, up to 1.0 v as in Fig. 3A; the circuit was broken for 1 min, then again completed, the anode potential being 1.0 v, i.e., greater than the potential at which the etching region and high peak value of the C.D. occurred at C in Fig. 3A. The C.D. rose rapidly to about 0.37 amp/cm^2 as recorded in Fig. 3B; the green film fell away to be replaced by a thick green layer of rapidly dissolving salt which streamed away from the anode; the anode was brilliantly polished. The rest of the graph was plotted as Fig. 3A.[1]

It is clear that in this electrolyte there are two limiting C.D.'s of approximately 0.10 and 0.40 amp/cm^2.[2] The operation of raising the potential to 1.0 v, breaking, and remaking the circuit will be called prepolarization.

If a prepolarized anode in 9*N* HCl is electrolyzed in the limiting C.D. region for about 5 min then I_{LIM} sinks gradually to the value for the nonprepolarized anode; the layer of rapidly dissolving salt is replaced by a thick green film. This is shown in Fig. 4, the anode potential being 1.0 v.

The nature of the anodic process occurring in each section of the curve was determined by carrying out constant-potential electrolyses at a series of increasing potentials and comparing the loss in weight of a nickel micro-electrode with the gain in weight of a cathode in a copper coulometer in series with the cell. Results obtained in electrolytes varying from 0.5*N* to 9.0*N* HCl showed that up to a potential of 2.5 v the current efficiency for dissolution of nickel in the nickelous state was practically 100%; above 2.5 v gas evolution set in and the current efficiency dropped.

Influence of experimental factors on I_{LIM}.—The limiting C.D.'s for the ascending curves were found to be reproducible with an accuracy of about ± 5% and ± 7% using potentiostats A and B, respectively.

In Table I are summarized the limiting C.D.'s for solutions of HCl of concentration from 10*N* to 0.1*N*.

The prepolarized values are the greater until the concentration drops below 7*N* HCl when the two sets of figures approximate the same values. Below a concentration of 7*N* HCl the thick green film at the nonprepolarized anodes does not appear, and all the electrodes are surrounded by a thick layer of rapidly dissolving salt streaming away. The limiting C.D.'s for both nonprepolarized and prepolarized anodes increase as the concentration of HCl decreases until 0.5*N* HCl when they decrease rapidly.

Potential/C.D. graphs were constructed for solutions of 7*N* HCl alone and with additions of 5, 10, 20, 25, and 30% glycerol to increase the viscosity, using both nonprepolarized and prepolarized anodes. Results are shown in Fig. 5, I_{LIM} being plotted against the reciprocal viscosity. For the prepolarized

Table I. Influence of concentration of HCl on I_{LIM} at 20°C

Concentration, g mole/l	10	9	8	7	6	4	2	1	0.5	0.1
Limiting C.D., amp/cm^2	0.07*	0.10*	0.24*	0.68*	1.18	1.83	2.37	2.54	1.59	0.19
Limiting C.D., amp/cm^2, prepolarized	0.34*	0.45*	0.54*	0.95*	1.22	1.83	2.24	2.43	1.62	0.19

* Values marked with an asterisk were obtained using potentiostat A, the rest potentiostat B.

[1] The limiting C.D. regions for the ascending and descending curves could not be brought any closer together by leaving the anode potential for 15 sec at each 0.2 v step for both Fig. 3A and B.

[2] When the C.D. passing in the limiting C.D. region is not constant a mean value is taken; the limiting C.D. is denoted in all cases by I_{LIM}.

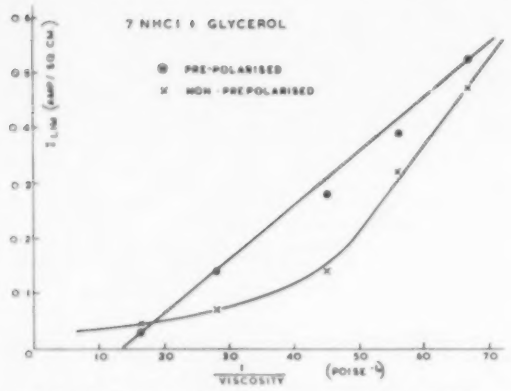

Fig. 5. Nickel in 7N HCl with glycerol additions : Influence of viscosity on limiting C.D.

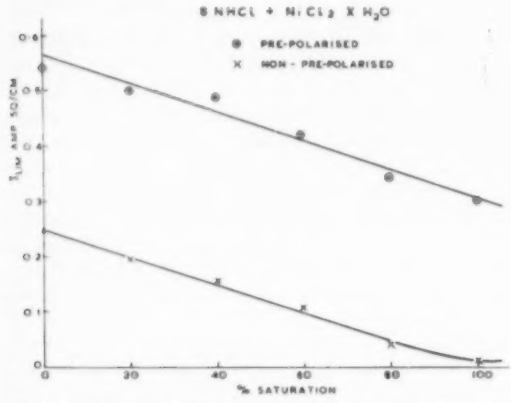

Fig. 6. Nickel in 8N HCl with nickelous ion addition; influence of dissolved nickel on limiting C.D.

anodes I_{LIM} varies linearly as the reciprocal viscosity, but this is not so for the nonprepolarized anodes.

Stirring solutions of 7*N* HCl + 20, 25, and 30% glycerol, at 450 rpm with a glass paddle stirrer, results in an increase in I_{LIM} of 3.9, 5.6, and 4.5 times for nonprepolarized anodes; increases for prepolarized anodes were 3.1, 5.6, and 3.7 times. In the case of 7*N* HCl + 20% glycerol, I_{LIM} increased from 0.09 to 0.35 amp/cm^2 for nonprepolarized anodes and from 0.14 to 0.43 amp/cm^2 for prepolarized anodes.

Rise in temperature from 20° to 70°C caused a rise in the limiting C.D. of 1.5 and 1.9 times for anodes in 0.5 and 6*N* HCl.

Solutions of 8*N*, 4*N*, and 0.5*N* HCl were saturated with A.R. $NiCl_2$. 6 H_2O by mechanical shaking for a few hours; by diluting these with the pure acid, solutions 80, 60, 40, and 20% saturated with nickel salt were obtained. Potential/C.D. curves were of the usual type. Typical curves of I_{LIM} against per cent saturation are given in Fig. 6 and 7 for 8*N* and 0.5*N* HCl.

For the nonprepolarized anodes in 8*N* and 0.5*N* HCl the values of I_{LIM} decrease linearly with per cent saturation of nickel salt; the value of I_{LIM} at 100% saturation is very nearly zero. Although there is a linear decrease in I_{LIM} for prepolarized anodes,

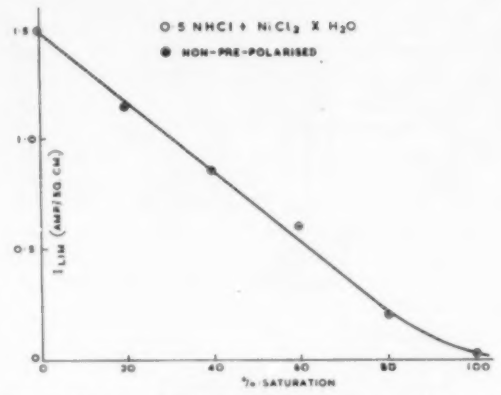

Fig. 7. Nickel in 0.5N HCl with nickelous ion addition; influence of dissolved nickel on limiting C.D.

the graph does not cut the x axis at 100% saturation.

Copper in Potassium Cyanide

The anodic dissolution and electrolytic polishing of copper in potassium cyanide has been discussed in a previous paper (2). An attempt was made to induce passivity gradually by slowly increasing the alkalinity of the electrolyte.

In Fig. 8 is given a typical potential/C.D. graph for a copper anode in 2M KCN. The anode was etched in the rapidly ascending region; it was polished in the limiting C.D. region, although the polish was not comparable in brilliance with those obtained at nickel anodes in hydrochloric acid or copper anodes in phosphoric acid. When the anode potential exceeded 1.0 v a thick brown film formed on it.

In Fig. 9, which is a graph for 2M KCN + 0.5M KOH solution, a pronounced dip occurs in both ascending and descending curves. If the concentration of KOH is increased to 0.75M, then the behavior shown in Fig. 10 is observed. The C.D. attains a high peak value of about 0.09 amp/cm^2 before it drops almost to zero on increasing the potential beyond 0 v; at 1.0 v the next process, formation of the brown film, sets in and the C.D. can again rise. The descending curve does not show a limiting C.D. region but the C.D. remains almost zero until about

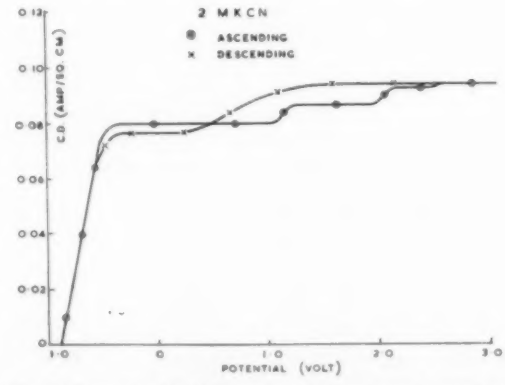

Fig. 8. Copper in 2M KCN; anode C.D. vs. anode potential

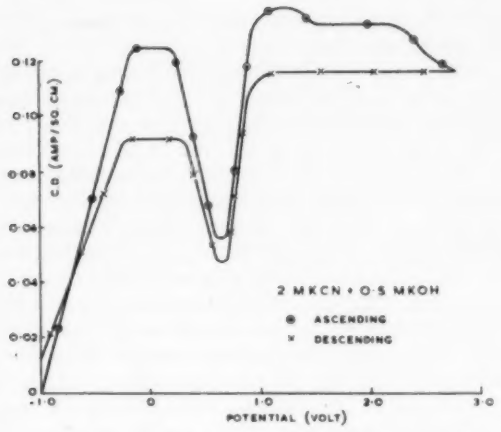

Fig. 9. Copper in 2M KCN + 0.5M KOH; anode C.D. vs. anode potential.

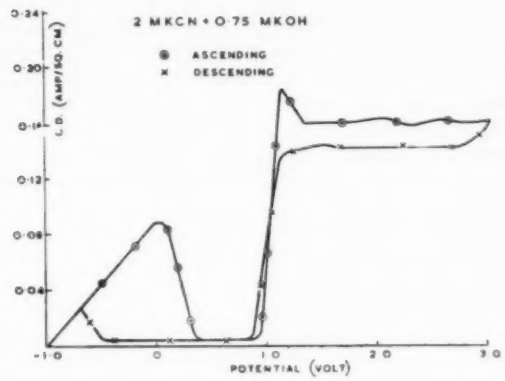

Fig. 10. Copper in 2M KCN + 0.75M KOH; anode C.D. vs. anode potential.

−0.5 v when it rises to the value for the ascending curve.[3]

The behavior in 2M KCN + 0.75M KOH solution up to a potential of 1.0 v is typical of an anode undergoing passivity (5) and the anode was not polished in this electrolyte. Passivity can be induced gradually by increasing the alkalinity of the medium in small steps.

Discussion

The increase in the limiting C.D.'s on stirring and the decrease when the viscosity is increased, together with the effect of temperature, constitute a clear indication that the anodic dissolution of nickel in hydrochloric acid is diffusion controlled at high current densities. The effect on the limiting C.D. of the addition of nickel salts to the solution suggests that it is the diffusion of the nickelous ion away from the anode which is rate determining.

Assuming Fick's law and the existence of a linear concentration gradient over the diffusion layer, the limiting C.D. is given by (2, 6).

$$I_{LIM}\ (\text{amp/cm}^2) = \frac{DFZ\ (C_s - C_o)}{\delta} \qquad [1]$$

[3] The ascending and descending curves in Fig. 9 and 10 could not be brought closer together by leaving the anode potenial for 15 sec at each 0.2-v step.

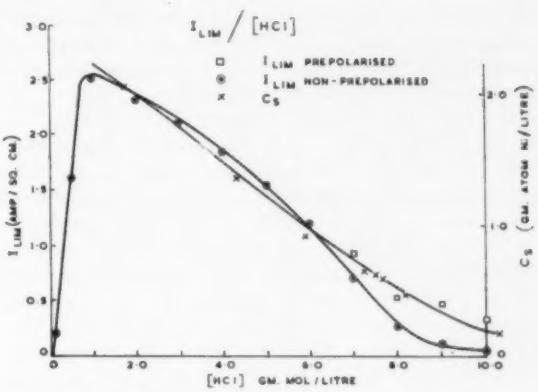

Fig. 11. Comparison of influence of HCl concentration on limiting C.D. and nickel chloride solubility.

where D is the diffusion coefficient of the nickelous ion, **F** the Faraday, Z the valency of the dissolving ion, and δ the thickness of the diffusion layer; C_s and C_o (g ion/liter) are the solubility and bulk concentration, respectively, of the nickelous ion. For a solution initially free from nickel $C_o = 0$, and we have

$$I_{LIM} = \frac{DFZ\,C_s}{\delta} \qquad [2]$$

According to Eq. [1] for constant values of C_s any factor such as stirring, tending to decrease δ, should increase I_{LIM}. Increasing the viscosity of the solution should decrease D and therefore I_{LIM}, while increase of temperature should increase D and therefore I_{LIM}. All these predictions are borne out by experiment.

For constant values of D and δ in Eq. [1], I_{LIM} should be proportional to $(C_s - C_o)$ and zero when $C_s = C_o$, i.e., at 100% saturation with nickel salt. This is confirmed experimentally as shown in Fig. 6 and 7 except for prepolarized anodes in 8*N* HCl.

If Eq. [2] is correct, I_{LIM} should be proportional to C_s in the simple acid solutions. In Fig. 11 the graphs of I_{LIM} and C_s are plotted against concentration of HCl; the shape of the two curves is similar, confirming the above prediction.

By substituting values of D, C_s, and I_{LIM} in [2] it is possible to calculate δ. The values of D were calculated from the equation (6)

$$D = \lambda RT/\mathbf{F}^2 \qquad [3]$$

where λ, reciprocal ohms, is the equivalent conductivity of nickel chloride at 18°C (7). The results obtained using λ values from the International Critical Tables for the solutions shown are: $D = 1.85 \times 10^{-6}$ cm²/sec⁻¹, 18°C, 10*N*, 8*N* HCl; $D = 1.74 \times 10^{-6}$ cm²/sec⁻¹, 18°C, 7*N* HCl; $D = 1.63 \times 10^{-6}$ cm²/sec⁻¹, 18°C, 6*N*, 1*N* HCl. Substituting these values in [2] the values

Table II. Thickness of diffusion layer in HCl solutions

Concentration HCl, g mole/l	10	9	8	7	6	4	2	1
δ cm	0.0110	0.0112	0.0070	0.0033	0.0024	0.0024	0.0026	0.0028
δ cm, prepolarized	0.0021	0.0021	0.0030	0.0023	0.0024	0.0024	0.0029	0.0028

of δ for the nonprepolarized and prepolarized anodes are given in Table II for the simple HCl solutions. Apart from the first four values for the nonprepolarized anodes δ is between 0.002 and 0.003 cm; this is much less than the 0.03 cm normally found for cathodic diffusion processes in unstirred solutions. However, at the present vertical anodes and the high C.D.'s encountered there will be a large amount of convective stirring which will decrease δ as discussed by Tobias, Eisenberg, and Wilke (8). Values of δ for nonprepolarized anodes in the concentrated HCl ($> 7N$) solutions are higher than the rest. When the thick salt film is removed, i.e., the anodes are prepolarized, then δ is lowered and is of the same order as the values found in the dilute solutions. It is clear that the simple diffusion mechanism does not hold for the nonprepolarized anodes in the concentrated acid solutions.

The above conclusion is borne out by the graphs of Fig. 11; the I_{LIM} and C_c curves agree most closely for the prepolarized anodes. Finally, Fig. 5, where I_{LIM} is plotted against the reciprocal viscosity for solutions of HCl containing glycerol, shows that the linear relationship holds for prepolarized anodes only. This relationship has been found for the anodic dissolution of copper in phosphoric acid and potassium cyanide; both are examples of diffusion-controlled processes (2). It would seem that the process in the dilute ($< 7N$ HCl) solutions is diffusion controlled as it is at the prepolarized anodes in the more concentrated ($> 7N$ HCl) solutions. At the nonprepolarized anodes in the concentrated solutions complications set in due to the formation of thick salt films.

The hydrate of nickel chloride stable in HCl solutions from 1.75 to 7.26N is the hexahydrate, at 7.5N the pentahydrate, and from 7.65 to 10.35N the tetrahydrate (9). It is probable that the thick salt films observed in HCl solutions more concentrated than 7N are films of the tetrahydrate; Fig. 11 shows that this salt, stable in concentrated acid solutions, is less soluble than the more hydrated forms.

If the prepolarized anode in 9N HCl is electrolyzed in the limiting C.D. region for about 5 min, then I_{LIM} sinks gradually to the value for the nonprepolarized anode (see Fig. 4); the diffusion layer is replaced by a thick light green film. It would seem at the prepolarized anode that the nickel first dissolves as an unstable species which then gradually reverts to the sparingly soluble tetrahydrate which forms a film on the anode.

Results for the dissolution of prepolarized anodes in 8N HCl, partly and completely saturated with nickel chloride, are puzzling (Fig. 6). All the evidence suggests that it is the reaction at the prepolarized anodes which is diffusion controlled, and yet it is the nonprepolarized anodes which show nearly zero I_{LIM} in solutions 100% saturated, as would be expected from Eq. [1] for a diffusion-controlled process. It may be because the prepolarized anodes are dissolving as an unstable species that I_{LIM} remains so high in solutions containing nickel chloride; when the nickel goes into solution directly as the stable tetrahydrate (nonprepolarized anodes) then the predictions of Eq. [1] are verified.

On the basis of the diffusion treatment given it is to be expected that in the limiting C.D. region, when the layer of electrolyte adjacent to the anode becomes saturated with salt, a film of salt will be deposited. This film usually dissolves as quickly as it is formed, its thickness depending on the solubility of the salt and its degree of hydration. Williams and Barrett (10) have identified the film formed on copper anodes in phosphoric acid as copper phosphate by electron diffraction measurements. It is invisible during electrolysis as are the films formed in the dilute HCl solutions at nickel anodes. In concentrated HCl solutions at nonprepolarized anodes the salt films are clearly visible, the electrode still being polished underneath.

The smoothing action during electrolytic polishing in the limiting C.D. region can be explained satisfactorily by assuming the absence of a concentration gradient of metallic cations between peaks and cavities in a roughened surface and consequently faster dissolution of the peaks. An additional factor aiding smoothing is the earlier deposition of a salt film in the cavities than on the peaks. However, while this theory is satisfactory for the dilute solutions of HCl, it is not sufficient to explain why nonprepolarized nickel anodes are polished underneath the thick salt film in the concentrated ($> 7N$) HCl solutions; the films are much thicker than the cavity depth of a few microns. Hoar and Mowat (3) have explained the absence of crystallographic etching in the limiting C.D. region by assuming that the metallic cations pass from the metallic surface into vacant sites in an oxide lattice, the oxide dissolving as fast as it is formed. The random distribution of vacant sites would then account for the absence of etch figures. If it is assumed that the oxide film is present underneath the salt film, then the brightening of the nickel in solutions where a very thick film of salt is formed can be understood. Probably both the smoothing and brightening mechanism are present at polishing anodes in dilute solutions.

It is well known from the work of Evans and others (5) that the occurrence of passivity is associated with the formation of a thin, coherent, insoluble oxide film on the anode. The fact that the transition from polishing to passivity behavior can be brought about gradually (Cu in KCN + KOH) by increasing the alkalinity of the electrolyte is evidence for the presence of a dissolving oxide film during polishing and leads to the view that polishing and passivity are two limiting cases of the same general phenomenon.

Conclusions

1. The anodic dissolution of nickel in dilute ($< 7N$) HCl solutions is diffusion controlled.

2. At prepolarized anodes in concentrated ($> 7N$) HCl solutions the dissolution is diffusion controlled.

3. At nonprepolarized anodes in conc. ($> 7N$) HCl solutions the simple diffusion mechanism breaks down.

4. The onset of thick salt film formation in the

more concentrated (> 7*N* HCl) solutions is associated with a decrease in the degree of hydration of the dissolving salt.

5. The state of the prepolarized anode is unstable; it reverts to the nonprepolarized condition in a short time.

6. Polishing in the dilute solutions can be explained satisfactorily by the differential solution of peaks and cavities due to different concentration gradients at peaks and cavities and the deposition of freely soluble salt films.

7. The brightening effect observed under very thick salt films in concentrated acid solutions is best explained by the dissolving oxide theory of polishing.

8. Passivity can be induced gradually in a polishing bath by increasing the alkalinity of the electrolyte in steps and this supports the theory mentioned in 7.

Manuscript received March 3, 1959.

Any discussion of this paper will appear in a Discussion Section to be published in the June 1960 JOURNAL.

REFERENCES

1. P. A. Jacquet, *Trans. Electrochem. Soc.*, **69**, 629 (1936); *Bull. Soc. Chim.*, **3**, 706 (1936); W. C. Elmore, *J. Appl. Phys.*, **10**, 724 (1939); **11**, 797 (1940); H. F. Walton, *This Journal*, **97**, 219 (1950); J. Edwards, *J. Electrodepositors, Tech. Soc.*, **28**, 133 (1952); J. Edwards, *This Journal*, **100**, 189C, 223C (1953).
2. A. Hickling and J. K. Higgins, *Trans. Inst. Met. Finishing*, **29**, 274 (1953).
3. T. P. Hoar and J. A. S. Mowat, *Nature*, **165**, 64 (1950); *J. Electrodepositors' Tech. Soc.*, **26**, 7 (1950); T. P. Hoar and T. W. Farthing, *Nature*, **169**, 324 (1952).
4. A. Hickling, *Trans. Faraday Soc.*, **38**, 27 (1942).
5. U. R. Evans, *Nature*, **126**, 130 (1930); L. Stephenson and J. H. Bartlett, *This Journal*, **101**, 571 (1954).
6. S. Glasstone, "An Introduction to Electrochemistry," p. 449, D. Van Nostrand & Co., New York (1949).
7. International Critical Tables 6, 231.
8. C. W. Tobias, M. Eisenberg, and C. R. Wilke, *This Journal*, **99**, 359C (1952).
9. Seidel, "Solubilities of Inorganic and Metal Organic Compounds," Vol. 1, p. 1342, D. Van Nostrand & Co., New York.
10. E. C. Williams and M. A. Barrett, *This Journal*, **103**, 363 (1956).

An Investigation of Chemical Variables Affecting the Formation of Films on Copper in Aqueous Solutions

W. H. Davenport, V. F. Nole, and W. D. Robertson[1]

Chase Brass and Copper Company, Waterbury, Connecticut

ABSTRACT

The growth of copper oxide films in aqueous solutions has been studied by an electrometric method. Quantitative data have been obtained on the growth of films as a function of the solution variables; anion type and concentration, pH, and oxygen concentration. In air-stirred chloride solutions, film thickness increases with increasing chloride concentration, passes through a maximum in solutions approximately 0.01M, and then decreases. A maximum also is obtained for pH dependence in the range pH 5.9-9.0. Cuprous oxide is formed below about pH 10.5 and cupric oxide predominates at higher values. For equimolar solutions (0.1M), film growth rate in sodium chloride solutions is about double that in sodium sulfate. In both cases the rate is linear and limited by oxygen availability under the conditions described. In high-purity water, in the presence of excess oxygen, the rate of growth is approximately parabolic, but the extremely thin films formed preclude detailed analysis with the present technique.

Many investigators (1-8) have studied the rate of film formation on copper as a result of oxidation in air at various temperatures. The composition of these films, which is affected by environmental factors such as temperature and oxygen partial pressure, has been verified by electron diffraction studies (9-12). A generally accepted mechanism for the reaction relates oxidation rate to the movement of copper cations through vacancies in the oxide lattice and, it has been shown (4, 7, 8) that over a limited range of film thickness or temperature the parabolic equation may be used to express the growth of films with time. In the case of copper, all of the oxidized metal remains on the surface as a film, and a measure of film growth rate is also a direct measure of oxidation rate.

When copper corrodes in an open aqueous solution the rate of reaction is affected likewise by the nature of the corrosion product film formed on the surface. However, in an aqueous solution, all of the products of corrosion do not necessarily remain on the surface; depending on solution composition and pH, corrosion products may dissolve in the solution or form at a site removed from the reacting area. Accordingly a study of oxidation of copper in aqueous solution, based on film growth, can become quite complex. This perhaps explains why very little quantitative information is available on this subject.

The growth of films on copper in aqueous potas-

[1] Yale University, New Haven, Connecticut, Consultant.

sium chloride solutions was measured by Hill (13) in a study of the initial corrosion reaction. His tests, however, were limited to the pH range 7.0-8.3 in which the films were essentially insoluble. Kruger (14) studied the effect of illumination on films formed in air-saturated distilled water.

The present paper describes an investigation of the effect of certain solution variables on the growth and composition of films formed on copper in solutions where information appears to be lacking. It is designed to supplement previous work (15) dealing with the effect of the same variables on the corrosion rate of copper under similar conditions.

Experimental Procedure

Specimens.—Rod specimens, 0.125 in. diameter x 12 in. long, were prepared from oxygen-free high-conductivity copper drawn 85%. Chemical composition was: Cu-99.98%, Fe-<0.003%, Ni-<0.005%, Pb-<0.0005%, and Zn-<0.01%. The surface was scrubbed with water and pumice, rinsed in distilled water, and dried in alcohol. Specimens then were inserted in 3/16 in. ID glass tubes through a short section of ⅛ x ¼ in. rubber tubing which served as a gasket. By sliding the rod in or out, the specimen area could be varied. For very thin films the area was adjusted to 4 cm^2. Thicker films were developed on a 2 cm^2 area. Prior to exposure, the projecting portion was etched for 3 min in 10% ammonium persulfate and rinsed in high-purity demineralized water. The specimen assembly then was transferred quickly to the test solution without drying.

This chemical etching technique for preparing the specimen surface was adopted as a reproducible method which minimizes the blank reading that is obtained by other chemical or mechanical methods, not involving preparation in an inert atmosphere. In view of the fact that film growth was to be studied over some considerable period of time, and that the increased thickness is an average quantity, more elaborate methods did not seem warranted for this preliminary investigation of the comparative effects of solution variables.

Film development.—Films were developed at room temperature in the corrosion cell previously described (15), using a continuous flow technique to maintain essentially constant solution composition. The test solution was fed to the bottom of the cell at 220 ml/hr and the appropriate gas stirring mixture was introduced by means of a gas lift side arm at 500 ml/hr (28 bubbles/min). Alternatively, in tests where increased oxygen availability was desired, the stirring gas was supplied to the bottom of the cell through a medium porosity, 10-15 micron pore size, fritted disk (10 mm diameter) at a rate of 250 ml/min.

When gas mixtures other than air were used, the system was kept under a slight positive pressure to maintain the desired atmosphere over the solution.

Three specimen assemblies were inserted in each cell and held in a uniform geometrical arrangement by means of a plastic spacer ring placed approximately at the mid point of the cell.

Air-formed films also were prepared by exposing specimens in an electric furnace equipped with a circulating fan.

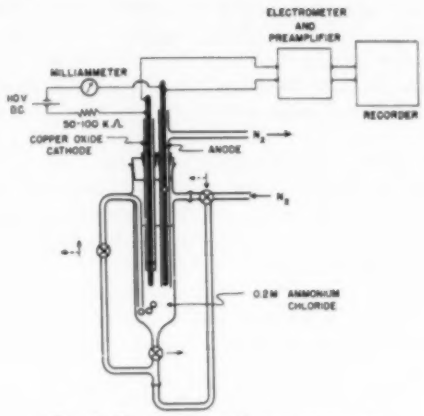

Fig. 1. Electrolytic reduction apparatus

Film analysis.—Following exposure, films were analyzed by an electrometric method, Fig. 1, similar to that used by Miley (4) in his investigation of air-formed films on copper. In principle, the copper compound composing the film is reduced cathodically and the thickness is calculated from the number of coulombs required and the bulk density. This calculation assumes that the surface is a plane and that the film is uniformly distributed. The errors resulting from these assumptions will depend on the magnitude of surface roughness, relative to film thickness, and on the degree of conformity of the contour of oxide and original metal surface. Certainly in the early stages the absolute value of the thickness may be largely in error due to nonuniformity of film and roughness of surface; the error should decrease significantly as the film thickness increases. In the present case the thickness has been used as a measure of changing conditions in the solution usually after 48 hr when a considerable thickness of film has been formed.

Reduction was carried out in a closed glass cell designed so that nitrogen could be either bubbled through the solution or passed over the surface to maintain a protective atmosphere. The film bearing specimen was made the cathode, a copper rod the anode, and 0.2M ammonium chloride was used as the electrolyte. Although the data reported herein were obtained using rod specimens, the apparatus can also be adapted to sheet or tube by using a hooked platinum wire as the cathode and hanging the specimen from this hook.

Current was obtained from a 110 v d-c source consisting of a 90-v "B" battery and a 22½-v "C" battery connected in series. Voltage was applied through a high resistance of 50,000-100,000 ohms. The use of such a large external resistance resulted in a small constant current of 1-2 ma which was unaffected by the relatively minor changes which took place in the cell. The potential developed by the voltage drop across the cell was fed to a Brown electrometer and preamplifier (an instrument which draws no significant current while measuring voltage) and then to a high speed recording potentiometer.

Table I. Oxidation of OFHC copper rod (0.125 in. diameter) in air at 245°C

Time, min	Film thickness, Å			
	Present data			Miley
	Cu_2O	CuO	Total	Total
3	760	10	770	
5				1100
6	1260	25	1285	
9	1580	0	1580	
10				1450
12	1745	20	1765	
15	1770	55	1825	
20				1900
25				2050
30	1780	385	2165	
43	2145	450	2595	
60	2180	535	2715	2700
90	2365	650	3015	
120	2145	810	2955	
150	2360	900	3260	
300	3000	940	3940	

Prior to analysis the electrolyte was deaerated by bubbling nitrogen for 30 min. The stopcock was turned to pass the gas over the surface and the exposed specimen assembly was inserted.

During the course of reduction the cell potential was followed and recorded to obtain the potential-time curves characteristic of the method. Film thickness then was calculated from the time and current required for reduction using the appropriate factors.

On the basis of Miley's observations and also x-ray diffraction studies, cuprous oxide, Cu_2O, was assumed to be the product which was reduced at a potential of approximately 300 mv and cupric oxide, CuO, the product reduced at 550 mv. Measured against a saturated calomel reference electrode, the corresponding reduction potentials would be 350 mv and 600 mv, respectively.

Experimental Results and Discussion

In order to check the apparatus and the procedure, a portion of Miley's work, dealing with film growth rate in air at 245°C, was repeated. The results are shown in Table I and in Fig. 2.

Good agreement was obtained. Miley's data did not indicate the ratios of cuprous and cupric oxide encountered but, in later work in conjunction with Cruzan (5), they reported that the proportions of the two oxides varied with film thickness. Below 400Å, films contained only cuprous oxide, above 800Å, all films contained a mixture of both, and in the intermediate range some films contained a mixture and others cuprous oxide alone. The films produced in the present work were all too thick to verify the latter conclusions; however, the increase in the proportion of cupric oxide with increasing film thickness does appear to agree with the trend established in the work of Cruzan and Miley.

Since the apparatus and analytical procedure proved reliable, the method was applied to the study of film formation in various aqueous salt solutions. The solution variables investigated were anion type and concentration, pH, and oxygen. Reproducibility of results varied with exposure conditions, with the greatest spread, ±5%, appearing in nearly neutral solutions where pH was quite sensitive to small changes in composition. A "blank" corresponding to a film thickness of 20Å is associated with the method and the necessary corrections have been made. The "blank" was traced to air oxidation during specimen preparation and probably could be reduced by preparing specimens in an inert atmosphere.

Effect of Anion Type and Concentration

The growth of films with time in 0.1M sodium chloride and 0.1M sodium sulfate solutions is shown in Fig. 3.

The rate of film growth is considerably higher in sodium chloride solutions and in each case it appears to be approximately linear over the range investigated. In both solutions only cuprous oxide was detected.

Results were about the same in either 0.1 or 0.01M sodium sulfate. However, a change in chloride concentration produced an appreciable change in film thickness as shown in Fig. 4.

For constant time and varying chloride concentration, maxima in thickness are obtained in 0.01M chloride solutions. The effect of chloride ion on film thickness does not correlate with previous observations (15) on the effect of chloride on corrosion rate, where it was shown that corrosion rate increased linearly with increasing chloride ion under the same conditions. The lack of correlation would appear to indicate that corrosion rate is not solely dependent

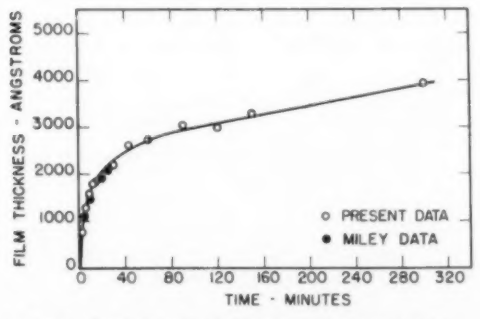

Fig. 2. Oxidation of OFHC copper in air at 245°C

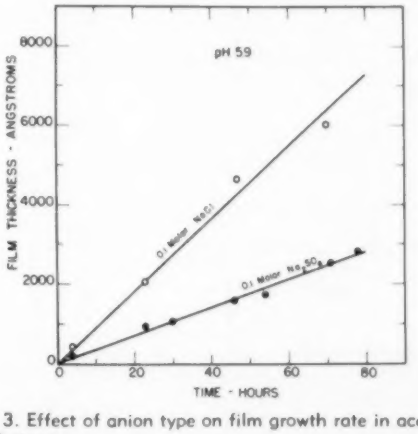

Fig. 3. Effect of anion type on film growth rate in aqueous salt solutions.

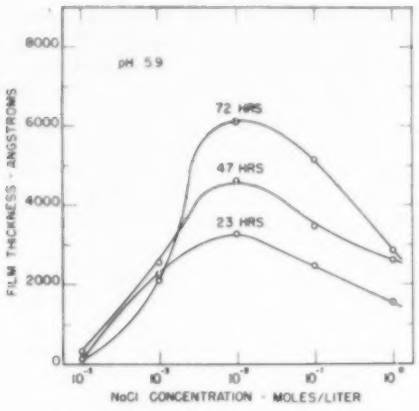

Fig. 4. Effect of concentration on film growth in sodium chloride solutions.

on film thickness for the conditions described. Further studies are being conducted.

Asselin and Rohrman (16) studied the corrosion rate of copper as a function of sodium chloride concentration and reported a maximum at much higher concentrations, 2-3*N*, but none in the range under consideration at present. They attributed the maximum to the net result of the opposing factors oxygen solubility and solution conductivity.

Effect of pH

The effect of pH was studied in solutions, 0.1M in chloride ion. Hydrochloric acid or sodium hydroxide was added to sodium chloride solutions as necessary in order to achieve the desired pH. It was also necessary to remove carbon dioxide from the incoming air in order to minimize drift in pH. Results are shown in Fig. 5.

A fairly flat maximum is obtained in the pH range 5.9-9.0. In this range films are essentially cuprous oxide, Cu_2O. Film thickness decreases rapidly below pH 5.9, or as the pH is raised from 9 to 10.5. At higher pH values, however, film growth again starts to increase. Films formed in the high pH range, around pH 12, are predominantly cupric oxide.

The effect of pH is complicated by the fact that

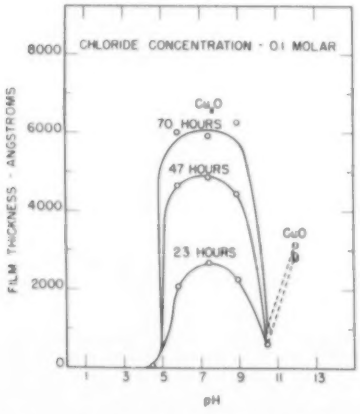

Fig. 5. Effect of pH on film growth in chloride solutions

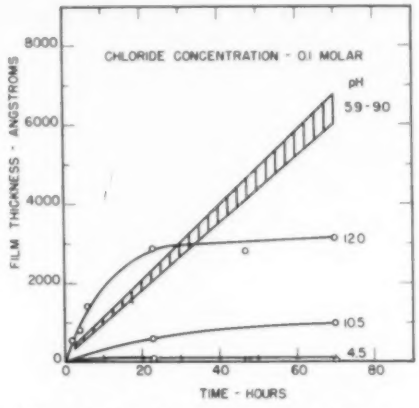

Fig. 6. Effect of pH on film growth rate in chloride solutions

the shapes of film growth rate curves vary at different pH values as shown in Fig. 6.

Films formed in the pH range 5.9-9.0 all fall in the band shown in Fig. 6 and they are still growing after 70 hr. Films formed below or above this range appear to reach a maximum thickness at shorter times and then remain fairly constant. Presumably, in the latter cases, a steady state has been reached where the film formation rate is equal to the dissolution rate.

The absence of measurable films below approximately pH 3 is consistent with previous observations (15) and, if the films can be assumed to be partially protective, then the effect of pH on films is also consistent with general experience regarding the increase in corrosion rate with decreasing pH.

Effect of Oxygen

The effect of oxygen was studied in 0.1M sodium chloride solutions by varying the composition of an oxygen-nitrogen mixture used as the stirring gas. Three mixtures were investigated; 21% (air), 50%, and 100% oxygen. Film thickness increased with increasing oxygen, as shown in Fig. 7, indicating that the process is under oxygen control in every case. The shape of the curve suggests that, at 100% oxygen, conditions were being approached where

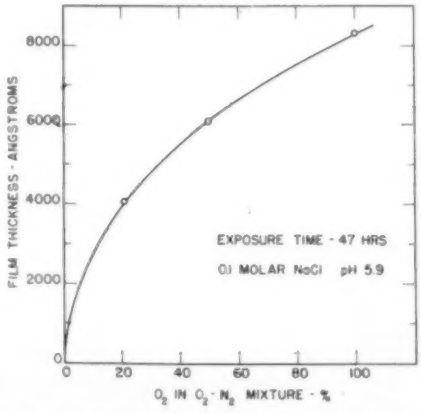

Fig. 7. Effect of oxygen on film growth in sodium chloride solutions.

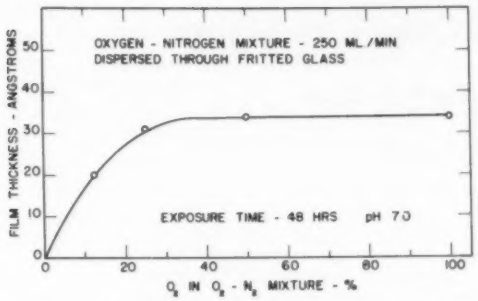
OXYGEN - NITROGEN MIXTURE - 250 ML/MIN
DISPERSED THROUGH FRITTED GLASS
EXPOSURE TIME - 48 HRS pH 7.0
FILM THICKNESS - ANGSTROMS
O_2 IN O_2 - N_2 MIXTURE - %

Fig. 8. Effect of oxygen on film growth in high-purity water

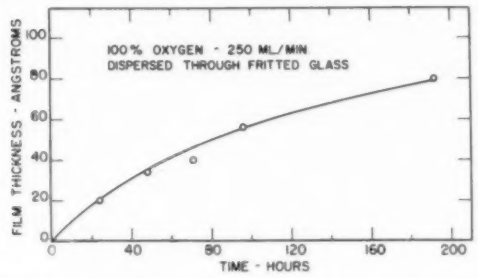

Fig. 9. Film growth rate in high-purity water in the presence of excess oxygen.

rate is independent of further increases in oxygen. This point has not been reached, however, and an increase in stirring rates at this point resulted in films of greater thickness for the same exposure times.

The interdependence of the variables anion concentration, pH, and oxygen makes it difficult to develop a general expression for the growth rate of films on copper in aqueous salt solutions. Thus, a statement regarding the rate in 0.1M chloride solutions must also define the conditions of pH and oxygen availability. In order to obtain a more general expression it was necessary to conduct tests under conditions where variables were either eliminated or reactants were supplied in excess. This was accomplished by using high-purity demineralized water as a corrosive medium. The effect of anions other than the hydroxyl ion present in water was thus eliminated and pH, which was determined before and after test, remained constant at 7.0. An oxygen-nitrogen mixture was supplied to the solution through the medium porosity fritted glass disk which served to increase the availability of oxygen. Under these conditions a mixture containing about 40% oxygen is sufficient to provide an excess of oxygen as shown in Fig. 8.

The film growth rate of copper in high-purity water in the presence of excess oxygen then was determined for times up to 200 hr, Fig. 9. However, under these conditions, the films formed are so thin that the limit of sensitivity of the method is approached. Reproducibility in film formation may also be a factor. Kruger (17) has shown that the nature of oxide films formed in pure water may vary considerably with method of surface preparation and environmental control. The curve is approximately parabolic in form, but the precision of the data, the blank correction, and possible failure of the assumptions involved in the calculations of thickness of thin films preclude detailed analysis of the rate law.

Conclusions

The growth of copper oxide films in aqueous solutions has been studied by an electrometric method. Quantitative data have been obtained on the growth of films as a function of the solution variables, anion type and concentration, pH, and oxygen concentration.

In air-stirred chloride solutions, film growth rate is affected by chloride concentration and pH with a maximum appearing in 0.01M solutions and in the pH range 5.9-9.0. Films are cuprous oxide exclusively except at very high pH values, >10.5, where the rate again increases and cupric oxide predominates.

In equimolar solutions (0.1M) the rate in sodium chloride is about double that in sodium sulfate. In both cases the rate is linear and limited by oxygen availability, even when oxygenation is effected by stirring with a 100% O_2 mixture.

Films formed in high-purity water in the presence of excess oxygen are relatively thin which precludes detailed analysis of the growth rate law from data obtained with the present technique.

Acknowledgment

The authors wish to thank D. K. Crampton and H. L. Burghoff for their interest and suggestions concerning this investigation and to acknowledge the assistance of S. Banisky and other members of the Research and Development Department of the Chase Brass and Copper Co.

Manuscript received April 10, 1959. This paper was prepared for delivery before the Columbus Meeting, Oct. 18-22, 1959.

Any discussion of this paper will appear in a Discussion Section to be published in the June 1960 JOURNAL.

REFERENCES

1. A. B. Winterbottom, *Nature*, **140**, 364 (1937); *Trans. Electrochem. Soc.*, **76**, 327 (1939).
2. B. Lustman and R. F. Mehl, *Trans. Am. Inst. Mining Met. Engrs.*, **43**, 246 (1941).
3. F. H. Constable, *Proc. Roy. Soc.*, **A115**, 570 (1927).
4. H. A. Miley, *J. Am. Chem. Soc.*, **59**, 2626 (1937).
5. C. G. Cruzan and H. A. Miley, *J. Appl. Phys.*, **11**, 631 (1940).
6. W. E. Campbell and U. B. Thomas, *Nature*, **142**, 253 (1938); *Trans. Electrochem. Soc.*, **76**, 303 (1939).
7. N. B. Pilling and R. E. Bedworth, *J. Inst. Met.*, **29**, 577 (1923).
8. J. S. Dunn, *Proc. Roy. Soc.*, **A111**, 241 (1926).
9. U. R. Evans and J. Stockdale, *J. Chem. Soc.*, **1929**, 2561.
10. G. D. Preston and L. L. Bircumshaw, *Phil. Mag.*, **20**, 706 (1935).
11. J. A. Darbyshire, *Trans. Faraday Soc.*, **27**, 675 (1931).
12. C. A. Murison, *Phil. Mag.*, **17**, 96 (1934).
13. G. R. Hill, *This Journal*, **100**, 345 (1953).
14. J. Kruger, *J. Appl. Phys.*, **28**, 1212 (1957).
15. W. D. Robertson, V. F. Nole, W. H. Davenport, and F. P. Talboom, *This Journal*, **105**, 569 (1958).
16. F. J. Asselin and F. A. Rohrman, *Ind. Eng. Chem.*, **32**, 1015 (1940).
17. J. Kruger, *ibid.*, **50**, 55A (March 1958).

The Formation of Porous Oxides on Metals

D. W. Aylmore, S. J. Gregg, and W. B. Jepson

Department of Chemistry, University of Exeter, Exeter, England

ABSTRACT

The porosity of the oxide scales formed on a number of metals during oxidation in dry oxygen has been investigated by measurements of specific surface and of density. The oxides formed during the linear oxidation of the eight metals: calcium, cerium, lead, magnesium, niobium, thorium, tungsten, and uranium are porous whereas those formed during the parabolic oxidation of copper and cobalt are impervious to oxygen gas.

The oxidative behavior of a metal in oxygen depends to a marked extent on the physicochemical properties of the oxide layer formed on its surface. If the layer of reaction product remains continuous during oxidation, reaction can proceed only by the diffusion of either one or both of the reactants in the ionized form through the oxide lattice. In some cases, as with aluminum (1, 2) at 600°C, the rate of oxidation falls off to a negligibly small value as time proceeds, while in others, as for example copper (3) at 1000°C, the oxidation follows a parabolic rate law and the rate of attack is such that a sheet of material is oxidized completely in a few hours.

On the other hand, some metals, usually above a certain characteristic temperature, oxidize at a constant rate which is maintained until the whole of the metal is consumed, a behavior exemplified by magnesium (4) at 500°C. This "linear oxidation" usually is interpreted in terms of the formation of an oxide scale which is porous in the sense that oxygen gas is able to pass freely through its thickness; the rate of oxidation is believed to be controlled by the rate of diffusion either of metal ions or oxygen anions through a thin barrier film of oxide adhering to the metal.

The present study was undertaken in order to provide experimental evidence for the postulated porosity of the oxide layer formed during linear, or almost linear, oxidation and to show that the oxide layer formed during parabolic oxidation is, in fact, impervious to oxygen gas. The metals whose oxides were investigated were calcium, cerium, lead, magnesium, niobium, thorium, tungsten, and uranium, which oxidize at a linear rate, and cobalt and copper which oxidize at a parabolic rate. Two distinct experimental techniques were used to investigate each of the oxide products: the specific surface was measured by the method of krypton sorption (5) at −195°C and the density (6) by immersion in mercury and in carbon tetrachloride, respectively.

Experimental

Each oxide was prepared by oxidizing the metal in dry oxygen at atmospheric pressure in a glass or silica reaction chamber on a thermal balance. The experimental arrangement was the same as that previously described (4) except that the oxygen was further dried by passing it through a column packed with Linde molecular sieves (7).

The percentage purity of the metals was: Ca, >99.4; Ce, >99.99; Co, 99.999; Cu, 99.999; Pb, 99.998; Mg, 99.95; Nb, >99.8; Th, >99.6; W, >99.95; and U, >99.9. Except for calcium, cerium, and lead, the metals were in the form of sheet, 1/32 in. thick for niobium and tungsten and 1/16 in. thick for the others; a sample in the form of a rectangle (4 x 1.5 cm) was cut from the sheet and abraded down to Grade 00 emery under petroleum ether and finally degreased in benzene vapor. The tungsten had to be hot-sheared (8) and the copper after abrasion was etched (9) in a 2.5% aqueous solution of ammonium persulfate for 15 min, washed with water followed by acetone, and finally dried. The calcium was oxidized in the form of a slice, 5 mm thick which was cut from the 1 in. diameter extruded rod; the surface treatment was filing on a "middle cut" file. Lead was oxidized in the molten state in an alumina crucible and cerium in the form of a single lump without surface preparation.

The temperatures of oxidation (Table I) were chosen so as to produce sufficient oxide within a reasonable period of time. The samples of cerium, cobalt, copper, niobium, and tungsten were oxidized to completion, while those of calcium, magnesium, and thorium were only partially oxidized since their oxides spalled from the respective metals on cooling. The oxides of uranium and lead were chipped and scraped from the cooled, oxidized samples.

The apparatus for measurement of krypton sorption (5) at −195°C was designed for the determination of an absolute area of about 1 m^2 of solid with a precision of about ±1%. The use of this quantity of material presented no difficulty with most of the oxides but, as will be seen, there were three whose specific surface was so small that a weight of solid equivalent to 1 m^2 could not be accommodated in the apparatus.

Special experimental techniques (6) were developed for the measurement of the density of the oxide by immersion in mercury and in carbon tetrachloride, respectively, in order to deal with the small amounts of oxide which were available. Briefly, the oxide, contained in a special density bottle, was first outgassed at 110°C to a pressure of 10^{-4} mm Hg and the

bottle then filled with liquid while still in the vacuum system. A quantity of solid equivalent to about 0.3 cm^3 was used for most of the measurements, and both the reproducibility and the absolute accuracy of the method were tested with Iceland spar. With 0.3 cm^3 of solid the density was reproducible to $\pm 0.1\%$ in mercury and to $\pm 0.3\%$ in carbon tetrachloride, and the absolute values agreed with the literature value (10) within these limits.

Results

Kinetic measurements.—The kinetic measurements were of course only ancillary to the main study and the results are described only briefly.

The oxidation curves (of weight gain against time) of magnesium (4) and calcium (11) were the same as those found in earlier work; the former was oxidized for a period such that only the white oxide scale was formed. The cerium was in the form of a single lump of irregular shape so that its oxidation curve could not be classified with certainty; the rate of oxidation at first decreased with time, then reached a constant value [cf. (12) and (13)], but subsequently increased possibly because of self-heating of the metal.

Thorium (Fig. 1) gave a complicated curve consisting of four branches, OA, AB, BC, and CD, over which, respectively, the rate of oxidation decreased, increased, was constant, and decreased; beyond D the rate of oxidation became constant again. Examination of a separate sample which had been oxidized for a shorter period indicated that, as with magnesium, the oxide scale gradually extended laterally over the sample surface. Levesque and Cubicciotti (14), in an experiment covering a much shorter period, found an increase in rate corresponding to branch AB, but the actual weight gains and times were different from those in the present work. The sharp rise in oxidation rate at A probably corresponds to a breakdown of the continuous oxide layer in local regions thus marking the beginning of lateral growth.

Niobium almost from the start of the experiment oxidized at a constant rate of 4.2 mg cm^{-2} hr^{-1} [Baur, Bridges, and Fassell (15) found 6 mg cm^{-2} hr^{-1}] and a breakaway reaction occurred after about 14 hr oxidation. The oxide consisted of a fairly brittle scale together with some powdered oxide, only the former being used for the physical measurements.

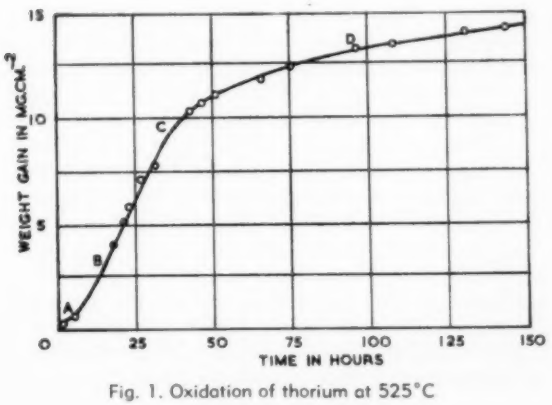

Fig. 1. Oxidation of thorium at 525°C

With tungsten, the rate of oxidation decreased in the very early stages but became constant after about 1 hr, the linear rate of 10.6 mg cm^{-2} hr^{-1} agreeing with the value of 11.5 mg cm^{-2} hr^{-1} found by Webb, Norton, and Wagner (16). The rate of oxidation fell below the linear rate after about 5 hr; the weight gain after this time corresponded to 30% conversion of the metal, and since there was no preferred oxidation at the edges of the sample (8) it is unlikely that the decrease in geometric area is the sole cause.

The rate of oxidation of uranium decreased with time, becoming constant after about 90 hr at 0.8 mg cm^{-2} hr^{-1} [Loriers (17) found 1.0 mg cm^{-2} hr^{-1}]. The oxidation of uranium is complicated by the fact that several oxides probably are involved, perhaps uranium dioxide being first formed and then itself oxidizing (18); at the end of the run the weight gain was in excess of that required for complete conversion to uranium dioxide and yet some metal remained unoxidized. With lead, the rate of oxidation became constant after about 80 hr.

Copper was found to oxidize according to a parabolic rate law ($w^2 = k_p t$), the value of k_p, viz., 238 mg^2 cm^{-4} hr^{-1}, being in good agreement with that calculated from literature data (9) for lower oxygen pressures. The temperature and oxygen pressure were such that both CuO and Cu_2O are stable (19) and the presence of some CuO in the oxide product was confirmed by the fact that the final weight gain

Table I. Values of the specific surface and densities of the oxides[a]

Metal oxide	T,[b] °C	S,[b] m^2 g^{-1}	ρ_m,[b] g cm^{-3}	ρ_o,[b] g cm^{-3}	ρ_o,[b] g cm^{-3}
		A			
Calcium oxide (CaO)	525	6.0±0.05	2.23	3.23	3.37
Cerium oxide (CeO_2)	175	26.3±0.4	5.22	n.d.[c]	7.22
Lead oxide (PbO_2)	575	2.1±0.4	n.d.	n.d.	9.70
Magnesium oxide (MgO)	525	56.0±0.5	0.969	3.33	3.61
Niobium pentoxide (Nb_2O_5)	500	11.3±0.2	4.20	5.15[d]	4.95[e]
Thorium oxide (ThO_2)	525	6.2±0.3	6.43	n.d.	10.04
Tungstic oxide (WO_3)	800	0.92±0.03	5.77	7.17	7.33[f]
Uranium oxide (UO_2)?	240	6.5±0.3	8.08	9.33	10.96
		B			
Cobalt oxide (CoO + Co_3O_4)	960	<0.01	—	—	—
Copper oxide (CuO + Cu_2O)	960	<0.01	—	—	—

[a] The oxides are classified into Groups A and B according to whether they were formed at a linear or a parabolic rate.
[b] T = temperature of formation, S = specific surface, ρ_m and ρ_o are the densities in mercury and in carbon tetrachloride, respectively, and ρ_o is the theoretical density calculated from the data of Wyckoff (21) unless otherwise stated.
[c] n.d. = not determined because of insufficient material.
[d] This value is significantly greater than the theoretical density. A second determination gave the same result.
[e] Quoted by Gulbransen and Andrew (22).
[f] Calculated from the data of Anderson (23).

was in excess of that required for complete conversion of the metal to Cu_2O; similarly with cobalt, two oxides, CoO and Co_3O_4, are stable (20) under the conditions of the reaction; this may account for the time dependence of k_p which increased from 45 mg^2 cm^{-4} hr^{-1} after 3.5 hr to 49 mg^2 cm^{-4} hr^{-1} after 90 hr oxidation.

Specific surface and density.—The values of the specific surface and of the density in mercury and in carbon tetrachloride are summarized in Table I. The density of each oxide has been calculated on the assumption that the density of the bulk liquid is unchanged at the solid-liquid interface: any error from this source is probably negligible.

With magnesium oxide and niobium pentoxide, it was noticed that the mercury only penetrated the oxide face which had been nearest to the metal. The other oxides did not appear to be penetrated at all by mercury.

Discussion

Group A Oxides

As seen in Table I, the measured specific surface S of the oxides exceeds the geometric surface by several orders of magnitude: the oxides possess an "internal surface" which is made up of the walls of numerous cracks and pores which permeate the solid. A crude but nevertheless useful measure of the degree of dispersion of the oxide is obtained by considering it to be made up of equal-sized cubelets of edge-length l. By simple geometry:

$$l = 6/S\rho_c$$

where ρ_c is the theoretical density of the oxide calculated from the x-ray lattice spacing. The measured surface area then comprises the faces of these cubelets which are accessible to krypton molecules, in other words there are gaps at least two molecules wide between the faces of neighboring cubes: the oxide scale is thus porous to krypton molecules and therefore to oxygen molecules [collision diameters (25): Kr, 4.16Å; O_2, 3.61Å]. The numerical values of l (Table II) cover a wide range, from 3×10^2Å for magnesium oxide to 9×10^5Å for tungstic oxide.

Somewhat more direct evidence as to the porosity is provided by the data for the density of the oxide in carbon tetrachloride (ρ_c) and in mercury (ρ_m). The difference between $1/\rho_c$ and $1/\rho_c$ or $1/\rho_m$ represents the volume, per gram of oxide, of those pores which are inaccessible to carbon tetrachloride or to mercury, respectively; the volumes of void ϵ_c and ϵ_m, expressed as a fraction of the total volume of the oxide, are thus given by:

$$\epsilon_c = 1 - \frac{\rho_c}{\rho_c}, \qquad \epsilon_m = 1 - \frac{\rho_m}{\rho_c} \qquad [1]$$

Since mercury at 1 atm pressure cannot enter pores of diameter less than about 10^5Å (26) while carbon tetrachloride can penetrate all pores with diameters in excess of about 5Å, ϵ_m and ϵ_c are made up of all the pores finer than 10^5Å and 5Å, respectively. Both values, of course, include those pores which are totally sealed off.

Table II. Calculated void fractions and cube and pore sizes of the Group A oxides

Oxide	α[a]	ϵ_c	ϵ_m	l, Å	δ, Å[b]
CaO	0.28	0.042	0.34	3000	880
CeO_2	0.20	—	0.28	320	73
PbO_2	—	—	—	3020	—
MgO	0.27	0.079	0.73	300	330
Nb_2O_5	0.43	0.00	0.15	1070	120
ThO_2	<0.26	—	0.36	960	310
WO_3	0.62	0.02	0.21	8900	150
UO_2 ?	0.21	(0.149)	(0.263)	(840)	180

[a] Values calculated from the melting points listed in (24).
[b] Calculated from Eq. [2] using ρ_c for ρ.

The values of ϵ_m (Table II) are all relatively large, varying from 0.15 for niobium pentoxide to 0.73 for magnesium oxide, a figure which implies that almost three-quarters of the oxide scale is composed of void. Values of ϵ_c are, as might be expected, considerably smaller and they vary over a narrower range.

The ϵ_m-value of 0.34 for calcium oxide agrees surprisingly well with the 34% porosity which was estimated by Pilling and Bedworth (27) from geometric measurements of the completely oxidized sample. The ϵ_m-value of 0.21 for tungstic oxide is significantly less than the figure of 30% for the porosity quoted by Webb, Norton, and Wagner (16); it is not clear, however, whether their solid had been outgassed.

The data all refer to the oxide scale after it has been cooled down from reaction temperature, but it is reasonable to assume that the state of subdivision of the scale at the temperature of the reaction is not markedly different. It must also be borne in mind that the scale tends to sinter after it has been formed. Such sintering, which would manifest itself in a reduction in specific surface and an increase in density, must come about as a result of either plastic (or viscous) flow or of transport of material through the crystallite by diffusion. Both processes are known to be greatly accelerated at temperatures above a critical value T_c, characteristic of the solid but lying within the range 0.37 T_f to 0.53 T_f where T_f is the mp of the oxide (28). (T_c often is termed the Tammann temperature and sometimes is defined as $T_c = 0.5\ T_f$.) The quantity $\alpha = T/T_f$, where T is the oxidation temperature, is given in Table II for each oxide: that tungstic oxide has the lowest specific surface and with it, the largest crystallite size of all the oxides in Group A, correlates in an interesting way with the fact that its α-value is the highest of the series and well above the Tammann range. It is also satisfactory that the values $\epsilon_c = 0$ and $\epsilon_c = 0.02$ for niobium and tungstic oxides, respectively, are in agreement with their relatively high α-values of 0.43 and 0.62, although it is perhaps surprising that all the fine pores in niobium pentoxide have apparently been eliminated. It is well known that in sintered oxides the measured density does not in general reach the true density unless the oxide is heated for very long periods near its melting point; indeed, sealed-off pores have been

seen with the electron microscope (29). Reference to Table I shows that for niobium pentoxide ρ_o was significantly greater than ρ_c, and it is possible that this oxide was not the exclusive reaction product (22, 30).

Yet another way of expressing the porosity of the oxide scale is to calculate the mean linear separation δ of the cubic blocks of our crude model; we have

$$\delta = 2l\left\{\left(\frac{\rho}{\rho_m}\right)^{1/3} - 1\right\} \qquad [2]$$

here ρ is within the range ρ_o and ρ_c, its exact value being dependent on the relative volumes of sealed and open pores making up the void fraction ϵ_o. Since the oxide scale contains a variety of pores of widely differing shapes and sizes, the numerical values of δ (Table II) can represent no more than the order of magnitude of the gaps within the oxide layer; but they clearly demonstrate the presence of pores sufficiently wide to permit the free passage of gaseous oxygen. A simple calculation, assuming Poiseuille flow, shows indeed that the pores could permit a flow of gas at a rate greater by many orders of magnitude than that actually required by the consumption of oxygen in the reaction.

Group B Oxides

The specific surface of the copper and the cobalt oxides was extremely small, being within the limits of the apparatus and probably representing little more than the geometric surface of the sample.

Conclusions

The findings of the present paper correlate in a satisfactory manner with inferences extant in the literature of metal oxidation as to the porosity of the oxide scale.

Thus the oxides formed during the linear oxidation of calcium, cerium, lead, magnesium, niobium, thorium, tungsten, and uranium are shown to be porous to molecular oxygen which therefore can diffuse freely through the oxide scale; the rate of oxidation probably is controlled by the diffusion, either of metal ions or of oxygen anions, through a thin barrier film of oxide (nonporous to gaseous oxygen) which remains adherent to the metal and whose thickness remains effectively constant.

For parabolic oxidation it generally is accepted that the rate determining step is the diffusion either of interstitial ions or of cation vacancies across the oxide layer which by implication is non-porous to oxygen gas. The present results provide evidence as to this lack of porosity with the oxide layer on copper and on cobalt.

Acknowledgments

Acknowledgment is gratefully made to the U.K. Atomic Energy Authority for financial support, and to Dr. J. E. Antill for some helpful comments.

Manuscript received April 1, 1959.

Any discussion of this paper will appear in a Discussion Section to be published in the June 1960 JOURNAL.

REFERENCES

1. W. W. Smeltzer, *This Journal*, **103**, 209 (1956).
2. D. W. Aylmore, S. J. Gregg, and W. B. Jepson, To be published in *J. Inst. Metals.*
3. C. Wagner, *Z. physik. Chem.*, (B), **21**, 25 (1933).
4. S. J. Gregg and W. B. Jepson, *J. Inst. Metals*, **87**, 187 (1958-1959).
5. D. G. Smith, Thesis, University of Exeter (1958).
6. W. B. Jepson, *J. Sci. Inst.*, **36**, 319 (1959).
7. C. C. Addison, E. Iberson, and J. B. Raynor, *Chem. and Ind.*, 96 (1958).
8. J. P. Baur, D. W. Bridges, and W. M. Fassell, Jr., *This Journal*, **103**, 266 (1956).
9. J. P. Baur, D. W. Bridges, and W. M. Fassell, Jr., *ibid.*, **103**, 273 (1956).
10. T. Batuecas and F. L. Casado, *Z. physik. Chem.*, (A), **181**, 197 (1937).
11. S. J. Gregg and W. B. Jepson, To be published in *J. Chem. Soc.*
12. J. Loriers, *Compt. rend.*, **231**, 522 (1950).
13. D. Cubicciotti, *J. Am. Chem. Soc.*, **74**, 1200 (1952).
14. P. Levesque and D. Cubicciotti, *ibid.*, **73**, 2028 (1951).
15. D. W. Bridges and W. M. Fassell, Jr., *This Journal*, **103**, 326 (1956).
16. W. W. Webb, J. T. Norton, and C. Wagner, *ibid.*, **103**, 107 (1956).
17. J. Loriers, *Compt. rend.*, **234**, 91 (1952).
18. P. E. Blackburn, J. Weissbart, and E. A. Gulbransen, *J. Phys. Chem.*, **62**, 902 (1958).
19. F. H. Smith and H. R. Roberts, *J. Am. Chem. Soc.*, **42**, 2582 (1920).
20. M. Watanabe, *Bull. Inst. Phys.-Chem. Research (Tokyo)*, **12**, 255 (1933).
21. R. G. Wyckoff, "Crystal Structures," Interscience Publishers Inc., New York.
22. E. A. Gulbransen and K. F. Andrew, *This Journal*, **105**, 4 (1958).
23. G. Anderson, *Acta Chem. Scand.*, **7**, 154 (1953).
24. "Handbook of Chemistry and Physics," C. D. Hodgman, Editor, Chemical Rubber Publishing Co., Cleveland (1950).
25. E. H. Kennard, "Kinetic Theory of Gases," p. 149, McGraw Hill Publishing Co., New York (1938).
26. J. F. Goodman and S. J. Gregg, *J. Chem. Soc.*, **1956**, 3612.
27. N. B. Pilling and R. E. Bedworth, *J. Inst. Metals*, **29**, 529 (1923).
28. G. I. Finch and K. P. Sinha, *Proc. Roy. Soc.*, **239A**, 145 (1957).
29. J. E. Bourke, *J. Am. Ceram. Soc.*, **40**, 80 (1957).
30. E. A. Gulbransen and K. F. Andrew, *J. Metals, Trans. AIME*, **188**, 586 (1950).

Galvanic Relationships between Aluminum Alloys and Magnesium Alloys

I. Galvanic Couples

M. R. Bothwell

Metallurgical Laboratory, The Dow Metal Products Company, Midland, Michigan

ABSTRACT

High-purity aluminum has nearly perfect galvanic compatibility with magnesium AZ31B alloy during saline exposure. This compatibility is little changed by additions to the aluminum of magnesium, silicon, or manganese, but it is rapidly and proportionately decreased by the addition of iron, copper, and nickel, and more gradually decreased by the addition of zinc. The addition of magnesium to the alloy or magnesium ion to the environment can greatly suppress the effect of the above deleterious constituents.

Their active potentials and lack of appreciable anodic polarization make magnesium alloys susceptible to galvanic effects during exposure to salt-laden environments. The suppression of these effects by the removal or metallurgical complexing of low hydrogen overvoltage constituents in magnesium alloys is one of the classic examples of the application of local-cell theory to a corrosion problem (1). Due to these operations the commercial magnesium alloys are generally serviceable in salt-laden atmospheres when they are painted with moderate care. However, when these alloys are incorporated in structures with other metals it is frequently not the inherent corrosion resistance of the magnesium alloy which determines the protective system needed, but rather the galvanic characteristics of the macro cells set up between the magnesium alloy and the other metals or alloys in the structure.

Galvanic relationships between magnesium alloys and aluminum alloys are extremely important since the two metals are combined so frequently in light metal structures. Even when the structure is dominantly magnesium, it will often be fastened together by aluminum rivets, for magnesium alloys generally lack the room-temperature plasticity necessary in the cold-driving rivet. Over the years it has been discovered that there is a tremendous range in the galvanic effect of the commercial aluminum alloys on magnesium alloys. Thus, the magnesium-rich aluminum alloys such as 5056 are generally quite compatible with magnesium alloys, whereas the copper-rich aluminum alloys such as 2024 alloy are generally poorly compatible. It is the purpose of this paper to demonstrate some of the principles which determine the compatibility of aluminum alloys toward magnesium alloys and to illustrate how these principles can be used in corrosion control.

Experimental

The cathodic polarization curves for the aluminum materials in Fig. 1 were obtained with an automatically regulated, linear current sweep rate of 30 min from nil to full current and 30 min full to no current. Each aluminum cathode consisted of a ⅜ in. diameter cylinder mounted as a section in a Bakelite holder of the same diameter and located at the axis of a magnesium AZ31B alloy hollow cylinder which was used as the anode. Potentials were recorded in respect to a Beckman Model 1170 saturated calomel electrode which was located in a Luggin capillary salt bridge filled with the corrodent solution. Potentials were recorded by a modified Brown recording potentiometer operating with its chart drive in synchronization with the current sweep. The one aluminum cathode consisted of commercial 2S aluminum rod which contained 0.47% Fe, 0.23% Si, and 0.087% Cu as determined by chemical analysis. The 99.99% purity electrode in these studies was machined from ingot containing 40 ppm respectively of Fe and Cu, 10 ppm Si, and 4 ppm Ni as determined by chemical analysis.

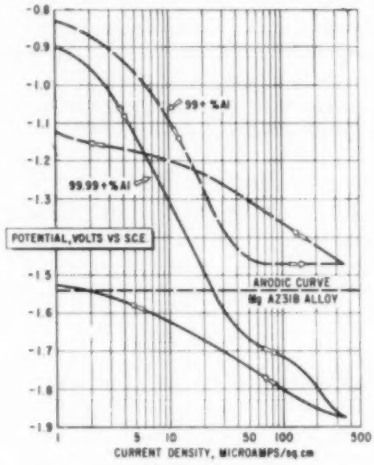

Fig. 1. Cathodic polarization of two grades of aluminum in 3% NaCl solution saturated with air and with $Mg(OH)_2$.

Except where a different base material is indicated, experimental aluminum alloys were prepared

starting with 99.99% purity Al from the same lot mentioned above or from another lot certified by the manufacturer to contain 10 ppm Cu, 20 ppm Fe, 10 ppm Mg, and <10 ppm of any other anticipated impurity. The 99.9% Al contained 300 ppm Fe, 270 ppm Si, 30 ppm Cu, and <100 ppm of any other anticipated constituent. Magnesium was alloyed directly from doubly sublimed material containing 5 ppm Fe. The zinc was also alloyed directly starting with 99.99% purity ingot. The copper, manganese, iron, and silicon bearing alloys were all prepared from master alloys based on 99.99% purity Al and respectively high conductivity, electrolytic copper, electrolytic manganese, high-purity alcoholized iron powder, and silicon of undefined quality. The basic alloying procedure was as follows: pure aluminum was melted in a spectroscopic-grade graphite crucible and heated to 1400°F, after which the alloying constituents were added and stirred in vigorously. This melt was heated to 1500°F for 30 min and then cooled to 1400°F before pouring into spectroscopic-grade graphite molds. Immediately after solidification each casting was water quenched.

Each melt produced two castings, a 1 x 4 x 4 in. miniature rolling slab and a disk specimen for spectroscopic analysis. After its surfaces were removed by grinding on Aloxite cloth, the rolling slab was reduced to sheet of 0.020 in. thickness on carefully cleaned and well-lubricated rolls at 300°F following the schedule, 25% reduction per pass with 15 min reheats at 700°F between passes.

The disk castings of all alloys were subjected to spectroscopic analysis. This was supplemented by chemical analysis in selected cases. Except where the level of an element is specified in the results, analysis has shown it to be negligibly different from the level in the aluminum base stock.

The galvanic corrosion specimens consisted of 2 pieces of the aluminum alloy sheet in the form of squares, ½ in. on the side, which were centrally mounted on the opposite sides of 1½ x 1½ in. squares of commercial, magnesium AZ31B alloy.[1] These specimens were held together by ⅛ in. diameter rivets of a high-purity aluminum-2% magnesium alloy. Prior to assembly the aluminum pieces were ground with fine Aloxite cloth to remove possible cathodic contamination introduced during the rolling, drilling, and shearing operations. The magnesium AZ31B alloy coupons were pickled to a depth of 1 mil per side in a solution of 25½ fluid oz of glacial acetic acid and 6 2/3 oz sodium nitrate per gal of aqueous solution. Following pickling and water rinsing, these magnesium alloy coupons were dried and weighed.

Following the exposure, the test pieces were disassembled and the magnesium alloy coupons were rinsed with gentle scrubbing under tap water. The corrosion product was then removed by immersion for 2 min in a solution of 20% chromic acid plus 1% silver nitrate at 180°F. Following this the specimens were rinsed in tap water, dried, and reweighed to obtain the weight loss due to corrosion. Since tests showed that this method caused <0.5 mg weight change on specimens not previously corroded, no correction for cleaning error was made. All test exposures were made by suspending each specimen in approximately 200 ml of the corrodent concerned. The test temperature was 95° ±2°F. The time of exposure was generally 1 week. However, this period had to be curtailed for those couples with which the galvanic effect was excessively large. The mean deviation for triplicate tests was generally <10% of the average rate and at no time did it exceed 20% of the average rate.

[1] The nominal composition of AZ31B alloy is Mg-3% Al-1% Zn-0.4% Mn.

Results and Discussion

The peculiarity of the pure aluminum cathode in respect to its extremely low limiting current for depolarization by dissolved oxygen has been pointed out by Pryor and Keir (2). It will be seen shortly that their hypothesis of impurity-rich sites as the effective cathodes in the aluminum macro cathode agrees with the data presented here. In fact, it was observation of this same phenomenon in the cathodic polarization of commercial aluminum alloys and a similar analysis of its implications which led to the work to be described here. Hansen and Wetmore (3) arrived at a similar conclusion when they noted that super purity aluminum has a much higher hydrogen overvoltage in acids than does commercial-purity aluminum.

In Fig. 1 can be seen the cathodic polarization curves of 99.99+% purity aluminum and commercially pure aluminum while exposed to 3% NaCl solution saturated with magnesium hydroxide and air. The dotted line represents the potential of magnesium AZ31B alloy which is without significant anodic polarization in this environment. It can be seen that the high-purity aluminum cathode polarizes so readily that it should cause very little galvanic attack to the magnesium alloy, whereas rather severe attack can be expected when the latter is coupled to commercially pure aluminum.

Because of the pronounced hysteresis in the cathodic polarization curves for aluminum and its alloys, the analysis of polarization data was abandoned in favor of measurements on the couples themselves. The configuration of the test couple chosen was felt to meet the following desiderata: (*a*) was easily prepared, (*b*) generally prevented electrolyte entry at faying surfaces, (*c*) invariably maintained contact, (*d*) was sensitive to cathode effects, and (*e*) introduced no significant third electrode effect.

Complete immersion of the test specimen was used rather than the more conventional alternate immersion or salt spray testing in order to utilize more effectively the available cathode and thus make the test more sensitive. While complete immersion testing was believed satisfactory here, since oxygen reduction is relatively unimportant in couples between magnesium alloys and aluminum alloys, such is generally not the case when magnesium alloys are coupled with other metals.

Iron is rarely a deliberate constituent in the commercial aluminum alloys but it is usually present in them to the extent of a few thousand ppm as a major

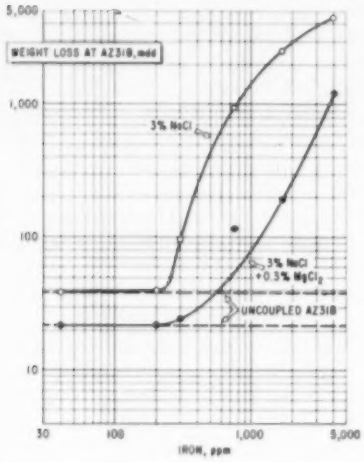

Fig. 2. Effect of iron in aluminum on the corrosion of AZ31B alloy coupled thereto.

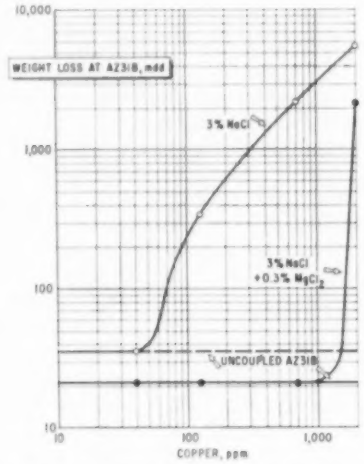

Fig. 3. Effect of copper in aluminum on the corrosion of AZ31B alloy coupled thereto.

impurity. In Fig. 2 it is seen that iron in the aluminum alloy can have a very adverse effect on its compatibility with magnesium AZ31B alloy. Up until the time that the iron content does not exceed 200 ppm, in this particular couple configuration, the iron is without appreciable galvanic effect, but as this level is exceeded, galvanic attack of the magnesium alloy increases rapidly. The addition of 0.3% magnesium chloride to the 3% sodium chloride solution was made to reproduce effects observed in natural seawater. The justification for this will be shown in Part II of this paper (4). Although this addition does not greatly change the iron level at which galvanic attack of the magnesium alloy becomes appreciable, it does greatly reduce such attack once the critical iron level is exceeded.

The results in Fig. 3 are in accord with past observations on the poor compatibility of copper-rich aluminum alloys with magnesium alloys. In the 3% NaCl environment, copper can have a deleterious effect at even lower levels than was seen in the case of iron in the previous figure. However, if 0.3% $MgCl_2$ is added to the environment, copper does not have a significant deleterious effect until it exceeds 1000 ppm.

Table I. Effect of various constituents on the galvanic compatibility of Al toward AZ31B alloy

	Weight loss at AZ31B, mdd	
	3% NaCl	3% NaCl + 0.3% $MgCl_2$
99.9+% Al (unalloyed)	94	24
+ 0.16% Zn	400	59
+ 0.27% Si (0.041% Fe)	78	33
99.99+% Al (unalloyed)	36	22
+ 0.015% Ni	127	
+ 0.30% Mn	34	23
Uncoupled control	38	23

In Table I it can be seen that nickel at low levels has a deleterious effect that is of the same order as that of iron and copper. The effect of nickel has been less extensively studied here because it is not of great importance in aluminum alloys either as a major impurity or a common alloying constituent. Zinc also has a deleterious effect, but it is much milder than that of iron, copper, and nickel. Furthermore, the effect of zinc is very effectively suppressed by the addition of magnesium chloride to the environment. Silicon and manganese have little effect even at moderate levels. Next to iron, silicon is the most prevalent impurity in commercial-purity aluminum and its alloys. Silicon is also an extremely important deliberate constituent in many aluminum alloys as are zinc and manganese as well. Since silicon is innocuous, the marked difference in the cathodic polarization behavior of the two purity grades of aluminum shown in Fig. 1 can be attributed primarily to the iron content of the less pure grade. This is substantiated by couple tests where it is found that the weight loss occasioned by the latter metal is nearly equal to that produced by a high-purity aluminum-iron binary alloy of the same iron content.

Figures 4, 5, and 6 illustrate the basis for the good performance in service of the magnesium-rich alu-

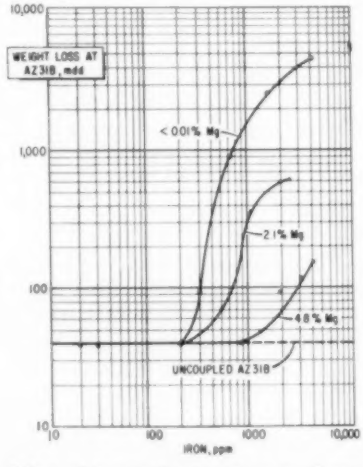

Fig. 4. Effect of iron and magnesium in aluminum on the corrosion in 3% NaCl solution of AZ31B alloy coupled thereto.

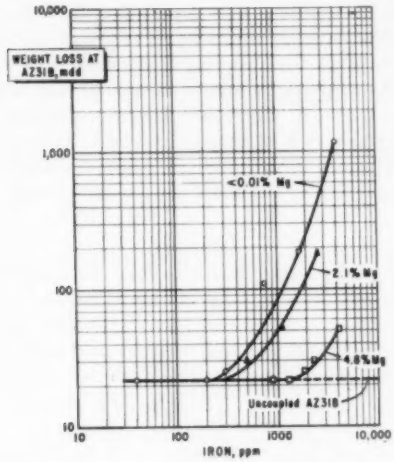

Fig. 5. Effect of iron and magnesium in aluminum on the corrosion in 3% NaCl plus 0.3% $MgCl_2$ solution of AZ31B alloy coupled thereto.

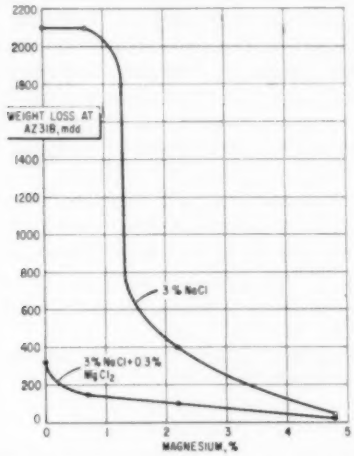

Fig. 6. Effect of magnesium in aluminum plus 0.13% iron on the corrosion of AZ31B alloy coupled thereto.

minum alloys in structures with magnesium alloys. It can be seen that the addition of magnesium to the aluminum alloy greatly improves its tolerance for iron. For example, aluminum 5056 alloy, which has long been used as the standard rivet material for magnesium alloy structures, has a nominal composition of aluminum-5.2% Mg-0.1% Mn-0.1% Cr. Its maximum permissible iron content is 0.4%, but in practice, it will generally be about one-half of this value. The results here indicate that 5.2% Mg should largely suppress the effect of 0.2% Fe and thus 5056 alloy should be a highly compatible material. This conclusion is substantiated by several years of trouble-free service with 5056 alloy rivets in AZ31B alloy structures.

In Table II it can be seen that magnesium can suppress the deleterious effects of copper and of iron and copper in combination. It is also extremely effective in suppressing the mildly deleterious effect of zinc that is observed in couple tests in 3% NaCl solution.

Table II. Suppression by alloyed Mg of the deleterious effects of Cu, Ni, and Zn on the galvanic compatibility of Al toward AZ31B alloy. (Al alloys containing Zn here were coupled with a different lot of AZ31B alloy from that used in remainder of study. Furthermore, duration of exposure to 3% NaCl was only one day.)

	Weight loss at AZ31B, mdd	
	3% NaCl	3% NaCl + 0.3% $MgCl_2$
Suppression of Cu effect		
Al + 0.013% Cu	332	24
Al + 0.014% Cu + 0.36% Mg	40	22
Al + 0.089% Fe + 0.018% Cu + 4.8% Mg	40	24
Al ± 0.078% Fe + 0.74% Cu	>4000	>2000
Al ± 0.078% Fe + 0.74% Cu + 4.5% Mg	81	35
Suppression of Ni effect		
Al + 0.015% Ni	127	
Al + 0.056 ± Ni + 4.8% Mg	46	
Suppression of Zn effect		
Al + 3.6% Zn + 0.05% Fe	3630	43
Al + 4.8% Zn + 0.05% Fe + 3.4% Mg	266	45
Uncoupled control	150	48

On the basis of these results, it can be seen that there is much freedom within which to design aluminum alloys which will have both satisfactory mechanical properties and excellent galvanic compatibility with magnesium alloys. The work hardening aluminum-magnesium alloys and the age hardening aluminum-magnesium-silicon and aluminum-magnesium-zinc alloys are the best prospects to meet these requirements. Contingent upon the magnesium content of the alloy, it may be necessary to reduce its iron content from the levels prevalent in the commercial purity materials.

An example of the effect of iron content on the compatibility of a commercial aluminum alloy is shown in Fig. 7. 6061 alloy is a moderately strong, age-hardening alloy with the nominal composition of aluminum-1.0% Mg-0.6% Si-0.25% Cu-0.25% Cr. The maximum permissible iron content for this alloy is 0.70% and, in practice, about one-half this amount is the general expectation. It can be seen here that this alloy cannot be made completely compatible with AZ31B alloy during exposure to 3% NaCl solu-

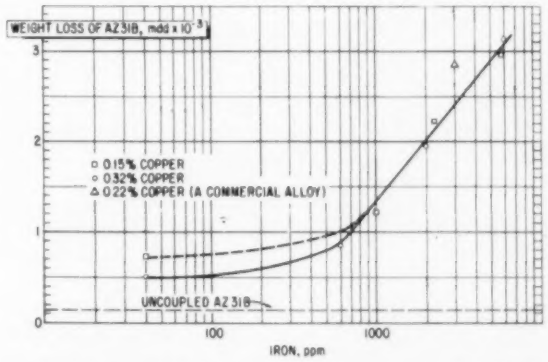

Fig. 7. Effect of iron and copper in aluminum 6061-T6 alloy on the corrosion of AZ31B alloy coupled thereto (48 hr immersion in 3% NaCl).

Table III. Compatibility of 6061-T6 alloy with AZ31B alloy during exposure to substitute ocean water per ASTM designation D-1141-52

	Weight loss at AZ31B, mdd
Commercial 6061-T6 (0.30% Fe, 0.22% Cu)	43
Experimental 6061-T6 (0.005% Fe, 0.15% Cu)	31
Experimental 6061-T6 (0.005% Fe, 0.32% Cu)	33
Uncoupled control	32

tion because the ratio of copper to magnesium is too high. Nevertheless, a decrease in the iron content from the usual levels of the commercial alloys can do much to improve the compatibility. In contrast to the results in 3% NaCl solution, even commercial purity 6061 alloy is highly compatible with AZ31B alloy during exposure to substitute ocean water (see Table III).

It is interesting to note that the constituents which have the greatest deleterious effect on the compatibility of the aluminum alloys with AZ31B alloy are iron, copper, and nickel. Since these are metals with rather low hydrogen overvoltages, it is reasonable to assume that the effective cathodes in an aluminum macro-cathode are regions rich in elements displaying substantially their bulk hydrogen overvoltage characteristics rather than areas in which elements have become incorporated in the film to make it semiconductive as Pryor and Keir have suggested for the case of extremely pure aluminum.

Magnesium constituent in the alloy may suppress the deleterious effect of the above constituents by increasing the resistance of the aluminum alloy to attack by cathodically generated alkali and thereby decreasing their rate of exposure. Since the pH should decrease as the distance from the low overvoltage phase is increased, it is reasonable to expect that enhancement in the alkali resistance of the matrix phase will favor a sharper gradient of cathodic attack and thus favor a higher ratio of impurity undercutting to impurity exposure. This view gains some support from the observation that, at the same deleterious impurity level, the addition of magnesium to the aluminum decreases its cathodic attack as well as the anodic attack of the AZ31B alloy coupled to it. However, this result is not readily resolved in terms of cause and effect. Efforts to confirm this mechanism through a cursory study of the metallography of cathodic attack have been unsuccessful.

Summary

High-purity aluminum causes substantially no galvanic corrosion to magnesium AZ31B alloy during exposure to 3% NaCl solution. The addition of increasing amounts of iron, copper, and nickel to the aluminum results in a rapid loss in compatibility whereas the addition of zinc causes more moderate loss at comparable levels. The addition of magnesium, silicon, and manganese is without noticeable deleterious effect. When magnesium is present in the alloy the deleterious effects of iron, copper, nickel, and zinc are greatly suppressed. The effects of these same deleterious constituents are also suppressed when a small amount of magnesium chloride is added to the corrosion environment. These results are consistent with the view that at the potential of magnesium AZ31B alloy, the bulk of the surface of an aluminum macro-cathode is galvanically inert while the effective cathodes are areas rich in low overvoltage constituents. The beneficial effect of magnesium in the alloy is probably related to its ability to suppress the accumulation of low overvoltage impurities at the alloy's surface.

Manuscript received Jan. 19, 1959. This paper was prepared for delivery before the Buffalo Meeting, Oct. 6-10, 1957.

Any discussion of this paper will appear in a Discussion Section to be published in the June 1960 JOURNAL.

REFERENCES

1. J. D. Hanawalt, C. E. Nelson, and J. Peloubet, *Trans., Am. Inst. Mining Met. Engrs.*, **147**, 273 (1942).
2. M. J. Pryor and D. S. Keir, *This Journal*, **102**, 605 (1955).
3. D. J. Hansen and F. E. W. Wetmore, *Can. Chem. Process Inds.*, **34**, 659 (1956).
4. M. R. Bothwell, *This Journal*, **106**, 1019 (1959).

Galvanic Relationships between Aluminum Alloys and Magnesium Alloys

II. Aluminum Claddings on Magnesium

M. R. Bothwell

Metallurgical Laboratory, The Dow Metal Products Company, Midland, Michigan

ABSTRACT

The cladding of magnesium AZ31A alloy with 99.99% aluminum greatly improves its resistance to saline environments. The protective ability of the cladding is little changed by incorporation therein of magnesium, silicon, or manganese, but it is impaired greatly by iron and copper and more mildly by zinc. The presence in seawater of soluble magnesium salts greatly diminishes the effects of iron, copper, and zinc from that seen in sodium chloride solution. This decrease is probably due to decreased cathodic attack of the aluminum at the lower equilibrium pH of the seawater environment.

While magnesium alloys generally withstand mild weathering very well without recourse to any protection beyond that of their naturally formed film, such weathering is accompanied by the gradual formation of a gray patina which is objectionable in some applications. Furthermore, it would be desirable for some applications to have magnesium sheet which could withstand moderately severe salt exposure when unpainted. Early experimental claddings of aluminum alloys on magnesium alloys showed a substantial improvement in the maintenance of a reflective surface during weathering, but unfortunately, rather than affording any protection to the magnesium alloy during salt exposure, they greatly accelerated corrosion due to strong galvanic effects. The experimental claddings described here were prompted by the recognition that extremely pure aluminum combines its well-known excellent resistance to corrosion in saline environments with remarkable galvanic inertness toward magnesium alloys.

Experimental

The aluminum alloys used here were prepared in the same manner as those in Part I of this paper (1). The aluminum base stocks used were 99.99% purity Al containing 40 ppm Fe, 40 ppm Cu, 4 ppm Ni, 10 ppm Si, and <10 ppm of any other anticipated constituent, and 99.9% purity Al containing 300 ppm Fe, 270 ppm Si, 30 ppm Cu, and <100 ppm of any other anticipated constituent.

Aluminum alloy sheet of 0.020 in. thickness was wire-brushed and then wrapped around 0.250 in. thick, magnesium AZ31A alloy[1] plate. This composite was rolled to 0.040 in. total thickness on clean, well-lubricated rolls according to the schedule described in Part I (1). The resulting thickness of the cladding was slightly over 0.003 in. per side.

These clad composites were cut into 1½ by 2½ in. coupons which were given a 1 min pickle in cold, 10% sodium hydroxide solution. After drying and weighing, they were subjected to alternate immersion testing at 95° ± 2°F in approximately 200 ml of the environments concerned by the method described by Hanawalt, *et al.* (2). Following the exposure, the samples were cleaned for 4 min in the chromic acid cleaning solution mentioned in Part I of this paper (1). Since it was found that individual coupons not previously corroded lost less than 1 mg during this cleaning, no correction for cleaning loss was made. Fortunately this cleaning process is sufficient to remove the corrosion product from all but the most severely corroded specimens, and thus the chromic acid-phosphoric acid baths that are used customarily to remove corrosion product from aluminum corrosion specimens, but which would attack the magnesium alloy wherever exposed, were not necessary.

The mean deviation for quintuplicate tests was generally <10% of the average rate and only rarely exceeded 20% of the average rate.

Results and Discussion

The clad coupons of this study can be considered as galvanic couples with an unusually high ratio of cathode area to anode area, e.g., approximately thirty to one when first exposed. In addition to the anodic attack of the core at the exposed edges, the cathodic attack of the cladding and the exposure of additional core metal thereby must be considered. Experience with galvanic couples shows that the cathodic attack of the aluminum alloy is almost as severe as the anodic attack of the magnesium alloy. Thus, it may be surmised that the aluminum cladding must polarize to the potential of the core with extraordinary ease if the composite is to have useful resistance to saline exposure.

In Fig. 1, it can be seen that a cladding of 99.99% purity Al meets this requirement very well, whereas a cladding of commercial purity aluminum is much worse than no cladding at all. At the edges of the

[1] The nominal composition of AZ31A alloy is Mg-3% Al-1% Zn-0.4% Mn-0.15% Ca.

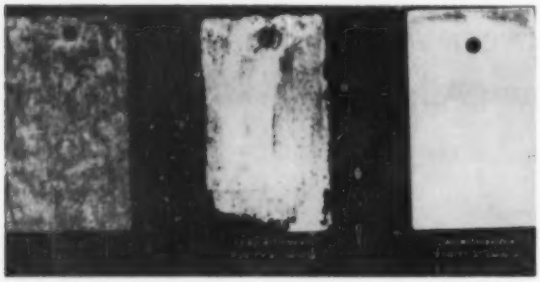

Fig. 1. Bare, 99% Al clad, and 99.99% Al clad AZ31A alloy after exposures to 3% sodium chloride. Period of exposure 7, 2, and 25 days, respectively.

coupons with 99.99% Al cladding, the AZ31A core exposed during shearing suffers little more than its open circuit corrosion. On the other hand, even beyond the edge damage apparent in Fig. 1, the cores of the coupons with commercial purity cladding were corroded to an average depth exceeding ⅛ in.

Not surprisingly, clad composites are more sensitive to low overvoltage constituents in aluminum than were the galvanic couples of Part I (1). Indeed from the shapes of the curves in Fig. 2 and 3, it may be surmised that even the 40 ppm Fe and 40 ppm Cu levels of the 99.99% Al are producing a significant harmful effect during exposure to 3% NaCl solution and that this level of iron, but not copper, is producing a significant harmful effect during exposure to seawater. However, if the limiting assumption is made that the exposed core alone suffers attack, the steady state rates of Fig. 4 correspond to core corrosion rates of about 180 mdd for sodium chloride exposure and about 120 mdd for seawater exposure. If these rates are compared to the steady-state rates of unclad core metal in each environment, it is deduced that the elimination of all cladding corrosion and all galvanic effects will only produce about a fivefold reduction in corrosion of the composite in either environment. This suggests that further purification of aluminum will yield comparatively small returns.

In Fig. 2 and 3 it can be seen that iron and copper are less deleterious during seawater exposure than

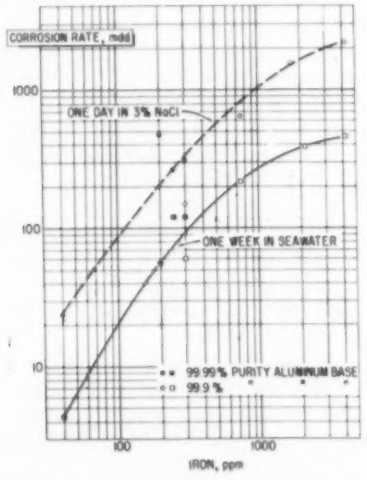

Fig. 2. Effect of iron in cladding on corrosion of Al clad AZ31A alloy sheet.

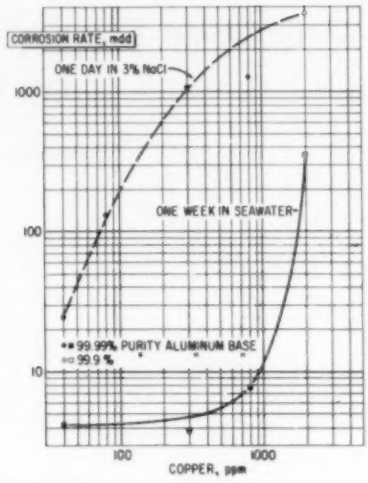

Fig. 3. Effect of copper in cladding on corrosion of Al clad AZ31A alloy sheet.

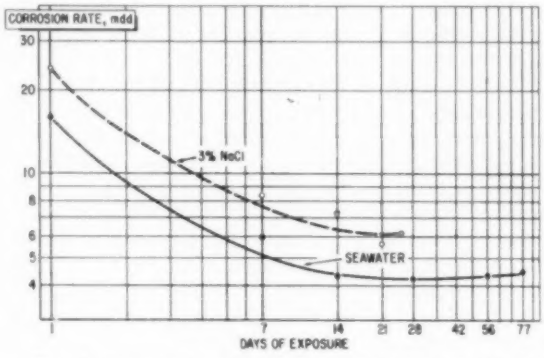

Fig. 4. Decrease in corrosion rate of 99.99+% Al clad AZ31A alloy sheet with time.

they are during exposure to 3% NaCl solution. Although the lesser test time in 3% NaCl solution prevents direct comparison of the environments from these results, there can be little doubt that iron constituent is much less aggressive and copper constituent enormously less aggressive during seawater exposure. Indeed the shorter test time in 3% NaCl was dictated by rapid disintegration of the coupons at the higher iron and copper levels. It is also interesting to note the appearance of a well-defined tolerance for copper in the cladding when exposure is made to seawater.

The effects of some additional cladding constituents are shown in Table I. Zinc is more mildly detrimental than iron and copper during exposure to 3% NaCl solution and, even at very high levels, it has no detrimental effect during seawater exposure. Magnesium, silicon, and manganese are substantially innocuous in either environment.

Difficulties in achieving bonding between magnesium AZ31A alloy cores and aluminum claddings containing large amounts of magnesium prevented a good test of the ability of magnesium constituent to suppress the effects of iron, copper, and zinc here as it did in the galvanic couples of Part I (1). Such an effect is likely in view of the similarity of all other results for the two types of specimens.

Table I. Effect of various constituents on corrosion of Al clad Mg AZ31A alloy sheet

	Corrosion rate, mdd	
	One day—3% NaCl	One week—seawater
99.9% Al	150	60
+0.16% Zn	300	28
+2.05% Zn	800	46
+0.53% Mg	190	86
+1.14% Mg	110	51
+0.10% Si (0.034% Fe)	250	86
+0.10% Si (0.038% Fe)	140	23
+0.27% Si (0.041% Fe)	250	130
+0.58% Si (0.039% Fe)	190	25
+0.05% Mn (0.036% Fe)	340	210
+0.29% Mn (0.042% Fe)	100	110
+0.51% Mn (0.059% Fe)	380	230
99.99% Al	29	4.3
+0.70% Mg	31	4.0
+0.05% Si	30	3.9
+0.30% Mn	69	4.9

The enormous difference in corrosivity between 3% NaCl solution and seawater toward some of the composites is of obvious interest. In Table II are shown the results on the corrosion of a particularly sensitive composite of the addition to 3% NaCl solution of two important seawater constituents, viz., Mg^{++} and $SO_4^{=}$. It can be seen that the addition of 0.3% Na_2SO_4 to the 3% NaCl solution decreases the corrosion of the composite by a small but probably significant amount. When 0.3% $MgCl_2$ is added to the sodium chloride solution, however, the corrosion of the composite is greatly reduced and indeed is nearly the same as the corrosion in seawater. The addition of 0.3% Na_2SO_4 to the above solution of sodium chloride plus $MgCl_2$ appears to have a rather trivial effect.

The difference in corrosivity between sodium chloride solutions and seawater probably depends on the difference in their buffering characteristics as shown in Fig. 5. Because of dissociation of the slightly soluble magnesium hydroxide corrosion product, the sodium chloride solution characteristically buffers at about pH 10.5. However, soluble magnesium salts in the seawater depress the solubility of the magnesium hydroxide and thus cause the system to buffer at a substantially lower pH. The lower bulk pH of the system in turn decreases the attack of the aluminum cladding by cathodically generated alkali. The consequences of this decreased attack of the cladding in order of increasing importance is probably: (*a*) reduction in the corrosion of the cladding per se, (*b*) slower exposure of the less resistant core at pits in the cladding, and (*c*) a smaller accumulation of low overvoltage constituents at the aluminum surface and thus less galvanic attack of the exposed core.

Table II. Effect of constituents in seawater on corrosion of AZ31A clad with 99.99% Al plus 0.08% Cu

Environment	Corrosion rate, mdd Two-day alternate immersion
3% NaCl	1980 ± 100
3% NaCl + 0.3% Na_2SO_4	1320 ± 80
3% NaCl + 0.3% $MgCl_2$	19 ± 1
3% NaCl + 0.3% $MgCl_2$ + 0.3% Na_2SO_4	17 ± 3
Seawater	15 ± 2

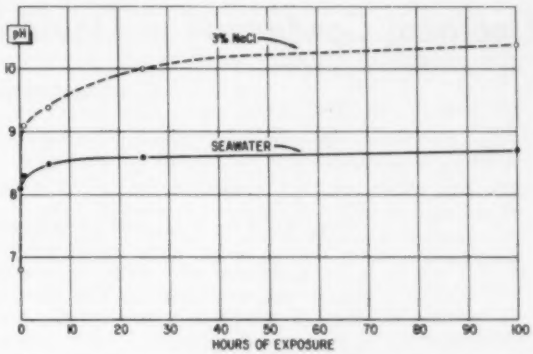

Fig. 5. pH as a function of time during corrosion in 3% NaCl and seawater of AZ31A clad with Al plus 0.08% Cu.

Just as in the case of the addition of magnesium to aluminum in the couples of Part I (1), the reduced galvanic effect from the addition of magnesium ion to the environment probably depends more on the distribution of cathodic attack rather than the total cathodic attack. Thus, a lower bulk pH should produce a sharper decrease in pH as a function of distance from each impurity-rich local cathode, and this should favor a higher ratio of impurity undercutting to impurity exposure.

Summary

High-purity aluminum cladding is extremely effective in protecting magnesium AZ31A alloy during saline exposure. The addition of iron or copper to the aluminum cladding materially impairs this protection by increasing the corrosion of the cladding and by making the cladding more aggressive galvanically toward the magnesium core. Zinc constituent has a milder effect than iron and copper while magnesium, silicon, and manganese are innocuous.

The above deleterious constituents have a much smaller effect during seawater exposure than they have during exposure to 3% NaCl solution because of the presence in seawater of a substantial concentration of magnesium ions which buffer the environment at a lower pH and thereby reduce the corrosion of the cladding by cathodically generated alkali. In addition to prolonging the life of the cladding, this also helps prevent the accumulation of low overvoltage constituents on the cladding surface and thus moderates its galvanic aggressiveness toward the magnesium core.

Manuscript received Jan. 19, 1959. This paper was prepared for delivery before the Buffalo Meeting, Oct. 6-10, 1957.

Any discussion of this paper will appear in a Discussion Section to be published in the June 1960 JOURNAL.

REFERENCES

1. M. R. Bothwell, *This Journal*, **106**, 1014 (1959).
2. J. D. Hanawalt, C. E. Nelson, and J. Peloubet, *Trans. Am. Inst. Mining Met. Engrs.*, **147**, 273 (1942).

Electrical Conduction in Liquid Dielectrics under Pulse Conditions

K. A. Macfadyen and G. C. Helliwell

Department of Physics, University of Birmingham, Birmingham, England

ABSTRACT

The need for a method of measuring conduction in pure nonpolar dielectric liquids under pulse conditions is considered, and details of a measurement technique are given. Experiments with hexane show that currents greater than 10^{-5} amp flow with certain electrode conditions, at a field strength of about 200 kv/cm, although the d-c conduction is much lower. A tentative explanation is offered.

Knowledge of the electrical conduction of dielectrics immediately after the application of an electric field is desirable not only as a means of understanding the mechanism of conduction in general but also to throw light on the breakdown process. This paper reports some experiments with a technique for revealing the time variation of conduction current during the first few microseconds after the application of a pulse of voltage between electrodes immersed in highly insulating liquids. Although applicable equally to polar liquids, the conduction mechanism of which is still not free from doubt (1), the method has so far been applied only to a typical nonpolar liquid (hexane) since views on the processes at work both in conduction and in electrical breakdown show considerable divergence.

Resumé of Present Theories

At low field strengths (about 1 kv/cm) the ultimate conduction in highly purified nonpolar liquids seems to be due to ionization by cosmic rays (2, 3) and other radiation. With stronger fields (over 100 kv/cm) there appears an added component of conduction attributed by different investigators to various forms of electron emission from the cathode with or without the additional influence of collision-ionization of the liquid molecules. Thus, Baker and Boltz (4) pictured thermionic emission from the cathode (without ionization) as the basic mechanism, a view modified in details by LePage and DuBridge (5) and by Dornte (6). Young (7) added the feature of collision ionization, a mechanism put forward earlier by Nikuradse (8). More recently Morant (9) and House (10) have produced evidence favoring a return to the thermionic emission theory. Green (11) considered cathode emission to be due to the combined effects of the applied field and the intense local fields set up by undischarged ions separated from the cathode by a superficial insulating layer.

Experiments leading to the foregoing views were carried out with d-c fields; some (10, 11) involved a lengthy process of "conditioning," whereby stable d-c conduction at field strengths near to breakdown could be obtained. It would clearly help in resolving these divergent views if the value of the conduction current during the first few microseconds after the application of the field, i.e., during the time of transit of an ion between the electrodes, could be established as a function of time. This is one object of the present research.

Apart from its intrinsic interest, the mechanism of conduction has an important bearing on our understanding of electrical breakdown in liquids. It was formerly held that there was no connection between these phenomena. In the case of pure, nonpolar liquids, however, present-day theories of breakdown are based mainly on the assumption that conduction and breakdown are in fact linked.

Thus, Goodwin and Macfadyen (12, 13) have explained their experimental results on the breakdown of various liquids under pulse conditions by a mechanism based on (*a*) a field-dependent cathode emission, and (*b*) intensification of the field at the cathode by positive space charge resulting from collision-ionization.

It is shown that these two relationships constitute a feedback mechanism leading to a catastrophic situation at a certain field strength even though emission and ionization may increase smoothly with field strength. Goodwin (14) later showed by electro-optical means that the predicted intensification of cathode field did in fact occur in certain cases. The breakdown condition is expressed in terms of ionic mobilities, ionization coefficients (Townsend's α), and cathode emission characteristics, all of which are hard to determine at field strengths approaching breakdown. The only estimates are either indirect or based on extrapolation from d-c measurements. Unless the "conditioning" process used by House (10) and by Green (11) is used, the available evidence points to conduction currents of the order of microamperes near breakdown. The object of the present investigation was to develop means for measuring currents of this order during a 5 μsec pulse. The fact that much of the experimental evidence on breakdown is derived from pulse tests is an added reason for the investigation.

The theory of Lewis (15), which has been strikingly successful in correlating breakdown strength with molecular vibration energy levels, does not enable specific predictions regarding conduction current to be made. The criterion here is that breakdown is contingent upon the setting-up of conditions

favorable for ionization by collision. Sharbaugh, Bragg, and Crowe (16), however, on the evidence of the effect of gap width on breakdown strength, suggest more explicitly that breakdown occurs when, on the average, each electron emitted by the cathode undergoes a certain fixed number n of ionizing collisions before reaching the anode. Their experiments suggest that for hexane $n = 9$ approximately. This would result in a current magnification by the factor 8100 (e^n) at breakdown. Cathode emissions of only 10^{-9} amp would thus be expected to yield currents of some microamperes, as in the theory of Goodwin and Macfadyen already considered.

Choice of Method

In order to facilitate interpretation, pulse breakdown measurements are usually carried out with a flat-topped pulse of voltage. The chief difficulty in measuring conduction under such conditions is the presence of very large charging and discharging currents at the beginning and end of the pulse. For example, in applying a 10 kv pulse to a pair of suitably spaced plane parallel electrodes (0.5 cm^2) the rate of rise of voltage (10^{11} v/sec) gives rise to a charging current of about 1 amp, which is many orders of magnitude higher than the conduction current expected. In a similar way, irregularities in the pulse-top would produce spurious indication of conduction. Some form of bridge circuit in which the capacitive current is balanced out is necessary.

Gledhill and Patterson (17) in their work on electrolytic conduction at high field strengths used a 3-winding differential pulse transformer to compare the conduction in two cells. This method was tried but found unsuitable for the present work for two reasons: first, a display of conduction current vs. time was required, comparison by null method against a standard resistance or conduction cell being unacceptable for this work; and, second, the above requirement coupled with the smallness of the currents to be measured compared with the large charging current pulses resulted in a transformer design problem impossible of solution with existing materials.

The Schering bridge circuit (Fig. 1) was therefore used, and although a pulse output transformer was ultimately necessary with this circuit the design problem was much less severe, the main requirement being extremely good electrostatic shielding.

In Fig. 1, C_s represents the capacitance in the conduction cell and i_c the conduction current. C_1 is a compensating condenser and C_2 an adjustable condenser for balancing the stray capacitance C_1. R_s, R_1, and R_2 are equal noninductive high-stability resistors. A flat-topped pulse, negative to ground, was applied to X.

An upper limit to the value of R_1 and R_2 was set by consideration of time constants (see below) and a lower limit by tube noise in the ensuing amplifiers. The first form of unbalance indicator to be used was a 2-stage differential amplifier. The requirements were onerous, since pulse potential differences of about a millivolt had to be amplified in the presence of unwanted pulses of some hundreds of volts. The method was abandoned because, whether triodes or pentodes were employed, it was found impossible to avoid spurious indications resulting from interelectrode capacitances. Nonlinearity was also troublesome.

The method of detecting the out-of-balance voltage finally adopted was to use a specially designed screened and balanced pulse transformer followed by conventional wide-band amplifiers and a cathode ray oscilloscope. Details are given below.

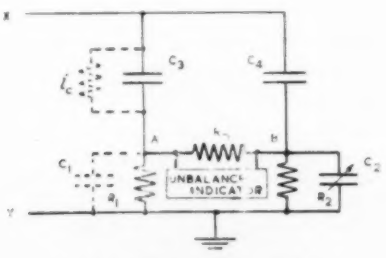

Fig. 1. Schering bridge circuit

The Conduction Cell

The removable parallel plane electrode system (Fig. 2) was enclosed in a borosilicate glass vessel V provided with plane windows for microscopic examination. The vessel was included in a closed-circuit distillation system with a sintered glass filter to exclude particles larger than 1.5 μ in diameter.

The electrode system was designed to be suitable for d.c. as well as pulse measurements. The cylindrical electrodes A, B were supported in accurately milled V-grooves in the blocks C, D. C was highly insulated by its composite quartz-metal mounting E, F, G. Contact with A was made by a spring attached to the rod J. The metal plate F acted as a guard ring to intercept surface conduction over the fused quartz blocks E, G. The quartz-metal joints were made by soft-soldering the chemically silvered quartz blocks to a nickel-iron alloy ("Nilo 36") of low thermal expansion. The bond was strong enough to permit the V-grooves in the block to be milled in one operation. Thus, if A and B were accurately

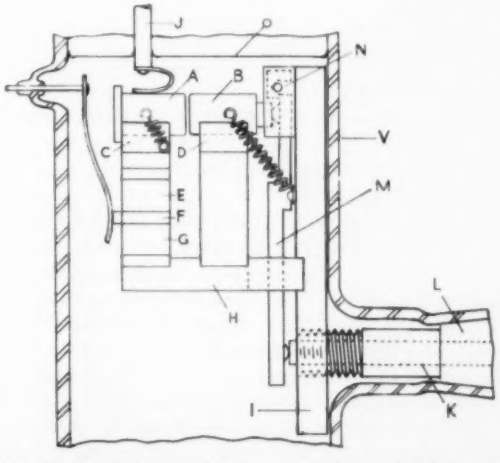

Fig. 2. Electrode assembly in conduction cell. Glass parts are shown in section.

turned, the adjacent surfaces automatically became exactly parallel. In lapping and polishing the end surfaces a special holder was used to preserve accurate geometry.

The pillars supporting A and B were attached to a base plate H. This was supported from the sideplate I which was curved to fit the inside of the glass vessel against which it was held by the screwed sleeve shown. Through this sleeve, to which was attached the cone L, there passed a spring-returned push-rod K sealed by a Neoprene O-ring and operated by a micrometer head (not shown) beyond L. Axial movement of the rod actuated the 10:1 lever M pivoted at N and thus enabled the gap between A and B to be adjusted to an accuracy of 1μ.

A phenomenon inseparable from measuring pulse currents at high field strengths is electrode movement resulting from electrostatic attraction. At a field strength of 1 megavolt/cm this force amounts to about 1 kg-wt/cm^2. With any practicable means of supporting the electrodes their natural frequency of vibration would be no higher than the "near ultrasonic" range; for 5 μsec pulses we may therefore regard the motion as limited by inertia rather than constraint, and attempts at extreme rigidity will be futile.

Solid cylindrical electrodes lightly constrained at the end remote from the gap were employed to make the movement predictable. If a mutual attraction of T dynes cm^{-2} is suddenly set up between the ends of the cylinders at a certain instant, the propagation of the tension pulse in one cylinder results in a steady rate of advance v of its end surface. If Y denotes Young's modulus of the material and ρ is density

$$v = T/\sqrt{(Y\rho)}$$

and since both electrodes move with this velocity the rate of change of capacitance C (in e.s.u.) is

$$\frac{dC}{dt} = 2\,CT/l\sqrt{(Y\rho)}$$

where l is the gap width. The value of T is given by

$$T = \epsilon E^2/8\pi$$

If the voltage, V, is maintained constant while this movement occurs the charging current will be

$$i_c = V\frac{dC}{dt} = E^2\,C\,\epsilon/4\pi\sqrt{(Y\rho)} \text{ e.s.u.} \qquad [1]$$

where E is the field strength in the gap and ϵ the permittivity of the liquid.

With a 10 kv pulse applied between cylinders 7 mm in diameter with ends 100 μ apart the charging current is 11 μa, the velocity of each electrode surface 0.3 cm sec^{-1} and the velocity of the tension wave 3.4 x 10^5 cm sec^{-1}. With cylinders 0.85 cm long the time of a double passage of the wave from the electrode face to the far end and back is 5 μsec. By this time the required information has been displayed by the oscilloscope. A correction must be applied, according to Eq. [1], for the current due to the electrode movement; this probably sets a lower limit of about 1 μa to the current that can be measured under these conditions. With narrower gaps the charging current is higher, (Eq. [1]).

In principle it is possible to balance out this current by means of a similarly constructed vacuum condenser on the other side of the Schering bridge. It can be deduced from Eq. [1] that if the vacuum condenser has electrode area S'

$$\frac{S'}{S} = \epsilon^{2/3}$$

for equalization of the charging currents.

This procedure has not been necessary in the experiments reported here as measurable currents were found with field strengths at which electrode movement was not serious. Polystyrene parallel plate condensers were used as compensators in the bridge circuit, the design being such as to make plate movement negligible. Bridge balancing was done by fine adjustment of the electrode separation in the conduction cell and by the variable condenser C_2 (Fig. 1).

The Bridge Circuit

Assuming a symmetrical bridge circuit (Fig. 1) with $R_1 = R_2 = R_0$ (=R, say) and other corresponding quantities approximately equal, an analysis of the effect of applying a step-function voltage V_s to the input terminals XY leads to the expression

$$v_{AB} = V_1\,e^{-t/\tau_1} + V_2\,e^{-t/\tau_2} \qquad [2]$$

for the potential of A relative to B at a time t after the application of the step. The time constants are given by

$$\tau_1 = \frac{1}{3}\,R(C_1 + C_3)$$

$$\tau_2 = R(C_1 + C_2)$$

In the present case τ_1 and τ_2 are about 20 and 60 mμsec, respectively. It is this time which limits the value permissible for R, for in the event of any capacity unbalance the oscilloscope deflection will not be a measure of the conduction current i_c until long after the lapse of time τ_2. Moreover, the indication of changes in i_c will be delayed by a time of the order of τ_2. This sets an upper limit to the value of R which can be used. A lower limit is set by tube noise in the amplifier which amplifies v_{AB}. The conduction current is related to v_{AB} thus

$$i_c = \frac{3\,v_{AB}}{R}$$

The factors V_1 and V_2 in Eq. [2] depend on the degree of capacity unbalance. If C_3 (capacity of the conduction cell) and C_2 are the adjustable capacitances we find

$$\left.\begin{aligned} V_1 &= \frac{3\delta(C_2C_3) - (C_2 + C_3)\delta C_2}{2(C_2 + C_3)^2}\,V_s \\ V_2 &= \frac{-\delta(C_2C_3) + (C_2 + C_3)\delta C_2}{2(C_2 + C_3)^2}\,V_s \end{aligned}\right\} \qquad [3]$$

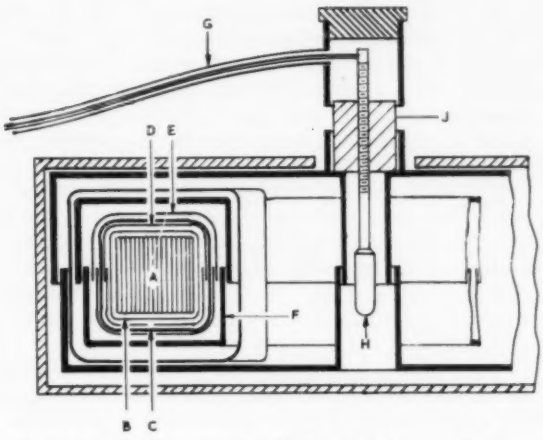

Fig. 3. Section of screened and balanced pulse transformer

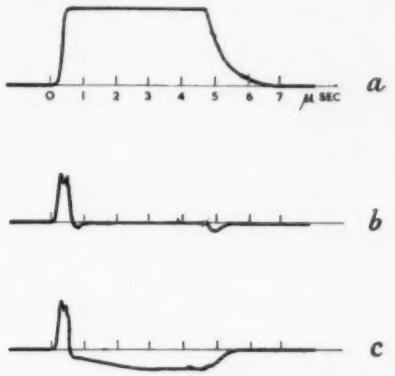

Fig. 4. Oscilloscope traces. (a) Voltage pulse applied to bridge circuit; (b) Output voltage pulse. The residual pulses are probably due to distributed inductance; (c) Output voltage pulse showing conduction current in cell. The shape of the conduction portion depended on the electrode surface conditions.

where δ represents the departure of the quantity in question from the value for perfect balance.

In practice the finite rise-time of the pulse renders Eq. [3] useful only in a general way. The final adjustments of C_2 and C_3 are made experimentally.

As mentioned earlier the essential feature of the unbalance indicator was a screened and balanced pulse transformer. This was wound on a spiral core (A, Fig. 3) of "Supermumetal" ($\mu \sim 50{,}000$) contained in a plastic case B. The primary winding C, occupying only a portion of the circumference, was surrounded by a complete earthed screen F, but in order to avoid spurious secondary emf's due to unbalanced capacity currents from primary to earth, two split foil screens D, E, each part being connected to the appropriate end of the winding, were interposed between the winding and its surroundings. In order to improve the balance still further the primary (52 turns of 38 S.W.G. enamelled wire) was wound back on itself. The final adjustment of balance was achieved by means of a "compensating turn" consisting of a short length of screened cable G leading from one primary terminal to the earthed case by way of a screw-plunger H having very low adjustable capacitance to the case. By joining both primary terminals to (say) point A (Fig. 1) the nut J could be adjusted to give the best discrimination against response to equal potential pulses at A and B simultaneously.

The whole transformer was enclosed in a "Mumetal" case and the entire circuit comprehensively screened. The first two stages of amplification, placed close to the transformer, gave a gain of about 100. When followed by the wide-band amplifier (5 Mc/s) in the oscilloscope (Solartron CD 513) this gave a screen sensitivity of 1 cm/75 μa of cell current.

Procedure

Early tests with the apparatus described were made with brass electrodes, lapped with wet rouge on a pitch block and lightly polished with "Silvo" polish on a "Selvyt" cloth stretched on a plate glass base. Then, after thorough degreasing, a layer of gold 1000Å thick was evaporated *in vacuo* onto the electrode faces. The electrodes were mounted as in Fig. 2 and the whole assembly continuously degreased in cold running refluxed hexane for at least an hour. The unit was mounted in its glass tube and washed out with several changes of hexane which had been dried with phosphorus pentoxide distilled and filtered in the same apparatus. The apparatus was normally filled with dried nitrogen from a cylinder. Microscopic examination of the gap was maintained during tests.

With a 1 kv pulse (Fig. 4a) applied to the bridge, balancing of capacitances was done by adjusting the electrode gap and the condenser C_2 (Fig. 1), giving an optimum oscilloscope trace as in Fig. 4b. The residual pulses were considered to be due to stray inductance in the connections, particularly those in the conduction vessel. Conduction was shown by the displacement of the trace in the center part of the pulse (Fig. 4c) and, although there seems to be some risk that "hangover" from the spurious initial pulse might invalidate this indication, it was possible to eliminate the uncertainty in the course of taking readings with different applied pulse voltages. The residual pulses were proportional to applied voltage while the conduction followed a different law.

Results

With the gold-plated electrodes described above the raising of the pulse input voltage from the balancing value of 1 kv to about 3 kv gave conduction as shown in Fig. 4c. The relatively slow rise of current with time was not an invariable feature.

Figure 5 shows the relationship between peak current and field strength. The two different symbols for the graph points indicate two experimental runs with different capacitance-balance conditions. In both cases breakdown occurred at a pulsed field strength of 0.52 mv/cm.

Similar results, with somewhat smaller currents, were obtained with other pairs of electrodes prepared in a similar way, but currents of this order could not always be obtained. A 5-times enhancement of the emission was obtained on occasion by prolonged exposure of the electrodes to air.

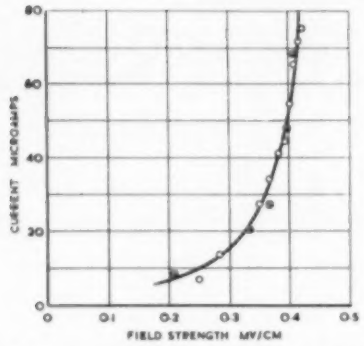

Fig. 5. Conduction characteristic of gold-coated electrodes in hexane. Electrode area: 0.35 cm². Electrode separation: 120μ.

With uncoated electrodes the conduction current was much lower. For example, stainless steel, mechanically polished with chromic oxide, gave a barely observable conduction, (about 5 μa). However, after several breakdowns had occurred currents up to about 150 μa were observed.

Experiments carried out to investigate the nature of the conduction included flushing the vessel and refilling with freshly distilled hexane. This produced no substantial change of conduction current. Conversely, when electrodes giving no measurable conduction were used with hexane which had been neither dried nor distilled, no conduction was observable.

Tests with double pulses, the second occurring at times down to 4 μsec after the first, showed no observable difference in behavior on the second occasion.

A further significant result was found in the course of comparing pulse and d-c conduction currents. A pair of electrodes giving a pulse current of 38 μa at 2.2 kv gave a steady conduction of only 0.07 μa with the same voltage and polarity. Furthermore, when the pulse test was again applied after a d-c test of this kind the pulse conduction was found to be reduced by about an order of magnitude.

In a similar way, the enhanced conduction from stainless steel after several breakdowns had occurred was largely suppressed by prolonged d-c testing, e.g., 45 hr with a current of 6×10^{-9} amp at 100 kv/cm. Microscopic examination of the electrodes after this treatment showed globular particles about 5μ in diameter mainly clustered around the 70μ craters left by previous breakdowns. These particles were apparently made of the wax-like substance reported by previous observers (5) and assumed to be a polymer resulting from electronic bombardment of the liquid molecules.

Discussion

In view of the preliminary nature of these experiments it would be unwise to attempt to deduce too much from them. The high values of pulse conduction current observed are far greater, having regard to the field strength, than the predictions of any previous measurements or theory. Ionic conduction seems to be ruled out by the dependence of conduction on electrode surface preparation and the lack of correlation between conduction and liquid sample.

Simple calculations show that the total charge during the 5 μ pulse is many orders of magnitude greater than could be explained by orientation of impurity dipoles. Time considerations also make this idea untenable. We are thus led to the conclusion that the conduction current originates at the electrode surfaces, the most likely mechanism being electron emission from the cathode, with or without magnification by collision-ionization in the liquid. The latter point must remain uncertain as conditions prevented a series of measurements with differing gap widths.

The magnitude of the current suggests that it may be limited by negative space charge. An analysis of the case of parallel plane electrodes of separation l and p.d. V volts drawing a space charge-limited current of negative ions having a mobility u cm/sec per volt/cm gives the expression

$$I = \frac{A\,u\,\epsilon}{32\,\pi\,10^{11}\,l^3}\,V^2 \text{ (amp)} \qquad [4]$$

where A is the plate area and ϵ the permittivity. With $l = 0.01$ cm, $\epsilon = 2$, $A = 0.5$ cm², $u = 4.4 \times 10^{-4}$ cm/sec per volt/cm (18) and $V = 4$ kv we find $I = 7 \times 10^{-4}$ amp, which is only one order of magnitude higher than the observed current. A logarithmic plot of Fig. 5, however, shows a law of variation of about the 5th power, which is different from Eq. [4], but the orders of magnitude of the quantities show that space charge cannot be ruled out as a factor in conduction of this kind, especially when it is remembered that emission from the cathode almost certainly occurs from small areas ($\sim 10^{-4}$ cm²) as the papers by Dornte (6) and by Goodwin (14) show. Although it can be proved in general that a law of the form $I \propto V^2$ is to be expected for a copiously emitting cathode and an anode, irrespective of their shapes, the argument does not apply when the emission is confined to limited areas on the cathode surface. In this case the influence of negative space charge will be enhanced.

The fact that prolonged exposure to air promoted emission from evaporated gold layers suggests an emission mechanism of the type envisaged by Green (11), namely, extraction of electrons by positive ions on a thin layer, in this case perhaps of CO (19). Some support for this view can be obtained for the high emissions after breakdown and from the effects observed after prolonged d-c conduction. A possible explanation of these phenomena is that a layer of wax (or other material) of suitable thickness results in copious emission according to the mechanism envisaged by Green, but that prolonged conduction results in a wax layer of excessive thickness, reducing emission and ultimately becoming visible under the microscope. Although the present experiments have not been carried far enough for a definite conclusion it seems possible that deposition of solid matter may be an important factor in "electrode conditioning." The experiments are continuing with improved apparatus including a Wagner earth to improve the accuracy of the capacity balance.

Acknowledgments

The authors wish to thank Professor P. B. Moon for placing the facilities of the Physics Department at their disposal. One of the authors (G.C.H.) acknowledges a grant from the British Department of Scientific Industrial Research.

Manuscript received April 8, 1959. This paper was prepared for delivery before the Philadelphia Meeting, May 2-7, 1959.

Any discussion of this paper will appear in a Discussion Section to be published in the June 1960 JOURNAL.

REFERENCES

1. J. Hart and A. G. Mungall, *Can. J. Phys.*, **34**, 491 (1956).
2. G. Jaffé, *Ann. der Phys.*, **29**, 125 (1909).
3. I. Adamczewski, *Nature*, **137**, 994 (1937).
4. E. H. Baker and H. A. Boltz, *Phys. Rev.*, **51**, 275 (1937).
5. W. R. LePage and L. A. DuBridge, *ibid.*, **58**, 61 (1940).
6. R. W. Dornte, *Ind. Eng. Chem.*, **32**, 1529 (1940).
7. D. R. Young, *J. Appl. Phys.*, **21**, 222 (1950).
8. A. Nikuradse, *Arch. Elektrotech.*, **26**, 250 (1932).
9. M. J. Morant, *Proc. Phys. Soc.*, **B68**, 513 (1955).
10. H. House, *ibid.*, **B70**, 913 (1957).
11. W. B. Green, *J. Appl. Phys.*, **26**, 1257 (1955).
12. D. W. Goodwin and K. A. Macfadyen, *Proc. Phys. Soc.*, **B66**, 85 (1953).
13. K. A. Macfadyen, *Brit. J. Appl. Phys.*, **6**, 1 (1955).
14. D. W. Goodwin, *Proc. Phys. Soc.*, **B69**, 61 (1956).
15. T. J. Lewis, *J. Appl. Phys.*, **27**, 645 (1956).
16. A. H. Sharbaugh, J. K. Bragg, and R. W. Crowe, *ibid.*, **26**, 434 (1955).
17. J. A. Gledhill and A. Patterson, Jr., *J. Phys. Chem.*, **56**, 999 (1952).
18. I. Adamczewski, *Ann. phys.*, **8**, 309 (1937).
19. B. M. W. Trapnell, *Proc. Roy. Soc. (London)*, **A218**, 566 (1953).

Luminescence of Copper-Activated Calcium and Strontium Orthophosphates

W. L. Wanmaker and C. Bakker

Light Division, N. V. Philips' Gloeilampenfabrieken, Eindhoven, Netherlands

ABSTRACT

Copper produces a strong luminescence in $Ca_3(PO_4)_2$. Luminescence in $Sr_3(PO_4)_2$ occurs only in the presence of small amounts of foreign ions such as Ca, Zn, Cd, Mg, or Al. These additions give rise to a new crystal phase which is probably isomorphous with β-$Ca_3(PO_4)_2$. The emission peaks under excitation with 2537Å of β-$Ca_3(PO_4)_2$, α-$Ca_3(PO_4)_2$, and of $Sr_3(PO_4)_2$ modified with Al are found at 4800, 5700, and 4950Å, respectively. Sensitization occurs with Mn, giving rise to a red emission peak. The temperature dependence of the fluorescence is good, especially that of β-$Ca_3(PO_4)_2$-Cu and $Sr_3(PO_4)_2$ partly substituted with Mg and Ca. Phosphor application in lamps presents difficulties due to the materials' sensitivity to air at binder bake-out temperatures.

In sulfides, copper is a well-known activator. In this type of phosphor copper does not in general act as a characteristic activator like manganese, but as an indirect one, facilitating the excitation of electrons of the neighboring sulfur ions (1).

In oxygen-dominated phosphors, however, activation by copper is not so generally known. It appears from the survey given by Kröger (2) that carbonates, oxides, halides, phosphates, and silicates may be activated by copper. In some cases copper acts only as an intensifier of the luminescence of the pure substance, as with $ThSiO_4$ described by Leverenz (3). Copper-activated alumino-silicate phosphors were investigated by Claffy and Schulman (4) and found to have a brightness of about one-third of that of calcium tungstate. Recently Wilke (5) also reported the preparation of copper-activated silicates.

Among copper-activated phosphates the following luminescent materials are known: AlBaMg-phosphate glass (6) with a pinkish white fluorescence; calcium apatites giving a blue emission (7); calcium metaphosphate, also with a blue emission (8); and finally the red-emitting magnesium orthophosphate (9).

Quite recently Uehara and Kofuya (10) described the properties of β-calcium orthophosphate activated with Cu and with Cu and Mn. The preparation of β-$Ca_3(PO_4)_2$ modified with the foreign ions Cd, Sr, Mg, and Zn is also given in the patent literature. With manganese, sensitization occurs, giving rise to a red emission band in addition to the blue band due to copper (11).

In this paper the preparation and properties of the efficient β-$Ca_3(PO_4)_2$-Cu and of $Sr_3(PO_4)_2$-Cu phosphors, substituted with small amounts of Al, Mg, Zn, and Cd, are described in some detail. Similar phosphors are prepared by substituting a small part of the Sr by Ca with a resulting green emission. While β-$Ca_3(PO_4)_2$-Cu has a narrow emission peak at 4800Å, the corresponding Sr compound with a small amount of Al has its peak wave length at 4950Å. Incorporation of zinc and magnesium into $Sr_3(PO_4)_2$-

Cu gives rise to an emission peak at about 4900Å, and incorporation of Cd and Ca gives a peak at 5100Å.

Method of Phosphor Preparation

The ingredients used in the firing mixtures were reagent grade $CaHPO_4$, $SrHPO_4$, $CaCO_3$, Cu_2O, $CuSO_4$, Al_2O_3, and $MnNH_4F_3$ or $MnCO_3$. The required amounts of the dry materials were thoroughly mixed and subsequently fired. The firing was done in a special tube furnace, in which alumina boats filled with the firing mixture were gradually passed through the heating zone in a neutral or slightly reducing atmosphere (N_2 with O to 0.5% of pure hydrogen). The furnace exit was provided with a gas lock to prevent the entry of air when the fired samples were removed from the furnace. The best results were obtained by a double firing at temperatures of 1160°-1240°C, in N_2 with 0.03% H_2, for periods of 1 hr each.

Incorporation of the Activator in the Host Crystal Lattice

Air-fired copper-activated phosphors give no luminescence at all or at best a very weak one, whereas firing in a slightly reducing atmosphere produces strongly luminescent materials. With too high a concentration of hydrogen in the firing atmosphere, metallic copper is produced, while too low a concentration of hydrogen gives products with a slightly blue body color, due to divalent copper. This shows that the copper ion should be present in the monovalent state.

Chemical analysis confirmed that, in the strongly luminescent products, all the copper is present in the monovalent state, e.g., in a β-$Ca_3(PO_4)_2$-Cu phosphor ($Cu/P_2O_5 = 0.01$ and $Al/P_2O_5 = 0.10$) the amounts of total and of monovalent copper were both found to be 0.19 wt%. The percentage of monovalent copper was determined by dissolving the phosphor sample in hydrochloric acid in the presence of an excess of potassium dichromate and measuring the amount of unused dichromate by titration with an 0.01N Fe^{II}-sulfate solution.

With large amounts of copper, brown colored products are mostly formed, indicating that part of the copper added is not incorporated in the crystal lattice. With the simultaneous addition of Al, the ratio of Cu/P_2O_5 at which the brownish discoloration occurs, increases. Obviously Al facilitates the incorporation of the monovalent Cu^+ ion in the crystal lattice. This phenomenon can be explained easily by the theory of charge compensation, with one Cu^+ and one Al^{3+} ion substituting for $2Ca^{2+}$ or $2Sr^{2+}$ ions, respectively (12).

Although this hypothesis may be applicable to β-$Ca_3(PO_4)_2$-Cu phosphors, other effects must also be taken into account with $Sr_3(PO_4)_2$-Cu.

The β-$Ca_3(PO_4)_2$-Cu phosphor is efficient without the addition of Al, whereas unsubstituted $Sr_3(PO_4)_2$-Cu shows only a very weak, deep blue emission (peak wave length at 4450Å). X-ray analysis showed that the latter substance has the normal $Sr_3(PO_4)_2$ lattice structure (13). However, with $Sr_3(PO_4)_2$-Cu a strong luminescence develops when ions such as Al, Ca, Mg, Zn, and Cd are added. At the same time, the partial substitution of Sr by Al, Ca, Zn, Mg, and Cd gives a pronounced change in the crystal lattice. A new structure appears which is identical with that of $Sr_3(PO_4)_2$-Sn phosphors, where part of the Sr has been replaced by smaller divalent ions like Mg. This structure is similar to the structure of the β-$Ca_3(PO_4)_2$ lattice, as described by Koelmans (14).

Apparently the presence of foreign ions transforms the $Sr_3(PO_4)_2$ structure in such a way that a different structure is obtained which is probably isomorphous with β-$Ca_3(PO_4)_2$ and which gives rise to a strong luminescence with Cu as the activator.

The brightest phosphors are made with a slight excess of P_2O_5, resulting in a total metal to P_2O_5 ratio of about 2.90-2.95. Usually better results are obtained with $CuSO_4$ than with Cu_2O. This may be due to the decomposition of the $CuSO_4$ during the firing process, which forms a more reactive copper compound in the process.

Calcium Orthophosphate Phosphors

$Ca_3(PO_4)_2$ exists in two crystal structures, viz., α-$Ca_3(PO_4)_2$, stable at a temperature above 1180°C, and β-$Ca_3(PO_4)_2$, stable below this temperature. Kroeger found (15) that the transition temperature is raised by the incorporation of small amounts of Ce, Al, or Mn in $Ca_3(PO_4)_2$·Ce,Mn. Similar results were obtained by Butler (16) who also found a high transition temperature with a composition different from the stoichiometric one and in the presence of the activator Sn. From the foregoing it is clear why we obtained the β-$Ca_3(PO_4)_2$ modification in nearly all cases. This compound, when activated with copper, gives a blue emission with a peak at 4800Å (Fig. 1).

It was interesting to investigate the luminescent properties of the α-modification. The α-$Ca_3(PO_4)_2$ structure (as identified with x-ray analysis) was obtained by firing unactivated $Ca_3(PO_4)_2$ at 1270°C

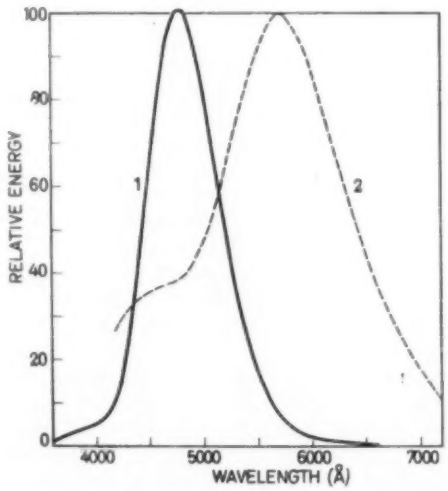

Fig. 1. Spectral energy distribution curves of the emission of β-$Ca_3(PO_4)_2$-Cu [curve 1] and of α-$Ca_3(PO_4)_2$-Cu [curve 2]. Mole ratios: $Cu/P_2O_5 = 0.005$ [2] and 0.01 [1]. $Me/P_2O_5 = 2.99$ [2] and 2.90 [1]. Firing temperature: 1160°C [1] and 1280°C [2]. Firing atmosphere: N_2 with 0.03% H_2.

in air. A low percentage of copper ($Cu/P_2O_5 = 0.005$) in the form of $CuSO_4$ was added to the fired product and the mixture was refired at 1280°C. X-ray analysis showed that the crystal structure did not change during this refiring process and that the crystal structure was entirely the same as that of α-$Ca_3(PO_4)_2$ described by Mackay (17). In this way a nearly white luminescent product (with 2537Å excitation) was prepared, the emission peak lying at 5700Å (Fig. 1). With 3650Å excitation a yellow emission occurs. The small emission peak at 4800Å is attributed to a small amount of β-$Ca_3(PO_4)_2$ in the refired product. When the refiring temperature is lowered to 1100°C only the blue-emitting phosphor is obtained.

With an increase of the amount of copper added, a shift of the emission peak of β-$Ca_3(PO_4)_2$-Cu to longer wave lengths is observed, the crystal structure remaining the same. The shift starts from a Cu/P_2O_5 ratio of 0.05 and reaches an emission peak of 4900Å at a ratio of $Cu/P_2O_5 = 0.20$. In order to obtain the high u.v. absorption desirable for application in fluorescent lamps, a Cu/P_2O_5 ratio of about 0.05 is needed. With the simultaneous addition of Cu^+ and Al^{3+}, the incorporation of the copper ion is obviously facilitated, as deduced from the increase in brightness found. The Al shifts the emission peak to shorter wave lengths and gives a narrower emission band.

With the introduction of manganese, a second emission peak arises at 6550Å. With increasing amounts of manganese, the intensity of the red manganese band is raised and that of the blue copper band is lowered, as is generally known to be the case with sensitized phosphors. This is illustrated in Fig. 2. The brightness of the phosphors activated with copper and manganese is lower than that of the single activated phosphors and falls off rapidly with increasing amounts of manganese. With $Mn/P_2O_5 = 0.08$ a brightness of about 25% of that of Mg-arsenate is reached.

In contrast to the modified Sr-orthophosphate phosphors the partial replacement of Ca in β-$Ca_3(PO_4)_2$ by foreign ions such as Mg, Zn, and Cd decreases the efficiency of the phosphor. Confirming the results of Uehara and Kofuya (11) the addition of a small amount of Mg and Zn, respectively, was found to shift the emission peak to shorter wave lengths. The partial substitution of Ca by Cd does not change the emission. With addition of La and Ce, a change in the spectral distribution is observed. For example, with a mole ratio of $Al/P_2O_5 = 0.06$, $Cu/P_2O_5 = 0.02$, and $Me/P_2O_5 = 0.25$ (Me = La or Ce), Ce, in addition to its own characteristic band at 3500Å, gives rise to the development of a sensitized Cu-band at 4700Å and La to one at 4900Å.

X-ray diffraction analysis shows that all of the latter substituted $Ca_3(PO_4)_2$ phosphors have the β-$Ca_3(PO_4)_2$ structure. Thus the variations observed in the emission spectra are not caused by a change in the crystal structure but by the perturbing action of the foreign ions on the ground and excited states of the activator ion.

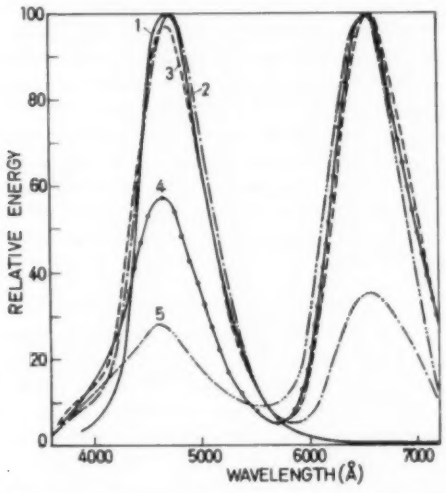

Fig. 2. Spectral energy distribution curves of the emission of β-$Ca_3(PO_4)_2$-Cu·Mn modified with Al, with increasing amounts of Mn. Mole ratios: $Cu/P_2O_5 = 0.02$ and $Al/P_2O_5 = 0.05$

Curve	Mole ratio Mn/P_2O_5
1	0
2	0.02
3	0.04
4	0.06
5	0.08

Strontium Orthophosphate Phosphors

$Sr_3(PO_4)_2$ phosphors with Cu give only a very weak deep-blue luminescence with an emission peak at 4450Å. In the presence of even a small amount of Al a strong blue-green emission occurs. With a sufficiently high amount of Al the deep blue emission disappears completely. This effect may be clearly seen from Fig. 3. The brightness of $Sr_3(PO_4)_2$-Cu modified with Al may reach a value of 125% of the brightness of Sb-activated calcium halophosphate.

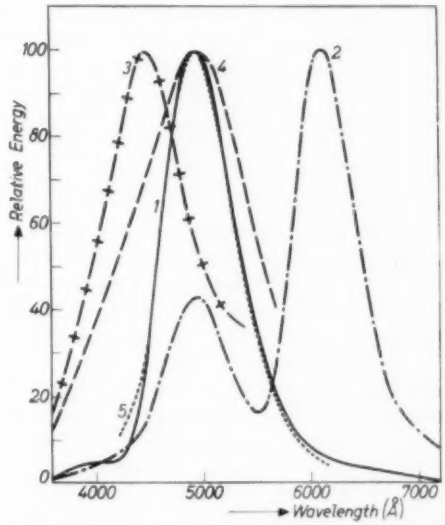

Fig. 3. Emission of Cu- and Cu,Mn-activated Sr orthophosphates. Mole ratio Cu/P_2O_5: curves 1 and 2 = 0.07, curves 3, 4, and 5 = 0.04; Al/P_2O_5: curves 1 and 2 = 0.21, curve 3 = 0, curve 4 = 0.005, curve 5 = 0.02; Mn/P_2O_5: curves 1, 3, 4, and 5 = 0, curve 2 = 0.06.

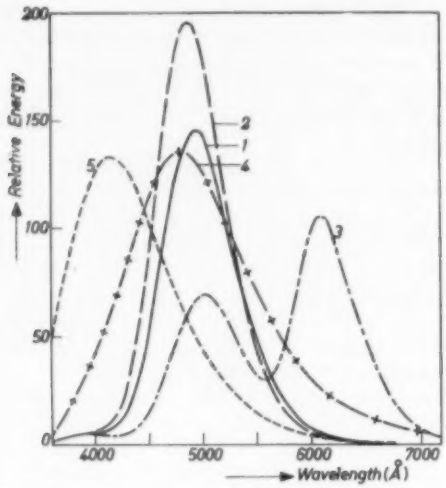

Fig. 4. Emission of Cu-activated Sr orthophosphates, modified with Zn [curve 1], Mg [curve 2], and Cd [curve 3]. The intensities are compared with those of Sb^{3+}-activated calcium halophosphate [curve 4] and of $CaWO_4$ [curve 5]. Composition of phosphors in Table I.

Besides Al, other foreign ions, such as Ca, Zn, Mg, and Cd also give strongly luminescent products, with a brightness higher than that of the known calcium tungstate and Sb-activated calcium halophosphate, as illustrated in Fig. 4. In this figure the intensities of the new phosphors are compared with those of the blue-emitting (Sb-activated) calcium halophosphate and of calcium tungstate. The influence of these foreign ions on the luminescence is due to the effect they have on the crystal structure. Koelmans (14) stated already that the normal Sn-activated $Sr_3(PO_4)_2$ gives only a weak u.v. emission, whereas ions such as Al and Mg cause a transformation into a structure analogous to that of β-$Ca_3(PO_4)_2$. Only the latter structure produces any luminescence. In fact the structures of the Sn-activated phosphors described by Koelmans and of the present Cu-activated ones are identical. As with calcium orthophosphate, the corresponding strontium compound can be activated by Cu and Mn and gives an additional red manganese band at 6100Å (Fig. 3). The intensities of the green Cu and the red Mn bands vary with increasing Mn content in the same manner as already described for the Ca-orthophosphate phosphor.

Modified Orthophosphate Phosphors

Koelmans (14) found that, starting from β-$Ca_3(PO_4)_2$, a gradual replacement of Ca by Sr results in a widening of the β-$Ca_3(PO_4)_2$ lattice until a Ca/Sr ratio of about 0.2 is reached. With more Sr, there is a rather sharp transition to the normal Sr orthophosphate structure and the emission of the Sn-activated phosphor changes from 6200 to 3700Å. With part of the Sr replaced by Ca ($CaO/P_2O_5 = 0.2$) the emission peak of the Cu-activated phosphor lies at 5150Å. The gradual replacement of Sr by Ca shifts this emission peak to shorter wave lengths, until the emission of pure β-$Ca_3(PO_4)_2$-Cu is reached. With the further addition of Al to the SrCa-orthophosphate activated with copper, the emission peak shifts to the blue region of the spectrum.

Table I. Quantum efficiency of Cu-activated orthophosphate phosphors with Al; excitation 2537Å; activator concentration $Cu/P_2O_5 = 0.02$; Al concentration $Al/P_2O_5 = 0.06$; x = Ca, Cd, Zn, and Mg

Phosphor	Activator	x/Sr	Q.R., %
β-$Ca_3(PO_4)_2$	Sn	—	81
$(Sr, Mg)_3(PO_4)_2$	Sn	0.12	87
β-$Ca_3(PO_4)_2$	Cu	—	76
$(Sr, Zn)_3(PO_4)_2$	Cu	0.07	68
$(Sr, Mg)_3(PO_4)_2$	Cu	0.09	82
$(Sr, Ca)_3(PO_4)_2$	Cu	0.11	73
$(Sr, Cd)_3(PO_4)_2$	Cu + Mn	0.11	69

With the partial substitution of Sr by Zn and Mg, respectively, the emission peak is found at 4900Å and at still shorter wave lengths in the presence of additional Al. In accordance with Koelmans' results (14) we found that the amount of foreign ion required to obtain the desired structure of $Sr_3(PO_4)_2$ is smallest with a small substituting ion, e.g., Mg. With the low ratio of $Mg/P_2O_5 = 0.08$ a fluorescence intensity of 70% of that of blue calcium halophosphate is already reached.

The substitution of Sr by Cd gives an emission peak at 5150Å. Besides the foreign ions already mentioned, it was also found that the addition of the rare earth ions La and Ce to $Sr_3(PO_4)_2$ produces luminescent products with an emission maximum at 4500Å. In accordance with Koelmans' results the maximum brightness of the substituted Sr-orthophosphates is achieved with a molar ratio Me/P_2O_5 of about 0.2-0.3 (Me being Mg, Zn, or Cd).

Quantum Efficiency

The efficiencies at room temperature of a number of phosphors, as measured by Bril (18), are given in Table I, together with the values for β-$Ca_3(PO_4)_2$-Sn and $Sr,Mg(PO_4)_2$-Sn, as reported by Koelmans (14). It is seen that the quantum efficiencies of the Cu-activated β-$Ca_3(PO_4)_2$ and of the modified Sr orthophosphates are nearly as high as those of the corresponding Sn-activated phosphors. We cannot state definitely that, for each of the phosphors mentioned in the table, the preparation has been studied sufficiently thoroughly so as to be certain that the figures given for the quantum efficiency are the highest attainable.

Reflection and Excitation Spectra

Figure 5 shows the reflection spectra of some Cu-activated phosphors, together with those of the unactivated product. The small amount of Al which is present does not affect the absorption materially. It may be seen that the introduction of the copper ions produces an absorption in the 2500-3500Å region. The excitation spectra of some phosphors are also shown. From this figure it may be seen that the phosphors investigated are strongly excited by the 2537Å mercury line. Thus this new type of phosphor might be very suitable for low-pressure mercury discharge lamp use, were it not for the difficulty presented by the application of these phosphors. This will be pointed out below. Excitation with cathode rays gives only a weak luminescence, the emission color being the same as with u.v.-excitation.

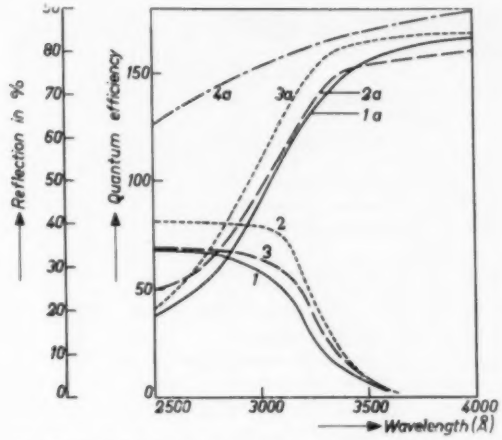

Fig. 5. Reflection (1a-4a) and excitation (1-4) spectra of some Cu- and Cu, Mn-activated Sr orthophosphates. Composition of phosphors in Table I. [1] $(Sr, Zn)_3 (PO_4)_2 \cdot Cu$; [2] $(Sr, Mg)_3 (PO_4)_2 \cdot Cu$; [3] $(Sr, Cd)_3 (PO_4)_2 \cdot Cu \cdot Mn$; [4] $Sr_3 (PO_4)_2$.

Temperature Dependence of Fluorescence

The temperature dependence of the fluorescence of phosphors can hardly be predicted, the behavior of an activator in different matrices varying considerably. Generally speaking, the fluorescence intensity decreases rapidly with increasing temperature when there is a large interaction between the activator ions and the surrounding ions, and vice versa. This is the reason why phosphors with activator ions such as Ce^{3+} and Mn^{4+} with an excited electron in an inner shell generally show a good temperature dependence of the fluorescence. A narrow emission band is, in many cases, evidence for a small disturbing action of the surrounding ions on the activator ion.

As the Cu-activated phosphors described have a band-width of 700-800Å, which is smaller than that of most phosphors, a good temperature dependence of fluorescence of these phosphors could be expected. Figure 6 shows that this is true for β-$Ca_3(PO_4)_2$-Cu and modified $Sr_3(PO_4)_2$-Cu phosphors. With the substitution of some of the Sr in $Sr_3(PO_4)_2$ by other ions, a marked effect on the quenching temperature (i.e., the temperature at which the fluorescence intensity drops sharply) is observed. Figure 6 shows that the quenching temperature decreases in the sequence: Ca, Mg, Zn, and Cd. Similar curves, but with a lower quenching temperature of about 20°C, were obtained with the corresponding phosphors activated with Cu and Mn. It is interesting to note that the ions of group IIa elements of the periodic table (Ca and Mg) have only a small influence on the quenching temperature, whereas the ions of the second sub-series (Zn and Cd) exert a strong one.

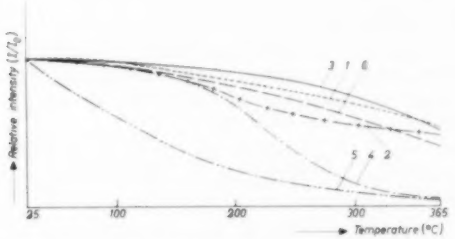

Fig. 6. Variation of fluorescent intensity with temperature for copper-activated calcium orthophosphate [curve 1], and modified strontium orthophosphates [curves 2, 3, 4, 5, and 6]. Composition: moles Me, etc., per 1 mole P_2O_5: Me = 2.90 or 2.95 [curve 2]. Me = Ca(Sr) + Cu + 3/2 Al. Cu = 0.02; Al = 0.06; X = 0.30 (X = Ca, Zn, Cd, or Mg). X = 0.30 (X = Ca, curve 3; Zn, curve 4; Cd, curve 5; or Mg, curve 6).

Obviously the Zn^{2+} and Cd^{2+} ions with a different electronic configuration have a greater disturbing effect on the copper ions than have the Mg and Ca ions. It should be noted that the emission peak of the phosphors investigated shifts to shorter wave lengths at increasing temperatures. An increased activator concentration gives a lower quenching temperature, as was also found with willemite (19) and Mg arsenate (20).

With a constant amount of Cu present, an increase in the Al content improves the temperature dependence of the fluorescence. From the shape of the curves it follows that this type of phosphor may be used in lamps in which good temperature stability is required, namely, high-pressure mercury discharge lamps with an outer bulb coated with a color-correcting phosphor. The difficulties encountered in the application, however, are the same as those met in fluorescent lamps (see below). Moreover the excitation with 3650Å radiation is rather poor (Fig. 5).

Decay of the Cu-Activated Phosphors

The decay of some Cu-activated orthophosphates was measured with the apparatus developed by Bril and Klasens (21). Decay curves are shown in Fig. 7 for Sr orthophosphate modified with Ca and activated with Cu and Mn. Similar curves were obtained with the other Cu-activated orthophosphates. The decay proved to be exponential for Cu, as may be expected for a characteristic activator. The decay constant for Cu in the various phosphors is approximately constant, viz., 40×10^{-4} sec. This means that the life time of the excited state is rather long. The decay constant of the Mn emission of some double-activated phosphors was also measured, using an RG 1 filter (transmitting only the radiation with a wave length greater than 6000Å), in order to remove the blue emission produced by the copper ions. For the Mn emission a decay of 1.9×10^{-2} was found, in accordance with the figures from the literature for the Mn^{2+} emission in other phosphors.

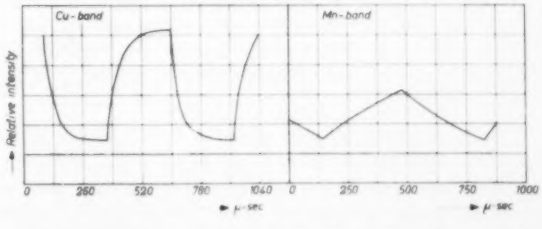

Fig. 7. Build-up and decay of $(Sr, Ca)_3 (PO_4)_2$-Cu, Mn. Composition: Me = 2.90; Cu = 0.02; Al = 0.06; Mn = 0.04; P_2O_5 = 1.

Application

From Fig. 4 and from the quantum efficiencies given in Table I, it is to be expected that this new type of phosphor may be of great importance for fluorescent lamps. In practice, however, serious difficulties arise when the current techniques of lamp making are followed. In order to remove the binder used for applying the phosphor coating, the bulbs are heated to 450°-550°C in air. However, the Cu-activated phosphors are very sensitive to oxidation at temperatures higher than 400°C. Thus after the binder bake-out at 550°C, the phosphor may lose as much as 80% of its efficiency. Phosphors of small grain size are especially sensitive in this respect.

From the foregoing it follows that the phosphors described cannot be applied in the usual way, but special techniques will be required in order to maintain the brightness of the phosphor. The problem of the application of the Cu-activated phosphors is analogous to that of some phosphors which are activated with trivalent cerium, as described by Henderson and Ranby for the calcium halophosphate phosphors (22).

Acknowledgments

The authors wish to express their thanks to Dr. A. Bril for the measurements of the quantum efficiency, the reflection and the excitation spectra of the phosphors; to Dr. H. Koelmans for many helpful discussions regarding the structure of the phosphors; to Mr. E. G. Berns for the determination of the monovalent copper; to Mr. J. Riemens for the measurement of the spectral emission curves; and to Mr. J. G. Verlijsdonk for part of the experimental work.

Manuscript received June 10, 1959. This paper was prepared for delivery before the Philadelphia Meeting, May 3-7, 1959.

Any discussion of this paper will appear in a Discussion Section to be published in the June 1960 JOURNAL.

REFERENCES

1. F. A. Kroeger, *Brit. J. Appl. Phys.*, Suppl. No. 4, 58 (1954).
2. F. A. Kroeger, "Some Aspects of the Luminescence of Solids," p. 266, Elsevier Publishing Co., Amsterdam-New York (1948).
3. H. W. Leverenz, "An Introduction to Luminescence of Solids," p. 192, John Wiley & Sons, New York (1950).
4. E. W. Claffy and J. H. Schulman, *This Journal*, **98**, 408 (1951).
5. K. Th. Wilke, *Z. Phys. Chem.*, **207**, 45 (1957).
6. Brit. Pat. 460,210 (1937).
7. E. Imore, *Sc. pap. Inst. Phys. Chem. Res. Tokyo*, **27**, 1 (1935).
8. D. G. Engle and B. S. Hopkins, *J. Opt. Soc. Am.*, **11**, 599 (1925).
9. J. de Ment, "Fluorescent Chemicals," pp. 76 and 141, Chemical Publishing Co. Inc., Brooklyn (1942).
10. Y. Uehara and Y. Kofuya, Japanese Pat. 1811 and 1812 (1957); *Chem. Abstr.*, **52**, 8754 (1958).
11. Y. Uehara, Y. Kobuke, and J. Masuda, *This Journal*, **106**, 200 (1959).
12. F. A. Kroeger and J. Dikhoff, *Physica*, **16**, 297 (1950).
13. W. H. Zachariasen, *Acta Cryst.*, **1**, 263 (1948).
14. H. Koelmans an A. P. M. Cox, *This Journal*, **104**, 442 (1957).
15. F. A. Kroeger, Unpublished work.
16. K. H. Butler, *This Journal*, **100**, 250 (1953).
17. A. L. Mackay, *Acta Cryst.*, **6**, 743 (1953).
18. A. Bril, Unpublished work.
19. G. R. Fonda, *J. Phys. Chem.*, **43**, 561 (1939).
20. H. A. Klasens, *Philips Res. Repts.*, **9**, 377 (1954).
21. A. Bril, H. A. Klasens, and P. Zalm, *ibid.*, **8**, 393 (1953).
22. S. T. Henderson and P. W. Ranby, *This Journal*, **104**, 612 (1957).

Copper and Tin-Activated Halophosphate Phosphors

B. E. Hunt and A. H. McKeag

Research Laboratories, The General Electric Company Limited, Wembley, England

ABSTRACT

New copper- and tin-activated halophosphate phosphors, fired in mildly reducing atmospheres and of potential practical importance, are described. They include copper- and tin-activated barium chlorophosphates with good thermal characteristics. Copper-activated barium chlorophosphate shows a moderate red fluorescence at ambient temperatures, under long u.v. excitation, which becomes brighter at higher temperatures due to a marked color shift toward the yellow. The same matrix, activated with tin, shows a strong pale green fluorescence at ambient temperatures when excited by 2537A radiation which is shifted toward the blue at elevated temperatures.

Since the introduction in 1942 of the alkaline earth halophosphate phosphors activated with antimony and manganese (1) a number of additional activators have been described. These include arsenic, bismuth, tin, lead (1), silver (2), uranium (3), and cerium (4). Copper has been mentioned as an activator of hydroxyphosphates (1) but has not been found previously to be very effective as an activator of halophosphates.

This paper describes a number of new copper-activated halophosphates prepared by heat treatment in mildly reducing conditions. Under similar conditions improved tin and tin-manganese activated halophosphates also have been prepared. Some of

these phosphors are of potential importance for use in discharge lamps of both high- and low-pressure mercury vapor types.

Preparation of Copper- and Tin-Activated Halophosphate Phosphors

Phosphors of this type were prepared by conventional halophosphate techniques, but firing treatments were carried out in mildly reducing atmospheres of nitrogen containing a low concentration of hydrogen. Tin-activated phosphors require about 0.5% vol/vol of hydrogen to nitrogen, while copper-activated phosphors, which are more sensitive to reducing conditions than those containing tin, require lower concentrations of hydrogen. With copper, the best results were obtained with about 0.25% vol/vol or less of hydrogen to nitrogen. Excessive reduction of copper and tin compounds is evidenced by discoloration of the samples, and this effect frequently can be corrected by subsequent refiring in "pure" nitrogen. Although nitrogen of the highest commercial purity was used throughout these experiments, it is possible that traces of oxygen present in the gas may contribute to the balance between reducing and oxidizing conditions necessary to maintain copper in the required valency state. It would seem probable that copper in the cuprous state and tin in the stannous state may be the conditions necessary for activation of these phosphors.

The useful ranges for copper and tin are from 0.1 to 1.0% (by weight) for copper and 0.5 to 5.0% for tin. Part of the copper is lost by volatilization during the firing treatment, and this may amount to as much as 50% of the initial quantity added. Preliminary analytical determinations suggest that part of the copper which remains may be present in the cuprous state. Firing temperatures depend on the nature of the halophosphate matrix but were usually in the range of 900° to 1200°C. Samples usually were prefired at a low temperature (900°C) to stabilize the matrix composition of the phosphors.

Fluorescence of Copper- and Tin-Activated Halophosphates

Copper- and tin-activated halophosphates of the alkaline earth metals (Ca, Sr, and Ba) were prepared with varying fluorine and chlorine ratios. X-ray examination of the more interesting phosphors confirmed that the apatite structure had been formed, and no noteworthy matrix impurities other than apatite phases were detected. The results of the various combinations tested are summarized below.

Calcium halophosphates.—Of this group, phosphors with a high chlorine content gives the best results. Copper activation produces a moderate blue fluorescence with short u.v. (2537Å) excitation, and the strongest emission occurs at a fluorine to chlorine molar ratio of 0.3:0.7.Manganese, in addition to copper, modifies the color to orange. Tin, by itself, gives a weak blue fluorescence which is modified to an orange-pink color by the addition of manganese.

Strontium halophosphates.—The best results are obtained in this group with strontium fluorophosphate activated with tin and manganese. Excitation by short u.v. radiation produces a strong yellow-green to orange-yellow fluorescence as the manganese content is increased. Replacement of fluorine by chlorine diminishes the brightness of these phosphors markedly. Copper, alone, (in strontium halophosphates) gives a weak red fluorescence with long u.v. excitation (3650Å).

Barium halophosphates.—These phosphors are more responsive to the effect of copper activation and give a moderately strong orange-red to red emission with long u.v. excitation. Tin, by itself, produces a moderate blue fluorescence in barium fluorophosphate and a strong greenish blue fluorescence with barium chlorophosphate. Manganese, in addition to copper or tin, is ineffective as an activator in these materials.

Among other phosphate combinations which were investigated with copper activation, calcium orthophosphate gives a strong blue fluorescence with short u.v. excitation which is modified to a pink fluorescence by the addition of manganese. This phosphor has also been described by Uehara and Kofuya (5).

Excitation and Emission Characteristics

Copper activation.—Two distinct types of emission are observed in the copper activated halophosphates, a blue or blue green emission in calcium halophosphates excited by short u.v. and a red emission in barium halophosphates excited by long u.v. radiation (Fig. 1, peak values normalized). With barium halophosphates the peak of the excitation curve for the red emission occurs at about 3000Å and declines rapidly at shorter wave lengths. In the presence of sulfate ions (added as copper or barium sulfate) these phosphors also show a weak blue fluorescence when excited by short u.v. radiation (2537Å). A

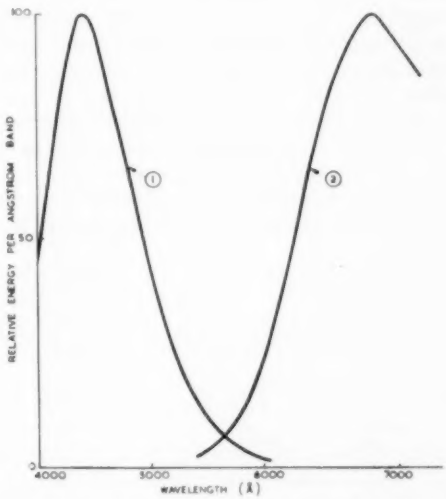

Fig. 1. Spectral energy distribution curves at ambient temperature of: 1. copper-activated calcium fluoro-chlorophosphate excited by 2537Å radiation $3Ca_3(PO_4)_2 \cdot 0.3\ CaF_2 \cdot 0.7\ CaCl_2$ (0.5% Cu by weight of matrix, as introduced), fired at 1200°C (0.1% vol/vol of H_2 to N_2; 2. copper-activated barium chlorophosphate, excited by 3650Å radiation (0.4% Cu, as introduced, fired at 1100°C, 0.25% vol/vol of H_2 to N_2).

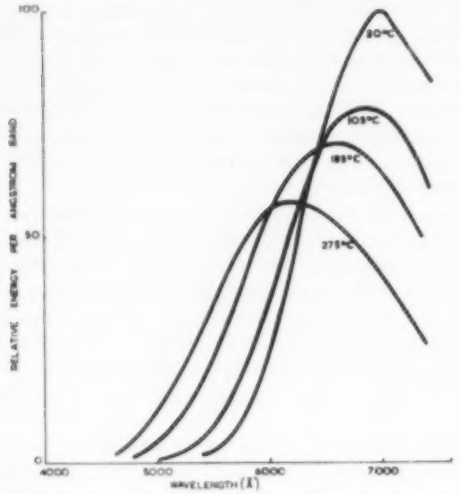

Fig. 2. Change of spectral energy distribution of copper-activated barium chlorophosphate with temperature, excited by 3650Å radiation (0.4% Cu, as introduced, fired at 1100°C, 0.2% vol/vol H_2 to N_2).

weak green emission is also obtained under short u.v. excitation if an attempt is made to compensate for charge difference between the monovalent cuprous ions and the divalent barium ions by the addition of trivalent cations such as cerium or lanthanum.

An unusual feature of the emission spectra of these phosphors is the marked shift in the position of the long u.v. excited band as the temperature of the phosphor is raised. This is most pronounced with barium chlorophosphate (Fig. 2) and is accompanied by an increase in visual brightness due to this shift in color from red toward the yellow.

Brightness-temperature measurements for copper-activated barium halophosphates, shown in Fig. 3, were made visually with a modified Macbeth photometer using suitable matched color filters of known transmission values. Curve 1 was normalized to give a peak value of 100, and curve 2 is relative to curve 1 on the same scale. With copper-activated barium chlorophosphate, the maximum brightness amounts to some three times the brightness at ambient temperatures and the maximum is reached at about 300°C. The corresponding fluorophosphate phosphor

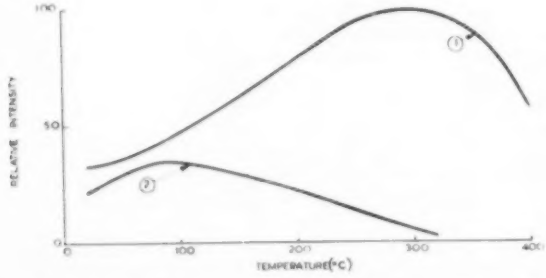

Fig. 3. Variation of visual brightness with temperature of: 1. copper-activated barium chlorophosphate, excited by 3650Å radiation (0.4% Cu, as introduced, fired at 1100°C, 0.2% vol/vol H_2 to N_2; 2. copper-activated barium fluorophosphate, excited by 3650Å radiation (0.4% Cu, as introduced, fired at 1100°C, 0.2% vol/vol of H_2 to N_2).

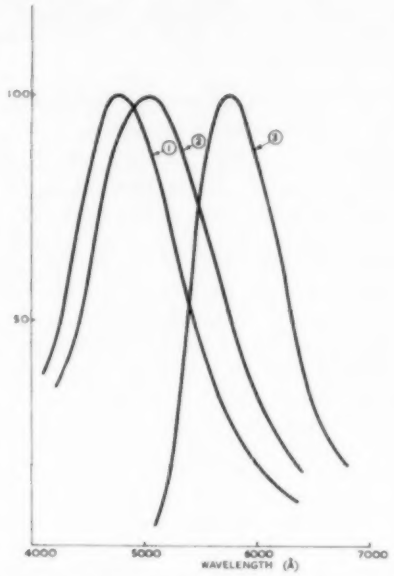

Fig. 4. Spectral energy distribution curves at ambient temperatures of: 1. tin-activated barium fluorophosphate, excited by 2537Å radiation (1% Sn, as introduced, fired at 1200°C, 0.5% vol/vol H_2 to N_2); 2. tin-activated barium chlorophosphate, excited by 2537Å radiation (1% Sn, as introduced, fired at 1150°C, 0.5% vol/vol H_2 to N_2). 3. Tin- and manganese-activated strontium fluorophosphate, excited by 2537 Å radiation (1% Sn, 2% Mn, as introduced, fired at 1050°C, 0.2% vol/vol of H_2 to N_2).

shows a much smaller change in color and has poorer temperature characteristics. These temperature effects are not critically dependent on activator concentration, although somewhat poorer results are obtained with high concentrations of copper. Phosphor samples which were heated in air during these measurements showed no marked permanent deterioration in brightness in the temperature range used for these observations.

Blue fluorescing calcium orthophosphate also shows good temperature characteristics and resembles in this respect certain copper activated aluminosilicates described by Claffy and Schulman (6). Instability of the calcium orthophosphate phosphor itself is evidenced by discoloration which occurs after baking the phosphor in air at temperatures of about 400°C.

Tin activation.—Barium halophosphates activated with tin are strongly excited by short u.v. radiation to give broad emission bands in the blue or blue-green regions of the spectrum (Fig. 4, peak values normalized). Barium chlorophosphate, activated with tin, like the corresponding copper activated phosphor, shows a marked shift in the position of the spectral band toward shorter wave lengths as the temperature is raised (Fig. 5). In this case, however, the shift in color is away from the green, and a reduction in visual intensity occurs (Fig. 6). Nevertheless, the phosphor is superior in temperature characteristics to most other blue emitting phosphors which are relatively poor in this respect, notable exceptions being copper-activated calcium orthophosphate and the aluminosilicates referred to above.

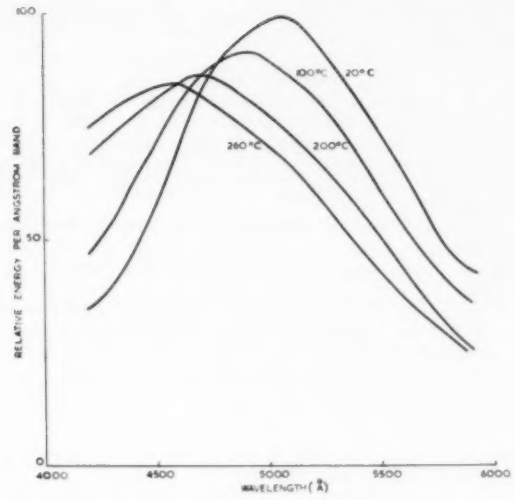

Fig. 5. Change of spectral energy distribution of tin-activated barium chlorophosphate with temperature, excited by 2537Å radiation (1% Sn, as introduced, fired at 1150°C, 0.5% vol/vol of H_2 to N_2).

Strontium fluorophosphate activated with tin and manganese is of potential importance because of the strong yellow emission excited by short u.v. radiation. The spectral energy distribution of a phosphor containing 1% by weight of tin and 2% by weight of manganese, fired at 1075°C, is shown in Fig. 4.

Applications in Lamps

Certain of the phosphors described above are of potential practical interest for use in discharge lamps. Barium chlorophosphate activated with copper, for example, applied to high-pressure mercury lamps is capable of utilizing the longer wave-length u.v. radiation (beyond 3000Å) from these lamps to give improved color rendering properties. In this instance it is an advantage to operate the phosphor at a relatively high temperature (ca. 250°C) in order to obtain the maximum light output.

Of the short u.v. excited phosphors, tin- and manganese-activated strontium fluorophosphates may be useful in mixtures with conventional red emitting phosphors to provide colors suitable for use in lamps of good color rendering qualities of the "De Luxe" types. The chromaticity values of 40-w fluorescent lamps coated with phosphors of varying manganese contents lie on an arc above the black body locus of the C.I.E. chromaticity diagram. The values range from $x = 0.400$, $y = 0.433$ for a phosphor containing 1.0% by weight of Mn to $x = 0.433$, $y = 0.445$ for a similar phosphor containing 2.0% Mn. Phosphors of this type show an appreciable and fairly rapid reduction in brightness when exposed externally to short u.v. radiation from a low-pressure mercury vapor quartz discharge tube. The effect occurs in air or in an evacuated quartz tube and is accompanied by a slight brown discoloration of the phosphor. After the initial reduction in brightness, further exposure produces little subsequent change. The effect is consistent with a chemical change in the surface state of the phosphor produced by the short u.v. radiation and may be similar to the formation of "color centers" produced in other materials by x-rays or cathode rays.

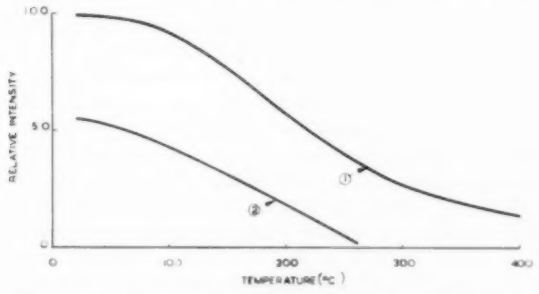

Fig. 6. Variation of visual brightness with temperature of: 1. tin-activated barium chlorophosphate, excited by 2537Å radiation (1% Sn, as introduced, fired at 1050°C, 0.2% vol/vol of H_2 to N_2); 2. tin-activated barium fluorophosphate, excited by 2537Å radiation (1% Sn, as introduced, fired at 1100°C, 0.2% vol/vol of H_2 to N_2).

Lumen maintenance characteristics of lamps coated with these phosphors show a rapid drop in efficiency during the first 100 hr of operation but this is succeeded by a relatively slow depreciation. In 40-w lamps "initial" (100 hr) efficiencies of 40-45 lpw have been obtained with these phosphors. After 4000 hr operation, lamp efficiencies were about 80% of the "initial" values. Of the other phosphors described, tin-activated barium chlorophosphate gives an "initial" efficiency in 40-w lamps of 45 lpw with a chromaticity value of $x = 0.250$, $y = 0.345$. The good temperature characteristics of this phosphor also make it potentially useful in high-pressure mercury vapor lamps.

Discussion

It has been shown that the temperature characteristics of barium chlorophosphates activated with copper and tin are markedly superior to the corresponding fluorophosphates. Both copper- and tin-activated barium chlorophosphates show a pronounced color shift as the temperature is raised. Uranium-activated barium halophosphates (3) also were tested for temperature dependence of fluorescence, but both fluoro- and chlorophosphates were markedly inferior to the copper- and tin-activated chlorophosphates and fluorophosphates. These observations support the view that temperature quenching effects are not a property of the lattice as such but of the emission centers and their surroundings (7). These differences in surroundings produce the marked difference in temperature characteristics between fluoro- and chlorophosphates activated with either copper or tin. As these phosphors are chemically and structurally similar, the differences observed may therefore be associated with the changes in spatial atomic arrangements in the matrix due to the replacement of fluorine by chlorine atoms in the apatite structure.

Besides the question of temperature properties the difference in emission characteristics between the various copper-activated phosphates is also of interest. Blue emission observed in halophosphates and calcium orthophosphate is typical of a number of

other copper-activated phosphors previously reported (1, 6). The long u.v. excited red emission observed in barium and to some degree in strontium halophosphates is more unusual. As both types of emission are obtained under certain conditions of preparation in the same barium halophosphate phosphor, it would seem that two different types of copper centers may be responsible for the blue and red emission bands. As the atmosphere conditions observed in the preparation are the same throughout, it may be assumed that copper is present in the same valency state in these phosphors. If this is so, the possibility of copper atoms occupying alternative sites in the halophosphate lattice might explain the observed differences in excitation and emission characteristics.

REFERENCES

1. H. G. Jenkins, A. H. McKeag, and P. W. Ranby, *J. (and Trans.) Electrochem. Soc.*, **96**, 1 (1949).
2. P. W. Ranby, *This Journal*, **98**, 299 (1949).
3. J. T. Anderson and R. S. Wells, *ibid.*, **98**, 414 (1951).
4. S. T. Henderson and P. W. Ranby, *ibid.*, **104**, 612 (1957).
5. Y. Uehara and Y. Kofuya, *Chem. Abs.*, **52**, 8754 (1958).
6. E. W. Claffy and J. H. Schulman, *This Journal*, **98**, 409 (1951).
7. F. A. Kroeger, "Some Aspects of the Luminescence of Solids," Chap. VI, Elsevier Publishing Co., Amsterdam (1948).

Electrical Properties of High-Purity Silicon Made from Silicon Tetraiodide

L. V. McCarty[1]

Research Laboratory, General Electric Company, Schenectady, New York

ABSTRACT

Resistivities, type of conduction, and lifetimes of minority carriers of single crystals of iodide silicon are recorded as a function of the purification procedure for silicon tetraiodide. Samples of silicon have been prepared by decomposition of silicon tetraiodide on hot tantalum and hot quartz surfaces in vacuum. Distillation in a 12 plate quartz column of silicon tetraiodide prepared from 99.7% silicon results in single crystals of silicon that are uniformly n-type with maximum resistivities at the seed end in the range 0.3-1 ohm-cm. Two recrystallizations from solvents before the distillation step result in both p- and n-type crystals with, respectively, 150-650 ohm-cm and 75-170 ohm-cm resistivity ranges at the seed ends. Distillation of silicon tetraiodide is particularly effective in removing boron, while recrystallization and zone melting are effective for removing group V impurity iodides.

Silicon tetraiodide has been recognized as a potential source of semiconductor silicon for several years. Litton and Andersen (1) first made iodide silicon from silicon powder using iodine vapor in a Van Arkel-de Boer type of apparatus and observed some purification, but, unfortunately, both donor (group V) and acceptor (group III) impurity elements were transferred in the operation. In order to improve the quality of their product they decided to isolate silicon tetraiodide, which probably carried the silicon through the vapor phase of their iodide cells, and to purify it by fractional distillation in an all-quartz column. The electrical properties of their product indicate that they met with considerable success.

Later Szekely (2) reported on the hydrogen reduction of silicon tetraiodide, but electrical data with which one might calculate the purity of the product are not included.

A different approach to the purification problem was adopted by Rubin and his associates (3). They took advantage of the solubility of silicon tetraiodide in toluene from which it can be recrystallized as the first step in their procedure. Their final steps are sublimation and zone melting of the solid, but the electrical properties of silicon made from their purified material are not discussed.

In this work still another sequence of purification steps has been used to prepare silicon tetraiodide for decomposition into silicon and iodine. These techniques include recrystallization from n-heptane and distillation in an all quartz column, and a very brief investigation of zone melting. Electrical properties of single crystals grown from the silicon are interpreted as a measure of crystal purity rather than depending on chemical analyses for individual elements, because the estimated quantity of electrically active impurities is in the range of parts per ten billion for elements that affect the resistivity of this silicon, and even less for those that affect the recombination of holes and electrons. It is true that the electrical properties do not give much detail concerning specific impurity elements, but the tests are more readily made and indicate the presence of broad classes of electrically active impurities. Any one of these would be much more difficult to detect

[1] Present address: Lamp Development Department, General Electric Company, Nela Park, Cleveland, Ohio.

chemically, and, if undetected, might render the silicon quite useless as a semiconductor. The objective of this work was the preparation of the purest silicon possible.

Experimental

Preparation of silicon tetraiodide.—The method of making silicon tetraiodide is quite similar to the one described by Szekely (2). A nitrogen purge was used instead of argon, and a reaction temperature of 600°C was sufficient when the Electrometallurgical Company's 99.7-99.9%, 30-80 mesh silicon powder was used. When DuPont hyper-pure silicon crystals were placed in the reactor, a temperature of 800°C was required to achieve about the same reaction rate. The higher temperature may have been necessary because there is less impurity present to act as catalyst in the latter silicon, but it was also much coarser and did not pack as well.

Recrystallization of silicon tetraiodide.—Silicon tetraiodide was dissolved in sufficient solvent in a Pyrex flask to make a 50 mole % solution at the boiling point. After cooling to room temperature the solvent is drained off, and residual solvent and tetraiodide are transferred to the distillation apparatus after two or more recrystallizations.

Solvents used include Phillips Petroleum 99+% n-heptane, Phillips Petroleum commercial heptane, and reagent grade toluene and benzene.

Distillation of silicon tetraiodide.—The distillation apparatus for most of this work is made entirely of quartz. The smaller column consists of a one liter pot sealed to a 4-ft length of 1 in. OD tubing which is packed with ¼ in. sections of ¼ in. tubing (Raschig rings). The condensing head is a conventional design with a magnetically operated quartz valve to control the take-off, and an electrically heated delivery tube to conduct the tetraiodide into its receiver flask. The larger column is made from a 5 liter pot sealed to a 2 in. OD tube 66 in. long. Both columns have a rectification efficiency equivalent to 12 theoretical plates as tested with a mixture of methycyclohexane and normal heptane. Either is purged with nitrogen before tetraiodide is melted or distilled into the pot, and a flow of 20-30 cc/min is maintained throughout the distillation. The apparatus remains on total reflux overnight before starting the first cut. The minimum reflux ratio is 24:1 while product is taken off at 50-150 g/hr into quartz storage flasks. A first cut of 25% of the charge is discarded, and the second cut, which is later decomposed to silicon and iodine, contains 50% of the tetraiodide.

Decomposition of SiI_4 *on tantalum.*—The deposition on tantalum is similar in many respects to the technique described by Litton and Andersen (1). A tantalum rod, ⅛ in. in diameter by 3 ft, in the form of a hairpin is suspended in an evacuable chamber by means of a 65/40 ball and socket joint to which are sealed ¼ in. molybdenum electrodes. The 2 in. OD deposition chamber and the reservoir for silicon tetraiodide are an integral unit made of quartz.

After drying the equipment thoroughly, silicon tetraiodide is transferred into its reservoir in a dry nitrogen atmosphere. The tantalum hairpin is placed in position next using silicone grease or, preferably, a silicone rubber gasket on the ball joint. A dry ice bath is placed around a trap to condense iodine and unreacted silicon tetraiodide, and the system is pumped down to about 1 μ. The tantalum rod is heated electrically to 950°C as observed without correction by an optical pyrometer, and, last, the tetraiodide is warmed to about 100°C. The estimated vapor pressure of tetraiodide in the system is of the order of 1 mm.

After all of the iodide in the pot has sublimed, the electrical power is turned off, permitting the silicon and tantalum to cool to room temperature. Cracking noises are heard as the two partially separate due to thermal fracture. When cool, the system is filled with dry nitrogen, and the tantalum rod and silicon are removed and wrapped in a sheet of polyethylene. Gentle flexing separates the silicon from the rod, and the larger spears are broken up. The yield of silicon is about 80-90% in a 20-30 hr run.

Decomposition of SiI_4 *on quartz.*—For reasons discussed later, tantalum did not seem to be the ideal deposition surface. Quartz is used at much higher temperatures in the crystal growing operation than are needed for the decomposition of silicon tetraiodide, so it seemed reasonable to use it for the latter operation because the requirements are not nearly so severe. Figure 1 shows the kind of equipment designed after preliminary experiments. The silicon tetraiodide storage pot and reactor tube are an integral unit made of quartz. A socket joint is ring sealed into the bottom of the reactor to support a thin walled quartz tube on which deposition actually occurs. The purpose of the tube within a tube construction is to keep the outer portion of the reactor from breaking when the furnace is allowed to cool after silicon has deposited. Silicon adheres to quartz very strongly and, since the coefficients of expansion are different, the deposit and tube fracture on cooling. A tungsten spiral in 1½ in. OD tubes kept fragments from falling into the flask.

The spiral winding on the connection between the decomposition apparatus and the trap is a nichrome ribbon to keep the tube warm and thus prevent condensation of unreacted silicon tetraiodide. The refrigerant usually used around the trap is trichloroethylene-dry ice, and during operation the pressure is of the order of 1 μ or less at the vacuum gauge, but it is much higher in the reactor.

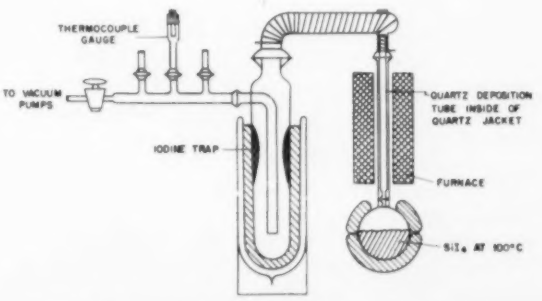

Fig. 1. Apparatus for deposition of silicon on quartz

At the end of a run the silicon with quartz adhering to it is placed in concentrated hydrofluoric acid for a day or two to dissolve the latter. Next it is thoroughly washed with water, then methyl alcohol, and air dried. The yield from 1000 g of SiI, is about 70% in a three day run at 1000°C. The reaction probably takes longer on quartz than on tantalum because the corrected temperature for the silicon deposit on the latter may be well above 1000°C.

Cleaning of equipment.—All equipment was thoroughly cleaned after each use with either 1% or 5% hydrofluoric acid followed by rinsing with water and drying by baking wherever possible. The hope was to standardize the surface of the vessels for each experiment rather than making it a function of the history of the equipment.

Crystal growing.—All crystals for this work were prepared in quartz crucibles by the Czochralski technique (4). A stainless steel pull rod held the single crystal seed, and the furnace atmosphere was argon. Heat was supplied to the crucible by a graphite resistance element supplied with a-c power from a Variac stabilized with a Sorensen regulator.

Electrical measurements.—Resistivities were generally measured with a calibrated four-point probe on a lapped surface. Occasionally there was reason to suspect the values obtained, and in these cases resistivities were checked by passing a small current through the sample and measuring the potential drop along the surface.

The relationship between the number of uncompensated impurity atoms per cubic centimeter and the resistivity (above 10 ohm-cm) can be approximated by (5, 6)

$$n = \frac{1}{\rho e \mu_n} \simeq \frac{3.6 \times 10^{15}}{\rho} \qquad [1]$$

$$p = \frac{1}{\rho e \mu_p} \simeq \frac{1.3 \times 10^{16}}{\rho} \qquad [2]$$

where ρ is the resistivity, e is the charge of one electron in coulombs, and μ_n and μ_p are the mobilities of electrons (~1750 cm^2/v sec) and holes (480 cm^2/v sec) at room temperature, respectively.

Another measurement which typifies the quality of silicon single crystals is the lifetime of the minority carriers. The method used for this measurement has been described by Watters and Ludwig (7) who give detailed data as a function of temperature for sample 3 of Table V, which is referred to as C-Si-170.

Drift and conductivity mobility data for C-Si-170 have also been determined by Ludwig and Watters (8).

Results and Discussion

Spectrographic Data

Impurity elements detected spectrographically in a typical sample of Electromet silicon as received, and after processing by conversion to silicon tetraiodide with subsequent decomposition to silicon, are shown in Table I. The four elements in the right-hand column were detected in a sample of iodide silicon made from unpurified silicon tetraiodide. When recrystallization from solvents or distillation of the tetraiodide were incorporated in the process, the aluminum concentration occasionally dropped so low as to become undetectable. The data show that the iodination and decomposition processes are powerful purification steps in their own right merely from the number of elements rejected. But for semiconductor purposes these spectrographic analyses of iodide silicon have only a very limited value because they are insufficiently sensitive.

Table I. Impurity elements detected spectrographically

Electromet silicon	Iodide silicon
Fe	Fe
Mg	Mg
Cu	Cu
Al	Al*
Ca	
Ti	
Ni	
Sn	
Co	
Cr	
Mn	
Zr	

* Not always detected.

Iodide Silicon Made from Unpurified Silicon Tetraiodide

The most difficult element to remove from silicon by zone melting or crystal growing techniques is boron, and it is almost imperative that it be removed from the compounds used to make silicon before the actual preparation. It is not difficult to recognize a crystal whose resistance is dominated or controlled by boron, however, because its segregation coefficient is about 0.9 (9), and such crystals have a characteristically "flat" resistivity profile.

Because of the importance of removing boron from silicon, it was desirable to determine how the various purification steps affect its removal. In order to establish a base line for comparison purposes, enough silicon was prepared by decomposition of unpurified silicon tetraiodide on quartz so that elements other than boron could be removed by 5 zone passes in a zone melting apparatus. A single crystal grown from the zone melt bar was p-type and had resistivities in the range 0.25-0.14 ohm-cm, about 0.20 ohm-cm on the average. (In this paper the first resistivity quoted will be for the "seed" end of the crystal, while the second number refers to a measurement near the "sprout", or tail end. In general, impurities segregate toward the sprout.) The conductivity mobility, μ_p, for this resistivity range (5) is about 350 cm^2 v^{-1} sec^{-1}, and the number of boron atoms per cubic centimeter, p, can be calculated as

$$p = \frac{1}{\rho e \mu_p} = \frac{1}{0.20 \times 1.60 \times 10^{-19} \times 350} = 9 \times 10^{16}$$

or about 1.7 boron atoms per million silicon atoms. Rubin, Moates, and Weiner (3) found considerably more boron than this in their silicon tetraiodide

Table II. Electrical properties of single crystals of iodide silicon prepared from distilled silicon tetraiodide[a]

Sample No.	Type	Resistivity range, ohm-cm
1	n	0.3-0.06
2	n	0.4 max.
3	n	0.7 max.
4	n	0.3 max.
5	n	0.4-0.2
6	n	0.8-0.2
7[b]	n	1-0.4

[a] SiI_4 prepared from 99.7% Electromet Si, distilled in 12 plate quartz column, and decomposed on ⅛ in. Ta rod.

[b] 5 g of KI added to still pot.

which was made from a different grade and different kind of silicon.

Iodide Silicon Made from Distilled Silicon Tetraiodide

In the first attempts in the present experiments at purification of silicon tetraiodide distillation in an all-quartz, 12 plate column was used. Results are shown in Table II. Two things about this data are impressive: all samples are n-type, and the resistivities near the seed end of the crystal (the first number quoted) are reasonably uniform. This means that some group V element, a donor impurity, is the chief contaminant rather than boron. The relatively slow decrease in resistivity along the crystals of samples 1, 5, and 7 indicates a material with a segregation coefficient similar to phosphorus or arsenic (9).

James and Richards have shown that phosphorus can be found in amounts of 0.1 to 10 ppm in iodine (10), and the very careful analysis of 97% silicon performed by the Bureau of Standards (11), as well as the work of Rubin, Moates, and Weiner (3), indicates that this quality of silicon can have as much as 80 ppm of phosphorus. The latter authors (3) also have shown the presence of 150 ppm of arsenic which is mostly eliminated by the iodination reaction.

Either n-type impurity as an iodide might be contaminating the crude silicon tetraiodide. Phosphorus triiodide is more volatile than silicon tetraiodide (1), and it should tend to concentrate in the condensing head of the apparatus. If it were not completely removed from the condenser through faulty technique, the electrical conductivities of Table II ought to show considerable scatter. Since they do not show a broad range of values, it seems more reasonable to believe that the source of n-type contamination is in the crude tetraiodide in the still pot, which should come to equilibrium with the still head during the prolonged initial operation at total reflux. Arsenic triiodide is less volatile than silicon tetraiodide (1). It would concentrate in the still pot, and it may be the n-type impurity responsible for these results.

Potassium iodide was added to the distillation pot of the last sample in an attempt to form complexes with group V iodides which would reduce their vapor pressure.

In order to determine the amount of boron in these samples it is necessary to prepare enough silicon for zone melting to remove n-type impurities. It would have been extremely tedious to do this with the original small quartz equipment, so a large 12 plate Pyrex column was used for the distillation. The use of Pyrex introduces certain complications which will be discussed later, but it is believed that the boron concentration obtained after zone melting represents the maximum amount coming through the distillation step. Sample No. 4 of Table VI was prepared in this way. Its maximum resistivity of 125 ohm-cm, which dropped only gradually over the first part of the crystal, corresponds to about 2 boron atoms per billion silicon atoms. This represents a reduction in the boron concentration by a factor of approximately 850 by a 12 plate distillation. Because of the experimental errors involved, however, it might be better to say that the factor is in the range 500 to 1000.

Litton and Andersen (1) have given a value of 6.8 for the relative volatility of boron triiodide compared to silicon tetraiodide. By assuming that the same relative volatility applies to a dilute solution of boron triiodide at 300°C, one can write

$$\frac{\dfrac{\text{mole fraction of } BI_3 \text{ in vapor}}{\text{mole fraction of } SiI_4 \text{ in vapor}}}{\dfrac{\text{mole fraction of } BI_3 \text{ in liquid}}{\text{mole fraction of } SiI_4 \text{ in liquid}}} =$$

$$\frac{\text{mole fraction of } BI_3 \text{ in vapor}}{\text{mole fraction of } BI_3 \text{ in liquid}} = 6.8$$

since the mole fraction of silicon tetraiodide is within parts per million of being unity in either phase. The number of effective plates realized from the observed separation in the "12 plate" column is:

$$6.8^x \sim 850$$

$$x \sim 3.5 \text{ effective plates}$$

If the total purification achieved in the best samples reported in this study were ascribed to the action of the distillation column, less than 4.5 plates would be required for the removal of boron triiodide to the indicated levels.

Green and Kafalas (12) have shown that the separation factor, α, for dilute solutions of arsenic trichloride in germanium trichloride is remarkably lower than in solutions containing an excess of arsenic trichloride. The α for the system boron triiodide-silicon tetraiodide may behave similarly, in which case many more theoretical plates would be realized than indicated.[1]

There are two other reasons that might be advanced for the discrepancy between the calibrated effectiveness of the column and that actually realized. The mixture of hydrocarbons is so different in physical properties from silicon tetraiodide that our calibration may indicate many more plates than can ever be realized in systems consisting mostly of silicon tetraiodide.[1] The other reason concerns the reduction and solution of boron impurities in quartz boats and crucibles containing molten silicon (13).

[1] The author is indebted to C. S. Herrick and J. G. Krieble for this suggestion.

Table III. Effect of tantalum doping on the electrical properties of silicon

	Type	Resistivity, ohm-cm	Lifetime of minority carriers, μsec
Starting material	p	150	125
Portion of crystal before Ta doping	p	150	150
After doping with 0.1% Ta	p	140	10

This effect may add a small amount of boron which places a limit on what can be achieved experimentally when molten silicon contacts quartz equipment as one of the processing steps.

Tantalum as an Impurity in Silicon

Litton and Andersen (1) have indicated that there is a discontinuous alloy zone formed at the tantalum-silicon interface during deposition. Neutron activation analyses of silicon removed from our tantalum rods showed that tantalum was present, and apparently in variable amounts[a] which supports their observation. In order to determine the effect of occluded alloy or metal, a silicon melt was doped with a small piece of tantalum metal when the crystal was partially grown (14). Table III gives data for the electrical properties of this crystal before and after tantalum doping. There is only a minor change in the resistivity of the silicon, but the lifetime of the minority carriers has dropped rather dramatically.

An n-type impurity in the tantalum metal could conceivably be diffusing through the metal-silicon interface to cause the low resistivities of Table II. Two samples of iodide silicon prepared on tantalum from distilled tetraiodide made from DuPont hyperpure silicon showed that this was not so, however. The resistivity range for an n-type single crystal was 114-8 ohm-cm, while a p-type crystal of another sample was in the range 200-100 ohm-cm.

Because of the tantalum contamination we decided to use another kind of deposition surface to try to avoid any adverse influence tantalum might have on the lifetime properties. Quartz is used at much higher temperatures in the crystal growing operation than is needed for the decomposition of silicon tetraiodide, so it seemed reasonable to use it for the latter operation because the requirements are not nearly so severe. Decomposition on quartz was used for all succeeding samples discussed in this paper.

Iodide Silicon Made from Recrystallized Silicon Tetraiodide

Residual solvent was removed from two samples of recrystallized silicon tetraiodide by heating to the boiling point and distilling a small portion to purge the apparatus. The first sample of Table IV indicates that two recrystallizations from a solvent are more effective than distillation in a 12 plate column, since this material contains less than one-fifth as many excess n-type impurities as the best example of Table II. [The mobility of the current carriers decreases as the resistivity drops in this range (9).] A detailed study of the effectiveness of two recrystallizations from other solvents was not carried out, but we believe that all would be approximately equally effective.

[a] W. W. Schultze performed the neutron activation analysis.

Table IV. Electrical properties of single crystals of iodide silicon prepared from recrystallized silicon tetraiodide[a]

Sample No.	Notes on purification of SiI_4	Type	Resistivity, ohm-cm	Lifetime of minority carriers, μsec
1	Recrystallized twice from toluene as a coarse powder; washed each time with 3 portions of n-heptane	n	5 max.	
2[b]	Recrystallized twice from commercial heptane, and then 6 times from n-heptane	n	94-130-94-22	200-75

[a] SiI_4 made from 99.8% Electromet Si and deposited on quartz.

[b] SiI_4 decomposed at 1200°C.

Eight recrystallizations from two kinds of heptane resulted in the second sample of Table IV which shows that the purity of the tetraiodide is a function of the number of recrystallizations. This sample had the same treatment as No. 4 of Table V except for the distillation step in the latter which seems to have removed the n-type impurity. Superficially the n-type sample appears purer because it has about 4×10^{13} excess carriers per cubic centimeter, while the distilled p-type sample has approximately 7×10^{13} excess carriers. Actually, the n-type sample might have as much as 11×10^{13} n-type carriers of which 7×10^{13} are compensated by p-type carriers.

Table V. Electrical properties of single crystals of iodide silicon prepared from recrystallized and distilled silicon tetraiodide[a]

Sample No.	Type	Resistivity, ohm-cm	Lifetime of minority carriers, μsec
	35 g lots of Si; n-heptane and commercial heptane as solvents:		
1[b, f]	p	420-700-1700	
2[d]	p	150-135-680	
3[c]	n	170-255-220	2000-2500
4[e]	p	200-80	250-75
	200 g lots of Si; n-heptane as solvent:		
5	n	75-30	
6	n	150-140	300-500 (seed end)
7	p	450-180	250-150 (middle-sprout)
8	p	250-50	750-300
	200 g lots of Si; benzene as a solvent:		
9	p	650-425-550	280-230 (seed-middle)
10	p	245-85	110-25

[a] SiI_4 made from 99.8% Electromet Si, recrystallized twice except where noted, distilled in 12 plate quartz column, and decomposed on quartz.

[b] Normal heptane used as solvent.

[c] Commercial heptane used as solvent.

[d] Distilled n-heptane used as solvent.

[e] Recrystallized 2X from commercial heptane, 6X from n-heptane.

[f] Quartz flask used for recrystallization.

If this latter picture is correct, the p-type distilled sample really is the purer, of course.

Iodide Silicon Made from Recrystallized and Distilled Silicon Tetraiodide

Table V contains data for experiments in which two recrystallizations were combined with distillation in a 12 plate quartz column as the purification steps. Comparing these results with those of Table II it is clear that two recrystallizations are exerting a very profound effect on the quality of silicon produced. Apparently the main function of recrystallization is the removal of n-type impurities.

In all but one of the experiments Pyrex flasks were used for the recrystallizations. As the next section shows there is some reason to be concerned about the extraction of impurities from Pyrex, so one set of the recrystallizations was performed in quartz. Sample 1 shows that no marked improvement over other samples was realized by this treatment.

The solvents used might also place a limit on the purification of the tetraiodide. For this reason the n-heptane for sample 2 was carefully distilled before use, but no decrease in impurity content was detected.

Since increasing the number of recrystallizations had improved the quality when this was the sole purification used (cf. Table IV), eight recrystallizations were combined with a distillation for sample 4 for Table V. Apparently two recrystallizations are as effective as more when combined with distillation because sample 4 showed no improvement.

One rather serious criticism of the first three samples of Table V is that they are obviously compensated because the resistivities tend to increase in some portion of the crystal proceeding from seed end to sprout (the portion which freezes last). This difficulty was rather common for the smaller size lots prepared, but it seemed to resolve itself in the larger batches. It may simply reflect a somewhat improved operating efficiency in the larger distillation column.

It was shown that, with very careful preparation of high resistivity crystals, boron contamination from the crucible amounted to only 2 to 3 x 10^{13} atoms/cc of silicon (14, 13). This corresponds so closely to the better resistivities for p-type crystals that contamination from the crucible may limit the results achieved for many crystals of this work. [Data for crystals with higher resistivities, however, are contained in a paper by Herrick and Krieble (15).]

In any event the chief impurity left in our best p-type samples is probably boron. If this assumption is correct, the best sample of Table V has at least 4 boron atoms per ten billion silicon atoms, which is a decrease in the boron content by a factor slightly greater than 4000 compared to the original silicon and represents only a modest improvement over distillation alone for purification.

Iodide Silicon Made from Silicon Tetraiodide Distilled in Pyrex

The distillation column for this work was a Pyrex duplicate of the larger of our quartz columns.

Table VI. Electrical properties of single crystals of iodide silicon prepared from silicon tetraiodide distilled in Pyrex[a]

Sample No.	Type	Resistivity, ohm-cm	Lifetime of minority carriers, μsec
	Recrystallized samples:		
1[b]	p outside n core	3000-120 not measured	
2[c]	p outside n core	1200-1800-25 not measured	
3[d]	p outside n core	2200-3500-250 11-140-35	
	Zone melted samples:		
4[e]	p	125-46	150 (seed end)
5[e, f]	p	200-50	100-10

[a] 12 plate Pyrex still used for all samples

[b] Recrystallized 2X from toluene.

[c] Recrystallized 2X from commercial heptane; decomposition apparatus broke at 800°C exposing sample to air; etched 12% from sample used to grow crystal.

[d] Recrystallized 2X from n-heptane; sample exposed to air at 400°C when decomposition apparatus broke.

[e] No recrystallization step used; Si zone melted with 5 zones.

[f] SiI_4 recovered from first and third cuts of previous distillations.

The complex pattern of electrical resistivities observed in the first three samples of Table VI is probably caused by the presence of traces of both donor and acceptor impurities which segregate at differing rates from liquid silicon as it circulates by the growing crystal to produce compensated p-type crystals near the surface with n-type cores of much lower resistivity. Toluene has not been thoroughly investigated as a solvent for silicon tetraiodide in this work, and, as the notes indicate, difficulties were experienced in handling the other two samples. A single crystal could not be grown from sample 2 before it was etched. In spite of these difficulties we believe that these data are characteristic of iodide silicon made from Pyrex-distilled tetraiodide.

Samples 4 and 5 were zone melted[a] after their preparation from silicon tetraiodide that was purified by distillation in the Pyrex column. This treatment effectively removes n-type impurities and reveals the amount of boron present as a p-type impurity. While the resistivities of these samples are not the best that have been obtained in this work, it is clear that the extraction of boron from Pyrex glass is not a serious problem even though boric oxide is a major constituent of this kind of glass.

Since the first three samples exhibited a kind of compensation which was not observed in comparable samples prepared from tetraiodide distilled in quartz equipment, it seems that the extraction of an n-type impurity from Pyrex is the real problem. Green and Kafalas (12) have shown that germanium tetrachloride can extract arsenic from Pyrex glass, and they have also explained the earlier results of Cluley and Chirnside (16) who found that Pyrex equipment was not suitable for the removal of traces of arsenic even though reasonably effective for relatively large amounts. Assuming that the arsenic is present as the pentoxide in Pyrex, thermodynamic estimates

[a] W. C. Dash performed these operations and evaluated the material.

of the free energy of extraction of arsenic as the triiodide are more favorable for silicon tetraiodide than for germanium tetrachloride. (Of course, it can also be estimated that the free energy for the extraction of boron as the triiodide is favorable.) While the present work does not unequivocally demonstrate the extraction of an n-type impurity from Pyrex, we feel that this is the real problem rather than the extraction of boron even though this may indeed seem like a paradox.

In view of these comments on the use of Pyrex glass for distillation, the use of Pyrex recrystallizing equipment may seem questionable. The best results were obtained when recrystallization was followed by distillation of the silicon tetraiodide, and all that was demanded of recrystallization is an upgrading of the quality of silicon tetraiodide rather than providing the ultimate in purity. If recrystallization alone were to be used for purification it might be desirable to use quartz equipment and specially purified solvents.

Iodide Silicon Made from Silicon Tetraiodide Purified by Zone Melting

The zone melting equipment differs from the kind described by Rubin and Moates (3). The main quartz tube, 2⅜ in. OD by 36 in. long, was held in a horizontal position and was not quite half filled by 2.5 kg of silicon tetraiodide. Alternate freezing and thawing caused no trouble with tube breakage. The rate of zone travel varied between 0.68 and 1.14 iph, but most of the time it was kept very nearly at 0.80 iph. The gas space above the iodide was continuously flushed with 40-50 cc/min of hydrogen.

After ten zones had passed down the tube (two passes of a 5 element heating unit), most of the first 40% of the silicon tetraiodide was a light clear yellow with a small wedge of salmon pink material towards the middle of the tube. The "impure" end of the tube was salmon pink to red in color, and this portion was removed first by rotating the tube 180° about its long axis, tipping slightly, and melting the impure tetraiodide with an air gas flame. The tube was then tipped in the opposite direction and the "pure" tetraiodide was transferred to the apparatus used for decomposition on quartz.

A single crystal prepared from the product was p-type over its entire length and had the following resistivity profile: (seed end) 20-20-20-20-20-100 (sprout end). The relatively uniform resistivity values indicate that boron is the impurity controlling this property except near the sprout end, where compensation results from the segregation of an n-type impurity.

A rather bad feature of the present equipment is the amount of back diffusion occurring in the gas phase as evidenced by needle-like crystals growing above the surface of the refrozen tetraiodide. Impurities that are more volatile than silicon tetraiodide, such as boron triiodide, would contaminate these needles resulting in a smaller degree of purification than actually realized by the zone melting.

In spite of the limitations of the equipment used in this work, the purification achieved is impressive. The n-type impurities have been effectively eliminated, and the boron content has been reduced by a factor of approximately 130 since 20 ohm-cm corresponds to about 1.3 boron atoms per hundred million silicon atoms. If the same ratio continued for ten additional zone passes, the rejection of boron would be impressive indeed.

According to Pfann (17), the boron content will have reached some equilibrium distribution after a sufficient number of zones have passed through a bar of tetraiodide, depending on its distribution coefficient and the ratio of zone length to bar length. In our equipment the zones were approximately one tenth as long as the quartz tube. Rubin, Moates, and Weiner (3) have given two figures for the distribution coefficient of boron in a silicon tetraiodide matrix: 0.16 ±0.07 for the boron contained in a sample of crude tetraiodide, and 0.42 ±0.22 for a boron triiodide doped sample. At equilibrium, zone melting would reduce the average boron content of the first 40% of the bar by a factor 2.3×10^7 for the first coefficient, and 4.1×10^8 for the second. There is room for a modest amount of improvement or a really significant improvement depending, apparently, on the chemical species containing the boron.

It is interesting, although perhaps superficial, that both recrystallization from solvents and zone melting seem to be particularly effective in removing n-type impurity iodides from silicon tetraiodide.

Acknowledgments

The author is particularly indebted to Dr. C. B. Collins and Dr. F. H. Horn for the preparation of single crystals of silicon, for the measurement and interpretation of the electrical properties, and much valued discussion. Mr. L. C. Landauer and Miss J. M. Binkowski prepared many of the samples of silicon.

Manuscript received April 3, 1959. This paper was prepared for delivery before the New York Meeting, April 28-May 1, 1958.

Any discussion of this paper will appear in a Discussion Section to be published in the June 1960 JOURNAL.

REFERENCES

1. F. B. Litton and H. C. Andersen, *This Journal*, **101**, 287 (1954).
2. Gustav Szekely, *ibid.*, **104**, 663 (1957).
3. B. Rubin, G. H. Moates, and J. R. Weiner, *ibid.*, **104**, 656 (1957).
4. J. Czochralski, *Z. Physik Chem.*, **92**, 219 (1917).
5. F. J. Morin and J. P. Maita, *Phys. Rev.*, **96**, 28 (1954).
6. P. P. Debye and T. Kohane, *ibid.*, **94**, 724 (1954).
7. R. L. Watters and G. W. Ludwig, *J. Appl. Phys.*, **27**, 489 (1956).
8. G. W. Ludwig and R. L. Watters, *Phys. Rev.*, **101**, 1699 (1956).
9. J. A. Burton, *Physica*, **20**, 845 (1954).
10. J. A. James and D. H. Richards, *Nature*, **177**, 1230 (1956).
11. Analysis of Bureau of Standards Sample No. 57, Silicon.
12. M. Green and J. A. Kafalas, *J. Chem. Soc.*, **1955**, 1604.
13. N. B. Hannay, Recent Advances in Silicon, pp. 6-7, chapter in "Progress in Semiconductors," Heywood and Co., Ltd., London (1956).
14. C. B. Collins, Private communication.
15. C. S. Herrick and J. G. Krieble, To be published, *This Journal*.
16. H. J. Cluley and R. C. Chirnside, *J. Chem. Soc.*, **1952**, 2275.
17. W. G. Pfann, *Trans. AIME, J. Metals*, **4**, 747 (1952).

Rare Earth Compound Semiconductors

J. F. Miller, F. J. Reid, and R. C. Himes

Battelle Memorial Institute, Columbus, Ohio

ABSTRACT

Selenides of La, Er, and Y, and tellurides of La, Er, Gd, and Y were prepared by direct reaction of the elements. Measured electrical characteristics indicate semiconducting behavior, with the possibility that a wide range of properties can be obtained within these series of rare earth compounds. Observed room-temperature resistivities, for example, ranged from about 10^{-4} ohm-cm for La_2Te_3 and ErSe to the insulator range for Y_2Se_3. All the compounds prepared possess high melting points (1400°-2000°C) and exhibit good thermal stability. The dissociation pressure of Gd_2Te_3 at its melting point appears to be as low as 0.01 atm.

Semiconductors with interesting and potentially useful properties have been found within a number of classes of intermetallic compounds. Several of these groups of compounds, notably the III-V's and II-VI's, are currently receiving considerable attention. This is the initial report on a study which is concerned with the electrical properties of a group of compounds which has, to date, received little attention—namely, binary intermetallic compounds containing a rare-earth element. Specifically, this paper deals with the preparation and observed electrical properties of the selenides of La, Er, and Y, and the tellurides of La, Er, Gd, and Y.

Preparation

The compounds were first prepared in granular form by reacting selenium or tellurium vapor with filings of the rare earth metal at moderate temperatures. The advantage of increased reaction rate was thought, for these initial experiments, to overcome any disadvantage of contamination through filing. Reactions were carried out in sealed, evacuated Vycor tubes, which were designed so as to maintain physical separation of the liquid selenium or tellurium and the solid rare earth metal. This measure was taken to preclude the possibility of the rapid, violent reaction which takes place on direct contact of the condensed phases. To carry out the desired reaction, vapor of the metalloid was distilled over the rare earth metal filings; temperature was increased slowly to 950°C over a period of about 24 hr and was held at this level for an additional 72 hr.

The granular reaction product was then melted down and cast into ingots to obtain bulk specimens which were suitable for electrical evaluation. The melting was done in tantalum or graphite containers under argon at 1 atm pressure; induction heating was used. Although relatively high temperatures were involved, residence times at temperature were short. Under these conditions, there was little evidence of reaction between the compounds and properly outgassed tantalum (i.e., tantalum which had been outgassed above 1600°C in a hard vacuum). Graphite also appeared to be satisfactory as a container material.

Procedures discussed to this point were used for initial preparations of the compounds. Additional studies concerned with more refined preparation and characterization of the compounds are in progress. Initial work of this type was done with gadolinium telluride. Table II, discussed in greater detail later, includes data for a series of specimens of this compound taken from ingots which were prepared under various conditions noted in the table. The first of these specimens was taken from an ingot which was prepared by distilling tellurium vapor over molten gadolinium metal. Since temperature of the protective quartz envelope was not controlled, the pressure of tellurium vapor prevailing during this initial experiment is not known. The remaining specimens were cut from ingots which were cast by carefully controlled directional freezing under various known pressures of tellurium vapor. Freezing rates varying from ½ in. to 1-½ in./hr were used. In this range, crystallization rate did not appear to have a significant effect on properties of the compound.

Whereas tantalum apparently had been satisfactory as a container material in which simple melting of the compounds could be carried out, the tantalum boats were attacked severely during the prolonged periods of exposure to tellurium vapor encountered in freezing the ingots directionally. Graphite containers appeared to be more satisfactory for this purpose since they were not attacked noticeably.

Physical Properties

Melting points have been determined for three of the compounds. In making the determinations, specimens were placed in a horizontal cylindrical cavity at a depth equal to 12 times the diameter of the cavity so as to obtain near black-body conditions (1). The specimens were of triangular cross section and were supported by contact of the edges with the wall of the cavity. Incipient melting at the edges produced readily detectable movement of the speci-

Table I. Observed electrical properties (measured at room temperature) rare earth selenides and tellurides

Compound	R_H, cm^3 coul^{-1}	ρ, ohm-cm	μ, cm^2 v^{-1} sec^{-1}	α, μ v deg^{-1}	η, cm^{-3}
La_2Se_3	Negative	0.024	—	—	$\sim 3 \times 10^{19}$
Er_2Se_3	Positive	7.9	—	—	—
ErSe	Negative	1.7×10^{-4}	—	—	$\sim 10^{20}$
Y_2Se_3			(Insulator)		
La_2Te_3	Negative	1.9×10^{-4}	—	−30	$\sim 10^{20}$
Gd_2Te_3	−3.25	0.019	170	−26	2×10^{18}
Gd_2Te_3	+3.3	0.2	17	>+200	2×10^{18}
Er_2Te_3	Negative	1.1×10^{-3}	—	—	$\sim 10^{19}$
Y_2Te_3	−1400	10.0	140	—	4×10^{18}

mens. Temperatures were measured by means of an optical pyrometer and are estimated to have an accuracy of ± 25°C. Values obtained were: 1520°C for the melting point of Er_2Se_3, 1420°C for Gd_2Te_3, and 1525°C for Y_2Te_3. Indirect observations made in the course of the preparative work indicate that melting points for some of the other compounds may be higher, ranging up to about 2000°C.

Thermal conductivity of Gd_2Te_3 has been determined at room temperature by use of the "Z-meter" (2, 3). Values for n- and p-type specimens were found to be 0.026 and 0.023 watts cm^{-1} deg^{-1}, respectively. Since the lattice component of thermal conductivity usually predominates at room temperature for materials of this type, the nearly identical values are to be expected.

Electrical Properties

Table I presents a tabulation of electrical properties observed for some of the selenides and tellurides in their initial preparations as polycrystalline, cast ingots. It will be noted that resistivities for the sesquiselenides are somewhat higher than those for the corresponding tellurides. In general, resistivities, in both classes of compounds, increase with progression through the rare earth series, the yttrium compounds falling at the end.

The resistivity of Y_2Se_3 appears to be in the insulator range. In attempts to eliminate possible high contact resistance, a number of different methods of contacting specimens of this compound were used. Various techniques explored utilized pressure contacts with probes of Pt, W, Mo, Cu, Fe, Al; contacts of conducting silver paint; leads of Cu, W, Fe applied by spot welding; solder contacts of Pb-Sn, In, Al, Ga applied with various fluxes by both normal and ultrasonic soldering techniques. However, under applied potentials up to 60 v, there was in no instance a detectable current through the sample.

At the other extreme, resistivity for the monoselenide of erbium was found to be quite low. Low resistivities would be expected for the 1:1 compounds if only two of the valence electrons of the rare-earth atom are involved in the chemical bonds, leaving the third free to act as a charge carrier with rather low activation energy. Iandelli (4) also concluded that this was the case through analysis of structures and interatomic spacings for the cerium-group compounds.

Seebeck coefficients were measured over a range of temperatures for specimens of Gd_2Te_3 and La_2Te_3 and were found to remain constant up to 450° and 525°C, respectively, the highest temperatures to which measurements were extended. High-temperature thermoelectric properties of these rare earth compounds may be of practical interest and are being investigated currently.

It will be noted that carrier concentrations for most of the specimens are high. In synthesizing the compounds, high-purity selenium and tellurium were used (i.e., better than 99.99%). However, purity of available rare earth metals is relatively low (i.e., 99+%). It is therefore probable that carriers, other than those resulting from excess of one of the component elements, were introduced principally as impurities present in the rare earth metals or as contaminants incorporated during synthesis of the compounds.

Electrical data for specimens of Gd_2Te_3 from ingots cast under various pressures of tellurium vapor (Table II) indicate that, if evolution of tellurium is permitted (specimens 67, 88), n-type material is

Table II. Effect of tellurium vapor pressure during casting on electrical properties of Gd_2Te_3

Specimen	Tellurium vapor pressure, atm	Container material	R_H, cm^3 coul^{-1}	ρ, ohm-cm	μ, cm^2 v^{-1} sec^{-1}	α, μ v deg^{-1}	η, cm^{-3}
9*	?	Tantalum	−3.25	0.019	170	−26	2×10^{18}
67	~0	Tantalum	−0.11	0.0031	35	−84	6×10^{19}
88	~0	Graphite	−0.1	0.0029	30	−70	6×10^{19}
71	0.5	Tantalum	Pos., small	0.091	(Large, numerous voids throughout ingot)		
73	0.2	Tantalum	+0.16	0.028	6	+160	4×10^{19}
74	0.1	Tantalum	Pos., small	0.68	—	+240	$\sim 10^{19}$
75	0.1	Graphite	Pos., small	0.51	—	+190	$\sim 10^{19}$
77	0.01	Graphite	+3.3	0.20	17	>+200	1.9×10^{18}

* Te distilled over Gd at ~1650°C.

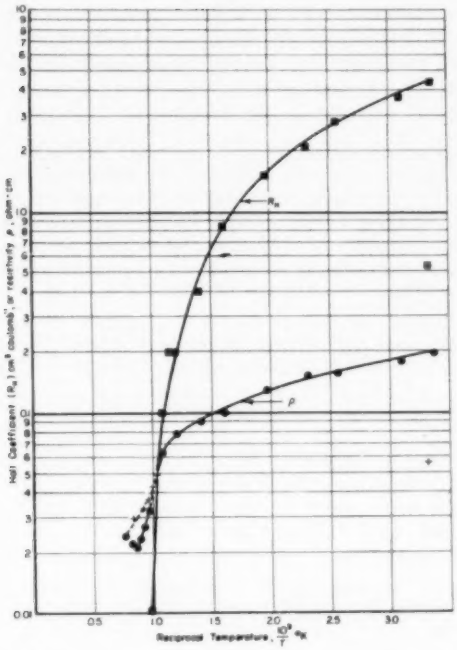

Fig. 1. Resistivity and Hall coefficient as functions of temperature for p-type Gd_2Te_3.

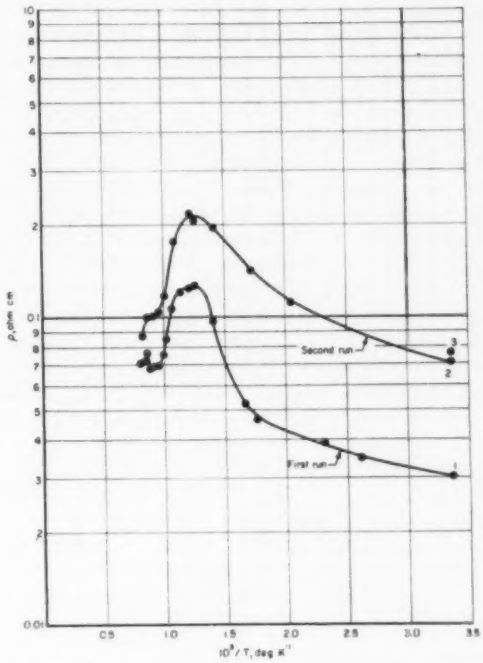

Fig. 2. Resistivity as function of temperature for n-type Gd_2Te_3.

obtained, but in the presence of moderate concentrations of tellerium vapor, (specimens 71-77), p-type material can be cast. However, dissociation pressure of the compound at its melting point appears to be relatively low since it was possible to cast a reasonably good p-type ingot (specimen 77) under only 0.01 atm of tellurium vapor pressure. Similarity of data for specimens from ingots which were cast under similar conditions in tantalum and graphite, (consider specimens 67 and 88, 74 and 75) indicates that any tantalum which may have been taken into solution, as a result of the aforementioned attack, had little effect on electrical properties of the compound at these carrier concentrations.

Figure 1 shows variation of Hall coefficient and resistivity with temperature for a p-type specimen of gadolinium telluride. Up to about 875°C, the curves are typical of those for an impure semiconductor. Above this temperature, however, behavior of resistivity is anomalous. As far as could be determined, the Hall coefficient continued to decrease (up to 950°C) and did not change sign. As temperature was decreased, resistivity followed the dotted curve, and room-temperature values for both Hall coefficient and resistivity were found to be lower following the run. (Points indicated by crosses, for both Hall coefficient and resistivity, were taken as temperature was decreased.) The variation of Hall mobility with temperature for this p-type specimen suggests that impurity scattering is important up to relatively high temperatures (i.e., at temperatures as high as several hundred degrees centigrade).

Figure 2 shows resistivity as a function of temperature for an n-type specimen of gadolinium telluride. Again, what appears to be typical behavior for an impure semiconductor was observed up to about 750°C, and anomalous variation of resistivity with temperature was noted through the range of higher temperatures. An irreversible heat-treating effect was also noted. Room-temperature resistivity was found to be considerably higher (point 2, Fig. 2) after the first temperature run. With the second

Table III. Heat-treatment of Gd_2Te_3 specimens*

Specimen	Heat treatment**	ρ, ohm-cm	μ, cm^2 v^{-1} sec^{-1}	η, cm^{-3}
67-1, n-type	None	0.0089	16	4×10^{19}
	2 hr at 950°C in vacuum	0.028	10	2.2×10^{19}
9, n-type	None	0.019	170	2×10^{19}
	120°C in vacuum†	0.03		
	950°C in vacuum†	0.072		
	950°C in vacuum†	0.076		
77, p-type	None	0.20	17	1.9×10^{18}
	950°C in vacuum†	0.056	10	1×10^{19}
75, p-type	None	0.51		$\sim 10^{19}$
	2 hr at 950°C in vacuum	0.067	6	1.7×10^{19}
73, p-type	None	0.027	6	4×10^{19}
	740°C in vacuum†	0.031	6	3×10^{19}
	Quenched after 2 hr at 950°C	0.032	6	3.5×10^{19}
	2 hr at 950°C in vacuum	0.037	4	4.2×10^{19}

* Data presented are from room-temperature measurements.

** All specimens cooled slowly except as otherwise noted.

† Heat treatment was that experienced in course of electrical measurements. Temperature given is the maximum attained.

temperature run, the specimen appeared to be approaching a stable condition, as is indicated by the much less pronounced irregularity in variation of resistivity with temperature above 700°C, and the fact that room-temperature resistivity (point 3) returned to approximately its initial value (point 2).

The effects of heat treatment on electrical properties of a number of specimens of gadolinium telluride were studied in an attempt to explain the observed behavior. Data for the heat-treated specimens, which are presented in Table III, indicate that after a sufficiently long period of heat treatment, the samples approach a stable condition.

Because of conflicts in the data (e.g., changes in carrier concentrations vs. changes in mobilities), it is not possible to reach a firm conclusion concerning the nature of heat treating effects. However, it may be seen that for the n-type specimens resistivity is increased and carrier concentration is decreased by heat treatment in vacuum, and for the p-type specimens resistivity is decreased and carrier concentration is increased by the same treatment. Such changes are consistent with loss of n-type impurities. This is a possibility since spectrographic analyses show that relatively high concentrations of Ca, Mg, Fe, Ni, Ta, Si, and Al are present in the specimens.[1] Since tellurium has already been shown to give p-type doping, loss of tellurium is not suspect as a cause for the changes observed.

Manuscript received June 15, 1959. This paper was prepared for delivery before the Philadelphia Meeting, May 3-7, 1959. This investigation was supported by the Rare-Earth Research Group (Davison Chemical Co., Union Carbide Metals Co., Heavy Minerals Co., Lindsay Chemical Div. of American Potash and Chemical Corp., Mallinckrodt Chemical Works, Rare Earths and Thorium Div. of Michigan Chemical Corp., and Molybdenum Corp. of America).

Any discussion of this paper will appear in a Discussion Section to be published in the June 1960 JOURNAL.

REFERENCES

1. I. E. Campbell, "High Temperature Technology," John Wiley & Sons, Inc., New York (1956).
2. T. C. Harman, *J. Appl. Phys.*, **29**, 1373 (1958).
3. T. C. Harman, J. H. Cahn, and M. J. Logan, To be published, *J. Appl. Phys.*
4. A. Iandelli, *Gazz. Chim. Ital.*, **85**, 881 (1955).

[1] Per cent by weight detected: 0:01 Ca, 0.05 Mg, 0.01 Fe, 0.001 Ni, <0.05-5.0 Ta, 0.001 Si, 0.005-0.01 Al.

Diffusion of Cerium and Zirconium in Molten Uranium

Tennyson Smith

Atomics International, A Division of North American Aviation Incorporated, Canoga Park, California

ABSTRACT

Coefficients for the diffusion of cerium in molten uranium have been measured over the temperature range 1170°-1480°C. An equation relating the diffusion coefficient with temperature is: $D = 4.5 \times 10^{-3}\, e - 11{,}000/RT$. At 1200°C the diffusion coefficient for cerium in uranium is $(1.00 \pm 0.17) \times 10^{-4}$ cm²/sec. An estimate of the coefficient of diffusion for zirconium in uranium at 1270°C is $(1.9 \pm 0.9) \times 10^{-4}$ cm²/sec. A discussion of experimental errors involved in measuring diffusion coefficients at high temperatures is given.

A study has been made of the reactions and mechanism involved in the oxide-drossing of fission products from uranium. The oxide-drossing process is a pyrometallurgical method of reprocessing spent uranium with an oxide such as urania, zirconia, or alumina. Those fission products that are more stable than the oxide used are removed selectively from the melt. Elements such as the rare earths react with the oxide, while elements such as cesium, iodine, and the rare gases volatize off.

The diffusion of cerium and zirconium in molten uranium was studied in a preliminary investigation. Cerium and zirconium were selected as representatives of the lanthanide series and high melting elements, respectively. Diffusion characteristics of fission products in uranium are of interest since the mass transfer of these elements to the oxide surface is the first step in the extraction mechanism. A knowledge of the diffusion coefficient for these elements in molten uranium will help determine the slow step in the mechanism.

Most of the studies on the diffusion of metals in molten metals have been done with low melting metals or alloys (300°-700°C) (1). Diffusion coefficients generally range from about 2×10^{-5} to 7×10^{-5} cm² sec^{-1}, which is close to that found for diffusion in other liquids.

At higher temperatures (between 1000° and 1700°C) only a few experiments have been reported, and the diffusion coefficients cover a wider range. Paschke and Hautmann (2) obtained 2.4×10^{-5} cm² sec^{-1} and 10.8×10^{-5} cm² sec^{-1} for the diffusion of silicon in molten iron at 1480° and 1560°C, respectively, and a value of 1.2×10^{-4} cm² sec^{-1} for manganese in iron in the same temperature range. Holbrook, Furnas, and Joseph (3) studied the diffusion of sulfur, manganese, phosphorus, silicon, and carbon in molten iron over the temperature range 1200°-1700°C. The average diffusion coefficients for silicon, phosphorus, sulfur, and manganese was about 1×10^{-4} cm² sec^{-1} in this temperature range. The variation of the diffusion coefficient with tem-

perature was less than the experimental error. They found the diffusion coefficient for carbon in liquid iron to be much larger, about 6 x 10^{-4} cm^2 sec^{-1}. Penetration curves did not correspond well with ideal diffusion curves, probably because of experimental errors such as convection. It is difficult to avoid this problem completely.

A recent paper by Morgan and Kitchener (4) describes an experiment to determine the diffusion coefficients of cobalt and carbon in iron. They obtained D values of 5.5 x 10^{-5} cm^2 sec^{-1} for cobalt at 1638°C and 4.3 to 6.7 x 10^{-5} cm^2 sec^{-1} for the diffusion of carbon in iron, depending on the carbon concentration and temperature. They took particular interest in eliminating the problem of convection.

Experiments to measure diffusion coefficients in molten metals generally have been carried out using one of the three techniques described by Niwa, *et al.* (5). Their third method, used by Kitchener and Morgan (4), was to place a pure metal or an alloy containing the diffusate next to a long, narrow column of solvent. Samples are taken along the length of the metal column after it had been to temperature for a specific time. Morgan and Kitchener point out that this method allows detection of deviations from Fick's law due to convection, etc. This same technique was used in the study reported here, except that metal columns of the order of 7 mm rather than 2 mm diameter were used in order to obtain larger samples for analysis. The larger diameter allowed convection at the higher temperatures which increased the uncertainty of the results at these temperatures (1400°-1480°C).

This paper reports experiments to measure the diffusion coefficient of cerium in molten uranium over the temperature range 1170°-1480°C. An estimate of the diffusion coefficient for zirconium in molten uranium is also given.

Experimental

A slug of natural uranium was machined to fit the crucible, then etched clean with dilute HNO_3. The desired amount of cleaned cerium or Zr-U alloy was placed on top of the uranium, and the unit was placed in the vacuum furnace tube (Fig. 1). The McDanel ceramic tube could be evacuated to 0.1 μ, filled with an inert gas, then placed in a Globar furnace. Three thermocouples were placed in the system so that the temperature could be

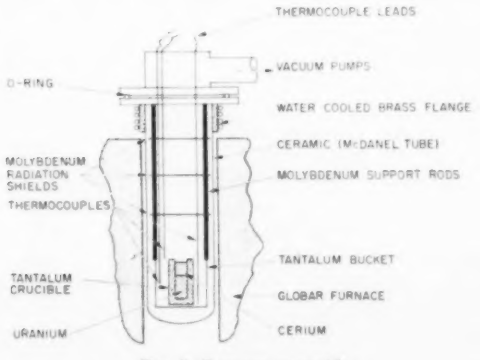

Fig. 1. Furnace assembly

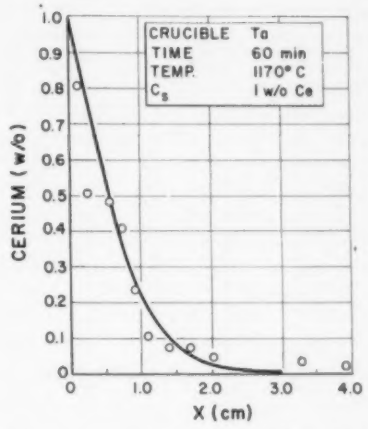

Fig. 2. Penetration curve: cerium diffusion into molten uranium at 1170°C. The solid line is based on an average value of D = 1 x 10^{-4} cm^2 sec^{-1}.

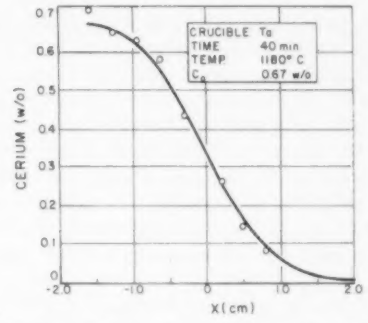

Fig. 3. Cerium diffusion into molten uranium from a Ce-U alloy at 1180°C. The solid line is based on an average value of D = 0.95 x 10^{-4} cm^2 sec^{-1}.

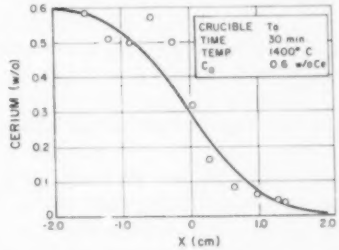

Fig. 4. Penetration curve: cerium diffusion into molten uranium from a Ce-U alloy at 1400°C. The solid line is based on an average value of D = 1.98 x 10^{-4} cm^2 sec^{-1}.

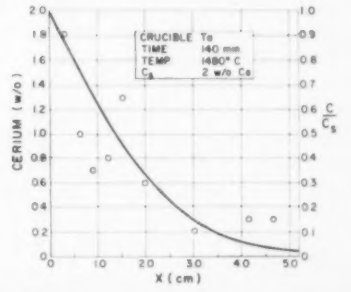

Fig. 5. Penetration curve: cerium diffusion from pure cerium into molten uranium at 1480°C. The solid line is based on an average value of D = 2.54 x 10^{-4} cm^2 sec^{-1}. Scatter of experimental points shows the effect of convection.

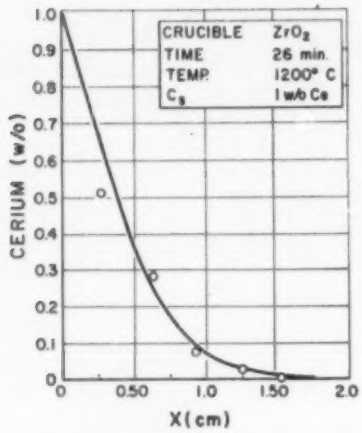

Fig. 6. Cerium diffusion into molten uranium (1200° C) in a ZrO_2 crucible. The solid line is based on an average value of $D = 1 \times 10^{-4}$ cm^2 sec^{-1}.

measured at various points with respect to the sample. The temperature was controlled with a temperature controller and recorded on a millivolt recorder.

In each experiment, the system was first evacuated to about 0.1 μ, then flushed and filled with argon to 1 atm of pressure. The argon was purified by passing it through a uranium trap held at about 600°C. The furnace was brought to the desired temperature, held at temperature for the experiment, then allowed to cool as fast as possible without breaking the ceramic tube. The time to heat the sample from the melting point of uranium to temperature was 3 or 4 min, and the time required to cool the sample below the freezing point of uranium was not more than 4 or 5 min.

Three different crucibles were used in the experiments. A tantalum crucible, 1.5 cm OD by 9 cm high, with a hole 0.75 cm ID and 7.5 cm deep, was used for the experiments reported in Fig. 2, 3, 4, and 5. In two of these experiments (Figs. 3 and 4) a 3 cm slug of uranium-cerium alloy (0.67 w/o, Fig. 3; 0.6 w/o, Fig. 4) was placed on top of a 3 cm slug of pure uranium. In the other two experiments, (Fig. 2 and 5) a thin layer of pure cerium about 2 mm thick was placed on top of a 6 cm slug of pure uranium. The slug of uranium was counter-sunk at the top, with a shallow hole, leaving thin uranium sides and just deep enough to contain the molten cerium when it melted. This was done so that the molten cerium would not run down the sides of the uranium before it melted (mp:Ce, 793°C; U,1133°C) (6).

For the experiment which corresponds to Fig. 6, the uranium was placed in a zirconia crucible approximately 1.5 cm OD x 5.5 cm high, with a hole 1 cm ID and 5 cm deep. In this experiment, pure cerium metal was placed on top of the uranium in the manner mentioned above, and the system was held at 1200°C for 26 min.

Figure 7 gives the results of an experiment carried out in a tungsten crucible at 1350°C for 155 min. Again, the pure cerium metal was placed on the counter-sunk uranium slug. The approximate

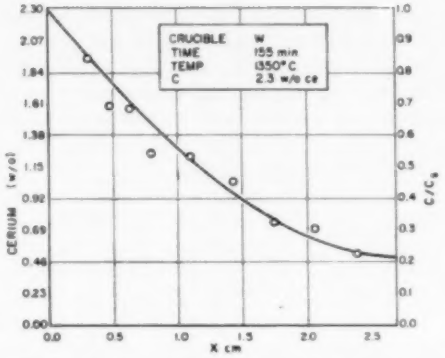

Fig. 7. Penetration curve: cerium diffusing into molten uranium at 1350°C from pure cerium. The solid line is based on an average value of $D = 1.46 \times 10^{-4}$ cm^2 sec^{-1}. The reflection principle was used.

dimensions of the tungsten crucible were: 2.5 cm OD by 4 cm high, with a hole 1.4 cm ID and 3.5 cm deep.

One experiment was conducted with a 3% zirconium-uranium alloy placed on top of pure uranium in the tantalum crucible. The system was held at 1270°C for 40 min.

After each experiment, samples were taken from the uranium at known distances from the top of the slug by drilling lengthwise through the center of the ingot. The samples were washed and dried, then weighed and analyzed. The higher concentrations of cerium were analyzed volumetrically (7) and the low concentrations calorimetrically (8). In two experiments, the cerium had been irradiated, and analysis was accomplished with a gamma-ray spectrometer after extracting the uranium with tributyl phosphate. Analyses for zirconium in uranium was made gravimetrically (9).

Errors and Uncertainties

When taking samples for analysis, there is an uncertainty as to the exact position of the interface due to its shape. The shape of the interface is a function of the interfacial tensions between cerium, uranium, and the crucible wall. Since the interface is not flat, there will be some samples at the interface that will cut both phases simultaneously and will give invalid results.

The uncertainty of the position of the interface generates an error in the value of X, which is increasingly significant as X approaches zero. This is shown by the equation: per cent error (in D) $= 100 (X_1^2 - X^2)/X^2$ where X is the true distance and X_1 is the apparent distance. In the present work, the uncertainty in X is approximately 0.2 cm; consequently, at $X = 0.2$ cm and $X_1 = 0.4$ cm, the per cent error is 300, while at $X = 4$ cm and $X_1 = 3.8$ cm, the per cent error is 10. This same effect is seen for uncertainties in λ (note Eq. [1] below) where λ is small, since $D \propto 1/\lambda^2$. Errors in λ result from uncertainties in the measured variables C or C_s since λ is obtained from a plot of C/C_s vs. λ. C is the concentration of the diffusate in the solvent at any specified time, and C_s is the constant concentration in the solvent at the interface between the solvent and the

Table I. Effect of an uncertainty in C_s on D with distance from the interface*

C_s, wt % Ce	X, cm	Ce, wt %	C/C_s	2	D, cm²/sec x 10^{-4}	% Error
1.1	0.12	0.81	0.737	0.48	0.18	45.5
0.9	0.12	0.81	0.900	0.20	1.00	20.0
1.1	0.59	0.49	0.445	1.05	0.90	10.0
0.9	0.59	0.49	0.545	0.86	1.35	35.0
1.1	1.39	0.07	0.064	2.63	0.77	6.1
0.9	1.39	0.07	0.078	2.49	0.87	6.1
1.1	2.02	0.04	0.036	3.00	1.26	2.3
0.9	2.02	0.04	0.044	2.88	1.37	6.2
1.1	2.30	0.03	0.027	3.15	3.00	32.0
0.9	2.30	0.03	0.033	2.52	4.77	54.0

* From data shown in Fig. 2.

diffusate. Small discrepancies in C or C_s cause increasingly larger uncertainties in λ as λ increases; therefore, large inherent errors are to be expected at small and at large values of X. This is clearly shown in Table I where the per cent error is given as a function of X for a difference of 0.2% in C_s. The most accurate values of D are those calculated for X between 1 and 2 cm.

The residuals for the values of D falling within the above mentioned band are considered random; only the values of D having random residuals are used in the determination of the average value of D.

The per cent error recorded in Table I is based on the assumption that the correct value for C_s is 1%.

It is well known that D, the diffusion coefficient, is rarely a constant with change in concentration; however, it does approach a constant value at low concentrations. Since the concentrations in these experiments were low, the assumption of D constant is good.

Although the uranium and the cerium were cleaned of oxide before each experiment, and the experiments were made in a purified argon atmosphere, it is quite possible that a thin film of oxide existed between the uranium and the cerium in the U-Ce couple. If the film was very thin or if no film existed, the value of C_s should be just the solubility of cerium in uranium at the temperature of the experiment. However, if the oxide film was thick enough to provide a resistance to the diffusion of cerium to the uranium surface, then the value of C_s might be something less than the solubility of cerium in uranium. With or without the oxide, correct values of the diffusion coefficients will be obtained as long as C_s is constant and can be measured.

The curve C/C_s vs. 2λ becomes linear as 2λ approaches zero. The best values of C_s, then, are those obtained by extrapolating the experimental curves of per cent cerium vs. X back to the interface, since $X \propto \lambda$, (note Fig. 2, 5, 6, and 7) this is the manner in which values of C_s were obtained for the calculations.

For the experiments in which an alloy was used instead of pure cerium (Fig. 3 and 4) only values of C_o, the initial concentration of the alloy, was needed rather than C_s. Values of C_s were found before the diffusion experiments were made by analyzing a number of samples from the alloy.

All but two experiments were made in a tantalum crucible. Tantalum is slightly soluble in uranium, and it is to be expected that some interference will result from its presence. Since the two experiments, in which a zirconia crucible and a tungsten crucible were used, gave results consistent with those of the experiments in which tantalum crucibles were used, the effect of the presence of tantalum can be considered to be within the experimental error. It is noted that the use of zirconia crucible will also cause interference, because some of the cerium reacts with the ZrO_2 at the surface. Every known container material would interfere to some extent. The best crucible would be one made of CeO_2, but this was not available for these experiments.

Discussion and Results

Results for diffusion experiments are shown in Fig. 2 through 7 as penetration curves for cerium in molten uranium. The weight per cent cerium plotted as open circles at various distances, X, from the cerium-uranium interface are average values for the concentration of cerium at that position. The length X is the distance from the cerium uranium interface to the center of the sample that was taken for analysis. The solid lines in the graphs are theoretical penetration curves based on average values of the diffusion coefficients.

Diffusion equations.—Diffusion coefficients were measured under three different experimental conditions requiring three separate solutions of Fick's equation.

Case 1.—The simplest experimental situation, that of nonsteady-state diffusion in a semi-infinite media, consisted of two elements in contact, having a sharp boundary between them initially, contained in a cylinder having impermeable sides. Consider only half of such a couple; the dimensions in the direction of diffusion must be large compared to the distance over which measurable composition change occurs during the experiment. The initial concentration of the diffusing element in the semi-infinite media must be uniform, and the surface must be brought instantaneously to some concentration C_s which remains constant during the experiment.

These boundary conditions may be written:

$$C = C_o \text{ at } t = 0 \text{ and } 0 < X < \infty$$

$$C = C_s \text{ at } X = 0 \text{ and } 0 < t < \infty,$$

where C is the concentration of the diffusing species at time, t, C_o is the initial homogeneous concentration of the diffusing species, and X is the distance from the interface in the direction of diffusion.

The solution (10) of Fick's second law corresponding to these boundary conditions and for a constant diffusion coefficient, D, is

$$\frac{C_s - C}{C_s - C_o} = \frac{2}{\sqrt{\pi}} \int_0^{X/(2\sqrt{Dt})} e^{-\lambda^2} d\lambda \qquad [1]$$

where λ is an integration variable. The term on the right is the normalized probability integral or the error function, (erf); its compliment, 1-erf, is known as erfc and is equal to $(C-C_o)/(C_s-C_o)$. Values of

Table II. Variation, with temperature, of the coefficient of diffusion for cerium in uranium

T, °C	$10^4/T$, °K	D (avg), cm² sec⁻¹ x 10⁶	Avg error x 10⁶	−LnD	Fig. No.
1170	6.93	1.00	0.21	9.20	2
1180	6.88	0.95	0.13	9.25	3
1200	6.79	1.00	0.17	9.20	4
1350	6.16	1.46	0.15	8.80	5
1400	5.98	1.98	0.73	8.52	6
1480	5.70	2.50	1.60	8.20	7

$(C-C_o)/(C_s-C_o)$ vs. 2λ are tabulated (10) and were used to determine the diffusion coefficients recorded in Tables I and II.

Case 1 is useful for experiments with low melting metals such as cerium and lanthanum where the pure metal is in contact with uranium.

Figures 2, 5, and 6 show penetration curves for cerium in uranium at 1170°, 1200°, and 1480°C, respectively. The experiments for 1170° and 1200°C were made at close to the same temperature but with different types of crucibles, tantalum and zirconia. Both experiments gave an average diffusion coefficient of 1.0×10^{-4} cm² sec⁻¹.

In these experiments, pure cerium was contacted with pure uranium and the data were interpreted as in Case 1.

Case 2.—In order to measure the diffusion coefficients of elements such as Zr, Mo, Y, Nb, and Ru that have high melting points, it is necessary to make alloys of these elements with uranium and measure the diffusion from the alloy into pure uranium. The boundary conditions are: $C = C_o$, $X < 0$; $C = 0$, $X > 0$, and $t = 0$. The solution (10) of Fick's second law for these boundary conditions is

$$C(X,t) = \tfrac{1}{2}\, C_o \operatorname{erfc} \frac{X}{2\sqrt{Dt}} \qquad [2]$$

or, $C/(\tfrac{1}{2}C_o) = \operatorname{erfc} \lambda$, which is identical with the expresssion for C/C_s in Case 1. It is seen, then, that the two processes are the same except that, in the second case, $C_s = \tfrac{1}{2}C_o$. It is interesting to note that at $X = 0$ the concentration remains constant, at $\tfrac{1}{2}C_o$, with time.

In order to evaluate D, the experimental value for C/C_s at X is determined and a corresponding value for 2λ is found from the error function tables, then $D = (1/t)\ (X/2\lambda)^2$.

The data reported in Fig. 3 and 4 for cerium and one experiment with zirconium were interpreted as in Case 2 above; pure uranium was contacted with a U-Ce or U-Zr alloy.

Case 3.—One other case must be considered to interpret the data from the experiment shown in Fig. 7. In this experiment the time period was long enough that at $X = l$ (where l is the distance from the interface to the bottom of the crucible), C was not equal to zero as in Case 1. The boundary conditions are:

$$C = C_s, X = 0; C = 0, t = 0; \text{and } \frac{\partial C}{\partial X} = 0, x = l$$

It becomes necessary to use the principle of reflection. The appropriate solution to Fick's second law can be found in Crank's (10) book on diffusion, if his equation 2.54 (section 2.43) has X replaced by $(1-x)$ and C_o replaced by C_s. The equation becomes:

$$C/C_s = \operatorname{erfc} \frac{X}{2\sqrt{Dt}} + \sum_{n=1}^{\infty} (-1)^n \operatorname{erfc} \frac{2nl+x}{2\sqrt{Dt}} - \operatorname{erfc} \frac{2nl-x}{2\sqrt{Dt}} \qquad [3]$$

This equation reduces to Eq. [1] if only the first term is needed, i.e., where x is small or t is short. Only two terms of this equation are needed to interpret the results in Fig. 7:

$$C/C_s = \operatorname{erfc} \left(\frac{X}{2\sqrt{Dt}}\right) + \operatorname{erfc} \frac{2l-x}{2\sqrt{Dt}} \qquad [4]$$

since the other terms are too small to be significant. Diffusion coefficients for the experiment reported in Fig. 7 were obtained by using the family of curves on page 46 of Crank's book (10).

Temperature Effect

Although an attempt was made to reduce thermal convection by controlling the temperature along the diffusion couple, it appears that convection currents did occur, particularly at the higher temperatures. If one assumes that deviation of the experimental points from the theoretical penetration curves is an indication of convective interference (4), it is seen from Fig. 2 through 7 that convection becomes more of a problem as the temperature increases.

Table II reports the average diffusion coefficients which correspond to Fig. 2 through 7 as a function of temperature. This table also gives the values for the average error and LnD.

It is felt that the diffusion coefficients reported in Table II up to 1350°C are accurate to within the error recorded for two reasons: first, the experimental points fall fairly close to the theoretical penetration curves in Fig. 2, 3, 6, and 7; second, even though the experiments reported in Fig. 2 and 3 were conducted in a crucible with different dimensions (0.75 cm ID) than that reported in Fig. 6, (1 cm ID), the diffusion coefficients proved to be the same. However, the experimental points at 1400° and 1480°C deviate considerably from the penetration curves (Fig. 4 and 5). It is thought that this deviation is due to convection and that the resultant average values for the diffusion coefficients are too high.

Data in Table II are plotted in Fig. 8; the open circles are based on the average diffusion coefficients and the solid lines indicate the maximum deviation from the mean. An estimate of the activation energy for diffusion, neglecting the data at 1400° and 1480°C, is 11 kcal moles⁻¹, and an equation relating the diffusion coefficient and temperature is: $D = 4.5 \times 10^{-3}\, e^{-11,000/RT}$.

For low melting metals (up to 700°C) activation energies have been reported from 4 to 10 kcal moles⁻¹ (1, 4, 11, 12). At higher temperatures (1100°-1500°C) the approximate activation energy reported here for cerium in uranium (11 kcal

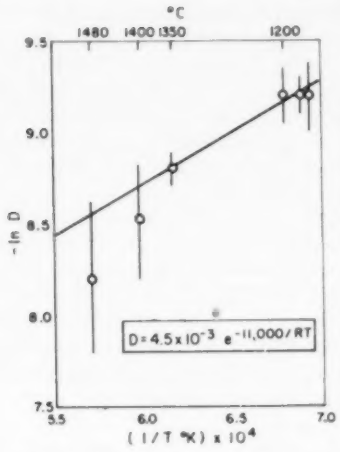

Fig. 8. An Arrhenius plot of the diffusion coefficient of cerium in molten uranium.

mole^{-1}) is close to that reported by Morgan and Kitchener (4) of about 10 to 11 kcal mole^{-1} for cobalt and carbon in molten iron (1350°-1650°C).

An estimate of the diffusion coefficient of zirconium in molten uranium at 1270°C was found from one experiment to be $(1.9 \pm 0.9) \times 10^{-4}$ cm^2 sec^{-1}. The large experimental error for this experiment is attributed to the error in chemical analysis although some turbulence may have had effect.

The diffusion of cerium and zirconium in molten uranium is somewhat faster than diffusion in other molten metal systems. The diffusion coefficients for many elements in molten metals (1) varies between (1 and 10) x 10^{-5} cm^2 sec^{-1}. Most of the work has been carried out below 1000°C, and it may be that the higher melting metals behave differently. Further experimentation with particular attention given to the convection problem is needed for measuring diffusion coefficients in metals at high temperatures.

Manuscript received April 23, 1959.

Any discussion of this paper will appear in a Discussion Section to be published in the June 1960 JOURNAL.

REFERENCES

1. W. Jost, "Diffusion in Solids, Liquids, Gases," Academic Press, New York (1952).
2. M. Paschke and A. Hautmann, *Arch. Eisenhüttenw*, **9**, 305 (1935).
3. W. F. Holbrook, C. C. Furnas, and T. L. Joseph, *Ind. Eng. Chem.*, **24**, 993 (1932).
4. D. W. Morgan and J. Kitchener, *Trans. Faraday Soc.*, **50**, 51 (January 1954).
5. K. Niwa, M. Shimozi, S. Kado, Y. Watanabe, and T. Yokokawa, *Trans. AIME*, **209**, 96 (1957).
6. *"Rare Metals Handbook,"* Reinhardt Publishing Co., New York.
7. C. V. Banks and J. W. O'Laughlin, *Anal. Chem.*, **28**, 1338 (1956).
8. J. Hure nd MMe. R. Saint James Shonberg, *Anal. Chim. Acta*, **9**, 415 (1953).
9. J. J. Klingenberg and R. A. Popucci, *Anal. Chem.*, **24**, 1861 (1952).
10. J. Crank, "The Mathematics of Diffusion," Clarendon Press, Oxford (1956).
11. S. J. Rothman University Microfilms (Ann Arbor Michigan) Publication No. 11, 185, 102 pp. (1954).
12. T. Saito and K. Maruya, *Bull. Research Inst. Mineral Dressing*, Tohoku University, **10**, 167 (1954).

Diffusion-Exchange of Exchange Ions and Nonexchange Electrolyte in Ion-Exchange Membrane Systems

Marvin A. Peterson and Harry P. Gregor

Department of Chemistry, Polytechnic Institute of Brooklyn, Brooklyn, New York

ABSTRACT

The following parameters of cation- and anion-permeable membrane systems were measured: water content; ohmic resistance; exchange capacity; diffusible electrolyte content; concentration potential; rate of exchange-diffusion of electrolytes; rate of diffusion of nonelectrolytes; effect of rate of stirring on diffusive flux. From these were calculated: the thickness of the unstirred film, which varied from 1 to 30 microns; the diffusion coefficient of the potassium ion in a sulfonic acid cation-permeable membrane, which was found to vary from 1.09 x 10^{-7} cm^2 sec^{-1} to twice that value as the ambient solution concentration was changed from 0.001 to 0.1M; the diffusion coefficient of the chloride ion which remained at about 3 x 10^{-7}; the diffusion coefficients of nonelectrolytes. A theoretical treatment showed that diffusion coefficients and other parameters could be estimated from a consideration of pore diameters, a tortuosity factor, and water contents.

Of primary importance in any detailed analysis of free and forced transport of ions across ion-selective membranes is the determination of boundary conditions which define film, membrane or coupled film-membrane diffusion mechanisms as being rate controlling. The appropriate application of Fick's law to diffusion across a membrane and its bounding unstirred films results in an expression which dictates the rate-controlling mechanism under given experimental conditions. The general theory of diffusive processes in ion-exchange resin systems has been described previously by several authors (1-3)

and analyzed by Tetenbaum and Gregor (4). Two different mechanisms, namely, film or particle diffusion, were found to be distinguishable when the resin system was operating in certain limited extremes, and a coupled mechanism was found to be operative in the region between these extremes.

With ion-exchange resin systems it was found that the diffusion coefficient of the exchange ion or the counter ion decreased as the degree of crosslinking or the density of the resin increased and that the diffusion coefficient of nonexchange or co-ions (anions in the case of cation-exchange resins) was proportional to that of the exchange ions and generally somewhat larger (1-6).

Diffusion studies are more complex for ion-selective membrane systems than for ion-exchange resin systems in that two diffusion films are encountered in membrane studies. Matters generally become simplified for the membrane case, however, once concentration gradients are established as compared to the resin system where a point source, nonstationary state prevails. Until steady state has been attained in the membrane system, the application of Fick's law presented by Lowan (7) holds for each of the successive layers, namely, film-membrane-film. Once concentration gradients have been established in each of the layers and a steady state is allowed to prevail, a new set of relations may be developed using Fick's law so as to determine the conditions which will dictate whether film, membrane, or a coupled diffusion mechanism is controlling.

The membrane-system model is characterized by the chain:

Solution′ | Film′ | Membrane | Film″ | Solution″

Subscripts on concentration terms denote ionic species. Primed terms refer to solution′ and solution″, respectively; o and l refer to interfacial concentrations at $x = 0$ and $x = l$, respectively; a superscript bar refers to concentrations within the membrane phase (see Fig. 1). Assumptions applied to the membrane system include the following: (*a*) steady state prevails; (*b*) the membrane is ideally ion-selective; (*c*) discontinuities at the interfaces present no resistance to interfacial diffusion; (*d*) negligible transfer of solvent occurs; (*e*) the ratio of the diffusion constants of the two diffusing counter ions remains constant throughout the system. The use and validity of these assumptions have been described in detail by many authors including Helfferich (8) and Soldano and Boyd (9).

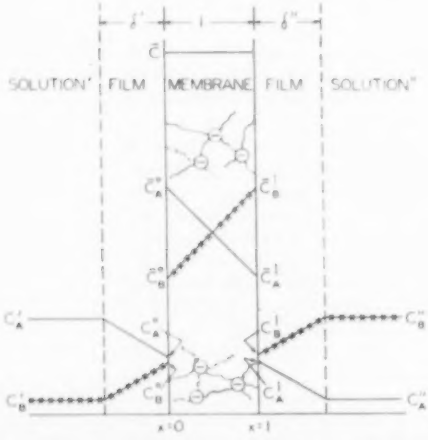

Fig. 1. Concentration profiles for the steady state where a coupled mechanism is rate controlling and where $Z_A = Z_B$ and $\overline{D}_A = \overline{D}_B$. Total membrane capacity is $\overline{C}_A + \overline{C}_B = \overline{C}$ and $C' = C''$.

The flux of ions across a membrane can be defined as the product of mobility, concentration, and driving force. Components of the driving force include gradients of activity, electric potential, and hydraulic pressure. These are summed up algebraically in the Nernst-Planck flux equation and the resulting flux, J, for a cation across a cation-permeable membrane is generally expressed as

$$J_i = -\overline{U}_i\overline{C}_i\left(\frac{RT}{\overline{C}_i}\frac{d\overline{C}_i}{dx} + Z_i\mathbf{F}\frac{d\phi}{dx}\right) \qquad [1]$$

where $\overline{U}_i$ and $\overline{C}_i$ represent the mobility and concentration of a single ionic species within the membrane and where the potential ϕ is generally taken as $\phi = 0$ at $x = 0$, and where $\mathbf{F}$ is the Faraday. With the aid of the Nernst-Einstein equation it is possible to relate the mobility of an ion in the membrane phase to its self-diffusion coefficient in the membrane phase (10). Direct or modified application of the above expression allows one to calculate interfacial concentrations, but this is a cumbersome approach.

A more direct approach may be made by defining an integral diffusion coefficient, D_{AB},

$$\overline{D}_{AB} = J_A\frac{l}{\overline{C}^{\circ}_A - \overline{C}^{l}_A} = J_B\frac{l}{\overline{C}^{l}_B - \overline{C}^{\circ}_B} \qquad [2]$$

where the total concentration $C = C_AZ_A + C_BZ_B$ and where similar defining expressions apply for the integral diffusion coefficients in the unstirred films.

Because of discontinuities at the membrane-film interface, a partition coefficient k must be defined for each interface, such that $k_i = \overline{C}_iC/C_i\overline{C}$. For steady-state conditions the flux J for each ionic species remains constant through each layer so that $J_i' = \overline{J}_i = J_i''$.

Application of Fick's law to this model results in the following expressions for the interfacial concentration of ion A at the coordinates $x = 0$ and $x = l$, in the case where $C = C' = C''$,

$$C^{\circ}_A = C - \frac{k^{\circ}_AC + \dfrac{D'_{AB}Cl}{\overline{D}_{AB}\overline{C}\delta}C'_B + k^{l}_A\dfrac{D'_{AB}}{D''_{AB}}C'_B - k^{l}_AC''_A}{\dfrac{D'_{AB}Cl}{\overline{D}_{AB}\overline{C}\delta} + k^{l}_A\dfrac{D'_{AB}}{D''_{AB}} + k^{\circ}_A} \qquad [3]$$

$$C^{l}_A = \frac{k^{\circ}_AC + \dfrac{D''_{AB}Cl}{\overline{D}_{AB}\overline{C}\delta}C''_A + k^{\circ}_A\dfrac{D''_{AB}}{D'_{AB}}C''_A - k^{\circ}_AC'_B}{\dfrac{D''_{AB}Cl}{\overline{D}_{AB}\overline{C}\delta} + k^{\circ}_A\dfrac{D''_{AB}}{D'_{AB}} + k^{l}_A} \qquad [4]$$

Partition coefficients must be determined experimentally. Integral diffusion coefficients can be eval-

uated from flux data by assuming activity coefficients independent of ionic composition and $\bar{D}_i$ constant throughout the membrane phase.

With the aid of these expressions the flux across any layer may be written. For the unstirred film[1] on the side adjacent to solution" and for the case where A and B have equivalent diffusive characteristics ($D_A = D_B = D$) and where $\delta' = \delta''$, the flux for ion A becomes,

$$J''_A = \frac{D}{\delta}(C'_A - C''_A) = \frac{D}{\delta}\left[\frac{C}{\frac{DCl}{\bar{D}\bar{C}\delta} + 2} - C''_A\right] \quad [5]$$

For the same conditions the flux across the unstirred film on the side adjacent to solution' becomes,

$$J'_A = \frac{D}{\delta}(C'_A - C^\circ_A) = \frac{D}{\delta}\left[C'_A - C\left[1 - \frac{1}{\frac{DCl}{\bar{D}\bar{C}\delta} + 2}\right]\right] \quad [6]$$

These expressions are exact when applied to the unstirred films and dictate whether film, membrane, or a coupled film-membrane diffusion mechanism is controlling. Expressions for the flux of ion B may be written similarly; these must satisfy the electroneutrality assumption inherent in the above derivation. The key parameter in these expressions is $DCl/(\bar{D}\bar{C}\delta)$ which is the ratio of the maximum attainable flux in the unstirred film to that in the membrane and has been used by Helfferich (8).

From these expressions it is noted that if $DCl/(\bar{D}\bar{C}\delta) << 1$, corresponding to a case where, under the same concentration gradient, the flux in the membrane phase is much larger than that in the unstirred film, then where $C'_A >> C'_B$ and $C''_B >> C''_A$ the expression for C°_A simplifies to $C^\circ_A = C/2$. Here the gradient in the unstirred film has reached its maximum value, or pure film control exists. The gradients are almost entirely in the unstirred films, and $C^\circ_A = C^\circ_B = C'_A = C'_B = C/2$. Similarly, if $DCl/(\bar{D}\bar{C}\delta) >> 1$, corresponding to cases where the resistance of the film to diffusion is much less than that of the membrane, then $C^\circ_A = C'_B = C$ and $C'_A = C^\circ_B = 0$, or the gradients are located almost entirely in the membrane phase. Where the ratio $DCl/(\bar{D}\bar{C}\delta)$ has intermediate values, neither process is purely rate-determining and a coupled mechanism prevails, as shown in Fig. 1. Analogous systems wherein water transport occurs have been described by Schlögl and Schödel (11).

Experimental

Homogeneous interpolymer membranes have been described by Gregor, *et al.* (12-16). These may be prepared by casting a homogeneous film from a solution of a polyelectrolyte and a hydrophobic film-forming polymer in a suitable solvent, allowing the film to dry, and using directly. A series of interpolymer films were examined in a preliminary way to ascertain their characteristics as regards transport phenomena. Transport across ion-exchange membranes proceeds by essentially the same process for all membrane types; however, there are certain basic differences between homogeneous and heterogeneous films as regards the exact mechanisms of transport, particularly of water transport (16). Since there are commercially available membranes of the homogeneous type, ones which show similar properties to the interpolymer membranes, it was decided to carry out the detailed examination of transport processes in commercial membranes. The films selected were quite strong mechanically and capable of withstanding high rates of stirring. The cation-permeable membrane used was the sulfonic acid-type film Nalfilm 1;[2] the anion-permeable membrane was Nalfilm 2, a quaternary ammonium-type obtained from the same source.

The effective exchange capacity of a membrane is the number of acidic or basic exchange sites within the membrane structure which are titrable while leaving the membrane intact. With strong acid (sulfonic) or strong base (quaternary ammonium) membranes simple mass-action exchange of neutral ions (potassium or nitrate) for counter ions (hydrogen or chloride) was utilized to make all exchangeable groups readily titrable (12).

All of the experiments were performed at room temperature, 24°-26°C, unless otherwise stated. In most cases the systems were thermostated at 25.0°C. All data were corrected to 25°C, unless the temperature deviation or the effect of temperature was negligible.

The cation-permeable membranes were equilibrated with 1M hydrochloric acid, washed with water to remove diffusible salt, and then blotted. Elution of the hydrogen ions was accomplished by placing the membrane samples, each having an area of about 100 cm², in 250 ml of 1M potassium chloride; these conditions provided at least a 250-fold excess of potassium ion. After a 24-hr period of shaking (much longer than the time required for equilibrium), an aliquot of the solution was titrated. The molality of this membrane was 2.86 ± 0.02, defined as milliequivalents of hydrogen ions per gram of sorbed water.

The anion-permeable membranes were equilibrated in potassium chloride solutions, the diffusible salts removed by washing with water and blotting, and elution of the chloride accomplished by shaking in 250 ml of 1M potassium nitrate for 24 hr. The membrane was removed, rinsed into the eluate, and the latter titrated potentiometrically with silver nitrate. The anion-permeable membrane was found to have a molality of 4.58 ± 0.04.

The thickness of each membrane was determined, following equilibration in 0.1M potassium chloride, with a micrometer which provided results accurate to ±1%. The water content of each membrane in the same state was determined by first eluting the diffusible salt, blotting with filter paper to remove surface moisture, and weighing immediately. This procedure was shown by Gregor and Sollner (17) to yield accurate and reproducible wet weights. The membranes were then dried at 10 mm Hg and 60°C

[1] The "diffusion layer" of "effective thickness" δ.

[2] Obtained from the National Aluminate Corporation.

for 24 hr and reweighed. Drying for an additional 24 hr under these conditions removed less than 0.2% additional water.

Characterization ohmic resistance measurements were made with a Klett conductivity bridge at 1000 cps on membranes in a plastic flow cell with fixed platinized platinum electrodes and provisions to interpose the membrane (18). The cell resistance was determined for various potassium chloride solutions with and without the membrane. Membrane resistance was calculated from the difference in resistance and consideration of the cell constant and the thickness of the membrane. In the more concentrated solutions the calculated resistance is quite accurate, while in dilute (0.001M) solutions the reliability decreases to ±4%.

Concentration potentials were determined for the chain:

$$\text{S.C.E.} \mid C_2 \mid \text{Memb.} \mid C_1 \mid \text{S.C.E.}$$

where S.C.E. refers to the saturated calomel electrode and where $C_2:C_1 = 2:1$. These measurements were carried out in a plastic cell with provisions for stirring at the membrane-solution interface by means of an air stream. The measuring circuit employed a L&N Type K-2 potentiometer and a Type E galvanometer. Corrections were applied as described by Wetstone (19) to the concentration potential measurements for the salt bridge liquid junction, the S.C.E. asymmetry and temperature. These measurements are summarized in Table I.

Nonexchange of diffusible electrolyte is that which enters the membrane phase in excess of those ions which compensate electrically for the fixed ions. In a cation-permeable membrane system in potassium chloride solution, for example, the mobile potassium ions are designated as counter-ions and the chloride ions as co-ions. Then the molality of co-ions is numerically equal to that of the diffusible electrolyte and is equal to the number of equivalents per gram of sorbed water. Membrane samples approximately 40 cm² in area were equilibrated in 0.100, 0.500, and 1.00M potassium chloride solutions, blotted quickly to remove surface solution, and placed in 25 ml of distilled water with gentle shaking for 24 hr. The amount of eluted diffusible electrolyte was evaluated from resistance measurements of the eluate. Water contents were determined on similar samples in equilibrium with the same solutions. Calculated molalities are presented in Table II.

Table I. Membrane properties

	Cation-permeable membrane	Anion-permeable membrane
Thickness (microns)	96 ±1	84 ±1
Water content		
% by weight	23.5 ±0.2	17.1 ±0.3
% by volume	30.9	20.6
ml. cm^{-2} of membrane ($\times 10^3$)	2.97	1.73
Resistance in ohm-cm^2		
1.0M KCl	8.03	
0.5M	14.5	
0.1M	16.5	28.8
0.01M	20.1	
0.001M	28.0	
Concentration*		
Molality — meq g^{-1} water	2.86 ±0.02	4.58 ±0.04
Capacity—meq cm^{-2} membrane area x 10^3	8.46	7.89
Molarity—meg cm^{-3} membrane	0.882	0.939
Co. P.,† mv (corrected)	15.45	—15.61

* These do not include nonexchange electrolyte.
† Concentration potential of chain: S.C.E. | 0.2M KCl | Memb. | 0.1M KCl | S.C.E. Theoretical, $E_{max} = \pm 16.11$.

Table II. Diffusible electrolyte or co-ion content of cation-permeable membrane

Potassium chloride, M	Area, cm^2	Water content, g cm^{-2}	Molality, meq g^{-1} water
0.100	38.4	0.119	0.0270 ±0.007
0.500	36.9	0.110	0.162 ±0.002
1.00	40.1	0.114	0.474 ±0.009

Ion-exchange membranes, like the ion-exchange resins, show some variation in the properties of different samples. This is particularly the case with materials still in the developmental stage. For a given batch of membranes, a high level of uniformity was encountered; all of the work described in this contribution was carried out on the same batch.

Rate of exchange studies were conducted in an apparatus which consisted essentially of two identical plastic (methylmethacrylate) chambers with a common window such that an interposed membrane was exposed on one side to solution' and on the other side to solution". Each chamber had provisions for an inlet and outlet stream, identical rates of stirring, and cooling coils for precise temperature control. Identical high rates of stirring very near the membrane-solution interface were obtained by means of a 3-bladed flat paddle stirrer which swept the entire exposed membrane area with controlled peripheral linear velocities of 55 to 330 cm sec^{-1} at a distance of

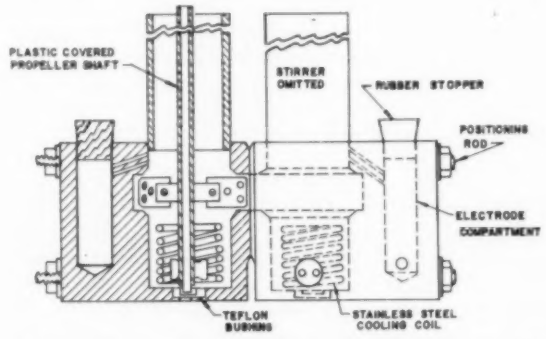

Fig. 2. Cell used for variable, high rates of stirring. The three detachable plastic flat-paddle blades are 0.1 to 0.2 cm from the interposed membrane. The assembly is symmetrical, and each compartment has provision for an entrance and exit stream. Volume of each compartment—115 ml.

1 to 2 mm from the interposed membrane. This cell is illustrated schematically in Fig. 2.

Water can be transported across ion-exchange membrane systems as a result of differences in the activity of water in solution′ and solution″, or by electro-osmosis. This was recognized by Donnan in his earliest papers, where he suggested the addition of a nonpermeable nonelectrolyte such as sugar to the side of higher solvent activity. Water transport can manifest itself in the measurement of any irreversible phenomenon, including that of a concentration potential, transport number, and diffusion coefficient. Water transport is negligble under almost all experimental conditions (excepting electro-osmosis) with membranes of low water content, such as the homogeneous membranes of Gregor and Sollner (17), the interpolymer membranes (12-16), and the films used in this study. Water contents of about 25% or less usually mean that water transport may be neglected; at water contents of 50% and greater, large effects are observed and have been evaluated by Schlögl and Schödel (11).

Another cell similar to that shown in Fig. 2 was constructed, where the exposed membrane area was about 15 cm². One side was maintained at constant volume with a mercury-sealed stirrer, and a capillary permitted direct observation of any volume changes. The imposition of an osmotic concentration difference as large as 1M gave such low rates of water transport as to be neglected.

Three series of runs at solution concentrations of 0.001, 0.1, and 0.5M were made using the cation-permeable membrane with potassium chloride as solution′ and ammonium nitrate as solution″. These ions resemble one another closely enough to serve as "tracers" for each other. Similar runs including a 0.0001M series were made using the anion-permeable membrane. Each series consisted of a number of runs ranging in time from 10 to 30 min and at stirring rates from 200 to 1200 rpm (corresponding to linear rates of 55 to 330 cm sec^{-1}).

The membranes were equilibrated in the respective potassium chloride solution for 24 hr prior to the rate experiments. Zero time for each run was not critical because essentially no potassium could be detected in the ammonium nitrate solution after a period of 1 hr with no stirring. That the membrane was highly ion-selective was verified when essentially no chloride could be detected in the nitrate solution after 15 min at 800 rpm in the 0.1M series, at which time an appreciable amount of cation-exchange had occurred. Duplicate runs gave essentially identical results.

The cation-permeable membrane contained 0.00846 meq of potassium per square centimeter of surface area. A constant area of 3.422 cm² was common to both solutions, so that before steady-state concentration gradients could be established approximately 0.015 meq of potassium (50% of capacity) would, of necessity, be displaced from the membrane sites to the ammonium nitrate cell side in return for the ammonium ion since the membrane was initially equilibrated in 0.001M potassium chloride for the 0.001M series of runs, etc.

Rate data were collected as follows: after a 10-min run both cells were drained and replenished with the original solutions. This was repeated once and followed by a third run for 20 min and a fourth for about 30 min. Once the 0.015 meq of potassium had been displaced it was assumed that the membrane retained a steady-state concentration gradient with respect to potassium and ammonium.

Solutions were analyzed for potassium with a Perkin-Elmer 52A flame photometer. These determinations were accurate to better than ±2% at a solution concentration above 5 x 10^{-4}M. A colorimetric method of analysis was used for chloride, capable of detecting chloride ion quantitatively at concentrations as low as 2 x 10^{-5}M with an accuracy better than 2% (20). The procedure involves the indirect evaluation of the chloride ion by displacement of the chromate ion from silver chromate solution. Analysis of the chromate ion was made using a Beckman DU spectrophotometer at 370 mμ against a

Table III. Exchange-diffusion of potassium

Chain: 0.001M KCl | Cation-Permeable Memb. | 0.001M NH_4NO_3

Elapsed time, min	Final conc soln′, M x 10^3	Final conc soln″, M x 10^3	Amount in soln″, meq x 10^3	Flux, meq cm^{-2} sec^{-1} x 10^6
	Stirring rate—200 rpm			
0				0.236
10	0.946	0.042	0.482	0.234
10	0.948	0.042	0.482	0.234
19	0.910	0.078	0.895	0.224
28	0.880	0.110	1.26	0.197
	Stirring rate—300 rpm			
0				0.318
10	0.933	0.055	0.632	0.308
16	0.910	0.080	0.977	0.280
19	0.888	0.100	1.15	0.280
28	0.850	0.140	1.61	0.249
28	0.848	0.142	1.63	0.260
	Stirring rate—400 rpm			
0				0.386
10	0.923	0.065	0.748	0.365
10	0.925	0.065	0.748	0.365
15	0.894	0.096	1.10	0.343
15	0.895	0.095	1.09	0.334
20	0.868	0.120	1.38	0.308
29	0.825	0.165	1.90	0.281
29	0.823	0.167	1.88	0.271
	Stirring rate—800 rpm			
0				0.664
10	0.876	0.114	1.31	0.638
10	0.875	0.113	1.30	0.632
15	0.824	0.166	1.91	0.595
19	0.784	0.206	2.37	0.574
28	0.699	0.291	3.35	0.530
28	0.698	0.290	3.34	0.524
	Stirring rate—1200 rpm			
0				0.856
10	0.843	0.147	1.69	0.822
10	0.843	0.145	1.67	0.813
15	0.776	0.214	2.46	0.771
19	0.722	0.268	3.08	0.753
28	0.609	0.381	4.38	0.703
28	0.609	0.379	4.36	0.694

$$\text{Flux} = \frac{\Delta M''_{final}\,(115)}{\Delta t_{sec}\,(3.422)} \text{ meq cm}^{-2}\text{ sec}^{-1}$$, where 115 cm³ is volume of cell, 3.422 cm² is membrane area.

suitable standard. The nonelectrolytes employed were analyzed for by standard procedures.

Table III gives the results of a series of exchange-diffusion experiments performed with the solution chain:

0.001M KCl | Cation-Permeable Memb. | 0.001M NH_4NO_3

measured at 25°C and with different rates of stirring. The amount of potassium exchanged was not proportional to the elapsed time at a given rate of stirring because the concentration gradients had changed. The flux for each time interval was evaluated, and by extrapolation to zero time it was possible to calculate the flux under the initial conditions J^*; then $C'_B = C''_A = 0$ and the calculation of δ and $\bar{D}$ followed.

Initial flux values were used to evaluate δ from the following general expression for the case where a coupled-mechanism prevails

$$J = \frac{D(C'_{K^+} - C^\circ_{K^+})}{\delta} \qquad [7]$$

At the zero time under steady-state conditions

$$C^\circ_{K^+} = C\left[1 - \frac{1}{\frac{DCl}{\bar{D}\,\bar{C}\delta} + 2}\right] \qquad [8]$$

$C'_{K^+} = C$ and $k = 1$. The general expression becomes,

$$J^* = \frac{D}{\delta}\left[\frac{C}{\frac{DCl}{\bar{D}\,\bar{C}\delta} + 2}\right] \qquad [9]$$

or

$$\delta = \frac{DC}{2}\left(\frac{1}{J^*} - \frac{l}{\bar{D}\,\bar{C}}\right) \qquad [10]$$

In order to evaluate δ as a function of the stirring rate it was necessary to determine $\bar{D}_{K^+}$. This was obtainable for the 0.001M system from conductance data using the appropriate application of the Nernst-Einstein equation (10)

$$\bar{\kappa} = \frac{l}{\Omega} = \frac{\mathbf{F}^2}{1000\,RT}(Z_+\bar{D}_+\bar{C}_+ + Z_-\bar{D}_-\bar{C}_-) \qquad [11]$$

and $\bar{D}_+ = 2.66 \times 10^{-7}\,\bar{\lambda}_+/Z_+$ where $\bar{\lambda}_+ = 1000\,\bar{\kappa}_+/\bar{C}_+$ where λ is the equivalent ionic conductance (mho cm^2 eq^{-1}) in the absence of electro-osmosis, κ is the specific conductance (ohm^{-1} cm^{-1}), Ω is the membrane resistance in ohm cm^2, and $\bar{C}$ the concentration (meq cm^{-3}) of the membrane phase. From Table II the concentration of nonexchange electrolyte would be negligible at 0.001M compared to that of the exchange ions and $\bar{D}_+ = 1.03 \times 10^{-7}$ cm^2 sec^{-1} in 0.001M solutions.

Values of δ and $DCl/(\bar{D}\,\bar{C}\delta)$ as a function of rate of stirring were calculated then, based on the $\bar{D}_+$ value from conductance data, for all experiments performed at 0.001M concentrations. Film thicknesses were found to range from 1 to 30 μ at stirring rates ranging from 1200 to 200 rpm. Values of $DCl/(\bar{D}\,\bar{C}\delta)$ for this 0.001M series ranged from 18.8 at 1200 rpm to 0.99 at 300 rpm and 0.65 at 200 rpm. This, on the basis of these calculations, a coupled mechanism prevailed at all rates of stirring.

Table IV. Evaluation of unstirred film thickness

Rate of stirring—200 rpm (55 cm sec^{-1})
Chain: 0.0001M KCl | Anion-Permeable Memb. | 0.0001M NH_4NO_3
All concentrations are for the chloride ion.

Elapsed time, min	C', M x 10^4	C'', M x 10^4	Amount in soln", meq x 10^5	$C' - C''_{avg}$, M x 10^4	δ, μ
0	1.00	0.000	0.00		
				0.474	31.3
10	0.948	0.052	0.0598		
				0.435	29.9
15	0.923	0.077	0.0885		
				0.412	31.9
20	0.901	0.099	0.114		
				0.379	30.7
30	0.858	0.142	0.163		

$\delta_{avg} = 30.9 \pm 0.6$.

Experimental results for a series of runs at 0.0001M and 200 rpm are presented in Table IV. Since the parameter $DCl/(\bar{D}\,\bar{C}\delta)$ equals 0.65 at 200 rpm in 0.001M solution, it was postulated that film control would predominate in 0.0001M solutions at 200 rpm where $DCl/(\bar{D}\,\bar{C}\delta)$ would equal 0.065 if all values other than C were unchanged. Under these conditions $C^\circ_A = C'_A$ and the concentrations at the membrane surfaces would be equal to the mean value of C' and C'', or $C/2$. For this determination, an anion-permeable membrane was used because chloride analysis could be performed with greater accuracy at these extreme dilutions. Postulating pure film control, $J = DA/\delta(0.00005 - C''_{avg})$ since C° and C' are constant and equal to 5×10^{-5}M. Table IV presents calculated values of δ where C''_{avg} is the average concentration of chloride in solution" during the appropriate time interval and A the membrane area.

Table IV shows that δ is 30.9 ± 0.6 μ at 200 rpm, agreeing well with δ as determined in 0.001M solutions wherein the coupled mechanism prevailed, as will be shown later. The constant values of δ over each time interval verifies the assumption that diffusion through the unstirred film was rate determining for 0.0001M concentrations.

The establishment of δ at 200 rpm in the 0.0001M series allowed an independent evaluation of $\bar{D}_+$ for 0.001M solutions from flux data for the 0.001M series, and good agreement was noted between $\bar{D}_+$ (conductance) and $\bar{D}_+$ (flux), as will be shown later.

From consideration of the dimensionless parameter $DCl/(\bar{D}\,\bar{C}\delta)$ it is seen that membrane control will predominate at values greater than 50, with the film being rate controlling at values less than 0.1. In the system under investigation, $l \cong 0.01$ cm, $\bar{C} \cong 1.0$M, $D/\bar{D} \cong 100$ and $0.0001 < \delta < 0.0030$ cm. Accordingly, film control can be expected at $C <$ 0.00001M at 1200 rpm and $C < 0.0003$M at 200 rpm; deviations from membrane control can be expected at $C < 0.005$M at 1200 rpm and $C < 0.15$M at 200

Table V. Flux of exchange ions

Stirring rate, rpm	δ, μ	J_{K^+} in cation-permeable membrane, meq sec^{-1} cm^{-2} x 10^5		J_{Cl^-} in anion-permeable membrane, meq sec^{-1} cm^{-2} x 10^5	
		0.1M	0.5M	0.1M	0.5M
200	31.0	1.51	1.65	0.850	—
400	14.4	1.53	1.66	0.866	0.99
800	4.25	1.57	1.68	0.894	1.02

Table VI. Chloride exchange-diffusion across cation-permeable membrane

Chain: KCl | Membrane | NH_4NO_3
Rate of stirring—400 rpm

Original conc. C'	Duration of run, min	Chloride conc. C'', M x 10^4	Chloride leak avg flux, meq cm^{-2} sec^{-1} x 10^5
0.100	60	1.90	28
0.100	180	2.50	28
0.100	300	3.10	
0.500	60	1.90	157
0.500	180	5.25	163
0.500	300	8.75	
1.000	60	1.90	443
1.000	110	5.85	443
1.000	160	9.80	

rpm. Intermediate ranges should exhibit a coupled mechanism.

The rate of diffusion-exchange processes in 0.1 and 0.5M solutions was measured with anion- and cation-permeable membranes. Solution concentrations remained essentially constant throughout the experiments, changing by less than one part in 500, and a constant flux was observed over the various time intervals. Table V presents the flux values. Values of δ were assumed to be concentration independent and taken from the 0.001M data. Corresponding data for the diffusion-exchange of chloride ions in the cation-permeable membrane are given in Table VI.

From the general flux expression it is noted that J^* approaches $\bar{D}\,\bar{C}/l$ in the limiting case of $DCl/(\bar{D}\,\bar{C}\delta) >> 1$ where membrane control prevails. The general expression for $\bar{D}$ in the coupled diffusive process is

$$\bar{D}_+ = \left[\frac{\bar{C}}{Jl} - \frac{2\bar{C}\delta}{DCl}\right]^{-1} \qquad [12]$$

From the expression relating specific conductance and diffusion coefficient, the diffusion coefficient for the anion is given by

$$\bar{D}_- = \left[\frac{\bar{\kappa}RT}{\mathbf{F}^2} - \frac{Z_+\bar{D}_+\bar{C}_+}{1000}\right]\frac{1000}{Z_-\bar{C}_-} \qquad [13]$$

Exact values of $\bar{D}_i$ can be calculated from flux data for that ion and values of δ; these can be calculated also from values of the specific conductance of the membrane phase together with values of $\bar{C}_i$ for each ionic species present and values of $\bar{D}_i$ for all other ionic species, subject to the applicability of the Nernst-Einstein equation. Where both kinds of data are available, an independent check is possible. Diffusion coefficients and other parameters for the cation-permeable membrane system are presented in Table VII.

From Table VII it is seen that within experimental accuracy the diffusion coefficients in the membrane phase for a given solution concentration are independent of the rate of stirring. This is not true of the flux unless complete membrane control prevails. As fluxes in the 0.1M solution series decrease, with lower rates of stirring, $\bar{C}/Jl$ increases; however, there is a corresponding increase in the values of $2\bar{C}\delta/(D_{Cl})$ due to an increase in δ, resulting in a constant value of $\bar{D}$. At higher concentrations (C = 0.5M) the film effect is diminished and in the limit

Table VII. Parameters for cation-permeable membrane

Rpm	$\bar{J}_+$ x 10^5, meq cm^{-2} sec^{-1}	$\bar{J}_-$ x 10^5, meq cm^{-2} sec^{-1}	$\bar{C}_+$, M	$\bar{C}_-$, M	$\bar{\kappa}$ x 10^2, ohm-cm^{-1}	$\bar{D}_+$ x 10^7, cm^2 sec^{-1}	$\bar{D}_-$ x 10^7, cm^2 sec^{-1}
			C = 0.001M				
			0.882	(0.000)	0.343	1.03*	
200	0.236					1.09	
			C = 0.01M				
			0.882	(0.000)	0.478	1.44*	
			C = 0.1M				
200	1.51		0.889	0.00832	0.582	1.72	3.24*
400	1.53	0.028				1.69	3.23
800	1.57					1.71	
			C = 0.5M				
200	1.65		0.931	0.0499	0.662	1.73	3.01*
400	1.66	0.160				1.72	3.08
800	1.68					1.74	
			C = 1M				
400		0.443	1.03	0.146	1.197	1.75*	2.91

* Calculated from conductance data.

Table VIII. Value of parameter $DCl/(\overline{DC}\delta)$ for cation-exchange membrane

Stirring rate, rpm	Stirring rate, cm sec^{-1}	$\delta \times 10^4$, cm	Ambient concentration 0.001M	0.1M	0.5M	1.0M
1200	330	1.04	18.8	1120	4930	8650
800	220	4.25	4.59	273	1200	2120
400	110	14.4	1.36	80.5	356	625
300	83	19.7	0.99	58.8	260	457
200	55	30.1	0.65	38.6	170	299

where membrane control is absolute, it is essentially zero and $\overline{D} = Jl/\overline{C}$.

In order to illustrate increasing membrane control with increasing solution concentration, $DCl/(\overline{D}\,\overline{C}\delta)$ values for 0.001, 0.1, 0.5, and 1M solutions are presented in Table VIII. Parameter values ranged from 0.65 at 200 rpm with 0.001M solutions to 8650 at 1200 rpm with 1M solutions.

From values of diffusion coefficients of exchange and nonexchange electrolyte, mobilities and transport numbers can be evaluated. A sequence of concentration potential measurements was made and is presented in Table IX. Good agreement is noted between transport numbers determined from exchange-diffusion studies and those calculated from potential measurements.

From flux data obtained with anion-permeable membranes, values of the anionic diffusion coefficients were calculated to be $(\overline{D}_{Cl})_{0.1M} = 0.78 \times 10^{-7}$ and $(\overline{D}_{Cl})_{0.5M} = 0.85 \times 10^{-7}$ cm^2 sec^{-1}. Subscripts outside the parentheses refer to the ambient solution concentrations.

A calculation of $(\overline{D}_{K^+})_{0.1M}$ in this membrane requires either nonexchange electrolyte content and flux data or the former and conductance data. A good approximation of the nonexchange electrolyte concentration can be made by analogy with the ion-exchange resins. Gregor, Gutoff, and Bregman (21), Gregor and Gottlieb (22), and Gottlieb and Gregor (23) measured diffusible electrolyte contents and mean activity coefficients for sulfonic acid cation- and quaternary ammonium anion-exchange resins of different resin phase molalities. Postulating that these systems are comparable, as seems to be the case from nearly all points of view, one can evaluate these parameters for the membranes.

Table IX. Transport numbers in membranes calculated from potential and exchange-diffusion measurements

C_{avg} $C' = 2C''$, M	E_{max}, mv	Cation-permeable membrane E_{corr}, mv	t_+	t_+^*	Anion-permeable membrane E_{corr}, mv	t_-
0.0015	17.43	17.42	0.999	(1.000)	−17.42	0.999
0.006	17.14	17.07	0.998		−17.09	0.999
0.015	16.87	16.77	0.997		−16.80	0.998
0.06	16.39	16.08	0.990		−16.13	0.992
0.15	16.11	15.45	0.979	0.983	−15.61	0.985
0.60	15.89	12.17	0.883	0.915	−12.80	0.903
1.5	17.18	10.11	0.794	0.810	−12.43	0.862

t_+^*—Transport numbers from exchange-diffusion experiments in 0.001, 0.1, 0.5, and 1M solutions.

Cation-exchange resin mean activity coefficients were calculated from the Gibbs-Donnan equations applied to systems of this type by Gregor, *et al.* (21-25). It was shown that mean activity coefficients for uni-univalent electrolytes defined by the expression $\overline{m}_+\overline{m}_-\overline{\gamma}_\pm^2 = m_+m_-\gamma_\pm^2$ were, for cation-exchange resins, as follows: where $(\overline{m}_+)_{0.1M} = 1.6$, $(\overline{\gamma}_\pm)_{0.1M} = 0.37$; for $(\overline{m}_+)_{0.1M} = 4.0$, $(\overline{\gamma}_\pm)_{0.1M} = 0.31$. For anion-exchange resins, where $(\overline{m}_-)_{0.1M} = 2.9$, $(\overline{\gamma}_\pm)_{0.1M} = 0.32$ and where $(\overline{m}_-)_{0.1M} = 4.6$, $(\overline{\gamma}_\pm)_{0.1M} = 0.28$. Accordingly, $\overline{\gamma}_\pm$ values for both resin types are quite similar when systems of the same resin phase molality are compared.

Since diffusible and nondiffusible electrolyte contents were determined for the cation-permeable membranes, values of $(\overline{\gamma}_\pm)$ could be calculated. These were: $(\overline{\gamma}_\pm)_{0.1M} = 0.273$ at $(\overline{m}_+)_{0.1M} = 2.89$; $(\overline{\gamma}_\pm)_{0.5M} = 0.465$ at $(\overline{m}_+)_{0.5M} = 3.02$; $(\overline{\gamma}_\pm)_{1M} = 0.483$ at $(\overline{m}_+)_{1M} = 3.33$. With the sulfonic acid resins, $(\overline{\gamma}_\pm)_{0.5M} = 0.40$ at $(\overline{m}_+)_{0.5M} = 2.3$, while $(\overline{\gamma}_\pm)_{1M} = 0.44$ at $(\overline{m}_+)_{1M} = 3.1$. Good agreement between the resin and membrane systems is observed.

Accordingly, it is possible to estimate diffusible nonexchange electrolyte contents for the anion-permeable membrane and calculate a $\overline{D}_-$ value from flux data for the anion and conductance data. Having determined $(\overline{m}_-)_{0.1M} = 4.58$, and assuming a value of $(\overline{\gamma}_\pm)_{0.1M} = 0.28$ (since $\overline{m}_-$ is quite constant in dilute solutions), then one can calculate $(\overline{m}_+)_{0.1M} = 0.017$. The calculated value of $(\overline{D}_K)_{0.1M}$ in the anion-permeable membrane was 2.41×10^{-7} cm^2 sec^{-1}, or three times that of the counter-ion.

Measurements were also made of flux values of urea and acetic acid in the cation-permeable membrane in 0.1M potassium chloride solution. In both cases the solution concentration of the nonelectrolyte (also treating the acid as such) was 0.1M. A high rate of stirring was not required since these solutes were not strongly accumulated by the membrane; concentration gradients of these solutes in the membrane phase were about 5% of those found for exchange species. The parameter $DCl/(\overline{D}\,\overline{C}\delta)$, accordingly, increased by a factor of 20, meaning that in all cases where even moderate stirring prevailed, diffusion was almost entirely membrane controlled. Flux values were constant in every case over an interval of several hours. For urea it was found that the flux was 2.37×10^{-10} moles sec^{-1} cm^{-2} from a 0.1M solution stirred at 400 rpm into water across the membrane (0.0096 cm) where the molality of urea in the membrane was 0.180 or its molar concentration was 0.0555 moles liter^{-1} of membrane phase. Then, $\overline{D}_{urea} = 4.11 \times 10^{-6}$ cm^2 sec^{-1}. In free solution, $D_{urea} = 1.36 \times 10^{-5}$ cm^2 sec^{-1}, so that $\overline{D}/D = 0.0030$.

These figures should be compared with those for the diffusion of urea in a sulfonic acid cation-exchange resin system, as measured by Gregor, Col-

lins, and Pope (26). Here $\overline{D}_{urea} = 12.2 \times 10^{-7}$ cm² sec⁻¹ in a 10% cross-linked resin where the distribution coefficient or $\overline{m}/m = 1.31$, where the water content of the resin was 40%, and where $(\overline{D}_{K^+})_{0.1M\ KCl} = 4.7 \times 10^{-6}$ cm² sec⁻¹ (4).

For acetic acid, the flux was 3.91×10^{-10} moles sec⁻¹ cm⁻² from a 0.1M solution of the acid in 0.1M potassium chloride. Here a determination of the solution phase molality was not made, but from other sources (26, 27) it appears likely that the distribution coefficient is nearly unity. The diffusion coefficient for acetic acid was calculated to be 3.76×10^{-6}, compared to the free solution value of 1.20×10^{-5} cm² sec⁻¹; then $\overline{D}/D = 0.0031$. Manecke and Heller (28) also measured the diffusion of acetic acid across a phenolsulfonic acid-formaldehyde cation-permeable membrane, but diffusion coefficients were not calculated.

Discussion

This discussion is concerned with the cation-permeable membrane systems, unless otherwise stated. Turning first to a comparison between the cation-selective membrane and a cation-exchange resin of the sulfonate type, it is seen that the two systems are quite comparable from almost all points of view. For systems of equal cationic molality, it is seen that the concentrations of diffusible electrolytes vary in the same way with the ambient solution concentration, with respect to both absolute and relative values. These Donnan systems absorb an amount of diffusible electrolyte at low concentrations which is much larger than that calculated for ideal systems. This is presumably because the counter-ion is bound electrostatically to the polymeric chains by their high potential. The system cannot exert its ideal Donnan potential, and excess diffusible electrolyte enters so that low values of mean activity coefficients are calculated.

As additional diffusible electrolyte enters the resin or membrane system with increasing solution phase concentration, the concentration of co-ions increases quite sharply and has a profound influence on the mean activity coefficient. Presumably, at high external solution concentrations the activity coefficient of diffusible electrolyte in the membrane phase would approach that in the solution phase, as was observed with the resin systems.

Turning to the change in the diffusion coefficient of the mobile ions in the cation-permeable membrane phase, it is observed that the diffusion coefficient of the cation rises significantly with increasing concentration of the ambient solution phase, while that of the anion decreases slightly, although the latter effect is within experimental error. This rise in the diffusion coefficient of the counter-ion with increasing ambient solution concentration amounted to a 1.7-fold increase in $\overline{D}_+$; this has been observed by Schlögl (29), Schlögl and Helferich (30), Ishibashi, Seiyama, and Sakai (31), Despic and Hills (32), and Richman and Thomas (33). Some of these authors observed a larger increase in the diffusion coefficient of the counter-ion with ambient solution concentrations than was observed here; this was probably due to their use of systems having a lower fixed-ion concentration and consequently a larger and more variable diffusible electrolyte content. In some cases the resistance due to the unstirred film has been neglected; such calculations are suspect.

In the cation-permeable membrane systems, the diffusion coefficient of the chloride ion was found to be significantly larger than that of the cation, varying by a factor of 3:1 to one of 2:1 as the solutions became more concentrated. At a 0.1M ambient solution concentration, the factor was approximately 2:1. With the anion-permeable membranes, a factor of 3:1 for the co-/counter-ion diffusion coefficients was observed. These differences are expected because the chloride ion is bound significantly to the fixed groups in anion-exchange resin systems and presumably also in anion-exchange membrane systems. The former effect was observed by Gregor, Belle, and Marcus (34). These differences have been observed previously by Schlögl (29) in his study on the diffusion of sodium bromide in an anion-selective membrane system.

As was shown in Table IX, transport numbers calculated from emf data are in good agreement with those calculated from the product of diffusion coefficients and membrane phase concentrations. This agreement is as expected in view of the fact that the solvent transport correction term is negligible in these membranes of low (15-25%) water content.

The absolute magnitude of the diffusion coefficients of the counter- and co-ions is of considerable interest. In dilute solutions (0.001M) the ratio $\overline{D}_+/D_+ = 0.0050$, taking $D_+ = 22 \times 10^{-6}$ cm² sec⁻¹, the value for potassium chloride of approximately the same molal concentration (4*M*) as in the membrane. As the ambient solution concentration increased to 0.1M, $\overline{D}_+/D_+$ increased to 0.0078. The value of $\overline{D}_-/D_-$ was 0.014.

It is of considerable interest to compare the diffusion coefficient of an ion in a condensed phase (such as a membrane phase) with the value it has in free solution, and examine each of the factors contributing to the markedly lower diffusion coefficient. Here, three factors must be considered. A large fraction of the membrane area is composed of the matrix polymer and the bulk of the polyelectrolyte. Consequently, ions are free to diffuse only in the interstitial solution, or the true area for diffusion is proportional to the water content; a factor of 0.235 must be applied.

Second, in a membrane system composed of interconnecting pores, a "tortuosity factor" must be applied because presumably only one-third of the pore lengths permit diffusion in a direction perpendicular to the face of the membrane; a factor of 0.333 is assumed. Carman (35) discusses this factor in porous media; Schlögl and Stein (36) have also considered the tortuosity factor.

The third is the so-called "drag factor." The viscous drag on a sphere moving in a homogeneous medium contained in a cylindrical pore will increase as the sphere diameter approaches that of the pore itself. While Stokes' law technically should not be

applied to the motion of an ion in water where both are of comparable size, nevertheless a considerable body of data has shown that Stokes' treatment does apply, although the constant term may be different. The applicability of Walden's rule is a case in point.

The determination of average pore diameters in the same cation-permeable membrane system was made by Gregor and Jacobson (37) who measured the conductivity of the unhydrated quaternary ammonium ions of different size, and applied the equation of Faxen (38),

$$F = \overline{D}/D = 1 - 2.104(s/S) + 2.09(s/S)^3 - 0.95(s/S)^5 \quad [14]$$

where s is the diameter of the sphere, S the diameter of the uniform pore, and F the drag factor. Gregor and Jacobson calculated an effective pore diameter of 6.0Å for a Nalfilm 1 membrane.

From this value of the pore diameter, Gregor and Jacobson (37) were able to calculate the diameter of the hydrated potassium ion *in the same membrane* from its conductivity. While several authors have observed that the conductances of the alkali metal cations in a resin or membrane phase were approximately proportional to their conductances in free solution, the importance of the drag factor was not considered. This proportionality is the result of a diminution in the size of the hydrated ion, proportional to its hydration. Since the velocity of an ion is $v_i \sim F_i/r_i$, where r_i is the hydrated radius, and since F_i increases with r_i, for the alkali metal cations the effect of viscous drag is compensated by an equivalent reduction in the hydrated diameter. An effective hydrodynamic diameter for the potassium ion of 2.5Å was calculated, while for the chloride ion the diameter was 4.0Å. The drag factor for the potassium ion in the cation-permeable membrane was calculated to be 0.54, and for the chloride ion, 0.21.

Accordingly, in the cation-permeable membrane the diffusion coefficient of the potassium ion is calculated to be $22 \times 10^{-5} \times 0.235 \times 0.333 \times 0.54 = 9.3 \times 10^{-7}$. The calculated value for the diffusion coefficient of the chloride ion is 3.6×10^{-7}. Then, the calculated value of $\overline{D}_+/D_+ = 0.042$ and $\overline{D}_-/D_- = 0.016$; in 0.1M solutions, the corresponding experimental ratios are 0.0078 and 0.014. For the co-ion, the agreement is excellent indeed for these ions are not bound electrostatically to fixed charges. For the counter-ions, the experimental value is but one-eighth the calculated value at $M = 0.001$, and one-fifth the value at $M = 0.1$. Obviously, electrostatic binding makes for a significantly higher activation energy for its diffusion.

Since the co-ion can act as a "carrier" for the counter-ions, it is easy to see why it can exert such a strong effect on the diffusion rate of the latter even when present at very low relative concentrations; in 0.1M solution, $\overline{m}_-/\overline{m}_+$ is only 0.01.

Various attempts have been made to calculate from purely theoretical considerations the diffusion coefficient of a counter-ion in a system of fixed charges. These calculations are made difficult by lack of accurate information on the sizes of the fixed and mobile ions and the distance of nearest approach, and on the effective dielectric constant of the system between unlike charges. Robinson and Stokes (39) discuss in some detail the uncertainties in each of these parameters.

Turning to the cation-permeable membrane systems, the average distance between fixed charges cannot be calculated from the molality alone since the fixed charges and the membrane matrix make up a large part of the volume of the system. However, since the actual pore structure is comparable to an ion-exchange resin of the same type and molality, the properties of the latter can be used as a first approximation. The volume of a potassium polystyrenesulfonate resin cross-linked with 6% divinylbenzene and having approximately the same volume of $\overline{m}_+$ as the cation-permeable membrane was found to be 2.02 ml for 5.09 millimoles of exchange groups (21). Assuming that each fixed site is at the corner of a simple cubic lattice, an average distance of separation of 8.7Å can be calculated.

An estimation of the distance of closest approach certainly cannot be made using the conditions that prevail in dilute solution, for in the membrane phase a considerably smaller hydration of the ions occurs. The variation of selectivity coefficients with temperature constitutes direct experimental evidence (40). In dilute solutions the distance of closest approach $\mathring{a}$ for potassium methanesulfonate was calculated from activity coefficient data using the extended Debye-Hückel equation,

$$\log_{10} \gamma_\pm = \frac{0.509\sqrt{M}}{1 + 0.329 \times 10^{-8}\mathring{a}\sqrt{M}} \quad [15]$$

by Fine, Rothenberg, and Gregor (41), and found to be 3.96Å. This compares with 4.0Å calculated from similar measurements with potassium chloride.

It is evident that $\mathring{a} = 4$Å is not a realistic value for this system; the value of 2.5Å (37) is more realistic.

In view of the fact that most of the water present in these membrane systems must be part of hydration spheres, one must take a value of $\bar{\epsilon}$, the dielectric constant in the membrane phase, as being considerably less than its value in dilute solution. The discussion in Robinson and Stokes (39) suggests a value of $20 < \bar{\epsilon} < 60$, which means that the exponential term can vary by e^3 or a factor of about 20. Obviously, agreement between theory and experiment is fortuitous indeed. Actually, in making these calculations an error in $\mathring{a}$ of 0.1Å can alter the result by a factor of two.

That the activation energy for the diffusion of counter-ions is larger than in free solution has been noted by several authors, particularly Boyd and Soldano (5). Frenkel (42) and Carman and Raal (43) have shown that surface diffusion coefficients likewise have higher activation energies.

Turning to any correlation that might exist between the diffusion coefficients of ions and of neutral molecules in the same cation-permeable membrane system, it was found that $\overline{D}_+/D_+ = 0.014$, $\overline{D}/D = 0.0030$ for urea and 0.0031 for acetic acid. The relatively greater retardation of urea and acetic acid may be due to their adsorption and immobilization by the matrix, or because they must diffuse *around* the counter-ions. The generally good agreement between the relative diffusion coefficients of all mobile species corroborates our general picture of the relative simplicity of these membrane systems.

Any correlation between diffusion coefficients of counter-ions in systems of different degrees of cross-linking or matrices will depend in large part upon pore diameter data. For example, $\overline{D}_+$ here was 2×10^{-7}, compared to 5×10^{-6} in an approximately 10% cross-linked resin (26). However, the latter system is highly permeable to sucrose molecules, while the pores of our membrane system exclude this solute to a pronounced degree (37).

Acknowledgment

The authors wish to express their thanks to the Office of Saline Water, Department of the Interior and to the National Science Foundation for their support of this study. This paper was abstracted from the thesis of one of the authors (M.A.P.) submitted in partial fulfillment of the requirements for a Ph.D. degree in chemistry at the Polytechnic Institute of Brooklyn.

Manuscript received April 6, 1959. This paper was prepared, in part, for delivery before the New York Meeting, April 27-May 1, 1958.

Any discussion of this paper will appear in a Discussion Section to be published in the June 1960 JOURNAL.

LIST OF SYMBOLS

Subscripts on concentration terms denote ionic species; superscripts on concentration terms denote interfacial solution concentration. The superscript bar refers to parameters within the membrane phase. Primed terms refer to ambient solutions.

- A, B — Cationic species.
- l — thickness of membrane, cm.
- δ — thickness of unstirred film, cm.
- C — concentration, molarity, meq cm^{-3} of membrane.
- x — spatial coordinate in membrane in cm.
- D — diffusion coefficient, $cm^2\ sec^{-1}$.
- U — mobility, $cm^2\ sec^{-1}\ volt^{-1}$.
- J — flux in equivalents (or coulombs) $cm^{-2}\ sec^{-1}$.
- ϕ — potential, volts.
- R — gas constant.
- T — absolute temperature, °K.
- Z — valence.
- $\mathbf{F}$ — the Faraday.
- k — partition coefficient.
- κ — specific conductance, ohm^{-1}, cm^{-1}.
- Ω — membrane resistance, ohm cm^2.
- λ — equivalent conductance, mho $cm^{-2}\ eq^{-1}$.
- m — concentration, molality, meq g^{-1} water.
- M — ambient solution concentration, molarity.
- $\gamma_\pm$ — mean activity coefficient.
- F — drag factor.
- s — diameter of sphere in cm.
- S — diameter of uniform pore in cm.
- ϵ — dielectric constant.
- $\mathring{a}$ — distance of closest approach in Å.

REFERENCES

1. G. E. Boyd, A. W. Adamson, and L. S. Myers, *J. Am. Chem. Soc.*, **69**, 2836 (1947).
2. T. R. E. Kressman and J. A. Kitchener, *Discussions Faraday Soc.*, **7**, 90 (1949).
3. J. J. Grossman and A. W. Adamson, *J. Phys. Chem.*, **56**, 97 (1952).
4. M. Tetenbaum and H. P. Gregor, *ibid.*, **58**, 1156 (1954).
5. G. E. Boyd and B. Soldano, *J. Am. Chem. Soc.*, **75**, 6091, 6096 (1953).
6. G. E. Boyd and B. Soldano, *ibid.*, **75**, 6105 (1953).
7. A. Lowan, *Duke Math. J.*, **7**, 94 (1935).
8. F. Helfferich, *Discussions Faraday Soc.*, **21**, 83 (1956).
9. B. A. Soldano and G. E. Boyd, *J. Am. Chem. Soc.*, **75**, 6107 (1953).
10. G. Schulze, *Z. physik. Chem.*, **89**, 168 (1914).
11. R. Schlögl and U. Schödel, *Z. physik. Chem.*, **5**, 372 (1955).
12. H. P. Gregor, H. Jacobson, R. C. Shair, and D. M. Wetstone, *J. Phys. Chem.*, **61**, 141 (1957).
13. H. P. Gregor and D. M. Wetstone, *ibid.*, **61**, 147 (1957).
14. D. M. Wetstone and H. P. Gregor, *ibid.*, **61**, 151 (1957).
15. D. M. Wetstone and H. P. Gregor, *Z. Elektrochem.*, **62**, 3, 274 (1958).
16. H. P. Gregor, *Proc. Natl. Acad. Sci.*, Pub. 568, 240 (1957).
17. H. P. Gregor and K. Sollner, *J. Phys. Chem.*, **50**, 53 (1946).
18. J. Andelman and H. P. Gregor, To be published.
19. D. M. Wetstone, Dissertation, Polytechnic Institute of Brooklyn, 1957.
20. L. Isaacs, *J. Biol. Chem.*, **53**, 17 (1922).
21. H. P. Gregor, F. Gutoff, and J. I. Bregman, *J. Colloid Sci.*, **6**, 245 (1951).
22. H. P. Gregor and M. H. Gottlieb, *J. Am. Chem. Soc.*, **75**, 3539 (1953).
23. M. H. Gottlieb and H. P. Gregor, *ibid.*, **76**, 4639 (1954).
24. H. P. Gregor, *ibid.*, **70**, 1293 (1948).
25. H. P. Gregor, *ibid.*, **73**, 642 (1951).
26. H. P. Gregor, F. C. Collins, and M. Pope, *J. Colloid Sci.*, **6**, 304 (1951).
27. R. M. Wheaton and W. C. Bauman, *Ind. Eng. Chem.*, **45**, 228 (1953).
28. G. Manecke and H. Heller, *Discussions Faraday Soc.*, **21**, 101 (1956).
29. R. Schlögl, *Z. Elektrochem.*, **57**, 195 (1953).
30. R. Schlögl and F. Helfferich, *Z. Elektrochem.*, **56**, 644 (1952).
31. N. Ishibashi, T. Seiyama, and W. Sakai, *J. Electrochem. Soc. Japan*, **23**, 182 (1954).
32. A. Despic and G. J. Hills, *Discussions Faraday Soc.*, **21**, 150 (1956).
33. D. Richman and H. C. Thomas, *J. Phys. Chem.*, **60**, 237 (1956).
34. H. P. Gregor, J. Belle, and R. A. Marcus, *J. Am. Chem. Soc.*, **77**, 2713 (1955).
35. P. C. Carman, "Flow of Gases through Porous Media," Academic Press, Inc., New York (1956).
36. R. Schlögl and B. Stein, *Z. physik. Chem.*, **13**, 111 (1957).
37. H. P. Gregor and H. Jacobson, To be published.
38. L. R. Bacon, *J. Franklin Inst.*, **221**, 251 (1936).
39. R. A. Robinson and R. H. Stokes, "Electrolyte Solutions," Butterworth Scientific Publications, London (1955).
40. H. P. Gregor and J. I. Bregman, *J. Colloid Sci.*, **6**, 323 (1951).
41. N. Fine, M. Rothenberg, and H. P. Gregor, To be published.
42. J. Frenkel, "Kinetic Theory of Liquids," Oxford University Press (1947).
43. P. C. Carman and F. A. Raal, *Proc. Roy. Soc.*, **209A**, 38 (1951).

A Method for Evaluating Battery Grade Manganese Dioxide

F. Kornfeil

U. S. Army Signal Research and Development Laboratory, Fort Monmouth, New Jersey

It is well known that, apart from its composition, several factors determine the quality of MnO_2 for use in Leclanché cells. Methods of chemical analysis have, therefore, in the past been supplemented by investigations of the structure of MnO_2, chiefly by studying the diffraction of x-rays and electrons and by measurements of certain magnetic and thermal properties.

In view of the large number of properties which determine the electrochemical behavior of the MnO_2 electrode, it is not surprising that no single test method has as yet been devised which would provide by itself the complete information necessary to predict the performance of the cathode in a dry cell. It is indeed doubtful that such a method will ever be found. Nevertheless, various attempts have been made in recent years to develop relatively simple laboratory techniques for the evaluation of MnO_2 (1, 2). These techniques permit a rather broad classification of the oxides but fail to show a clear quantitative relationship between a measured quantity and the capacities obtained from complete dry cells containing the same oxides.

Experimental

Another method and device for evaluating MnO_2 is suggested in this paper. The principle of operation of this method is quite similar to that of the discharge tests of dry cells. However, the tedious and expensive procedure of manufacturing dry cells for testing purposes is eliminated. Moreover, the length of the discharge period is reduced to approximately one-eighth of the time required in the 16-2/3 ohm continuous drain discharge test on A-size dry cells. The reduction of a 0.500-g compressed pellet of a mixture of MnO_2 and Shawinigan black (weight ratio 10:1) is accomplished in a test cell (Fig. 1) consisting of the two Lucite halves A and B and a plastic piston ("Hysol No. 3110")[1] through the center of which a graphite rod insures good electrical contact with the depolarizer mixture. The pellet is discharged against a circular amalgamated Zn anode to an end-voltage of 1.00 v at 63.5 ma, corresponding to a current density of 50.0 ma cm^{-2} of the cathode-electrolyte interface. The electrolyte is an aqueous solution of 280 g NH_4Cl and 145 g $ZnCl_2$ per liter.

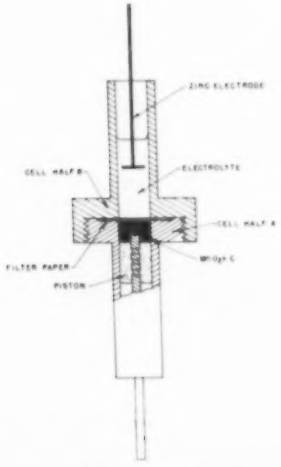

Fig. 1. Completely assembled test apparatus

The test circuit is based on the interrupter principle and is described in detail elsewhere (3, 4). Its essential feature is that the drop of potential due to the internal resistance of the cell is eliminated from the reading of the cell voltage. Therefore, it is not necessary to control some of the factors contributing to the internal resistance, such as the distance between the electrodes, conductance of the graphite rod, and, within a rather wide range, the pressure used in the preparation of the depolarizer pellet.

The results obtained with this method, expressed as length of time required to decrease the cell voltage to 1.00 v (*IR*-drop eliminated), are reproducible within $\pm 2.5\%$. This agreement is remarkably good compared to the results of dry cell tests which normally show a scatter of $\pm 10\%$.

About fifty different samples of MnO_2 were selected for each of which high drain dry cell test results were available of a uniformity considerably greater than $\pm 10\%$. These samples then were discharged in the apparatus at 25°C. Three typical discharge curves are shown in Fig. 2. The results of these tests are plotted against the corresponding dry cell test results (A-size cells) in Fig. 3. The resulting curve was used subsequently to predict the capacities in dry cells of about two hundred additional samples of MnO_2.

The agreement between the present method and the dry cell test results is generally very satisfactory. However, it should be pointed out that, although this method in its present form gives a quantitative measure of the inherent capacity of the

[1] Houghton Laboratories, Olean, N. Y.

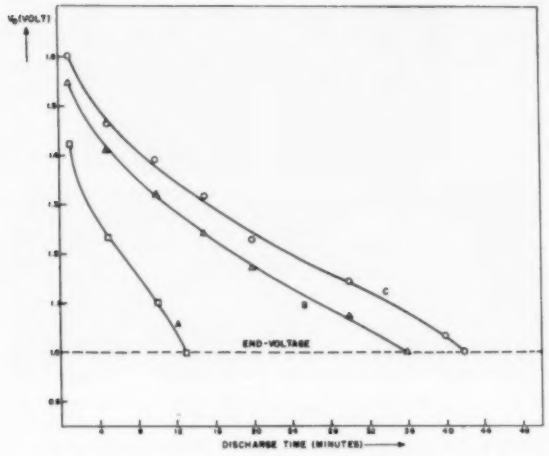

Fig. 2. Discharge curves. Curve A: African ore; Curves B, C: electrolytic manganese dioxides. V_o: Terminal voltage minus IR-drop.

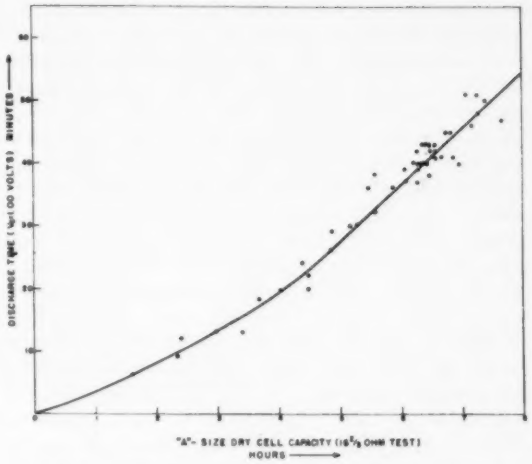

Fig. 3. Correlation between discharge time in test apparatus (end-voltage 1.00 v) and 16-2/3 ohm continuous drain dry cell test.

MnO_2 tested, this capacity need not necessarily be obtainable in an actual dry cell. For example, it has been observed that an oxide of an extremely low apparent density has a lower capacity in a dry cell than would be expected using the curve in Fig. 3, because the dry cell simply contains a comparatively smaller quantity of this particular oxide. This difficulty probably can be overcome by modifying the test procedure so that a constant volume is used instead of a constant mass of the depolarizer.

Acknowledgments

The author wishes to express his appreciation to Mr. H. L. Suchan who carried out a large number of the discharge tests, and to Mr. W. F. Nye, this Laboratory, and Mr. F. Keller, Bright Star Industries, for their continued interest and many helpful suggestions.

Manuscript received Oct. 8, 1958.

Any discussion of this paper will appear in a Discussion Section to be published in the June 1960 JOURNAL.

REFERENCES

1. N. C. Cahoon, *This Journal*, **99**, 343 (1952).
2. C. K. Morehouse and R. Glicksman, *ibid.*, **103**, 94 (1956).
3. A. Marko and K. Kordesch, U.S. Pat. 2,662,211 (1953).
4. F. Kornfeil, Doctoral Thesis, University of Vienna, Austria (1952).

A Study of Stripping Anodized Coatings from an Aluminum Alloy

Walter Beck, John Danovich, and Sara J. Ketcham

Aeronautical Materials Laboratory, Naval Air Material Center, Philadelphia, Pennsylvania

A study has been made of the effect of a HF-HNO_3 mixture in stripping anodized coatings from an aluminum alloy. Comparison of efficacy and amount of metal attack was made with that of the CrO_3-H_3PO_4 solution usually used for this purpose. Information about some of the variables which control the process of film stripping was obtained from weight loss determinations, microscopic and electron microscopic studies.

Experimental Procedure

Pretreatment, anodizing, and stripping.—Unless otherwise reported, panels 5 x 10 x 0.13 cm of 5052 aluminum alloy, which contains 2.5% Mg and 0.25% Cr, were vapor degreased, immersed for 15 min in a nonetching alkaline cleaning solution, and water rinsed. Immediately following this pretreatment cycle, the panels were anodized in a 7% CrO_3 bath, operated at 35°C with air agitation. The average current density was 155 ma/dm^2 and the applied voltage 40 (1). Specimens to be used for weight loss measurements were anodized to a coating weight[1] of 48 mg/dm^2 (450 mg/ft^2). Samples for microscopic studies were buffed to a mirror finish, then anodized to a weight of 113 mg/dm^2 (1050 mg/ft^2), the heavier coating being required to permit metallographic examination at a reasonably low magnification.

The CrO_3-H_3PO_4 solution which contained 0.6*N* CrO_3 and 1.6*N* H_3PO_4, was used at 88°C, the HF-HNO_3 solution which contained 0.1*N* HF and 3.5*N* HNO_3 at room temperature.

Preparation of specimens for photo and electron micrographs.—Before sectioning and mounting, the

[1] The weight of an anodic coating is determined by weighing the anodized panel, stripping the coating in the CrO-H_3PO_4 acid mixture described here for 10 min, and reweighing the panel. The weight loss represents coating only, as this solution does not attack the base metal in any measurable amount.

specimens were covered with an epoxy resin to protect the anodized film against damage during the preparation for microscopic examination. Specimens were sectioned at an angle of 45° to obtain a greater thickness for study.

For electron microscopic inspection, the panels were cut into 1.59 by 1.59 cm (0.625 by 0.625 in.) squares, cleaned with benzene, and molded between layers of polystyrene at 121°C-149°C (250°-300°F) under 3000 to 4000 psi. The plastic was cut along the edge of the specimen and removed after cooling on dry ice. In order to depict the pore structure of the coatings, silicon monoxide replicas were employed. In this technique, a thick film of silicon monoxide was vapor deposited approximately normal to the surface of the impression. The pores in the impression are represented as peaks, and because of their geometry, they appear as holes in the silicon monoxide replica.

To obtain greater surface detail, a thin carbon replica, shadowed with chromium at an angle of 30°, was employed.

The replicas were floated off the polystyrene impression in benzene, washed twice in this liquid, placed on screen supports, and examined in the electron microscope.

Experimental Results and Discussion

Microscopic and electron microscopic observations.—The photomicrographs in Fig. 1 illustrate the effect of the CrO_3-H_3PO_4 stripping solution, showing the coating as anodized (Fig. 1*a*), after immersion for 10 sec during which the thickness was reduced very slightly but uniformly (Fig. 1*b*), and after immersion for 30 sec during which the coating was completely removed (Fig. 1*c*).

Results of electron microscope studies are given in Fig. 2. The surface of the aluminum alloy after buffing but before anodizing shows the typical furrow structure of sub-grain boundaries and some contaminants (Fig. 2*a*). The as-anodized surface

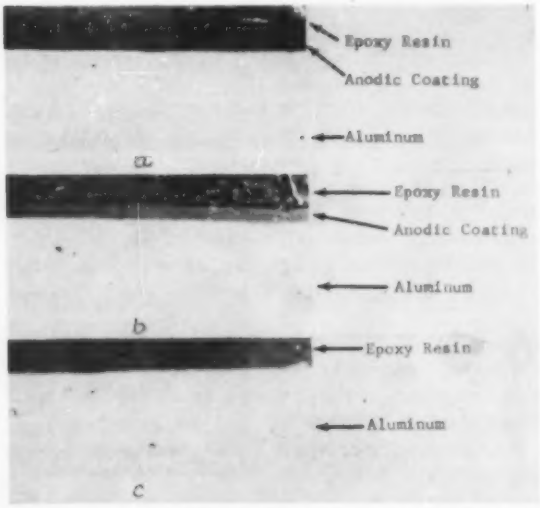

Fig. 1. a, As-anodized; b, stripped for 10 sec in CrO_3-H_3PO_4; c, stripped for 30 sec in CrO_3-H_3PO_4. Magnification 500X before reduction for publication.

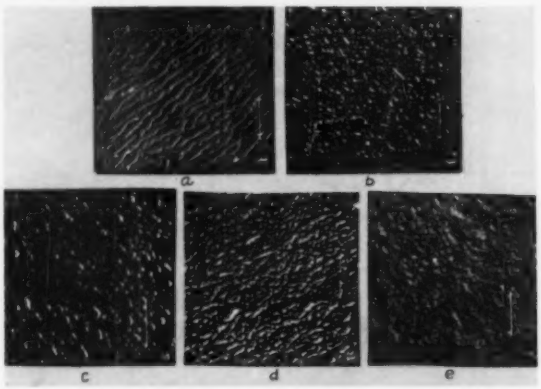

Fig. 2. a, Surface of the aluminum alloy before anodizing; chromium shadowed carbon replica of a polystyrene impression; b, surface of a specimen in as-anodized condition; average pore diameter is 300Å; thick silicon monoxide replica of a polystyrene impression; c, anodized specimen exposed for 10 sec in CrO_3-H_3PO_4; average pore diameter is 600Å; thick silicon monoxide replica of a polystyrene impression; d, same surface as in c; chromium shadowed carbon replica of a polystyrene impression; e, anodized specimen exposed for 30 sec in CrO_3-H_3PO_4; chromium shadowed carbon replica of a polystyrene impression. Magnification 10,000X before reduction for publication.

reveals an average pore diameter of 300Å, the pores being the white areas (Fig. 2*b*). Immersion in the CrO_3-H_3PO_4 for 10 sec enlarged the average pore diameter to 600Å (Fig. 2*c*), attack of the pore walls is following an elliptical pattern and produces ridges in the coating (Fig. 2*d*). After 30 sec immersion, weight loss measurements (to be discussed in the last section) indicate complete removal of the coating and (Fig. 2*e*) shows that the surface of the base metal has been roughened to a considerable degree, an effect which has been related to the anodizing process (2).

The mechanism which controls the action of the CrO_3-H_3PO_4 system may be discussed in the light of the well-known oxide cell structure of anodized coatings (3). By the attack of the pore walls demonstrated in Fig. 2*d*, the enlargement of the pores, shown in Fig. 2*c* is achieved (4).

It may be surmised that the enlargement of pores due to the dissolution of oxides which build up the pore walls, in the CrO_3-H_3PO_4 solution, facilitates its access to the barrier at the base of the pores.

The HF-HNO_3 *System*

The electron micrograph depicted in Fig. 3*a* reveals a random attack of the coating which, after an

Fig. 3. a, Anodized specimen exposed for 150 sec in HF-HNO_3; chromium shadowed carbon replica of a polystyrene impression, magnification 10,000X before reduction for publication; b, anodized specimen exposed for 450 sec in HF-HNO_3; magnification 500X before reduction for publication.

immersion period of 150 sec, is in a progressive stage of decay; pits can be distinguished in the layer. As depicted in Fig. 3*b*, after an immersion period of 450 sec, the metal underneath the coating is attacked at numerous spots (5) and the layer partially loosened but not yet completely removed.

Figure 3*a* indicates that oxide dissolution is again one of the variables involved in the mechanism which determines the removal of the coating. In addition, as demonstrated in the photomicrograph in Fig. 3*b*, undermining of the coating because of metal attack is another parameter (5). Apparently, in the HF-HNO_3 solution, the rate of oxide dissolution is slower than in the CrO_3-H_3PO_4 solution, and coating removal is partially dependent on film undermining.

Coating Weight Loss

Since the CrO_3-H_3PO_4 stripper does not attack the base metal to any measurable extent, differences in weight found before and after exposure to this solution can be assumed to represent coating weight loss only. However, in HF-HNO_3 solution, the possibility of metal attack had to be considered because immersion of an uncoated specimen in this solution had resulted in considerable weight loss.

After the total weight loss in this solution was obtained for each exposure time, the amount that represented only coating weight loss was determined in the following manner: These specimens were subsequently immersed in the CrO_3-H_3PO_4 acid stripper to see whether any residual coating remained. The weight of this residual coating (if any was present) was then subtracted from the average coating weight of 48 mg/dm^2 (3.1 mg/in.^{2}) to obtain the coating weight loss only. The difference between this figure and the total weight loss was considered to be the amount of metal attack. If no residual coating was present, the amount of weight loss in excess of 48 mg/dm^2 (3.1 mg/in.^{2}) was considered to be the amount of metal attack.

Weight losses plotted in Fig. 4 are the averages of 3 measurements with a maximum deviation not exceeding 6%. With the CrO_3-H_3PO_4 system, a coating

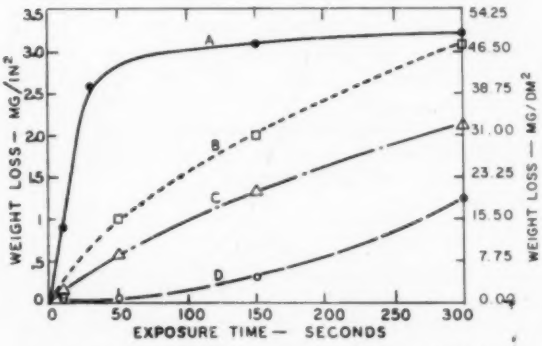

Fig. 4. Plot of weight loss vs. exposure time. Weight loss due to: A, solvation of anodized coating in CrO_3-H_3PO_4; B, removal of anodized coating in HF-HNO_3; C, dissolution of metal from uncoated specimen in HF-HNO_3; D, dissolution of metal from underneath anodized coating in HF-HNO_3.

weight loss of 25%, determined after a 10-sec exposure, correlates qualitatively with a 10% loss in coating thickness (measured microscopically) and the appreciable increase in pore diameter, as shown in Fig. 2c. Also, a coating weight loss of about 75% can be considered to be in a fair agreement with the fact that, after the 30-sec exposure, both the microscopic and the electron microscopic investigation disclosed complete removal of the anodized layer. In the HF-HNO_3 solution, the weight loss determinations and the optical findings indicated a much slower rate of coating removal than in the CrO_3-H_3PO_4 system. Figure 4 also illustrates that almost from the very beginning of the stripping process the removal of the coating is accompanied by the dissolution of metal from beneath the oxide layer when specimens were exposed to the HF-HNO_3 solution. Within an initial period of about 100-sec duration, the rate of dissolution of the aluminum from underneath the anodized layer is considerably slower than that of an uncoated specimen. After exceeding this time interval, the metal is dissolved at a rate similar to that resulting on the unanodized specimen. Also, the electron micrograph 3*a* taken after an immersion of 150 sec showed that the coating was strongly attacked and pitted, while the photomicrograph taken after 450 sec revealed strong metal attack underneath a partially loosened coating. From the last experiments, it has to be concluded that uncritical use of the HF-HNO_3 system may lead to a much greater metal attack than is necessary for coating removal.

HF-HNO_3 solutions have come into widespread use for removal of oxide coatings not only from aluminum alloys but also from numerous other metals such as Ti, Mo, Zr, and Ta (6). Metal losses due to over etching are avoidable, and the HF-HNO_3 containing systems should only be used when the concentrations and time of exposure are controlled carefully.

Acknowledgment

The authors are much indebted to Mr. F. S. Williams and Dr. G. K. Holmes, Superintendents of the Metallurgical and Chemical Engineering Divisions, respectively, Aeronautical Materials Laboratory, and Mr. Jack Smith, Head of the Chemical Branch for the great interest taken in this study.

Manuscript received Dec. 29, 1958. This paper was prepared for delivery before the Ottawa Meeting, Sept. 28-Oct. 2, 1958.

Any discussion of this paper will appear in a Discussion Section to be published in the June 1960 JOURNAL.

REFERENCES

1. MIL-A-8625 (issued December 14, 1954).
2. S. Wernick and R. Pinner, "Surface Treatment and Finishing Aluminum and its Alloys," p. 225, Robert Draper Ltd., Teddington Middle Essex, England (1956).
3. F. Keller, M. S. Hunter, and D. L. Robinson, *This Journal*, **100**, 416 (1953).
4. D. J. Stirland and R. W. Bicknell, *ibid.*, **106**, 483 (1959).
5. N. C. Welsh, *J. Inst. Met.*, **85**, Pt. 4, 133 (1956).
6. D. A. Vermilyea, *This Journal*, **104**, 213 (1957).

The Gudden-Pohl Effect of ZnS:Cu

Yoshihide Kotera and Kiyotake Naraoka

Government Chemical Industrial Research Institute, Tokyo, Japan

The Gudden-Pohl effect (1) on the phosphorescence of various ZnS:Cu phosphors was studied by means of an applied alternating electric field. The phosphors were prepared by a method similar to that described by Bube (2). They comprised two series of hexagonal and cubic ZnS:Cu (2% NaCl) phosphors and contained 10^{-6}, 3×10^{-6}, 10^{-5}, 3×10^{-5}, 10^{-4}, 3×10^{-4}, and 10^{-3} moles Cu per mole ZnS. The hexagonal and cubic phosphors were fired at 1200° and 900°C, respectively.

All phosphors were embedded in Acrylite (polymethylmethacrylate) and measured in an electroluminescent cell of common construction. The electric field was obtained from a 50 cps source, and the field intensity was estimated to be about 10,000 v/cm. The integral of the light flash (i.e., the area under the curve shown in Fig. 1, in which the abscissa is time and the ordinate is the photocurrent from a photomultiplier) during the application of the field was taken as a measure of the magnitude of the Gudden-Pohl effect (Fig. 1). Prior to the measurement the phosphors had been excited with near ultraviolet radiation. The exciting radiation was then removed and the electric field was applied 1 min after removal of the radiation.

The integrals of the light flashes of both hexagonal and cubic ZnS:Cu increased with increasing copper content and reached a maximum at a content of 10^{-4} mole. With further increasing copper contents they decreased again. In general, the effect was stronger with cubic phosphors than with hexagonal ones of the same copper content. The phosphorescent intensity after one minute's decay and the infrared stimulation during illumination with infrared after one minute of normal phosphorescent decay were measured. Results were nearly identical with those reported by Bube (3).

It has been known that the Gudden-Pohl effect may be caused by electrons released from filled traps by the action of a field. Accordingly, from the knowledge of trap characteristics, the existence of a Gudden-Pohl effect might be predicted. Figure 2 shows the temperature dependence of the Gudden-Pohl effect and the thermoluminescence above room temperature. For cubic ZnS:Cu, the effect becomes smaller at rising temperatures between 20° and 120°C. There is no glow peak in this temperature range. In contrast, the effect increases at higher temperatures with hexagonal ZnS:Cu and it reaches a maximum at 70°C, while the glow curve has its peak at 550°C (Fig. 2).

Two glow curves were obtained for hexagonal ZnS:Cu (10^{-4}), one with and the other without previous application of an electric field. It was found that the two glow curves have about the same height.

From the above observations it is concluded that the deeper traps which correspond to a glow peak at 55°C do not produce the Gudden-Pohl effect at room temperature. Rather, the increase of the effect at higher temperatures may be ascribed to the emptying of the deeper traps which are able to release their electrons thermally at higher temperatures.

Manuscript received March 10, 1959.

Any discussion of this paper will appear in a Discussion Section to be published in the June 1960 JOURNAL.

REFERENCES

1. H. F. Ivey, *This Journal*, **104**, 740 (1957).
2. R. H. Bube, *Phys. Rev.*, **80**, 655 (1950).
3. R. H. Bube, *ibid.*, **80**, 764 (1950).

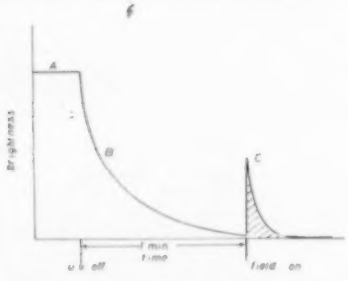

Fig. 1. Schematic representation of the Gudden-Pohl effect. A, Steady luminescence; B, phosphorescent decay; C, Gudden-Pohl effect.

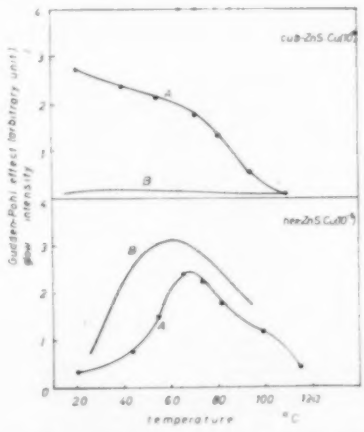

Fig. 2. The Gudden-Pohl effect as a function of temperature (Curves A) and glow curves (B) for ZnS:Cu.

Diffusion of Oxygen in Hafnium

J. Paul Pemsler

Nuclear Metals, Inc., Concord, Massachusetts

Hafnium shares with titanium and zirconium the unusual ability to dissolve large amounts of oxygen in interstitial solid solution. No data have been found regarding the hafnium-oxygen phase diagram other than the existence of a stable oxide HfO_2, and no studies on the diffusion of oxygen in hafnium are reported. The techniques used in this study are similar to those used by the author in a study of the diffusion of oxygen in zirconium (1).

Experimental

The diffusion of oxygen in hafnium was measured by following the rate of dissolution of anodically deposited thin oxide films when annealed *in vacuo*. The thickness of the oxide film was determined periodically during the experiment by observing its color (arising from optical interference) and comparing it with a series of standards.

Reactor grade hafnium samples containing 1.45 w/o Zr and measuring 1.8 x 4.5 x 0.4 cm were obtained from Knolls Atomic Power Laboratory. They were annealed in a vacuum for 1 hr at 800°C, furnace cooled, paper polished on 4/0 emery paper, and then etched for 2 min in a bath of 50% HNO_3, 5% HF, 45% H_2O.

Oxide films were deposited anodically from a 1% KOH solution in distilled water, with the sample as anode and a platinum wire as cathode. Several thicknesses of oxide were deposited on different areas of the same sample. The weight gain on anodization, as measured on a microbalance, was found in separate experiments to be a linear function of the applied voltage over the range studied (0-120 v), and independent of time. Assuming a value of 10.22 g/cm^3 for the density of HfO_2, the oxide thickness deposited during anodization corresponds to 18.9Å/v.

Anodized hafnium samples, sealed off in a Vycor tube, were placed in a horizontal furnace having a view hole for continuous observation of the sample while at temperature. The color of each zone changed with time, indicating a decreasing film thickness. At any given time, the decrease in film thickness was found to be independent of the original film thickness in a particular anodized area; thus identical results were obtained from any one of the color areas.

Results

Microscopic examination of samples which had been anodized and subsequently vacuum annealed revealed that, as in zirconium (1), the dissolution process was not homogeneous, and that, macroscopically, an average process was being observed. A wide range of colors, sharply defined by grain boundaries, was observed under a microscope. The diffusion coefficients calculated are therefore based on a macroscopic, average estimate of color. Variation in the diffusion coefficient by a factor of about two among the differently oriented grains was observed.

The parabolic rate of disappearance of the oxide film on hafnium suggests that the rate-determining step in the dissolution process is the diffusion of oxygen in hafnium metal. The consumption of oxide, generating additional metal, is accompanied by an outward motion of the oxide-metal boundary until the oxide is entirely consumed. Mathematically this case falls within a limited class of moving-boundary diffusion problems, for which solutions are readily found. The diffusion equation is discussed in detail elsewhere (2). From the solution found on the assumption of constant diffusivity, D can be expressed as

$$D = \frac{1}{4b^2}\left(\frac{x'}{\sqrt{t}}\right)^2$$

where b satisfies the equation

$$b\,(1 + \operatorname{erf} b) = \frac{1}{\sqrt{\pi}}\frac{C_o}{m_o}e^{-b^2}$$

Here in time, t, there is a displacement of the oxide-metal boundary, x', which is related to the observed decrease ΔL in thickness of oxide film by the following expression involving the respective molecular volumes

$$x' = \frac{\rho HfO_2}{\rho Hf\ \text{saturated}}\,\frac{\text{Formula weight } (HfO_{sat})}{\text{Formula weight } (HfO_2)}\,\Delta L$$

The quantity ρ is the density, and C_o is the difference between the saturated concentration, C_s, and initial concentration of oxygen in the metal. The quantity m_o represents the weight of oxygen removed from the HfO_2 consumed in the generation of unit volume of saturated hafnium (HfO_{sat}), and may be expressed as

$$m_o = \frac{\text{Formula weight } (HfO_2) - \text{Formula weight } (HfO_{sat})}{\text{Formula weight } (HfO_{sat})}\,\rho HfO_{sat}$$

The precise value of the diffusion coefficient cannot be calculated at this time because the saturation concentration of oxygen in hafnium (O_{sat}) is not known. Nevertheless, by considering the titanium-oxygen and zirconium-oxygen systems (saturation oxygen concentration values 34 a/o and 29 a/o, respectively), reasonable estimates of this value may be made. In this work the diffusion coefficient was calculated for each of three saturation values: 20 a/o, 30 a/o, and 40 a/o oxygen in hafnium. Thus,

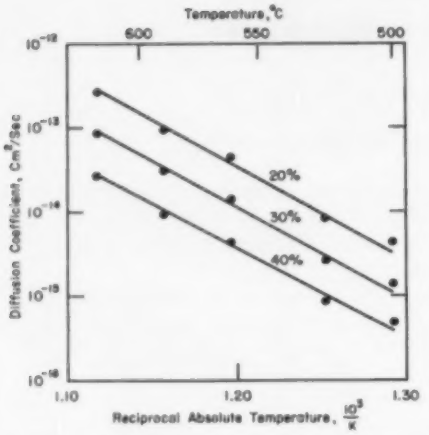

Fig. 1. Temperature dependence of the diffusion coefficient of oxygen in hafnium. The three curves represent results calculated assuming the three indicated oxygen solubilities in hafnium.

$C_o = C_i = 0.30$ g/cm³, 0.50 g/cm³, or 0.76 g/cm³ (the initial concentration was taken as zero); $m_o = 2.07$ g/cm³, 1.83 g/cm³, or 1.52 g/cm³; $x' = 0.657\ \Delta L$ cm, $0.667\ \Delta L$ cm, or $0.678\ \Delta L$ cm; $b = 0.067$, 0.120, 0.218. The density of HfO_2 was taken as the calculated x-ray value equal to 10.22 g/cm³, and the density of hafnium saturated with oxygen was estimated to be about 13.5 g/cm³.

A plot of the logarithms of the diffusion coefficients vs. the reciprocal of the absolute temperature for each of the three assumed oxygen solubilities is shown in Fig. 1. The equation for the diffusion coefficient of oxygen in hafnium in the temperature range of 500°-620°C is given by D, cm²/sec $= 1.4$ exp $[(-51{,}850 \pm 200/RT)]$ for 20 a/o; 0.47 exp $[(-51{,}850 \pm 200/RT)]$ for 30 a/o; and 0.14 exp $[(-51{,}850 \pm 200/RT)]$ for 40 a/o oxygen saturation solubility in hafnium.

The diffusion coefficient of oxygen in hafnium is smaller by a factor of about ten than that of oxygen in zirconium, but the energies of activation are identical.

This work was performed under AEC Contract No. AT(30-1)-1565.

Manuscript received April 24, 1959.

Any discussion of this paper will appear in a Discussion Section to be published in the June 1960 JOURNAL.

REFERENCES

1. J. Paul Pemsler, *This Journal*, **105**, 315 (1958).
2. J. Paul Pemsler, "The Diffusion of Oxygen in Zirconium and Its Relation to Oxidation and Corrosion," Report NMI-1177 (1957).

Technical Feature

The Fuel Cell and the Carnot Cycle

Herman A. Liebhafsky

Research Laboratory, General Electric Company, Schenectady, New York

ABSTRACT

To provide a basis for considering the combination of nuclear reactor (or other heat source) and fuel cell, the well-known fact that the fuel cell escapes the Carnot-cycle limitation is reviewed briefly. Then it is shown that the combination cannot escape this limitation and, in some cases, can only approach the Carnot-cycle efficiency.

The Fuel Cell Alone

The fuel cell is an electrochemical device in which the chemical energy of a conventional fuel is converted directly and usefully into electrical work. As has long been appreciated (1), the fuel cell is potentially attractive because the energy conversion it accomplishes is not subject to the Carnot-cycle limitation. This electrochemical conversion can be isothermal: for the Carnot-cycle limitation to operate, heat must flow from a higher to a lower temperature and be partially converted into work.

More precisely, the chemical energy mentioned above is the free energy

$$\Delta G = \Delta H - T\Delta S \qquad [1]$$

of the reaction

$$\text{Fuel} + \text{Oxygen} = \text{Reaction Products} \qquad [2]$$

(In Eq. [1], ΔH is the change in heat content, and ΔS the change in entropy for reaction [2].) Note, however, that the heat $T\Delta S$ absorbed or liberated in reaction [2] is characteristic of the reaction carried

out reversibly. It can be absorbed or liberated isothermally, and it must on no account be confused with heat that is converted into work in a Carnot-cycle process.

A more detailed analysis of this thermodynamic argument is desirable. In Eq. [1], ΔG is the maximum useful work realizable if reaction [2] is carried out isothermally and reversibly. If, instead, we choose to carry out this reaction nonisothermally with no work done, all the chemical energy will appear as heat. Because heat is random in nature, and work is a directed process, a price must be paid to convert heat into work; this price is the Carnot-cycle limitation. To escape this price, it is necessary to avoid randomizing the chemical energy as heat.

The electrochemical cell permits one to avoid this randomization. In such a cell, reaction [2] will occur in two parts (or half-cell reactions) schematically as follows:

Anode Reaction: Fuel = Ions + Electrons [2a]

Cathode Reaction: Oxygen + Electrons = Ions [2b]

When reaction [2] is carried out in this way, randomization never occurs because the electrons liberated at the anode flow unidirectionally to the cathode through the external circuit. They flow in this direction because they are driven by an electromotive force proportional in the limit to the free energy change. Because of this driving force, it is possible to make the electrons do work before they reach the cathode. Randomization of the chemical energy is thus avoided, and the Carnot-cycle limitation does not apply.

If the chemical energy of reaction [2] is randomized as heat that is later converted to work in a heat engine, the maximum useful work recoverable will be the familiar $\Delta H(T_1 - T_2)/T_1$, where the temperatures apply to the heat engine; that is, T_1 might be the inlet temperature of the first stage in a turbine; of course it is less than the temperature under the boiler.

In assessing the possible advantage a fuel cell might have over a conventional power plant, it is thus necessary to compare $\Delta H(T_1 - T_2)/T_1$ with ΔG (Eq. [1]). But the relationship of ΔH to ΔG depends on $T\Delta S$. Now, the sign and magnitude of this last term depend on the heat capacities of the substances in reaction [2] because

$$d(\Delta S) = \Delta Cp \, d\ln T \text{ (at constant pressure)} \quad [3]$$

(Assume ΔCp constant. In general, the integration of this equation also requires the statement about entropy changes at the absolute zero that is known as the Third Law of Thermodynamics. This need not concern us here.)

The three possible relationships of ΔH and ΔG are summarized in Table I.

The present outlook is that all successful fuel cells will use gaseous fuels, hydrogen and carbon monoxide being the most likely. These gases may prove necessary intermediates even when hydrocarbons are used, for the direct anodic oxidation of hydrocarbons to water and carbon dioxide is difficult to accomplish. Because the oxidation of hydrogen and of carbon monoxide to gaseous products reduces the number of gaseous molecules, only Case 3, Table I, is of immediate practical concern. (The sign and magnitude of ΔCp for reaction [2] are determined primarily by the change in the number of gaseous molecules during reaction. Note that this change is zero for the oxidation of methane.)

Table I. Maximum useful work and change in heat content for reaction [2]

Case	ΔCp	Heat exchange*	Arithmetic relationship
1	Positive	Absorbed by cell	$\Delta G > \Delta H$
2	Zero	None	$\Delta G = \Delta H$
3	Negative	Rejected by cell	$\Delta G < \Delta H$

* Heat exchange with environment when reaction [2] proceeds isothermally and reversibly.

To illustrate the relationship between ΔG and ΔH, let us examine the gaseous reaction

$$H_2 + \tfrac{1}{2} O_2 = H_2O \quad [4]$$

for which data (2) are given in Table II.

The ratio in the last column may be compared with $(T_1 - T_2)/T_1$ equals 64%, which is the Carnot efficiency for a good modern steam plant that might attain an actual over-all efficiency of 40%. Table II shows clearly that the potential advantage of this fuel cell over the steam plant will disappear with increasing temperature unless the rejected heat is properly used. This is a much more serious consideration in our day than in Ostwald's (1), when a fuel cell would have been called on to compete with steam plants having an over-all efficiency of only 10%.

Nuclear Reactor and Fuel Cell

As nuclear power bcomes increasingly available, one hears more frequently the suggestion that a fuel cell (or other battery) be combined with a nuclear reactor so as to convert heat into electric energy. Any other source of heat could in principle serve as well. In the fuel cell, for example, elements A and B would be consumed at temperature T_2 to produce electric energy and to form the compound AB, which would flow to the reactor at temperature T_1, where it would be dissociated to regenerate A and B.

The compound AB and its elements may be regarded as a working fluid in a thermal cycle in which heat is changed into work. On general grounds, one is justified in concluding that this conversion of heat into work must be Carnot-cycle limited in accord with the Second Law. The conclusion applies even though the working fluid is un-

Table II. ΔG° and ΔH for a hydrogen fuel cell

T, °K	ΔH, cal/mole	ΔG°, cal/mole*	$\Delta G^\circ/\Delta H$
400	−58,040	−53,520	0.92
500	−58,270	−52,360	0.90
1000	−59,210	−46,030	0.78
2000	−60,260	−32,310	0.54

* This free energy change, ΔG°, is for all three gases in their standard states (about 1 atm). The superscript must be used also for entropy changes at the standard state (ΔS°), but may be omitted in the present cases from ΔH because this function is virtually independent of volume.

usual in that it undergoes dissociation and recombination. Although the fuel cell alone escapes the Carnot-cycle limitation, the combination of fuel cell and nuclear reactor does not. Detailed analysis is necessary, however, to show whether the Carnot-cycle efficiency can actually be attained.

To make the analysis, let us represent the cycle as follows:

Dissociation in Reactor: AB = A + B at T_1 (I)
Recombination in Fuel Cell: A + B = AB at T_2 (II)

Heat Exchange (connecting link) A and B initially at T_1 (III)
with AB initially at T_2

The maximum efficiency will be attained if the cycle is reversible throughout. We would then have a reversible isothermal process (I) at T_1, which is the reverse of a reversible isothermal process (II) at T_2. The heat exchange process (III) cannot, however, be reversible unless ΔCp is zero.

That a value of ΔCp other than zero lead to irreversible heat flow in process (III) is easily shown. If, for example, ΔCp in process (II) is negative, then the combined molal heat capacities of A and B exceed that of AB. If ΔCp is negative also at T_1, then AB in passing from fuel cell to reactor cannot en route absorb enough heat from A and B to keep infinitesimal the temperature difference between the two legs of the heat exchanger. Consequently, A and B will reach the fuel cell at a temperature above T_2, where the irreversible flow of heat will continue until temperature equilibrium is established.

Because further discussion of such irreversible heat flow is not necessary to the main argument, let us proceed with Table I, Case 3, for which ΔCp is negative.

We need not inquire into the nature of the isothermal reversible processes (I) and (II). We know that each (and the cycle) must obey the Laws of Thermodynamics. We obtain the ideal efficiency in three steps. We postulate A, B, and AB to be in their standard states at T_1 and at T_2.

1. For the two isothermal processes only, with the working fluid initially at T_1, the net maximum useful work under the postulated conditions is

$$\Delta G^\circ_2 - \Delta G^\circ_1 = (\Delta H_2 - \Delta H_1) - (T_2\Delta S^\circ_2 - T_1\Delta S^\circ_1)$$

or

$$\Delta G^\circ_2 - \Delta G^\circ_1 = (\Delta H_2 - \Delta H_1) + (T_1\Delta S^\circ_1 - T_2\Delta S^\circ_2) \quad [5]$$

(Here, as in Table II, the superscripts indicate that standard states are involved. In practice, of course, A, B, and AB are not likely to be in their standard states, but this does not affect the argument.)

2. The heat absorbed from the nuclear reactor is $T_1\Delta S^\circ_1$.

3. The ideal efficiency is

$$\frac{\Delta G^\circ_2 - \Delta G^\circ_1}{T_1\Delta S^\circ_1} = \frac{(\Delta H_2 - \Delta H_1) + (T_1\Delta S^\circ_1 - T_2\Delta S^\circ_2)}{T_1\Delta S^\circ_1} \quad [6]$$

Were our thermal cycle completely reversible, we should expect it to have the Carnot efficiency. The right side of Eq. [6] degenerates to the Carnot efficiency if

$$\Delta H_1 = \Delta H_2 \text{ and } \Delta S^\circ_1 = \Delta S^\circ_2 \quad [7]$$

Noting that

$$d(\Delta H) = \Delta Cp\, dT \quad [8]$$

(assume ΔCp constant)

and considering Eq. [3], we conclude that Eq. [7] is valid if ΔCp is zero. This is true for Table I, Case 2, in which the heat exchange process (III) can be made reversible. With complete reversibility, the combination of nuclear reactor and fuel cell will attain Carnot efficiency.

Let us now examine Table I, Case 3, beginning with a numerical illustration. Let us consider that a hydrogen fuel cell at 500°K (T_2) is combined with a nuclear reactor at 2000°K (T_1). By use of Eq. [6] and of data in Table II, we find

$$\frac{-20{,}050}{\dfrac{-52{,}360 + 32{,}310}{-27{,}950}} =$$

$$\frac{+1990 \qquad -22{,}040}{\dfrac{(-58{,}270 + 60{,}260) + (-27{,}950 + 5910)}{-27{,}950}} \text{ or } 73.3\% \quad [9]$$

This efficiency is less than 75%, the efficiency of a Carnot cycle operating between 2000° and 500°K. Why? Because of the irreversibility in the heat flow process (III), which is traceable to the negative ΔCp.

The difference between 73.3 and 75% subdivides into (*a*) the effect of changing temperature on ΔH and (*b*) the effect of changing temperature on ΔS. (*a*) As Eq. [9] shows, the heat of reaction [4] increases numerically (from −58,270 to −60,260 cal) as the temperature increases from 500° to 2000°K. Consequently, the numerator in Eq. [9] decreases by 1990 cal and this acts to *reduce* the efficiency below the Carnot value. (*b*) Suppose the reduction just described were absent. Then Eq. [6] would yield the Carnot efficiency if ΔS°_2 were replaced by ΔS°_1. What is the effect of this replacement? $T_2\Delta S^\circ_2$ is −5910 cal, and $T_2\Delta S^\circ_1$ is −6990 cal; consequently, the use of the (correct) $T_2\Delta S^\circ_2$ term in Eq. [9] gives a larger (negative) number (by 1080 cal) in the numerator than would the insertion of $T_2\Delta S^\circ_1$, which insertion would yield the Carnot efficiency under the conditions stipulated. On this basis, we may say that the effect of changing temperature on ΔS° tends to *counteract* the analogous effect on ΔH.

It will now be shown that the effect on ΔH is always numerically the larger.

For this to be true, we must have (Eq. [3] and [8])

$$\int_{T_2}^{T_1} \Delta Cp\, dT > T_2 \int_{T_2}^{T_1} \Delta Cp\, d\ln T \quad [10]$$

If we write $T_1 = T_2 + \Delta T$, relation [10] is tantamount to

$$\Delta T > T_2 \ln \frac{T_2 + \Delta T}{T_2} \quad [11]$$

or

$$e^{\Delta T/T_2} > 1 + \frac{\Delta T}{T_2} \quad [12]$$

The correctness of relation [12] is easily established by comparing it with the series

$$e^x = 1 + x + \frac{x^2}{2!} + \frac{x^3}{3!} + - - - \qquad [13]$$

It follows therefore that the combination of nuclear reactor and fuel cell will, even under ideal conditions, have an efficiency somewhat below the Carnot if ΔCp for reaction [2] is negative. As the foregoing analysis has shown, the difference generally will be small owing to the interaction of the changes in heat content and in entropy.

If ΔCp were positive, A and B could not heat AB to temperature T_1 in the heat exchange process (III). The deficit would have to be made up from the nuclear reactor, and it would therefore appear as an added term in the denominator of Eq. [6]. No doubt detailed calculations for the case of positive ΔCp would also show the Carnot-cycle efficiency to be an upper limit.

Although thermodynamics does not require it, let us examine the combination of nuclear reactor and fuel cell in more detail. Water, especially water vapor, is a poor electrolyte. We shall therefore have to add an electrolyte so that the cell can function. This electrolyte may very well interact with water, and the energy of such interaction will have to be considered. In particular, the work required to separate the water from the salt will have to be subtracted from the work output of the nuclear reactor-fuel cell system. This will reduce the attractiveness of the scheme.

To bring the entire picture nearer reality, we point out, as did Yeager (3), that electrolysis is the simplest process for dissociating AB reversibly and isothermally at temperature T_1. From the electrical energy ΔG_2, ΔG_1 will have to be diverted to accomplish this dissociation. If A and B are gases, electrolysis has the great advantage of separating them at the minimum energy cost, which is ΔG_1. This seems the simplest solution to the separation problem, a problem that can be formidable enough to make the nuclear reactor-fuel cell scheme unattractive.

The energy cost of transferring the gases from reactor to cell and back to reactor has been neglected. No matter how small the cost, the need for this transfer will further reduce the attractiveness of the scheme.

Instead of behaving like water, AB might be stable in state 2 but unstable in state 1. One might then assume that AB does not dissociate until it is passed over a catalyst at temperature T_1, when it dissociates *spontaneously* to regenerate A and B. A substance such as this is unlikely to have a large value of ΔG°_2, and the useful work recoverable from the cycle is likely to be small. Appreciable irreversibility anywhere in the cycle, for example, in the separation of A and B at temperature T_1, will then be a serious matter.

In summary, the combination of nuclear reactor and fuel cell cannot operate at an efficiency exceeding that of a Carnot cycle. It cannot attain this efficiency if the heat capacity relationships among the reacting substances lead to irreversibility in heat transfer. The combination has other limitations that will not usually be offset by factors such as elimination of the need for turbines and generators.

This paper has been restricted to simple fuel cells. In more complex systems (the "redox systems") for the generation of electricity, oxidation-reduction couples are used as intermediates to promote reaction [2]. The conclusions about the Carnot cycle apply to these systems also.

Acknowledgment

The author wishes to thank his colleagues, E. J. Cairns, D. L. Douglas, G. E. Moore, and B. H. Zimm, for helpful discussions of the material in this report.

Manuscript received April 8, 1959.

Any discussion of this paper will appear in a Discussion Section to be published in the June 1960 JOURNAL.

REFERENCES

1. W. Ostwald, *Z.Elektrochem.*, **1**, 122 (1894).
2. J. P. Coughlin, Bureau of Mines Bull. 542, p. 23, U. S. Govt. Printing Office, Washington (1954).
3. E. Yeager, Proceedings 12th Annual Battery Res. and Dev. Conference, Asbury Park, New Jersey, p. 2 (1958); See also R. Roberts, *This Journal*, **105**, 428 (1958).

Discussion Section

This Discussion Section includes discussion of papers appearing in the JOURNAL of The Electrochemical Society, Vol. 105, No. 1, 8, and 9 (January, August, and September 1958), and Vol. 106, No. 1-6 (January-June 1959). Discussion not available for this issue will appear in the Discussion Section of the June 1960 JOURNAL.

The Anodic Oxidation of Zinc and Zinc-Tin Alloys at Very Low Current Density

S. E. S. El Wakkad,[1] A. M. Shams El Din, and H. Kotb (pp. 47-51, Vol. 105)

M. Prazák[2]: The fact described by Dr. S. E. S. El Wakkad and co-workers, namely that Sn-Zn alloy is more easily passivated than pure zinc or pure tin, is very interesting indeed. According to the binary diagram, two phases exist in this alloy: practically pure tin and zinc. According to x-ray investigation, this is true also for electrolytically deposited alloy. Nevertheless, the electrochemical behavior of the alloy does not correspond to the sum for both components present, as we found in the case of the alloys Fe-Cr-Ni.[3]

We have studied the electrochemical behavior of the Sn-Zn alloy and that of pure zinc and tin in 1*N*-NaOH by means of impedance measurements and also by the potentiostatic method (*see* the polarization curves in Fig. 1 and 2 of this discussion). We found that:

(*A*) The corrosion current in the passive state for the alloy is lower (about 0.5 ma/cm^2) than would correspond to 25% Zn and 75% Sn (2.1 ma/cm^2), as shown in Fig. 1 and 2 at +0.2 to 0.8 v.

(*B*) On pure zinc, two types of passive layers may be found according to the potential imposed. In the range −0.92 to −0.56 v (vs. the normal hydrogen electrode), there exists a colorless thin layer possessing good electron conductance; in the range above +0.2 v, a thicker dark layer grows up, showing a higher corrosion current in the passive state. On this type of layer, oxygen is evolved with an overpotential of about 0.8 v (*see*, also, the paper of

[1] Deceased.
[2] Vyzkumny Ustav Ochrany Materialu, G. V. Akimova, Prague, Czechoslovakia.
[3] M. Prazák, Vl. Cihal, and M. Holinka, *Chem. listy*, 52, 1693 (1958); *Collection Czechoslov. Chem. Commun.*, 24, 9 (1959).

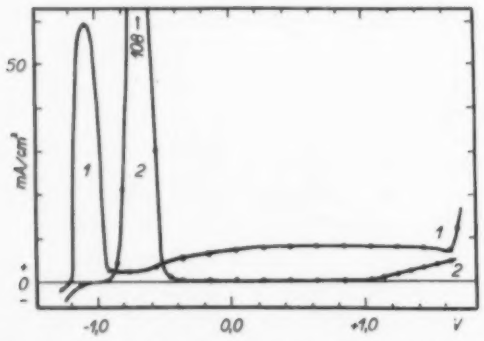

Fig. 1. Potential-polarization curves of Zn (1) and Sn (2) in 1N-NaOH.

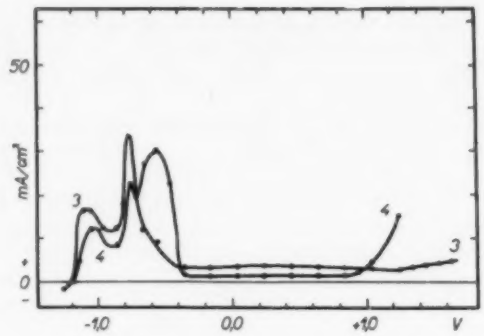

Fig. 2. Potential polarization curves of Sn75-Zn alloy (3—prepared by melting, 4—electrodeposited) in 1N-NaOH.

Landsberg[4]). In the case of the Sn-Zn alloy, this change in the behavior of the zinc component was not found.

To explain these facts, it must be accepted that a homogenous passive layer grows up on the nonhomogenous Sn-Zn alloy.

We believe that this and the other works of Dr. El Wakkad and co-workers will do much to clear up the problems concerning passivity of alloys of different types.

Higher Oxides of Silver

W. S. Graff and H. H. Stadelmaier (pp. 446-449, Vol. 105)

J. A. McMillan[5]: Graff and Stadelmaier, in an interesting paper dealing with the higher oxides of silver, have affirmed that Ag_2NO_{11} cannot exist since the same product is obtained from AgF as from $AgNO_3$ solutions. They assume that the x-ray diffraction pattern is due to the presence of silver in an oxidation state higher than two (Ag_2O_3?). The discussor wishes to add that the same pattern is obtained from $AgClO_4$[6] and Ag_2SO_4 solutions. These facts, however, do not necessarily mean that all of the four products are the same oxide with different impurities, as believed by Graff and Stadelmaier, since the patterns could be due to isomorphous substances. The discussor believes that a series of compounds $(Ag_2O_4)_2Ag^IAn$, where An stands for NO_3, ClO_4, F, or SO_4H, exists, on the basis of the following facts.

I. Skanavi Grigoieva and Shimanovich[7] have obtained, during the electrolysis of $AgClO_4$ solutions, a black deposit whose composition was $(Ag_2O_4)_2Ag^ICIO_4$.

[4] R. Landsberg, *Zeitschr. f. Physik. Chemie*, 206, 291 (1957).
[5] Instituto de Física de San Carlos de Bariloche, Bariloche, Río Negro, Argentina; present address: Chemistry Div., Argonne National Lab., Lemont, Ill., where the discussor is spending the duration of a Guggenheim Fellowship.
[6] W. S. Graff and H. H. Stadelmaier, *This Journal*, 105, 446 (1958).
[7] M. S. Skanavi Grigoieva and I. L. Shimanovich, *Zhur. Obshchei Khim.*, 24, 1490 (1955); *Chem. Abstracts*, 49, 5165a (1955).

II. de Boer and van Ormondt[8] have obtained, on electrolyzing Ag_2SO_4 solutions under similar conditions, black deposits whose composition was $(Ag_2O_4)_2Ag^{II}SO_4$ with $a = 2 - 2.5$. These authors believed that all silver atoms were in higher oxidation states. Nevertheless, if one hydrogen is added (impossible to identify from the results of the analysis) and only the value $a = 2$ is taken into account (values of a greater than 2 correspond to partial decomposition), the formula becomes $(Ag_2O_4)_2Ag^{I}SO_4H$. It should be noted that the oxysalts give insoluble AgO when boiled with water, according to

$$(Ag_2O_4)_2Ag^{I}An \rightarrow 6\,AgO + Ag^{+} + An^{-} + O_2,$$

which permits a straightforward analysis.

III. Kappanna and Talaty[9] have observed a black deposit during the electrolysis of AgF solutions, whose magnetic susceptibility was $+0.37 \times 10^{-6}$ emu/g. Comparing this with the value observed by the discussor[10] in the case of oxynitrate and oxyperchlorate, $+0.41$ and $+0.49 \times 10^{-6}$ emu/g, respectively, it is plausible to infer that the compound was $(Ag_2O_4)_2Ag^{I}F$, earlier reported by Tanatar,[11] and found to exhibit the same x-ray diffraction pattern as the other oxysalts.[6]

IV. $Ag_7NO_{11} = (Ag_2O_4)_2Ag^{I}NO_3$ is a chemical compound that certainly could be questioned until the outstanding papers of Noyes and co-workers, cited by Graff and Stadelmaier, appeared, but not later.

In addition to the above, the discussor's own results[10] support the existence of such a series of compounds. Their space group is $\bar{F}43m - T_d^2$, with $a \cong 10$Å, the anions occupying the tetrahedron (¼, ¼, ¼), the tetrahedron (¾, ¾, ¾) being occupied by monovalent silver atoms. The anions orient as the trigonal axes. Interchanging of different anions gives the different oxysalts. Twenty-four silver atoms center the edges of each of the eight ½a-cubes. Oxygen atoms arrange in two sets of four tetrahedrons each, surrounding anions and monovalent silver atoms, respectively. This structure explains the magnetic behavior.

The interpretation of these patterns is straightforward, and the discussor's experience, in disagreement with Graff and Stadelmaier's, is that quite pure patterns can be obtained, free from AgO lines, at least in the cases of oxynitrate and oxyperchlorate.

With respect to AgO, Graff and Stadelmaier have arrived at the same conclusion as the discussor, although the discussor believes that their values for a, b, and c are more accurate than his own.

Independently, Scatturin, Bellon, and Zannetti[12] have arrived at the same conclusion. Nevertheless, if AgO were a divalent silver oxide, it would be strongly paramagnetic (Ag^{2+} is a $4d^9$ ion), which is not the case. AgO is diamagnetic, its susceptibility having been found to be[13]

$$\chi = -0.15 \times 10^{-6}\ \text{emu/g}.$$

The discussor[10] has modified the structure and adopted the space group $P2_1c - C_{2h}^5$, the oxide then being a silver(I)-silver(III)-oxide, with silver(III) ions coordinated in a planar arrangement with four oxygens (hybridization dsp^2), which explains its diamagnetism.

These results, together with the results on the oxysalts, will be published in detail.

H. E. Swanson[14]: Graff and Stadelmaier have pointed out that the sample we used in reporting the x-ray diffraction powder pattern of argentic oxynitrate $Ag_7O_8NO_3$[15] was not analyzed to show the existence of the NO^-_3 ion and that the nature of the compound was dependent only upon documentation in the literature.[16-20] Graff and Stadelmaier believe this compound to be a higher oxide of silver.

In the four years that have elapsed since our x-ray pattern was prepared, a recent x-ray analysis of the original material shows that it has decomposed, in the vial in which it was stored, into the components AgO and $AgNO_3$, indicating the presence of nitrogen in the original sample. When compared to physical mixtures of AgO and $AgNO_3$, the peak heights of the decomposed sample agree with a six to one molecular ratio mixture.

Graff and Stadelmaier also showed that the $Ag_7O_8NO_3$ is decomposed by boiling in water to AgO. What they did not note was that, when it is so treated, oxygen is released and $AgNO_3$ remains in this solution which may be readily analyzed quantitatively.

This decomposition procedure was used to break down a fresh sample prepared by D. Norman Craig at the National Bureau of Standards. We obtain stoichiometric percentages of 6AgO, O_2, and $AgNO_3$. Oxygen was determined volumetrically over water at 90°C. $AgNO_3$ was obtained by evaporation of the filtrate, and weighed as such.

	AgO	$AgNO_3$	O
Found	785 mg/g	181 mg/g	31.4 mg/g
Calc.	784	179	33.8 oxygen

The reported close similarity of the x-ray patterns of the salts formed by electrolysis of a silver fluoride bath and that of a silver nitrate bath may be easily explained if they are found to be of the same type structure. However, the two patterns published by Graff and Stadelmaier show significant differences in both spacing and intensity values which we feel are due to difference in composition.

We recently have been able to check the similarity in cell dimensions of these two crystals and find about the same values reported by Graff and Stadelmaier.

[8] J. H. de Boer and J. van Ormondt, *Proc. Intern. Symposium on Reactivity of Solids, Gothenburg 1952*, 557 (pub. 1954); *Chem. Abstracts*, **48**, 11972a (1954).
[9] A. N. Kappanna and E. R. Talaty, *J. Indian Chem. Soc.*, **28**, 413 (1951).
[10] J. A. McMillan, Results not yet published.
[11] S. Tanatar, *Z. anorg. Chem.*, **28**, 331 (1901).
[12] V. Scatturin, P. L. Bellon, and R. Zannetti, *J. Inorg. & Nuclear Chem.*, **8**, 462 (1958).
[13] A. B. Neiding and I. A. Kazarnovskii, *Dokl. Akad. Nauk S.S.S.R.*, **78**, 713 (1951); *Chem. Abstracts*, **45**, 8385g (1951).
[14] National Bureau of Standards, Washington 25, D. C.
[15] H. E. Swanson, R. K. Fuyat, and G. M. Ugrinic, *Nat. Bur. Standards Circ. 539*, **4**, 61 (1955).
[16] J. C. Poggendorff, *Ann. Physik.*, **75**, 337 (1848).
[17] O. Sulc, *Z. anorg. Chem.*, **12**, 89 (1896).
[18] E. Mulder and J. Heringa, *Rec. trav. chim.*, **15**, 1, 235 (1896).
[19] A. A. Noyes, D. DeVault, C. D. Coryell, and T. J. Deahl, *J. Am. Chem. Soc.*, **59**, 1326 (1937).
[20] K. Bräkken, *Norske Vidensk. Selskabs, Forh.* **7**, p. 143 (1935) as abstracted in *Chem. Zentr.*, **106**, 1, 3634 (1935).

	Silver oxynitrate	Silver (oxyfluoride?)
Graff and Stadelmaier	5.890	5.834
NBS	5.893 at 26°C	5.823 at 25°C

Since Graff and Stadelmaier's paper did not come to our attention until recently, we have not verified the composition of the fluoride bath material as the oxyfluoride counterpart of the oxynitrate. However, we are planning to investigate this portion of the problem further.

W. S. Graff and H. H. Stadelmaier: The authors do not agree that the compound they reported to be a higher silver oxide can be, as McMillan suggests, a series of isomorphous compounds of the type $(Ag_2O_3)_x \cdot Ag(I)AN$, where AN is NO_3^-, ClO_4^-, F^-, or SO_4H. Our points in answer to McMillan's and Swanson's arguments along this line are as follows.

I. All the preparations reported (Braekken, Swanson, Graff and Stadelmaier, Zvonkova and Zdanov), regardless of the anion present in the preparation (NO_3^-, ClO_4^-, F^-, or $SO_4^{=}$), yield a substance with a similar diffraction pattern and with lattice constants that differ from each other by no more than 0.5%. We attribute these small differences to varying amounts of absorbed impurities. An additional paper, not cited in our original bibliography,[21] also adds confirmation in that the preparation of a substance that yields the same diffraction pattern is reported from the oxidation of silver in a stream of $O_2 + 5\%$ O_3 with no N_2 present.

The regular presence of anions of such widely differing sizes (NO_3^-, ClO_4^-, F^-, or SO_4H^-) in the lattice as McMillan suggests would likely cause a larger variation in lattice constants than observed, even if we assume that such a series of isomorphous compounds does exist. Furthermore, it seems to us that the structure as postulated by McMillan with Ag(I) and the complex anion tetrahedrally surrounded by oxygen atoms is impossible from the standpoint of Pauling's radius ratio rules. The radius ratio of Ag(I) to $O^=$ is 0.9 and the radius ratio of NO_3^- to $O^=$ is 1.26. These ratios do not appear to be compatible with a coordination number of four.

II. We do not question the validity of Noyes' work in identifying Ag_2NO_{11}; we only feel that after the preparation is washed and dried the resulting decomposition product is the same as can be obtained from other means of preparation (fluoride, perchlorate, etc.) and very probably is a higher oxide of silver.

McMillan's comment on the structure of AgO is very interesting. If the compound is in fact diamagnetic, we agree that this would preclude the existence of a simple Ag^{++} state, because this state would involve an unpaired electron in the bonding with surrounding oxygen atoms and hence would be paramagnetic. Neiding and Kazarnovskii[22] also report that AgO is diamagnetic. This, we agree, indicates that AgO is a more complex structure, and not similar to CuO where Cu^{++} is known to exist.

[21] G. M. Schwab and G. Hartmann, *Z. anorg. u. allgem. Chem.*, **281**, 184 (1955).
[22] A. B. Neiding and I. A. Kazarnovskii, *Dokl. Akad. Nauk S.S.S.R.*, **78**, 713 (1951)

Preparation and Properties of Aluminum Antimonide

A. Herczog, R. R. Haberecht, and A. E. Middleton
(pp. 533-540, Vol. 105)

H. F. Matare[23]: Four years ago (1953), we[24] produced AlSb-diodes from laboratory-grown crystals. We found a possible use for high-frequency diodes, e.g., as mixer diodes. The characteristic feature was a small diffusion voltage. Blocking voltages were low and corresponding to the order of magnitude given by the authors. Stability over long time periods was not very good. Encapsulation under oil as proposed by the authors was used also.[25]

A. Herczog: In the production of mixer diodes, one has to apply a special surface treatment to bring out the lowest forward resistance. This treatment is known to make the surface rather sensitive and corrosive.

Other treatments capable of producing more stable surface conditions will yield inferior forward characteristic but much higher blocking voltage (85 v).

The Flade Potential of Iron Passivated by Various Inorganic Corrosion Inhibitors

H. H. Uhlig and P. F. King (pp. 1-7, Vol. 106)

G. H. Cartledge[26]: It is gratifying that the authors have independently confirmed the earlier work of Cartledge and Sympson,[27] which showed that the passivating films produced on iron or carbon steel in aerated solutions in inhibitors display the Flade potential upon activation. This indicates that the films have the same electrochemical character, although formed in a variety of ways. In later work, to be published elsewhere, it has been shown that the Flade potential may be demonstrated also on films produced by passivation in an aerated solution containing benzoate ions.

It is not believed that the apparent variation of the activation potential reported by Uhlig and King for different passivators is real. Their measurements were made after the specimens were transferred to unbuffered solutions, whereas those of Cartledge and Sympson were made in the inhibitor solution itself, in which the pH value was accurately determinable. With the exception of the pertechnetate ions, all the inhibitors used have some buffering action. It may be noted in Fig. 2 and 3 of Uhlig and King that the observed points fell on the noble side of the curve of Franck[28] when passivation was conducted in acid media, and on the other side for passivation in alkaline media. The data make one suspicious that the films had some "memory" of their origin, because of incomplete equilibration with the new, unbuffered environment. No such variation was apparent in the observations of Cartledge and Sympson.

[23] Semiconductor Section, Solid State Lab., Sylvania Electric Products Inc., Bayside, N. Y.; present address: Laboratorium Halbleiter, Suddeutsche Telefon-Apparate-, Kabel- und Drahtwerke A.-G. 185 Allersberger Str., Nurnberg, Germany.
[24] Intermetal Corp., Düsseldorf, Germany.
[25] G. Zielasch, *Arch. elektr. Uebertragung, Stuttgart*, **8**, 529 (1954).
[26] Chemistry Div., Oak Ridge National Lab., Operated by Union Carbide Corp. for the U. S. Atomic Energy Commission, Oak Ridge, Tenn.
[27] G. H. Cartledge and R. F. Sympson, *J. Phys. Chem.*, **61**, 973 (1957).
[28] U. F. Franck, *Z. Naturforsch.*, **4a**, 378 (1949).

From the standpoint of theory, if the Flade potential actually corresponds to some electrochemical state that is reproducible, albeit metastable, one should expect to measure it best in as nearly a steady state as possible, rather than during rapid activation. This was the justification of the procedure used by Cartledge and Sympson.

The attempt of the authors to relate the Flade potential to a free energy calculable from data on heat of adsorption of gaseous oxygen on iron powder suffers from the weakness that two entirely different processes are being compared. Adsorption of oxygen in an aqueous medium involves both displacement of adsorbed water and competitive adsorption with all other species present. It would, therefore, be a strange coincidence if the adsorption in the two environments were the same in extent or energy.

The authors' discussion of the passivation process in the presence of a pertechnetate also must be questioned. They suggested that the writer's failure to find more than minute amounts of a technetium compound on the passivated specimen might be due to the formation of a soluble reduction product. This is quite contrary to the facts. Thorough study of the chemistry of technetium in this laboratory has shown that soluble compounds derived from the quadrivalent state (the important one) can be made only by forming complexes in strongly acidic solutions, such as hydrochloric acid of 1*N* concentration or greater.[29] Furthermore, in one experiment on the passivation of cast iron, which reduced an appreciable amount of the inhibitor, a material balance was obtained, within analytical accuracy, by adding the amount found from the beta activity of the specimen to the residual technetium in solution as determined spectrophotometrically as TcO_4^-.

Finally, if one uses the authors' estimate of the free energy of "$Fe{\cdot}O{\cdot}O_2$" in combination with the normal potential of the Tc(VII)-(IV) couple,[30] in accordance with their Eq. [9], it is calculable that 10^{-4} *f* TcO_4^- could passivate by this process only if the pH value were less than 4.9. The corresponding number is 4.0 if Franck's value for the Flade potential is used. As a matter of fact, passivation results best at higher pH values in aerated solutions. It is not believed, however, that such calculations are reliable, in view of the abnormal and unknown free energies of the surface components.[31]

H. H. Uhlig and P. F. King: In view of his extended studies along similar lines, Dr. Cartledge's comments are especially welcome. His comments indicate that he is reluctant to believe that the Flade potential varies with specific passivators, but the facts are quite clear that the observed variations are larger than the experimental error of our measurements, and we believe that the explanations that we have outlined suggest reasons why these variations are to be expected. The observed variation in stability of passivity depending on the passivator used is part of the evidence that differences in Flade potential can be predicted.

It is not likely that the deviations we find can be explained by a "memory" of the electrodes for the pH of the solution in which the electrodes were passivated, as Dr. Cartledge proposes. Other than the fact that each electrode was carefully washed in three separate beakers of distilled water before breakdown of passivity was followed by potential measurements, it is clear from Fig. 2 and 3 that acidity of the solution in which passivation occurred did not appreciably influence the observed Flade potential measurements. For example, iron passivated anodically in 5% H_2SO_4 or in concentrated HNO_3 (16*N*) gave the same Flade potential and the same slope of E_r plotted vs. pH of the solutions in which the passivity decayed despite a large difference in acidity. Furthermore, potassium ferrate solution, which by slow decomposition and hydrolysis was very alkaline, gave the same Flade potential as sodium molybdate or potassium chromate solutions which were near neutral.

We found that the use of buffer solutions is not ideal because of the tendency of some buffer anions in their usual high concentration to accelerate decay of passivity. This probably accounted for our observation that there was a variation in the Flade potential at the same pH when the buffer system was varied.

It is true that, when passivation occurs in an aqueous medium, competitive adsorption is expected to occur, and that this is not the case when oxygen is adsorbed directly on iron. In a subsequent paper,[32] we have shown that the calculated displacement effects amount to about 6000 cal/mole H_2O adsorbed on iron. This corresponds to only a minor part of the free energy accompanying adsorption of oxygen, and hence is not of great significance.

The relative absence of technetium on the surface of iron after passivation by TcO_4^- indicates that either TcO_4^- is not reduced at the surface of iron during passivation, which we discuss as being unlikely, or that the reduction products of TcO_4^- are soluble (or they are dispersed) in the solution. The latter situation is contrary to that for CrO_4^{--} for which chromium ions or compounds tend to remain on the iron surface after passivation and can be counted if the chromium is radioactive. It is difficult to foresee any other possibility explaining lack of Tc on an iron surface passivated by TcO_4^-.

The calculated value for critical pH in accord with our Eq. [9] depends on the particular value of the Flade potential which is assumed to apply to pertechnetates, and hence the calculated pH can be less than 4.9. We are somewhat more optimistic than Dr. Cartledge regarding thermodynamic calculations in which surface reactions are involved, provided that the composition of the surface product and the corresponding free energy are known. The practical use of the Ag-AgCl and Pb-$PbSO_4$ electrodes constitutes proof that thermodynamics also applies rigorously to thin films on metal surfaces. In many cases, of course, composition of surface films is not known, and cannot be readily established by the usual analyses, but potential

[29] R. H. Busey, Personal communication.
[30] G. H. Cartledge and W. T. Smith, Jr., *J. Phys. Chem.*, **59**, 1111 (1955).
[31] G. H. Cartledge, *Z. Elektrochem.*, **62**, 684 (1958).
[32] H. H. Uhlig and P. F. King, In press, *J. Phys. Chem.*

measurements are still useful nevertheless as a first step in diagnosing the possible composition and structure of such films.

D. M. Brasher [55]: If we have interpreted this paper correctly, Uhlig and King suggest that the very slow film growth on steel in dichromate solutions takes place by means of a dual mechanism. During depolarization of cathodic areas by $Cr_2O_7^{-2}$ ions, deposition of chromic oxide (possibly hydrated) or adsorbed Cr^{3+} ions occurs on these areas; this depolarization causes an equivalent amount of (chemisorbed) $O.O_2$ to be deposited on anodic areas, followed by (it is implied) the gradual conversion of this to Fe_2O_3 with fresh deposition of $O.O_2$.

This is of interest to us as the over-all reaction quoted:

$$Cr_2O_7^{2-} + 8H^+ + Fe_{surface} \rightarrow 2Cr^{3+} + 4H_2O + O.O_2$$

with, presumably, in addition

$$2Fe + O.O_2 \rightarrow Fe_2O_3$$

is stoichiometrically equivalent to the reactions we have assumed[54] in the interpretation of film growth in deaerated chromate or dichromate solutions. These reactions have been assumed to be, in the absence of oxygen:

$$2Fe + 2CrO_4^{2-} + 2H_2O \rightarrow Fe_2O_3 + Cr_2O_3 + 4\,OH^- \text{ (pH 7.5)}$$

or $$2Fe + 2HCrO_4^- \rightarrow Fe_2O_3 + Cr_2O_3 + 2\,OH^- \text{ (pH 4.2)}$$

In each case, the growing film should contain equivalent amounts of Fe and Cr.

In our work,[56] we have shown that Cr uptake, and hence film growth, proceeds as a function of the logarithm of time, and that the rate constant for this growth is similar to that for oxide film growth in dry air. We (Kubaschewski and Brasher) have explained this growth on the basis of theories of Mott, Hauffe, and Ilschner in which electron transfer through the film is the rate-controlling step. It would be interesting to know if Uhlig and King's suggested mechanism, cathodic deplorization with concomitant anodic polarization, can account for logarithmic film growth.

H. H. Uhlig and P. F. King: Miss Brasher's observations are a welcome supplement to our own, and in our opinion comprise a reasonable explanation of what may be expected if iron is passivated by chromates. In fact, similar continuous oxidation should be observed with any of the passivators, such as nitrites, molybdates, etc., for which the Flade potential is approximately the same as for iron anodically passivated in H_2SO_4.

If the passive film formed by passivators is essentially chemisorbed oxygen or an adsorbed oxygen complex, as our data lead us to believe, the further slow oxidation of iron to form iron oxide would be expected to follow a rate curve similar in shape to that observed when iron is exposed to dry oxygen. It has been demonstrated by others that the rate of oxidation in dry O_2 is logarithmic, and the fact that Miss Brasher finds this relation, assuming that reduced chromate is incorporated into the iron oxide film, is confirming evidence that the assumptions and explanations she and her co-workers propose are reasonably correct.

It is not certain that the absolute rates of oxidation should be identical. The presence of chromate adsorbed on the outer boundary of the passive film, and absence of chromate in dry oxidation, may well cause the rates to differ, but the logarithmic equation is expected to hold in either instance.

It may be well to point out that the application of Mott's early derivation of the logarithmic equation relating thin film oxidation to the tunnel effect, and its more recent adoption by Hauffe and Ilschner, is subject to some doubt. The Mott derivation leads to an oxidation rate independent of temperature, and suggests that the logarithmic equation should hold for films not thicker than about 40Å, both being contrary to observation, as Lustman pointed out.[58] A subsequent derivation of Cabrera and Mott based on a quasi-exponential migration of ions in an electric field within the oxide leads to the inverse logarithmic equation instead of the logarithmic equation, and does not account, as we have pointed out earlier, for the observed effects of grain orientation, lattice transformation, and Curie temperature on thin film oxidation rates.[57, 58]

Potential Studies on Passivity to Corrosion Induced by Pretreatment Processes for Metals, I. Aluminum

K. S. Rajagopalan (pp. 113-117, Vol. 106)

S. L. Chisholm[59]: Similar studies of passivating and corrosion inhibitive treatments and compounds have been performed on a variety of aircraft, nonferrous, and ferrous metals, by employing a Beckman pH meter and measurement of potentials against silver-silver chloride electrodes made in quantity by fusing silver chloride on strips of pure silver. The purpose was to develop direct screening methods and prospective specification requirements for useful corrosion inhibitors and inhibitive compounds, such as corrosion inhibitive paint films, since development and testing of such materials normally involves inordinate amounts of time for field test exposure. In the case of inhibitive paint primers, such as zinc chromate primer, an interesting variation of the test method is to determine the differential potential of the primed vs. the unprimed metal in separate cells when immersed in ground or saline water. Initial values are of the order of 450 mv on aluminum alloys, which decrease with extended time to a steady state. Increasing salinity increases the initial differential, but also the rate of change. In all of this work, it has been found difficult to obtain exact reproducibility. Replicate samples normally furnish families of similar curves of potential vs. time, as reported and illustrated in the subject paper. By

[55] National Chemical Lab., Teddington, Middlesex, England.
[56] O. Kubaschewski and D. M. Brasher, *Trans. Faraday Soc.*, 55, 1200 (1959).
[57] D. M. Brasher and Kingsbury, *Trans. Faraday Soc.*, 54, 1214 (1958).
[58] B. Lustman, *Trans. Electrochem. Soc.*, 81, 372 (1942).
[57] H. H. Uhlig, *Acta Met.*, 4, 541 (1956).
[58] H. H. Uhlig, J. Pickett, and J. MacNairn, *Acta Met.*, 7, 111 (1959).
[59] U. S. Naval Air Station, North Island, San Diego, Calif.

this method, it is also possible to detect and determine the persistence of nonvisible passivation effects, such as that produced by nitric or chromic acid treatment of corrosion resistant steels.

K. S. Rajagopalan: I am glad to note that observations similar to those made by me have also been made by Dr. Chisholm. Dr. Chisholm is correct in stating that the order of reproducibility of the potential changes observed should be higher from the point of view of using the changes as a method for the assessment of the performance of the pretreatments considered. This aspect has received particular attention in the paper. I think it should be possible to get better reproducibility if the conditions of treatment are better understood. However, it should be noted that the results have an even greater significance from the point of view of the light it throws on the mechanism of passivation of the metal surface. The results show that there are a number of systems where the potential shift is in a negative direction following passivation. The explanation given by the author brings into relief a factor which has not been given adequate attention in the consideration of changes in potential with time and changes in potential with application of external current. This is the important part played by changes in anodic and cathodic areas. It has been shown that, under certain ideal conditions assumed, the potential changes can be attributed either to a change in the ratio of anodic and cathodic areas or a change in the ratio of the velocity factors for the anodic and cathodic reactions. It may be that these two factors cannot be separated ordinarily. But it is possible to visualize the conditions under which one can be studied independent of the other.

Reaction of Aluminum and Carbon Tetrachloride, I

J. D. Minford, M. H. Brown, and R. H. Brown
(pp. 185-191, Vol. 106)

R. A. Hine[40]: The authors have presented a thorough and most useful study of this reaction, which has considerable practical importance in connection with the use of aluminum vessels and equipment for handling halogenated compounds.

Rather surprisingly, the tremendously increased rate of reaction brought about by mechanical activation has not been referred to; this was first described by Shaw.[41] In our laboratories, we have demonstrated that a very rapid and vigorous reaction takes place when aluminum is abraded, drilled, machined, or filed under the surface of warm carbon tetrachloride. In the case of aluminum powder ground in a mortar and pestle with a little warm carbon tetrachloride, the reaction starts suddenly and may be almost explosively violent with evolution of large amounts of hexachlorethane and aluminum chloride fume. If further portions of liquid and powder are added to the reacting mass, incandescence is reached and a secondary reaction involving direct formation of $AlCl_3$ and liberation of carbon takes place. In the primary reaction, the formation of the red intermediate complex is always strikingly produced.

[40] Aluminium Labs. Ltd., P. O. Box 84, Kingston, Ont., Canada.
[41] M. C. Shaw, *J. Appl. Mechanics*, 15, 37 (1948)

The reaction has been discussed by Grunberg[42] who explains it by taking account of the Kramer and Russell effects (emission of electrons from an abraded metal surface) and formulates the steps as:

$$Cl_3C{:}Cl^- + e \text{ (from abraded metal)}$$
$$\rightarrow Cl_3Cl{\cdot}Cl^- \rightarrow Cl_3Cl^{\cdot} + Cl^-$$
$$Al^{3+} + 3Cl^- \rightarrow AlCl_3$$
$$2Cl_3C^{\cdot} \rightarrow C_2Cl_6$$

The above sequence does not explain the formation of the red complex and in my view the present authors' electrochemical theory can be held just as tenable as the free radical theory.

R. H. Brown, E. H. Cook, M. H. Brown, and J. D. Minford: The authors appreciate R. A. Hine's interest in their paper.

It is not surprising that mechanical abrasion of the surface in warm carbon tetrachloride produces a rapid reaction. Our experiments to cathodically protect an aluminum rod whose surface was freshly scratched under boiling carbon tetrachloride were unsuccessful. In order to achieve cathodic protection, it is necessary to supply at least the minimum current as would be calculated from the initial reaction rate at the scratched surface. Because of the high resistance of the solution, such currents could only be obtained with excessively high applied potentials.

Conductivity measurements by the authors indicate the existence of an ionic species before the visible detection of the red complex, and that the conductivity continues to increase after the red complex is detected.

Principles and Applications of the Iodide Process

A. C. Loonam (pp. 238-244, Vol. 106)

A. A. Woolf[43]: We wish to comment on Loonam's conjecture that boron and rhenium can be deposited from the vapors of their iodides.

Recent work has confirmed that rhenium iodides cannot be made directly from the elements alone, or in complexing and noncomplexing solvents for iodine, but only indirectly via the hexaiodorhenates (IV).[44,45] The rhenium iodides so prepared are decomposed to rhenium by heating in vacuo without appreciable volatilization of the iodide, indicating that their dissociation pressures are high compared with their vapor pressures. Thus, refining of rhenium is impossible by a continuous iodide process. It is the kinetics, rather than the thermodynamic equilibria, of the reaction of iodine with some elements which limits the method, because reaction only occurs at an appreciable rate at temperatures at which the iodide is no longer stable. Boron is similar in that no appreciable reaction occurs with iodine at temperatures up to 1200°C.[46]

[42] L. Grunberg, *Proc. Phys. Soc. (London)*, 66B, 153 (1953).
[43] Research Lab., Associated Electrical Industries Ltd., Aldermaston Court, Aldermaston, Berkshire, England.
[44] A. A. Woolf, *J. Inorg. & Nuclear Chem.*, 7, 291 (1958).
[45] R. D. Peacock, A. J. E. Welch, and L. F. Wilson, *J. Chem. Soc.*, 2901 (1958)
[46] H. C. Oldland, Ph.D. Thesis, Imperial College, London (1956); "Gmelins Handbuch der Anorganischen Chemie," 13, 126 (1926).

A. C. Loonam: I am very grateful indeed for Dr. Woolf's comments. However, I believe that they were covered adequately in the paper by the "perhaps" before the "Re" in the statement to which he refers and by the succeeding one: "In some cases, e.g., carbon, it would be necessary to prepare the iodide by an external process," which, of course, includes indirect methods. These would almost certainly be necessary for the preparation of carbon-iodine compounds, since the common forms of this element, graphite and amorphous carbon, in my definite experience, do not react directly with iodine at temperatures up to at least 1100°C.

Formation of a volatile product by the direct action of iodine vapor on metallic rhenium has been reported [47,48] but, even if this should prove to be the oxyiodide found by Dr. Woolf, I would be unwilling to place the metal in the same category with carbon because of recent evidence that other metals ordinarily considered resistant can be made to react with iodine. Not long ago, it was stated that tantalum is resistant to iodine vapor up to 1000°C and that it can be used as a shield in the de Boer-van Arkel process; yet TaI_5 has been prepared by the action of iodine vapor on the metal at temperatures as low as 300° [49] and the metal has actually been refined by the iodide process[50] with bulb temperatures as low as 311°, using commercial sheet as the "crude" material. Moreover, molybdenum, which gives very satisfactory service in iodide process units, can react with iodine under suitable conditions;[51] while the recent announcement by the General Electric Co.,[52] of a compact high-intensity incandescent lamp containing a small amount of iodine to return the volatilized tungsten from the interior surface of the quartz bulb to the filament, shows that even this metal can be attacked and transferred. Even more pertinent to Dr. Woolf's remarks is the report that direct reaction of one form of crystalline boron with iodine at 900° gave as high as 70% yields of the triiodide; and that the vapor of this compound produced deposits of elementary boron at temperatures as low as 800°.[53] Indeed, a new allotropic modification of boron was produced.[54]

Furthermore, the rhenium iodides should be studied in the presence of a high partial pressure of iodine vapor before it is concluded that they cannot exist in the gaseous state. Dr. Woolf's finding of the volatile oxyiodide indicates that the Re-I bond is not excessively weak. Niobium, which forms a similar oxyiodide, has been refined by the iodide process[55] even though heating NbI_5 in an evacuated tube gave results similar to those obtained by Dr. Woolf with the rhenium iodides, the unvolatilized residue being converted slowly to metal at 540° and rapidly at 800°.[56] It is true that evidence for the existence of gaseous NbI_5 was found in these experiments, whereas Dr. Woolf obtained no similar evidence; but this may be due to a lower volatility of the rhenium compounds resulting from the lower valence state and the higher atomic weight of the metal.

I would not be at all astonished to learn that considerable volatilization occurs when the rhenium iodides are heated to 600°-1000° in a stream of iodine vapor at atmospheric pressure. If such proves to be the case, I believe that conditions will be found under which rhenium can be deposited from the vapors of its iodides, perhaps by a "straight-flow" process rather than the conventional de Boer-van Arkel method.

[47] W. Noddack, *Z. Elektrochem.*, **34**, 627 (1928).
[48] H. V. A. Briscoe, P. L. Robinson, and E. M. Stoddart, *J. Chem. Soc.*, 2263 (1931)
[49] R. F. Rolsten, *J. Am. Chem. Soc.*, **80**, 2952 (1958).
[50] R. F. Rolsten, *Trans. Met. Soc. AIME*, **215**, 472 (1959).
[51] T. L. Allen and D. M. Yost, *J. Chem. Phys.*, **22**, 855 (1954).
[52] E. G. Zubler and F. A. Mosby, Preprint No. 19, National Technical Conference, Illuminating Engineering Society, San Francisco, Calif., September 7-11, 1959.
[53] L. V. McCarty and D. R. Carpenter, *Abstracts of Papers, Am. Chem. Soc.*, 135th Meeting, Boston, Mass., April 5-10, 1959, pp. 17M, 18M (2 papers).
[54] L. V. McCarty, J. S. Kasper, F. H. Horn, B. F. Decker, and A. E. Newkirk, *J. Am. Chem. Soc.*, **80**, 2592 (1958).
[55] R. F. Rolsten, *Trans. Met. Soc. AIME*, **215**, 478 (1959).

The System LiF-LiCl, LiF-NaCl, LiF-KCl

H. M. Haendler, P. S. Sennett, and C. M. Wheeler, Jr.
(pp. 264-268, Vol 106)

M. A. Bredig[57]: It appears that the most recent values for the heat of fusion of LiF, NaCl, and KCl were used in the calculations presented in the tables. However, this does not seem to be true for the so-called Clausius-Clapeyron Limit in Fig. 1-3, especially for NaCl in Fig. 2 and above all for both LiF and LiCl in Fig. 1. If for the LiF-LiCl system the latest, correct heats of fusion of 4.80 kcal for LiCl[58] and 6.46 for LiF are used to draw the Clausius-Clapeyron Limit, it becomes apparent that as expected there is no positive deviation from Raoult's Law in this system, but rather very slight *negative* deviations due to the different size of the F^- and Cl^- ions.

H. M. Haendler, P. S. Sennett, and C. M. Wheeler, Jr.: The calculations presented in the tables of this paper used values for the heat of fusion of LiF, NaCl, and KCl listed by Flood. The Clausius-Clapeyron Limit was inadvertently drawn using values for the heat of fusion of these salts as found in National Bureau of Standards Circular 500. These values for, particularly, LiCl and LiF are low and should not be used. Replotting the Clausius-Clapeyron Limit using either the values from Flood or those supplied by Dr. Bredig indicates, as he states, that there is a slight negative deviation in the LiF rich systems.

The Stability and Solubility of AgO in Alkaline Solutions

T. P. Dirkse and B. Wiers (pp. 284-287, Vol. 106)

J. A. McMillan[59]: As Salkind and Zeek[60] have pointed out, the structure of AgO has been of interest to members of the Society, and I should add to chemists in general, during the last years. Dirkse and Wiers, in an interesting paper on the behavior of AgO in alkaline solutions, found that samples of an assumed AgO prepared by different methods ex-

[56] J. D. Corbett and P. X. Seabaugh, *J. Inorg. & Nuclear Chem.*, **6**, 207 (1958).
[57] Chemistry Div., Oak Ridge National Lab., P. O. Box X, Oak Ridge, Tenn.
[58] A. S. Dworkin and M. A. Bredig, In press.
[59] Chemistry Div., Argonne National Lab., Lemont, Ill., on leave of absence from Instituto de Fisica de San Carlos de Bariloche, Bariloche, Rio Negro, Argentina, spending the duration of a Guggenheim Fellowship.
[60] A. J. Salkind and W. C. Zeek, *This Journal*, **106**, 366 (1959).

hibit different x-ray diffraction patterns. They have a point, namely: difference in x-ray patterns indicates a difference in structure, or at least the existence of AgO samples with somewhat larger lattice parameters. This latter can be true, but I suspect that the results quoted above stand for the production of a black deposit obtained during the electrolytical oxidation of silver anodes in sulfuric acid medium[61] that should rather be identified with $(Ag_3O_4)_2AgSO_4H$, isomorphous with Ag_7NO_{11}, Ag_7ClO_{12}, and perhaps with Ag_7O_8F (interchanging NO_3, ClO_4, SO_4H, F),[62] also obtained by de Boer and van Ormond[63] during the oxidation of $AgNO_3$ solutions with $K_2S_2O_8$. It should be noted in this respect that the latter method leads to AgO if the medium is alkaline.[64]

The unit cell edge of Ag_7NO_{11} is 9.89Å. This value cannot vary strongly when substitution by other anions takes place. In fact it does not, as can be seen in the table, published here where values of spacings for silver oxinitrate[65,66] and oxifluoride[63] are given. The values found by Jones and Thirsk[61] are quoted in the same table, showing a good agreement with the exception of spacing 1.45Å, presumably due to reflections 311 or 022 of AgO.[67] It should be borne in mind that the oxisalts decompose to give rise to AgO, oxygen, and the corresponding monovalent silver salt. Jones and Thirsk's compound seems to be like the compound obtained by Schwab and Hartmann[68] using ozone for the oxidation, as can also be seen in the table.

I wish to make good use of the opportunity to call to the attention of workers on this problem that the compounds obtained from electrolytical oxidation of silver anodes are not at all clear up to the present time.

T. P. Dirkse and B. Wiers: One of the purposes in reporting on our work with AgO was to show that all that is called AgO is not necessarily AgO. The x-ray data of Schwab and Hartmann, Footnote 68, show that the AgO prepared by decomposition of Ag_7NO_{11} with boiling water is not the same as that prepared by oxidation of $AgNO_3$ with alkaline persulfate. There are also differences in chemical properties between these two substances, such as the effect of boiling water as noted in our article.

[61] P. Jones and H. R. Thirsk, *Trans. Faraday Soc.*, **50**, 732 (1954).
[62] J. A. McMillan, *This Journal*, this issue, Discussion on "Higher Oxides of Silver."
[63] J. H. de Boer and J. van Ormond, *Proc. Intern. Symposium on Reactivity of Solids, Gothenburg, 1952*, 557 (pub. 1954); *Chem. Abstracts*, 45, 11968f (1954).
[64] J. C. Bailar, "Inorganic Syntheses," p. 12, McGraw-Hill Book Co., New York (1953).
[65] H. E. Swanson R. K. Fuyat, and G. M. Ugrinic, *Nat Bur. Standards Circ. 539*, 4, 61 (1955).
[66] W. Graff and H. H. Stadelmaier, *This Journal*, **105**, 446 (1958).
[67] J. A. McMillan, *Acta Cryst.*, **7**, 640 (1954).
[68] G. M. Schwab and G. Hartmann, *Z. anorg. u. allgem. Chem.*, **281**, 183 (1955).

Table I. Spacings of some silver oxisalts

Ref., Footnote 66					
Fluoride	Nitrate	Ref., Footnote 65	Ref., Footnote 61	Ref., Footnote 68	HKL
...	...	...			...
2.836	2.855	2.856	2.85	2.85	222
2.457	2.472	2.474	2.46	2.46	400
...	...	...			...
1.483	1.491	1.491	1.49	1.50	622
- - -	- - -	- - -	1.45	- - -	- - -
...		...			...
1.230		1.237		1.24	800
...		...			...
1.1261		1.1348	1.136		662
1.0988		1.1062	1.106		840

Water-Stabilized Arc Tests on Nonmetallic Materials

M. Dank, R. A. Nelson, W. R. Sheridan, and W. H. Sutton
(pp. 317-321, Vol. 106)

Charles Sheer[69]: Comment on peak temperatures reported by Burham, Maecker, and Peters in Germany (~50,000°K): "Peak temperatures of this order exist only on the axis of the plasma jet over a very small radial distance (<1 mm). The extreme high temperature region extends a short distance beyond the nozzle opening into the plasma jet, but not enough to be useful in testing samples of materials at these temperatures."

On the subject of temperature measurement in plasma jet environments, rotational temperatures, determined spectroscopically, appear to be abnormally high. However, Stark effect broadening of the hydrogen lines is reported to yield effective temperature measurements with about 10% accuracy.

The Anodic Oxides of Lead

J. Burbank (pp. 369-376, Vol. 106)

P. Rüetschi and B. D. Cahan[70]: pH potential diagrams, as developed by Pourbaix, are convenient means to describe the regions of thermodynamic stability of solid phases or ionic species in solution. In applying these diagrams, one must keep in mind that concentration terms other than the H-ion concentration (pH) are determining the thermodynamic reversible potentials. For example, in the case of the pH-potential diagram of Pb, the nature of the particular anions present is of profound influence. Considering a pH of 1, the lead ion concentration could vary over many orders of magnitude with a corresponding shift in potential of several tenths of a volt. This means that, for each anion present, the pH-potential diagram might look entirely different.

In Fig. 1 of J. Burbank's paper, the regions of stability of corrosion products *at the solution interface* are given without specifying nature and concentration of other ionic species (in particular anions) present. Looking at the diagram, it is hard to understand the presence of PbO, $Pb(OH)_2$, and αPbO_2 in an acid media of, e.g., pH 1, in direct contact with the acid solution. At this pH, the existence of PbO, $Pb(OH)_2$, and αPbO_2 are difficult to picture thermodynamically or kinetically. In Fig. 3 of J. Burbank's paper, which refers to a pH of 1, no such substances are shown in direct contact with the acid media. Only $PbSO_4$ and βPbO_2 are shown in direct contact with the solution. This is in contrast with the data of Fig. 1.

It should be made clear that the definition of a pH *in the interior* of a corrosion layer is ambiguous. The pH in the very fine cracks and pores of the cor-

[69] Vitro Labs., West Orange, N. J.
[70] Electrochemistry Div., Electric Storage Battery Co., Yardley, Pa.

rosion layer must be quite different from the pH in the bulk of the electrolyte, due to strong diffusion and depletion effects. It does not make much sense to assume that only H^+ ions and water are penetrating into the layer, since equal amounts of anions and cations must be present in the pores at any time to maintain electroneutrality. In the double layer, an excess charge on the solution side is neutralized by an equal excess charge on the electrode side; however, in any case, the conditions in the interior of the corrosion layer are then not ideal, and the energetic states of the same ionic species in the interior of the corrosion layer and in the bulk must be different.

We feel that the experimental evidence of the presence of PbO, $Pb(OH)_2$, and αPbO_2, which is well confirmed, is connected with a pH effect in the interior of the corrosion layer, due to diffusion effects. It seems that J. Burbank does not sufficiently stress the importance of nonequilibrium conditions with regard to pH in the corrosion film. In a basic media, the formation of PbO, $Pb(OH)_2$, and αPbO_2 would be readily understood. One could visualize a system where the corroding electrode is separated from the solution by a diaphragm, such that the electrode compartment of the corroding electrode has much higher pH than the solution. This diaphragm insulating the electrode from the solution would in practice consist of a $PbSO_4$ or βPbO_2 layer. This would now mean that the corroding electrode would be at a higher pH and thus, for a given impressed over-all electrode potential, the formation of PbO_2 would become possible far below the theoretical thermodynamic value as determined from the bulk pH of the solution. If the undefined virtual pH in the interior of the corrosion layer were effectively basic, then PbO_2 could be formed down to an apparent external potential of 0.6 v or so as can easily be seen from the pH-potential diagram.

In practice, the corrosion of lead might proceed underneath a partially protecting coverage of $PbSO_4$ or βPbO_2 by migration of oxygen species (e.g., OH^-) along the surfaces of the $PbSO_4$ and PbO_2 grains or crystals to produce PbO, $Pb(OH)_2$, or αPbO_2 from metallic lead. The formation of these substances is therefore related to a lack of acid in the interior of the corrosion film.

It has been described by Rüetschi and Cahan[71] that the ratio of α to βPbO_2 in the corrosion layers of lead-antimony alloys in H_2SO_4 depends on the Sb concentration of the corroding grid. It was indicated that with high Sb content generally more βPbO_2 is formed due to the higher porosity of the corrosion film. The Sb, corroding out of the metal, is oxidized to Sb oxide and Sb sulfate.These substances subsequently are leached out of the corrosion film, rendering it more porous and more pervious to H_2SO_4, which is inducive for the formation of βPbO_2 rather than αPbO_2 or PbO. With pure lead or Pb-Ca alloys, one observes often very dense, impervious corrosion films, containing in the interior much PbO. The latter substance can impair, under certain conditions, the contact between grid and active material in positive plates of storage batteries made with Ca-alloy.

J. Burbank prefers not to make any reference to an article of Rüetschi and Cahan[72] where the occurrence of the second modification of PbO_2 (orthorhombic αPbO_2) has for the first time been reported in *corrosion layers of lead*. This material had been described previously in foreign papers, particularly of Russian origin. Its preparation with chemical and with electrochemical plating techniques had been established, but it had not been known as a corrosion product of lead. Prior to the publication date of the article of Rüetschi and Cahan, J. Burbank never mentioned the existence of αPbO_2 in her papers. But since, she also has found αPbO_2 as a corrosion product.

During prolonged corrosion at elevated potentials, αPbO_2 is the major corrosion product. Electrode potentials of α and βPbO_2 in H_2SO_4 solutions have been measured experimentally with good precision by Rüetschi and Cahan in the article referred to, and by S. J. Bone, Symposium of Batteries, Signal Research and Development Establishment, Ministry of Supply, Christchurch, Hampshire, England, October 21, 1958. These measurements agreed very well. In 5M H_2SO_4, e.g., αPbO_2 has an electrode potential 7 mv higher than βPbO_2. The presence of the two different corrosion products has also been demonstrated by the two-step reduction of the corrosion layer.[73] The experimentally determined potential values for α and βPbO_2 do not coincide with the theoretical pH potential diagram of J. Burbank, which is due, as discussed previously, to the presence of other ionic species in the electrolyte.

Recently, Kabonov (*loc. cit.*) has shown that on αPbO_2 less SO_4^{--} ions are adsorbed than on βPbO_2. Inversely, βPbO_2 is formed preferentially in the presence of SO_4^{--} ions, which means at low pH values. Addition of cobalt sulfate to the electrolyte is inducive for the formation of αPbO_2 and to the desorption of SO_4^{--} ions from the surface. Rüetschi and Cahan (*loc. cit.*) have demonstrated that αPbO_2 has a lower oxygen overvoltage than βPbO_2. The lower oxygen overvoltage for αPbO_2 can be associated with a smaller amount of SO_4^{--} ions adsorbed. Oxygen overvoltage is indeed decreased by the addition of cobalt sulfate to the electrolyte.[74]

J. Burbank has not been very consistent with the designations for the various anodic oxides of lead. For instance, she uses intermittently the designations $PbO_1 \cdot xPbO_2$ and $PbO \cdot xPbO_2$ for what is apparently the same material. More serious, however, is the use of such composite formulations. The formula $PbO_1 \cdot xPbO_2$ is misleading because these substances are not mixtures of PbO_1 and PbO_2, but have a definite and separate crystal structure. The designation PbOx is more satisfactory. However, Pb_2O_3 should not be included in the group of PbOx materials. The designation PbOx should be used for substances like Pb_7O_{11} ($PbO_{1.57}$), Pb_5O_8 ($PbO_{1.60}$), Pb_2O_3 ($PbO_{1.50}$), which have a very similar composi-

[71] P. Rüetschi and B. D. Cahan, *This Journal*, **105**, 369 (1958).

[72] P. Rüetschi and B. D. Cahan, *This Journal*, **104**, 406 (1957).

[73] P. Rüetschi and B. D. Cahan, *loc. cit.*, and B. Kabanov, *Dokl. Akad. Nauk S.S.S.R.*, **122**, 1042 (1958).

[74] P. Rüetschi and B. D. Cahan, *loc. cit.*, and D. F. A. Koch, *Electrochemica Acta*, **I**, 32 (1959).

tion, varying only by a few per cent. Also, these substances have basically an orthorhombic symmetry, whereas Pb_3O_4 is tetragonal.

The thermodynamic stability of Pb with regard to PbO_2 (Eq. [1] in J. Burbank's paper) has no practical implication, since both Pb and PbO_2 are unstable at the indicated potential with regard to other possible divalent corrosion products of lead (PbO, $PbSO_4$). Thus, at a potential of, e.g., 0.67 v at pH 1, metallic lead *is not stable* thermodynamically even in the presence of PbO_2 since it will form divalent corrosion products first, and the thermodynamic stability of Pb cannot approach that of PbO_2. On the other hand, PbO_2 is reduced to divalent corrosion products not only above 0.67 v but of course also below this value, and metallic lead is unstable above and below this potential. The experimental evidence for the presence of PbO_2 below the thermodynamic theoretical value is more plausibly explained by nonequilibrium concentration (in particular pH) in the interior of the corrosion layers.

J. Burbank: This extension of the discussion of the anodic reactions of lead is very interesting. A detailed discussion of ionic equilibria in general is contained in the work of Pourbaix[75,76] and the differences brought about by the presence of sulfates and carbonates was presented in the original lead diagrams.[77] The variations in solubilities among the salts of lead with other anions and the differences in free energies of formation will give rise to as many diagrams.

In the first part of the paper under discussion, solubilities, anions, and ionic equilibria were intentionally and specifically stated to be excluded, and a comprehension of the works of Pourbaix was assumed. The data recorded in Fig. 1 were obtained by diffraction examination of surfaces of anodes as stated in the paper. The picturization of Fig. 3 presented under the heading "anions and passivation" is thought to represent the conditions under which such oxide mixtures are possible—by formation of a salt layer. Fig. 1 must not be read out of context. The text appears clear enough on these points.

It is gratifying to know that Rüetschi and Cahan now accept the appearance of lower oxides of lead on the anode in acid solutions, a fact they were unable to verify at an earlier date. The concept of film formation in the passivation of Pb in H_2SO_4 is rather widely accepted. A change in pH toward higher values at local cathodes is a normal expectation of static corrosion phenomena. In the instance under discussion external anodic polarization was applied, and anodic reactions were to be considered. Rüetschi and Cahan did not state by what anodic reaction the area near an anode may become alkaline. The reactions believed to effect an increase in pH were not written out in full in the comments so as to permit a more considered analysis of the situation described. No difficulty whatsoever is encountered in visualizing a consumption of hydrogen ion during cathodic reactions, but merely stating that an increase in pH occurs adjacent to the film-carrying lead anode does not make it a fact. It would be most convenient if the anodic phenomena could be written off as an increase in pH.

Migration of hydroxyl ion along with others through a primary layer of $PbSO_4$ may take place, but it is not clear that a marked increase in pH adjacent to an anode may be developed. It is clear that an increase in pH can not accompany electrochemical formation of the oxides, oxygen, or similar anodic products.

Experimental work remains to be done to realize a final determination of the mechanisms of the anodic processes on lead, but it is believed that the Hirsch[78-80] effect describes the phenomena encountered with $PbSO_4$ films. If one accepts Hirsch's work, a $PbSO_4$ film is permeable to hydrogen ion and water but not to plumbous or sulfate ion. Furthermore, it appears likely that the charge exchange mechanism of the $PbSO_4/PbO_2$ electrode itself may be elucidated by such a process.

The paper contained no discussion regarding the cited work of Rüetschi and Cahan, but it may be well at this time to indicate that some of the experimental results reported by them may be otherwise interpreted. For one example, the two-step discharge of PbO_2 has been attributed to another phenomenon.[81] It is hoped that Rüetschi and Cahan will continue their experimental work, and that ultimately all experimental facts may be properly interpreted.

The designation $PbO_4 \cdot xPbO_2$ should have been uniform through the manuscript; this and several other typographical errors should cause no confusion. It is redundant to reiterate that the stoichiometry Pb_3O_4 is exhibited by at least two structurally different materials. It seems doubtful that a simple mechanical mixture of PbO and PbO_2 could possibly be understood by the definition given for the symbol in the paper.

Some would hesitate to state unreservedly that the equilibrium between Pb and PbO_2 is without "practical" implication. Other factors could prove this to be a most "practical" and significant equilibrium: consider the processing of positives for "dry charge" use.

Role of Thiourea in the Electrodeposition of Copper

B. Ke, J. J. Hoekstra, B. C. Sison, Jr., and D. Trivich
(pp. 382-388, Vol 106)

S. C. Barnes[82] and G. G. Storey[83]: We have studied the effect of thiourea additions to acid copper sulfate solutions on the type of deposit subsequently obtained on electrolysis. All our work has been carried out on flat single crystal cathodes: on which deposits formed at low current densities, from thiourea-free solutions, continue the base orientation

[75] M. Pourbaix, "Thermodynamics of Dilute Aqueous Solutions," Trans. by J. N. Agar, London (1949).
[76] M. Pourbaix, *Centre Belge d'Etude Corr. R.T. No. 49* (1957).
[77] P. Delahay, M. Pourbaix, and P. Van Rysselberghe, *This Journal*, **98**, 57 (1951).
[78] P. Hirsch-Ayalon, *Rec. trav. chim.*, **75**, 1065 (1956).
[79] P. Hirsch-Ayalon, *J. Polymer Sci.*, **23**, 697 (1957).
[80] C. J. Van Oss and P. Hirsch-Ayalon, *Science*, **129**, 1365 (1959).
[81] W. Feitknecht, *Z. Elektrochem.*, **62**, 795 (1958).
[82] Joseph Lucas Lab., Dept. of Industrial Metallurgy, University of Birmingham, Edgbaston, Birmingham 15, England.
[83] Messrs. Joseph Lucas Ltd., Birmingham, England; formerly at Dept. of Industrial Metallurgy, University of Birmingham, Edgbaston, Birmingham, England.

and develop well-defined crystallographic surface structures.[86, 88] The particular surface plane studied in the thiourea investigation was near to {100} on the <110> zone: this develops a sharp straight-edged platelet surface structure (when the deposit is approximately 14 μ thick) at 20 ma/cm^2 and 35°C, and a partially polycrystalline deposit at 40 ma/cm^2.[88] Additions of thiourea in concentrations ranging from 5×10^{-10} to 10^{-2}M were made to the bath, and effects on the deposit structures obtained at these two current densities noted. The results obtained from the solution containing an approximately equal amount of thiourea to the one used by Ke, *et al.*[87] (10^{-4}M) were in complete agreement with their observations and conclusions. Our evidence for adsorption was that the overpotential associated with the deposition was considerably increased by the addition of this amount of thiourea, indicating some interference with the normal growth process. However, the results obtained from solutions containing lower concentrations of the addition agent were more interesting. These are briefly summarized below.

At 20 ma/cm^2, 10^{-9} to 10^{-6}M thiourea decreased the overpotential and led to development of deposits characteristic of lower current densities in a thiourea-free solution.[88] 10^{-5}M had negligible effect on polarization but caused a habit change in the deposit: pyramids with sides near {211} developed instead of platelets. Above 10^{-4}M overpotential was increased in proportion to the thiourea content, the deposits becoming increasingly uneven and containing polycrystalline material. With 10^{-2}M thiourea, the deposit was very uneven, nodular, and cracked.

Deposits produced at 40 ma/cm^2 from solutions containing thiourea showed more variations: concentrations from 5×10^{-10} to 10^{-6}M caused an increase in overvoltage and more polycrystalline material to develop. 5×10^{-6} to 10^{-4}M reduced overpotential and platelet type deposits were obtained; 5×10^{-4} to 10^{-3}M produced deposits with pyramidal habit and only small changes in polarization. These deposits from solutions containing 5×10^{-3} to 10^{-2}M, at this current density, were complete continuations of the base, and contained no polycrystalline material. Bright even deposits were produced when 5×10^{-5} and 10^{-4}M thiourea was added, that at the higher concentration being almost featureless. At all concentrations above 5×10^{-6}M, polarization was increased. 10^{-2}M caused uneven nodular deposits to form, while that obtained from the solution containing the highest concentration studied (10^{-2}M) was covered with needle-like growths at a small angle to the surface. Deposits formed at this current density from solutions containing more than 5×10^{-3}M contained polycrystalline material.

This work at present is continuing and an explanation of these, and allied, phenomena is being sought in the relation between relative rates of crystal growth and adsorption of surface active material.

[86] H. J. Pick and J. Wilcock, *Trans. Inst. Metal Finishing, Advance Copy*, No. 9, 35 (1958).
[88] H. J. Pick, G. G. Storey, and T. B. Vaughan, In press, *Electrochemica Acta*.
[88] S. C. Barnes, G. G. Storey, and H. J. Pick, In press, *Electrochemica Acta*.
[87] B. Ke, J. J. Hoekstra, B. C. Sison, and D. Trivich, *This Journal*, **106**, 382 (1959).

The Role of the Metal-Ion Concentration Cell in Crevice Corrosion

G. J. Schafer and P. K. Foster (p. 468, Vol. 106)

Saul B. Bien[89] and Herbert D. Ayers, Jr.[90]: It was suggested by Schafer and Foster that the metal-ion concentration cell cannot be a cause of crevice corrosion and that crevice mouth attack is a special case of differential aeration. In the case of solder joints, it was clearly demonstrated[90] with autoradiographs made by flux tagged with fluorine-18 that fluoride salts are deposited at the interface between the solder and chromium alloys. We postulated that the crevice mouth attack was initiated by solution through convection and/or diffusion of irregular areas of residue at the interface. Following this, the development of the crevice continues. We discussed[91] the role of the differential aeration cell as described by LaQue[92] and the active-passive cell of Logan[93] in the continued development of the crevice.

A further significant finding was that, after one year of exposure to the room atmosphere in the laboratory, discoloration appeared (at X375) on the polished surface of the cross sections of the solder joints on areas corresponding approximately to those which produced radiopacities on the autoradiographs. The surface was repolished removing all stains. After six months of re-exposure to the air in the laboratory, discoloration again reappeared in the same areas of the surface adjacent to the interface. There is therefore a correlation between the areas of the autoradiographs showing the deposition of fluoride salts at the interface and the discolored areas observed on surface of the cross section of the solder joints. The discoloration appears to result from corrosive action in the areas which were most radioactive. The dissociation of salts deposited at the interface between the solder and the chromium alloy and the movement of ions over the polished surface of the specimen may have been facilitated by moisture from the atmosphere.

G. J. Schafer and P. K. Foster: The investigations of Bien and Ayers[90, 91] are not related to crevice corrosion in the sense used by us in the discussed paper. Their work is concerned with the initiation and propagation of failure at bimetallic soldered joints containing entrapped flux residues. Perhaps it should have been explicitly stated that our concern was solely with the mechanism responsible for maintaining steady-state corrosion in crevices consisting of only *one* homogeneous alloy.

We agree that once a crevice is present between a solder and the base metal due to incomplete bonding in the soldering operation, differential aeration

[89] 76 Union Ave., Lynbrook, N. Y.
[90] Dental Materials Lab., Columbia University School of Dental and Oral Surgery, New York, N. Y.
[90] S. M. Bien and H. D. Ayers, Jr., *J. Dental Research*, **38**, 428 (1959).
[91] S. M. Bien and H. D. Ayers, Jr., *J. Am. Dental Assoc.*, **58**, 74 (1959).
[92] F. L. LaQue, "Nature of Corrosion of Metals," New York Chapter American Society for Metals, October 10, 1955.
[93] H. L. Logan, *J. Research Nat. Bur. Standards*, **48**, 99 (1952).

would have an important effect[91] particularly with stainless steels which are passivated by oxygen. It seems to us, however, that the potential difference between the two different alloys (solder and base metal) should have been considered. Evidence of potential differences is provided by preferential attack of the base metal in Fig. 7 (upper) and Fig. 10 (upper) in the work cited in Footnote 91.

The "crevice corrosion" failures observed by Bien and Ayers[91] may be due to purely physical effects, i.e., the solution of flux from the interface, since "crevice corrosion is characterized by a failure of the bond with little or no macro corrosion of the soldered joints or the solder. In the appliances where the bond failed either clinically or experimentally, there was no obvious corrosion or pitting of any metal."[91]

Alternatively, it may be that a thin layer of a base metal/solder alloy is formed at the interface, and that this layer is anodic to both the solder and the base metal under the conditions of test.[91] This would explain the formation of crevices sufficiently long and narrow to cause separation of the joint without gross corrosion of either the solder or the base metal.

We agree that the experiments cited in the second paragraph of Bien's and Ayer's comments confirm the entrapment of flux at the solder/base metal interface.

On the Internal Resistance of Dry Cells. A New Pulse Method

R. J. Brodd (pp. 471-475, Vol. 106)

J. J. Coleman[95]: I have two specific comments to make on Dr. Brodd's paper, the first specific to the paper, and the second more general in character.

The author's method of measurement involves a comparison of a potential developed across a dry cell, by pulses ranging from 1 to 10 μsec with a potential developed across a simple resistor. This assumes that the "equivalent circuit" in a dry cell is a simple resistor and not, for example, a resistor shunted by a condenser. The author directs his attention to the problem of what *is* a proper "equivalent circuit" in the first paragraph under "Results and Discussion." He found his internal resistance measurement unaffected by a change in the length of the pulse from 1 to 10 μsec and the change in the rate of the pulses from 100 to 5000 pulses per second. He concludes from this, mistakenly I believe, that the "equivalent circuit" can be taken as a simple resistor. Fig. 2 indicates that the pulse is approximately a square wave and the shape of the pulse as exhibited on the experimenter's oscilloscope is more important than its length. Dr. Brodd does not interpret the shape and hence does not come to grips with the problem of determining the "equivalent circuit" of a dry cell.

Now for the second comment, I believe that the method described by the author, and all similar methods, give the same results as conventional methods employing alternating currents. There is a feeling that a short, direct-current pulse is superior to an alternating current because the battery develops direct current and not alternating current. However, the phrases "direct current" and "alternating current" lose many of their usual meanings when applied to very short pulses. These phrases are usually applied to steady states. For example, one may say that a.c. will pass through a condenser and d.c. will not. Certainly this is not true if the d.c. is a very short pulse. A short d-c pulse has much more in common with steady state a.c. than with steady state d.c. This relationship appears mathematically in the Fourier analysis of a square wave. One represents a square wave pulse by the superposition of alternating currents of many frequencies.

Any steady state direct current in a dry cell must flow through the manganese dioxide particles or be coerced in some similar fashion. Alternating current or short pulses of direct current can pass directly from the black to the electrolyte. Hence, I do not regard measurements by short d-c pulses as pertinent to any study of the dry cell as a machine developing electrical energy.

R. J. Brodd: The comments of Dr. Coleman will serve to clear any misunderstanding in my original paper. The purpose of the paper was to report a method for measuring the true internal resistance of the battery. It appears that the method is successful in measuring the pure resistive element of a battery.

Dr. Coleman seems to have missed the significance of my statement concerning the shape of the voltage and current pulses. As was emphasized in the paper, the two traces were identical. The rise and decay of the pulses were instantaneous and the tops of both pulses were flat. This behavior is characteristic of a circuit containing a resistor with no capacitive effects. The ringing at the leading edges of the pulses, as suggested by Dr. Jacopetti,[98] is probably due to lead inductance of the instrument and cell. There is no evidence of a rounding of the leading edge of the pulses as would be expected from capacitive elements. The variation of repetition rate and pulse length without changing the measured resistance supports the conclusion reiterated above that the measuring technique reported in my paper determines the purely resistive element of a dry cell.

The equivalent circuit of a Leclanché cell which results from impedance measurements is

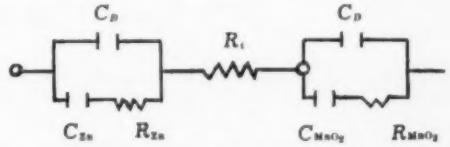

where R_i is the internal resistance, C_D the capacitance of the electrical double layer, C_{Zn}, R_{Zn} and C_{MnO_2}, R_{MnO_2} are the capacitance and resistance of the

[91] J. D. Dowd, *Welding J. (N. Y.)*, 33, 113s (1954).
[95] Burgess Battery Co., Freeport, Ill.
[98] M. M. Jacopetti, Private communication.

zinc and manganese dioxide electrode reactions.[27, 28] As Dr. Coleman mentioned, the pulse method used was essentially a very high-frequency a-c measurement as the pulse may be constructed from a suitable Fourier analysis. The very high-frequency character of the pulse method is emphasized by the 3000 repetition rate of 3 μsec pulse used in the paper. Inspecting the equivalent circuit above, we see that at very high frequencies the impedance of the electrode reactions would be shunted by the capacitance, C_p. At very high frequencies, the impedance of C_p will become negligible. As a result, the pulse measurement of the impedance of the Leclanché cell determines only the resistive element of the circuit R_i, the internal resistance of the cell. Thus, the conclusion reached in the pulse measurement concerning the measured resistive element of a cell is strengthened by results of impedance measurements on the cell.

The comparison of the a-c bridge measurements to the pulse method has been discussed elsewhere.[28] However, a few words of comment are in order. The a-c results reported in the past are often misleading for measurements often were made at only one frequency. The errors involved in this procedure are clearly evident considering the equivalent circuit of a cell. Also, the results of Euler and myself[27, 28] illustrate the effect of frequency on the measured resistance and capacitance of a cell.

It is possible to use the a-c bridge measurements of the resistance and capacitance at various frequencies to calculate the values of all components of the equivalent circuit. My results show that the resistive element R_i determined by the analysis of a-c bridge measurements is identical with the true internal resistance determined by the pulse method

I do not think it is accurate to say, as Dr. Coleman did, that a determination of R_i is not pertinent to the study of dry cells. The resistance polarization of a cell plays an important role in any experimental measurement or use of a cell. The change in R_i as a cell is discharged is interesting as it offers a clue to possible cell reactions and possibly a prediction of cell life. The internal resistance is the most important factor in determining the short circuit current a cell will deliver. The true internal resistance, R_i, is indeed an important part of a cell.

[27] J. Euler and K. Kahmelt, *Z. Elektrochem.*, **61**, 1200 (1957).

[28] R. J. Brodd, paper presented before Columbus Meeting of The Electrochemical Society, October 1959.

June 1960 Discussion Section

A Discussion Section, covering papers published in the July—December 1959 JOURNALS, is scheduled for publication in the June 1960 issue. Any discussion which did not reach the Editor in time for inclusion in the December 1959 Discussion Section will be included in the June 1960 issue.

Those who plan to contribute remarks for this Discussion Section should submit their comments or questions in triplicate to the Managing Editor of the JOURNAL, 1860 Broadway, New York 23, N. Y., *not later than March 1, 1960.* All discussion will be forwarded to the author(s) for reply before being printed in the JOURNAL.

Monographs of The Electrochemical Society

ECS Series

The following are books developed and sponsored by The Electrochemical Society and published by John Wiley & Sons, Inc., 440 Fourth Ave. New York 16, N. Y. Members of The Electrochemical Society can receive a 33 1/3% discount by ordering volumes from Society Headquarters, 1860 Broadway, New York 23, N. Y. Book and invoice will be mailed by John Wiley & Sons. Nonmembers (including subscribers) should order direct from Wiley.

Corrosion Handbook. Edited by Herbert H. Uhlig. Published 1948, 1188 pages, **$16.00**

Modern Electroplating. Edited by Allen G. Gray. Published 1953, 563 pages, **$8.50**

Abstracts of the Literature on Semiconducting and Luminescent Materials and Their Applications. Compiled by Battelle Memorial Institute.

Vol. I, 1953 Issue—published 1955, 169 pages, **$5.00** (soft cover)

Vol. II, 1954 Issue—published 1955, 200 pages, **$5.00** (soft cover)

Vol. III, 1955 Issue—Edited by E. Paskell; published 1957, 322 pages, **$10.00** (hard cover)

Vol. IV, 1956 Issue—Edited by E. Paskell; published 1959, 456 pages, **$12.00** (hard cover)

Electrochemistry in Biology and Medicine. Edited by Theodore Shedlovsky. Published 1955, 369 pages, **$11.50**

Vapor Plating (The Formation of Metallic and Refractory Coatings by Vapor Deposition), by C. F. Powell, I. E. Campbell, and B. W. Gonser. Published 1955, 158 pages, **$5.50**

High-Temperature Technology (Materials, Methods, and Measurements). Edited by I. E. Campbell. Published 1956, 526 pages, **$15.00**

Stress Corrosion Cracking and Embrittlement. Edited by W. D. Robertson. Published 1956, 202 pages, **$7.50**

Arcs in Inert Atmospheres and Vacuum. Edited by W. E. Kuhn. Published 1956, 188 pages, **$7.50**
(Papers Presented at the Symposium on Arcs in Inert Atmospheres and Vacuum of the Electrothermics and Metallurgy Division of The Electrochemical Society, April 30 and May 1, 1956, San Francisco, Calif.)

Technology of Columbium (Niobium). Edited by B. W. Gonser and E. M. Sherwood. Published 1958, 120 pages, **$7.00**
(Papers Presented at the Symposium on Columbium—Niobium of the Electrothermics and Metallurgy Division of The Electrochemical Society, May 15 and 16, 1958, Washington, D. C.)

The Structure of Electrolytic Solutions. Edited by Walter J. Hamer. Published 1959, 441 pages, **$18.50**
(Based on a Symposium held in Washington, D. C., in May 1957, sponsored by The Electrochemical Society, New York, and The National Science Foundation, Washington, D. C.)

Vacuum Metallurgy

Vacuum Metallurgy, third printing, 1958. Edited by J. M. Blocher, Jr.; 216 pages; **$5.00,** less a 20% discount to ECS members only. Available from Electrochemical Society Headquarters, 1860 Broadway, New York 23, N. Y.

(Papers Presented at the Vacuum Metallurgy Symposium of the Electrothermics and Metallurgy Division of The Electrochemical Society held in Boston, Mass., October 6 and 7, 1954)

FUTURE MEETINGS OF
The Electrochemical Society

Chicago, Ill., May 1, 2, 3, 4, and 5, 1960

Headquarters at the Lasalle Hotel

Sessions probably will be scheduled on

Electric Insulation (including a symposium on "Electrolytic Capacitors"),

Electronics (including Luminescence and Semiconductors),

Electrothermics and Metallurgy (including a symposium on "High-Purity Vanadium" and a round table on "Methods of Reducing Iron Ores"), Industrial Electrolytics,

and Theoretical Electrochemistry

★ ★ ★

Houston, Texas, October 9, 10, 11, 12, and 13, 1960

Headquarters at the Shamrock Hotel

★ ★ ★

Indianapolis, Ind., April 30, May 1, 2, 3, and 4, 1961

Headquarters at the Claypool Hotel

★ ★ ★

Detroit, Mich., October 1, 2, 3, 4, and 5, 1961

Headquarters at the Statler Hotel

Papers are now being solicited for the meeting to be held in Chicago, Ill., May 1-5, 1960. Triplicate copies of each abstract (*not exceeding 75 words in length*) are due at Society Headquarters, 1860 Broadway, New York 23, N. Y., *not later than January 4, 1960* in order to be included in the program. *Please indicate on abstract for which Division's symposium the paper is to be scheduled, and underline the name of the author who will present the paper.* Complete manuscripts should be sent in triplicate to the Managing Editor of the JOURNAL at 1860 Broadway, New York 23, N.Y.

Papers submitted for presentation at the meeting become the property of The Electrochemical Society and may not be published elsewhere, in whole or in part, unless permission is requested and granted by the Society. Papers already published elsewhere, or submitted for publication elsewhere are not acceptable for oral presentation except on invitation by a Divisional program Chairman.

Current Affairs

News Notes in the Electrochemical Field

New ECS Sustaining Member

Peerless Roll Leaf Co., Inc., Union City, N. J., recently became a Sustaining Member of The Electrochemical Society.

1960 ECS Membership Directory

The Electrochemical Society is pleased to announce that a new Membership Directory henceforth will be published each year. The 1960 edition will be off the press in the spring of 1960.

The Directory will be available only to members of the Society (not including subscribers) at the price of $1.00 per copy. Members who wish to purchase the Directory should indicate this in the space provided on the dues statement which has been mailed to them.

A form has been sent out to ECS members to enable them to bring their listing up to date. Members are urged to fill out and return this form to Society Headquarters, 1860 Broadway, New York 23, N. Y., immediately. The deadline for receipt of this information is *January 1, 1960.*

Auto-Lite Announces the Purchase of C & D

The Electric Auto-Lite Company of Toledo, Ohio, became owner of C & D Batteries on September 30, 1959 according to the joint announcement of Mr. Robert Davies, president of Auto-Lite, and Mr. John F. Rittenhouse, president of C & D. Mr. Rittenhouse has been named vice-president of Auto-Lite and general manager of the C & D Division of Auto-Lite. Mr. Henry E. Jensen has also been named vice-president of Auto-Lite and will continue as manager of marketing and engineering of the C & D Division. No change in personnel or policy is planned.

Auto-Lite is one of the three largest manufacturers of automobile batteries in the country. C & D is a rapidly growing manufacturer of industrial type lead-acid batteries with factories in Conshohocken and Pennsburg, Pa., and Attica, Ind. They make electric truck batteries; telephone batteries; railway, diesel, and car-lighting batteries; and control batteries for power stations.

C & D recently enlarged their research and development laboratory under the direction of Dr. Eugene Willihnganz. According to Mr. Rittenhouse, this work will now be expanded.

R. V. Williams Receives 1959 F. J. Tone Medal Award

Reginald V. Williams, president and director of research of the Williams Gold Refining Co., Inc., Buffalo, N. Y., is the recipient of the 1959 Frank J. Tone Medal Award.

R. V. Williams

The Medal is awarded annually by the Niagara Frontier Section of the American Institute of Mining, Metallurgical, and Petroleum Engineers.

The Medal was established in 1956 by F. Jerome Tone and Franchot Tone to honor the memory of their father, Dr. Frank J. Tone, pioneer industrialist of the Niagara Frontier, and Past President and Acheson Medalist of The Electrochemical Society. It is awarded to a person who has made outstanding and important contributions to the science and practice of metallurgy. The recipient must be a resident of the Niagara Frontier community.

Mr. Williams has been a leader in research and development in the field of precious metals metallurgy for the dental profession and industry throughout his entire career. He holds several patents on alloy compositions of precious metals. He is particularly known in the dental profession for his work on the perfection of the complex gold-platinum alloy system used in wire form for dental applications, particularly in orthondontics.

Mr. Williams is a member of long standing of many scientific societies, including The Electrochemical Society.

The Tone Medal Award was presented to Mr. Williams at the annual Award Meeting held in the Hotel Stuyvesant in Buffalo on November 18. The presentation was made by William W. Stevens, Carborundum Metals Co., chairman of the Niagara Frontier Section of the sponsoring society.

First Nationwide "Aerospace Finishing Symposium"

Following is the program for the first nationwide "Aerospace Finishing Symposium," to be held December 7, 8, and 9, 1959, at the Hotel Texas in Fort Worth.

Monday Morning, Dec. 7
Metal Depositions and Plating Processes

"Nickel Plating by Chemical Reduction" by G. Gutzeit

"New Developments in Precious Metals Plating" by A. Korbelak

"Vacuum Deposited Coatings for Aircraft, Space Vehicles, and Missiles" by P. J. Clough and H. M. Farrow

"High-Temperature Coatings for Aerospace Applications" by J. R. Myers

Tuesday Afternoon, Dec. 8
Coatings for the Future

"Application and Testing of High-Temperature Inorganic Coatings" by L. N. Hjelm

"Utilization of Pigmented Coatings for the Control of Equilibrium Skin Temperatures of Space Vehicles" by G. A. Zerlaut

"Experimental Application of Arc and Flame Sprayed Coatings" by J. D. Walton

"Some Important Factors for Coatings for High Temperatures" by C. L. Faust

"Surface Protection of Metals for Atmospheric Re-entry by the Diffusion Technique" by R. L. Wachtell

Wednesday Morning, Dec. 9

Special Processes and Finishing Treatments

"Developments in Aluminum Finishing" by R. E. Pettit

"Electroforming for Aircraft and Missiles—A Survey" by M. Rubinstein

"Precious Metal Coatings for Special Depositions and Surface Treatments" by R. T. Hopper

"Hard Anodizing of Aircraft and Missile Components" by H. J. Wiesner

Wednesday Afternoon

Organic Coatings and Polymeric Finishes

"A Better Priming System" by W. F. Smith

"Organic Finishing and Coatings" by E. D. Hood

"High-Temperature Resistant Organic Coatings" by M. A. Glaser, R. E. Caplan, and R. W. Clope

"The Development of Polyurethane Coatings for Atomic Thermal Control" by A. S. Dalton

Wednesday Evening

The Finishing Forum

Panel Discussions—The Finishing Forum comprises speakers from Wednesday's technical sessions, plus several specially invited finishing authorities.

Porosity of Plated Coatings

Because the protective value of a plated coating on metal is dependent, to a large extent, on the exclusion of pores and other flaws in the coating, the National Bureau of Standards has been investigating the causes, nature, and effect of porosity in plated coatings for the American Electroplaters' Society. As part of this program, several different aspects of porosity have been studied under the direction of Fielding Ogburn and Donald R. Ernst. These include the development of an improved technique[1] to study the porosity of metallic electroplated coatings with a microscope, evaluation of the sensitivity of the ferroxyl test[2]—one of the generally accepted methods for detecting porosity—and determination of the influence of gas[3] on pore formation.

Microscope Detection Method

"Parallel sectioning," a technique[1] developed by F. Ogburn and D. W. Ernst, an AES Research Associate, involves polishing off some of the coating *perpendicular* to the axis of the pore and parallel to the basis metal. When the cut section is studied under a microscope, the pore will appear as a small dot which can be seen easily at 400 magnification if the pore is larger than 0.05 ml in diameter. To make sure that the dot is not a surface defect introduced during polishing, successive layers are removed and examined until the underlying metal is reached. If the dot is a pore, it will reappear consistently at the same spot.

Four types of pore defects were found in these studies: Pits (dead-end pores), cavities (enclosed pores), continuous pores, and bridged-over pores.

Sensitivity of Ferroxyl Test

Perhaps the best known porosity test for nickel coatings on steel is the ferroxyl test. However, since the over-all sensitivity was not known, experiments[2] were conducted by the Bureau to determine the efficiency of the method.

Test specimens were prepared by plating steel sheets with gold on one side. The coating specimens were then tested with the modified ferroxyl test[4] (solution of sodium chloride-potassium ferricyanide). Next the basis metal was dissolved by an acid solution, leaving the coating. This gold foil was photographed[5] by placing it on a photographic film and exposing to light. The resulting photographic record of the porosity, supplemented with measurements of pore size obtained by microscopic examination, were compared, spot by spot, with the pattern produced by the ferroxyl test.

From this experiment, it was found that the sensitivity of the ferroxyl test decreased as the pore size decreased. Virtually all pores 0.5 ml or more in diameter were detected by the ferroxyl test while very few of the pores less than 0.1 ml in diameter were detected. Since smaller pores are more numerous than larger pores, it is evident that the ferroxyl test has rather severe limitations.

Influence of Gas on Porosity

One factor contributing to the formation of pores involves the growth of a deposit around a gas bubble. To study the effect of gas on porosity, a cell[3] was developed with a transparent bottom that facilitates observation of metal deposition.

The relative rates of hydrogen discharge and metal deposition were found to determine whether a bubble is covered over by the deposit or enlarges itself. When a gas bubble is large enough to break away from the deposit, it leaves some gas in the pore formed by the deposit growing around the bubble. This gas effectively blocks the electrolyte from entering the pore and so prevents the deposit from forming across the pore opening. Although this experimental procedure differs from actual industrial plating conditions in several ways, observations seem to indicate that the pore growth mechanism it demonstrates is applicable on a broader scale.

NBS to Publish Four-Part Journal

On July 1, 1959, the National Bureau of Standards began publishing its *Journal of Research* in four separate sections, corresponding to subject matter fields. This change is being made to permit more effective dissemination of the Bureau's findings to science and industry. At the same time, the editorial scope of the journal is being broadened to cover the Bureau's technical program as completely as possible.

Henceforth, the individual reader need subscribe only to those sections of the journal that fall within his particular field of interest.

Four Sections

The journal is being divided into the following sections, each available upon subscription from the Government Printing Office: Section A—Physics and Chemistry, Section B—Mathematics and Mathematical Physics, Section C—Engineering and Instrumentation, Section D—Radio Propagation.

Section A, *Physics and Chemistry*, will cover a broad range of physical and chemical research, with major emphasis on standards of physical measurement, fundamental constants, and properties of matter. It

[1] F. Ogburn and D. W. Ernst, "Microscopic Detection of Porosity", *Plating*, 46, 831 (1959).

[2] F. Ogburn, D. W. Ernst, and W. H. Roberts, "An Evaluation of the Sensitivity of the Ferroxyl Test," *ibid.*, In press.

[3] F. Ogburn and D. W. Ernst, "Influence of Gas on Porosity," *ibid.*, 46, 957 (1959).

[4] P. W. C. Strausser, *Proc. Am. Electroplaters' Soc.*, 27, 194 (1939).

[5] F. Ogburn and M. Hilkert, "The Nature, Cause and Effect of the Porosity in Electrodeposits. II. Radiographic Detection of Porosity in Electrodeposits," *Ann. Proc. Tech. Sessions Am. Electroplaters' Soc.*, p. 256 (1956); "Porosity Detection in Plated Coatings", *Tech. News Bull.*, 41, 44 (1957).

will be issued six times a year, and the annual subscription will cost $4.00 (75 cents additional for foreign mailing).

Section B, *Mathematics and Mathematical Physics*, will present studies and compilations designed mainly for the mathematician and theoretical physicist. It will include topics in mathematical statistics, theory of experiment design, numerical analysis, theoretical physics and chemistry, and logical design and programming of computers. Short numerical tables will also be included from time to time. Section B will be issued quarterly, and the annual subscription cost will be $2.25 (foreign, 50 cents additional).

Section C, *Engineering and Instrumentation*, will report results of interest chiefly to the engineer and the applied scientist. This section will include many of the new developments in instrumentation resulting from the Bureau's work in physical measurement, data processing, and development of test methods. It will also cover some of the work in applied mechanics, properties of engineering materials, building research, and cryogenic engineering. Section C will be issued quarterly, and the annual subscription cost will be $2.25 (foreign, 50 cents additional).

Section D, *Radio Propagation*, is to be edited at the Bureau's Boulder (Colo.) Laboratories. It will report research in radio propagation, communications, and upper atmospheric physics. Topics to be covered include propagation in ionized media, scattering by turbulence, effect of irregular terrain on propagation, diffraction and scattering by solid obstacles, propagation through time-varying media, surface waves, and antennas. Section D will be issued six times a year, and the annual subscription cost will be $4.00 (foreign, 75 cents additional).

Broadened Scope

The editorial scope of the journal will be broadened in several ways. In addition to research reports, the new journal will present review articles by recognized authorities, and compilations of information on subjects closely related to the Bureau's basic mission. Much of the material which the Bureau has been publishing in nonperiodical form will henceforth be directed to the journal.

To provide complete coverage of the Bureau's technical program, all NBS nonperiodical publications and articles by the Bureau staff in professional journals will be abstracted in the appropriate section of the *Journal of Research*. In addition, each section will carry a complete listing of all Bureau publications that are not abstracted in that section. Thus, within a particular journal section, each individual Bureau publication will appear either in full, in abstract, or listed with appropriate reference data.

NBS Technical Notes have been designed to supplement the Bureau's regular publications program. They will provide a means for making available communications and reports that are of transitory or limited interest. *Technical Notes* will be offered for sale by the Office of Technical Services, U. S. Dept. of Commerce, Washington 25, D. C. All other NBS publications are available from the Superintendent of Documents, U.S. Government Printing Office, Washington 25, D. C.

52nd Annual Meeting of A.I.Ch.E.

The 52nd Annual Meeting of the American Institute of Chemical Engineers will be held in San Francisco, December 6-9, 1959. Electrochemists may be particularly interested in the Tuesday afternoon session, in which papers on mercury cell design, iodate production, aluminum cell design, and fuel cells will be presented. Numerous papers on heat transfer, turbulent mixing, fluid flow, and other fields of importance to electrochemistry, combined with the charm and beauty of San Francisco, will make your attendance at the meeting a rewarding experience.

Notice to Subscribers

Your subscription to the JOURNAL of The Electrochemical Society will expire on *December 31, 1959*. Avoid missing any issue. Send us your remittance now in the amount of $18.00 for your 1960 subscription. (Subscribers located outside the United States must add $1.00 to the subscription price for postage, and payment must be made by Money Order or New York draft, not local check.) A final expiration notice has been mailed to all subscribers.

A bound volume of the 1960 JOURNALS was obtainable at the prepublication price of $6.00 by adding this amount to remittance on orders placed by *December 1, 1959*, After this date the price will be increased to $18.00 subject to prior acceptance. Bound volumes are *not* offered independently of your JOURNAL subscription.

Development of New Science Teaching Aids Supported by NSF

Several ingenious scientists and engineers who are dissatisfied with the standard catalog offerings of items of equipment for science teaching are today working in laboratories from Vermont to New Mexico to develop tools they feel are desirable for improved science instruction. The National Science Foundation, an independent agency of the United States Government, recently announced support of 18 projects, totalling $189,000, to encourage mathematicians, scientists, and engineers to devise new laboratory equipment for school and college courses.

Nelson Walbridge, of the Dept. of Physics at the University of Vermont, is developing modified research apparatus for quantitative experiments on the properties of waves, for use in college courses in physics. R. K. Moore, of the Dept. of Electrical Engineering, University of New Mexico, is constructing a relatively inexpensive digital computer which students and teachers can put together for use in high school and college mathematics courses. Others are devising such science-instruction tools as dissectible models of skulls, an operating model to demonstrate the principles of hemodynamics in vertebrate circulatory systems, an inexpensive supersonic wind tunnel, and an electronic planetarium. Grants for these and other projects have been made by the Foundation to colleges, universities, professional scientific organizations, and research institutes in Arizona, the District of Columbia, Indiana, Iowa, Kansas, Maryland, Missouri, New Mexico, New York, Vermont, and West Virginia.

The Foundation does *not* provide for purchasing equipment for use by an individual school or college, nor for the development of equipment solely for local use. The objective is to aid competent scientists to develop new equipment of potentially wide usefulness. Grantees are expected to supply teachers with full information about apparatus they devise. Such information is commonly distributed in the form of reports, articles in professional journals, and presentations at professional meetings. Once equipment

has been developed, grantees are expected, as well, to permit interested commercial suppliers to enter negotiations for production and marketing.

Support for the program will be extended during the current fiscal year, and proposals must be received by the National Science Foundation by December 31, 1959. Further information can be obtained from the Course Content Improvement Section, National Science Foundation, Washington 25, D. C.

Facts and Fancies in Pure Silicon

Contrary to the current popular thinking that silicon of higher and higher purities will be required by the semiconductor industry in the future, a survey completed by Aries Associates, consulting engineers of Stamford, Conn, indicates that the demand trend, based on actual interviews with users, is toward lower grades than now used and toward a lower-cost, uniform product.

The Aries survey shows that the current U. S. consumption, estimated at approximately 80,000 pounds in 1959, will continue to grow at a high rate for at least five years, even with improved efficiency of utilization.

Currently, pure silicon is being sold in four purity grades, determined by its resistivity, with the ultimate selling price based on purity, as indicated by the following recent quotations:

	Price/lb
Grade I	$330
Grade II	220
Grade III	130
Solar cell grade	90

The Aries survey discloses that semiconductor device manufacturers are tending to use the lower grades of silicon because of the price premium for higher purities. This has been accomplished through intensified development of improved "doping" procedures and designs utilizing the lower grades. The findings indicate that eventually Grade I or better will be used in comparatively few devices, such as power rectifiers, and that grades close to the present Grade III will be the dominant market type.

The implications of the Aries study on processes are significant. Only those processes capable of marketing silicon at a price of less than $100 per pound will survive the competitive shakedown. Nine manufacturers already have entered the ring and two others are known to be developing processes.

A study of the process economics conducted as part of the survey indicates that the most costly processes involve the reduction of silicon iodide, which can also potentially yield the purest material. Other processes, in order of estimated decreasing costs, are: the decomposition of silane, the hydrogen reduction of trichlorosilane, and the reduction of silicon tetrachloride. The trichlorosilane process is the simplest to get into and has attracted a number of companies, both here and abroad. Its costs are substantially higher than processes based on reduction of silicon tetrachloride. Because of its low raw material and conversion costs, silicon tetrachloride reduction is expected to be the workhorse of the industry in the foreseeable future, supplying the bulk of the needs of the electronics industry.

Fighting for markets, the current producers have already found that the expected profits by some processes have been illusory. Thus, some companies unable to sell in bulk have been compelled to pull single crystals; others are doing this since the return on bulk production is too low to justify direct marketing without further upgrading. Other companies, finding themselves with a Grade I product and little demand for it, are working at uneconomic capacities, adulterating to lower the grade or selling a Grade I product as if it were Grade III. The common complaint is that actual marketing is a hard job, contrary to the prognostications of market researchers whose viewpoint was colored by interviews with theoretical scientists.

The Aries survey indicates that increased demand will take up the slack in overcapacity in the near future, except for the higher grades which will remain as specialties on which researchers will still insist.

Monsanto Plans Research Center in St. Louis County, Mo.

Plans to develop a Research Center at Monsanto Chemical Co.'s General Offices location in Creve Coeur, St. Louis County, Mo., were announced recently by Charles Allen Thomas, Monsanto president.

In the initial phase, a building complex occupying about 400,000 square feet of total area, and consisting of two laboratories and supporting facilities, such as analytical laboratories, a library, glass-blowing facilities, and other services, will be constructed. Utilities and other special services will be provided from two separate structures. It is hoped to have all buildings completed in 1961.

The Center will house only laboratory and related activities similar to those already being conducted at the site; there will be no manufacturing or industrial activity involved.

"By centralizing this type of work at the General Offices location, we will be able to effect many efficiencies and economies," Mr. Thomas said. "There are also many benefits to be gained in having our research people in close proximity to our administrative headquarters. In addition, there is the important intellectual stimulus which may be found in a group working together rather than at separate locations," he added.

Designed to match the "campus atmosphere" of Monsanto's General Offices, the new buildings will provide facilities for about 800 scientific personnel. Ultimately, most of the company's research will be centered here. As part of the initial program, the new Center will provide research facilities for the Inorganic Chemicals, Organic Chemicals, Research and Engineering, Plastics, and Lion Oil Company Divisions.

RCA Plant for Transistors and Rectifiers to be Built in Mountaintop, Pa.

Plans for a major expansion of transistor and rectifier manufacturing facilities of the Radio Corp. of America, which call for the construction of a 120,000-square-foot plant in Mountaintop, Pa., were announced in September.

The plant, designed with a view toward future expansion, will be devoted exclusively to products of the RCA Semiconductor and Materials Division, including high reliability germanium and silicon semiconductor devices for military, industrial, and computer applications.

The new manufacturing facility will be situated on a 38-acre tract in the Crestwood Industrial Park, seven miles southwest of Wilkes-Barre, on U. S. Route 309.

The over-all operation of the electronic components activities of the corporation, including the RCA Semiconductor and Materials Division, is under the jurisdiction of W. W. Watts, RCA group executive vice-president. Dr. A. M. Glover is vice-president and general manager of the Division.

Construction of the new plant represents the third phase of the Semiconductor and Materials Divi-

sion's expansion program. The first step of this program was the addition of a 90,000-square-foot extension to the Division's headquarters plant at Somerville, N. J. Then, early this year, a 132,000-square-foot RCA plant at Findlay, Ohio, was acquired by the Division and converted to transistor manufacturing operations.

Initially, the new plant will concentrate its production on Mesa transistors and silicon rectifiers.

Personals

D. Gardner Foulke, formerly manager, electrochemical development with Hanson-Van Winkle-Munning Co., Matawan, N. J., has joined Sel-Rex Corp., Nutley, N. J., as research director, Precious Metals Division. Dr. Foulke will head up Sel-Rex's active research team, with the goal of developing additional precious metals electroplating processes to produce coatings with the metallurgical properties required in exacting industrial and decorative uses. He is past Executive Secretary of the American Electroplaters' Society and Managing Editor of *Plating* magazine, Vice-Chairman of the AES Research Committee, and current Vice-Chairman of the Electrodeposition Division of The Electrochemical Society.

A. E. Middleton, a pioneer in the study of semiconductors and the electrical properties of germanium, has joined the research staff of the Harshaw Chemical Co., Cleveland, Ohio. His new duties will be as senior research advisor on solid state physics, an area increasingly important to many of the products manufactured by Harshaw. Previously, he was with P. R. Mallory & Co., Inc., in Indianapolis, Ind. Dr. Middleton was one of the organizers of the Semiconductor section of the Electronics Division of The Electrochemical Society, and is associated with the solid state devices professional group of the Institute of Radio Engineers.

Otto L. Forchheimer has been named manager of the Chemistry Division of Trionics Corp., Madison, Wis. The Chemistry Division is one of three laboratory divisions of this contract research organization. Dr. Forchheimer will direct Trionics research on problems involving coatings and other surface treatments, adhesives and bonding agents, resins and plastics for special applications, corrosion chemistry, and electrochemistry. Before joining Trionics, he was assistant director of research at General Abrasive Co. and Nilok Chemicals, Inc., Niagara Falls, N.Y., and was a specialist in abrasive technology.

Harvey F. Haight has resigned his post with the Research Dept. of Columbia-Southern Chemical Corp., Corpus Christi, Texas, to become a member of the technical staff of Texas Instruments, Inc., Central Research Lab., Dallas, Texas.

Christopher L. Wilson, professor at the University of Notre Dame and Industrial Consultant, has been appointed vice-president of Phillips-Foscue Corp. of High Point, N. C.

Egon E. Nurmet, formerly of Newfoundland, Canada, recently joined the staff of the Contract Battery Manufacturing Co. in Tampa, Fla.

Paul R. Kruesi, former general manager of the Rare Earths Division of Heavy Minerals Co., Chattanooga, Tenn., has been named vice-president, research and development, of Vitro Chemical Co., a newly formed subsidiary of Vitro Corp. of America. Vitro Chemical Co. is engaged in the milling of uranium ores; production of thorium and rare earth chemicals, rare metals and metal alloys, and other industrial chemicals; and also is engaged in chemical and metallurgical research and development.

David A. Lupfer recently was appointed general manager of the Materials and Ceramics Division of Gulton Industries, Inc., Metuchen, N. J. Mr. Lupfer formerly was a research physicist and development engineer with the General Electric Co.

Book Reviews

Atomic Energy Facts (United States Atomic Energy Commission). Published September 1957. For sale by Superintendent of Documents, U. S. Government Printing Office, Washington 25, D. C. 216 pages; $2.00.

Quoting from the preface, this volume was intended primarily as a source book for industrial management. It should prove, however, illuminating to teachers, writers, and engineers connected in any way with the nuclear energy industry.

Its 216 pages include an extraordinarily lucid table of contents as well as a comprehensive index. The text is very readable, the language is as nontechnical as possible, and the many illustrations and diagrams add a great measure of clarity and perspective. The book does not report on programs concerned with weapons or on support of basic research in universities.

The text is well divided into nine appropriate chapters each of which is fairly complete in itself, so that the reader may pursue his particular interest without being concerned with continuity from chapter to chapter.

The first three chapters deal directly with organization of the appropriate Government agencies, and various matters of strong interest to the prospective manufacturer of reactors or associated equipment. Chapter II outlines the relationship

Brief Communications

The JOURNAL accepts short technical reports having unusual importance or timely interest, where speed of publication is a consideration. The communication may summarize results of important research justifying announcement before such time as a more detailed manuscript can be published. Consideration also will be given to reports of significant unfinished research which the author cannot pursue further, but the results of which are of potential use to others. Comments on papers already published in the JOURNAL should be reserved for the Discussion Section published biannually.

Submit communications in triplicate, typewritten double-spaced, to the Editor, Journal of The Electrochemical Society, 1860 Broadway, New York 23, N. Y.

of Government and the atomic industry. Tables which indicate where to go for unclassified and classified technical information, and how to obtain it, are included. In addition, directions are given for the acquisition of appropriate clearance and access permits. Information is provided indicating the basis on which fissionable and other required materials may be obtained from the Government, and the present efforts to establish cooperative ventures are summarized. Chapter III describes the operations of the Atomic Energy Commission, its organization, location of branch offices; summarizes the programs being conducted, future trends; and lists the current pertinent financial data.

Chapters IV through IX were prepared by the Vitro Corp. of America, and are somewhat more strongly technical in nature, although the broad scope of the book is preserved. These chapters have much material of interest to the teacher of courses in nuclear engineering, and to the engineering specialist who seeks information in related fields.

Topics covered in this section are the production of uranium and thorium, power reactors, fuel cycles, reactor materials, research reactors, and the use of radioisotopes.

Chapters IV and VII, dealing with the mining and production of uranium, thorium, and other reactor materials, such as heavy water, graphite, beryllium, and zirconium, are excellently illustrated with flow process charts and photographs. Considerable cost data are presented.

The chapters on power and research reactors include tables which list the major reactors operating or in construction, their operating characteristics and design features, and tabular data for most of them. Programs for future development are discussed.

A description is included of the manner in which radioisotopes are manufactured and shipped, and a number of typical uses are outlined.

In summary, this volume is so comprehensive that, if it does not in itself have the data which almost anyone might desire, it will describe how to go about obtaining it. It is a must as a general reference work.

Sherwood B. Menkes

Process Chemistry, Vol. II, Progress in Nuclear Energy Series III, by F. R. Bruce, J. M. Fletcher, and H. H. Hyman. Published by Pergamon Press Inc., New York City, 1959. 579 pages; $17.50.

Vol. I of this Process Chemistry series relied heavily on the information declassified for the 1955 Geneva Conference. This present volume brings the subject up to date and enlarges the scope to include recovery processes connected with the treatment of ores and irradiated fuels as well as the production of materials intermediate between ore concentrates and refined feeds. The plan is similar to that of Volume I in that the 35 papers are assembled logically in chapters. In addition, an Appendix of 6 papers is devoted mainly to data on systems of importance in solvent extraction.

Although the production of nuclear power hardly can be considered as standardized, it is becoming apparent that processing of spent fuel will be performed in central locations by a few well-tried methods. Therefore, much of the emphasis is very properly placed on the chemistry and practical results of techniques such as solvent extraction. However, electrochemists will probably be more interested in some of the processing schemes that are still in the development stage. One of these involves the recovery of uranium from leach liquors by electrolysis in cells compartmented by ion-selective membranes. Another proposes to decontaminate irradiated uranium metal by electrolytic refining in fused salts. Unfortunately, neither of these appears to be currently competitive with more standard approaches.

Presumably, additional volumes will be forthcoming to keep this Series abreast of new developments. The resultant collection should prove extremely valuable to trainees and workers in the chemical processing area of nuclear power.

M. Kolodney

Absorption and Dispersion of Ultrasonic Waves, by Karl F. Herzfeld and Theodore A. Litovitz. Published by Academic Press Inc., New York City, 1959. xviii + 535 pages; $14.50.

During the past decade, significant progress has been made in providing a molecular basis for the interpretation of ultrasonic velocity and absorption measurements in gases and liquids. Theoretical developments have been complimented by improvements in experimental techniques for measurements at frequencies from the audible through 10^9 cycles/sec. Many physical acousticians who have been concerned with these measurements are now of the opinion that the physical chemist should have an active interest in such measurements for structural and kinetic investigations.

The new book by Herzfeld and Litovitz should prove useful to physicists and physical chemists who are new to the field as well as to workers who already may have had considerable experience in such studies. These two authors are particularly well qualified to prepare such a book because of their extensive and outstanding contributions to this field.

In the words of the authors in the preface, the book is halfway between a textbook and a handbook. After a brief introduction to the so-called "classical" aspects of sound transmission and absorption in fluids, a general treatment of relaxation in fluids is presented. The mathematical treatment in this first section is particularly detailed and easily followed. Furthermore, the authors assist the reader in many instances to interpret the significance of the mathematical approach in terms of relatively simple physical concepts and models. Specific aspects of theory and experimental methods are presented for gases and liquids but not for solids. Experimental results obtained by ultrasonic velocity and absorption measurements are summarized in considerable detail. The authors include a good summary of the theories of the liquid state. Unfortunately, space limitations have prevented the authors from treating specifically ultrasonic relaxation in polymers and electrolytic solutions, which represent areas of considerable interest to the physical chemist. The general treatments of ultrasonic relaxation, however, provide the necessary background for the pursuit of these areas. Ultrasonic studies of relaxation also should be of considerable interest to physicists and physical chemists who have been concerned with dielectric relaxation because of the obvious overlap of effects.

Special features of the book which this reviewer believes the reader will particularly appreciate are: (a) the ample literature references which are very complete, (b) the good organization of the material, and (c)

Notice to Members
Re Voting Ballot

By now you have received your official voting ballot from Society Headquarters. If you have not already done so, please return the ballot by *December 15* so that your vote can be included in the final election count.

the list of symbols and their meanings included at the beginning of the book. The mathematical background required for readily assimilating the theoretical treatment is in accord with that which most research physical chemists and physicists are expected to have.

This reviewer is pleased to recommend enthusiastically this book to all physicists and physical chemists with an interest in the structure and the kinetics of fast processes in fluids.

Ernest Yeager

Announcements from Publishers

"European Technical Digests." Published monthly by European Productivity Agency, 2 rue André-Pascal, Paris, France. Price of yearly subscription, $12.00 (£3.10s.); six-month subscription $6.00 (£1.15s.).

The purpose of the Digests is twofold: first, to spread from one country to another, irrespective of language barriers, technical information and knowledge likely to increase productivity; second, to crossfeed ideas from one industry to another.

Each month over 1000 technical journals appearing in 13 different countries and in 11 different languages are searched by qualified engineers for information on new processes, methods, apparatus, or materials which could be employed readily in industry without large capital investment.

The Digests deal principally with all kinds of engineering and equipment, metallurgy, and agricultural machinery, and much importance is attached to subjects of general interest, such as corrosion, materials handling, packaging, safety, and management. Also covered are such sectors as glass, chemicals, leather, etc.

A number of countries have published translated versions of the publication so that, apart from the English edition, it now appears in German, Italian, Norwegian, Spanish, Turkish, Croat, and Japanese, and, on a selective basis, in Hebrew and Icelandic. Greece and the Netherlands produce translated title lists.

As a free readers' service, the European Productivity Agency supplies on request photocopies of the original articles on which the Digests are based, and also additional information wherever possible.

"Corrosion of Chemical Apparatus," by G. L. Shvartz and M. M. Kristal. Translated from Russian by Consultants Bureau, Inc., 227 W. 17 St., New York 11, N. Y. Price, cloth bound, $7.50.

This book is a monograph on intercrystalline corrosion and stress corrosion of various metals and alloys used in chemical machine construction. The fundamental causes of these types of corrosion are dealt with first, then specific cases of destruction of industrial equipment are described, and finally methods of protection of metals against corrosion cracking are discussed. The monograph was written as the result of investigations performed by the authors in the Scientific Research Institute of Chemical Machinery and the Moscow Institute of Chemical Machinery, and also on the basis of Soviet and foreign literature.

This work, available for the first time in complete English translation, is intended for workers in industrial laboratories and for designers, technologists, and scientific personnel concerned with chemical machine construction and the chemical industry.

Contents include: causes of corrosion cracking of metals; corrosion cracking of carbon and alloyed steels; corrosion cracking of stainless steels; corrosion of nonferrous metals and alloys; methods of protection against corrosion cracking; testing methods.

CB translations include all photographic, diagrammatic, and tabular material integral with the text. Free catalog describing current Russian translation program available on request.

"The Properties of the Rare Earth Metals and Compounds." Available from the Rare Earth Research Group, c/o Battelle Memorial Institute, Columbus 1, Ohio. 214 pages; $10.00.

This handbook was prepared for the Rare Earth Research Group, made up of the nation's principal producers of the rare earth metals and their compounds, by the staff of Battelle Memorial Institute, where an extensive research program on behalf of the Rare Earth Research Group is now being carried on. Some of the information appearing in the new handbook has appeared in recent technical papers, and the decision to make this handbook available has been prompted by the many requests received for data on rare earth materials.

Manuscripts and Abstracts for Spring 1960 Meeting

Papers are now being solicited for the Spring Meeting of the Society, to be held at the Lasalle Hotel in Chicago, Ill., May 1, 2, 3, 4, and 5, 1960. Technical sessions probably will be scheduled on Electric Insulation (including a Symposium on "Electrolytic Capacitors"), Electronics (including Luminescence and Semiconductors), Electrothermics and Metallurgy (including a symposium on "High-Purity Vanadium" and a round table on "Methods of Reducing Iron Ores"), Industrial Electrolytics, and Theoretical Electrochemistry.

To be considered for this meeting, triplicate copies of abstracts (*not exceeding 75 words in length*) must be received at Society Headquarters, 1860 Broadway, York 23, N. Y., *not later than January 4, 1960. Please indicate on abstract for which Division's symposium the paper is to be scheduled, and underline the name of the author who will present the paper.* Complete manuscripts should be sent in triplicate to the Managing Editor of the JOURNAL at the same address.

Papers submitted for presentation at the meeting become the property of The Electrochemical Society and may not be published elsewhere, in whole or in part, unless permission is requested and granted by the Society. Papers already published elsewhere, or submitted for publication elsewhere, are not acceptable for oral presentation except on invitation by a Divisional program Chairman.

• • •

The Fall 1960 Meeting will be held in Houston, Texas, October 9, 10, 11, 12, and 13, 1960, at the Shamrock Hotel. Sessions will be announced in a later issue.

The manual brings together for the first time the most recently available data on the physical, crystal, chemical, mechanical, electrical, magnetic, nuclear, and thermodynamic properties of each of the 15 rare earth metals, as well as for yttrium, a metal closely associated in nature with the rare earths. In addition, a 114-item reference list of leading sources of information on the rare earths is included.

"The Determination of Plutonium in Irradiated Uranium Fuel Solutions by Controlled Potential Coulometry," Dec. 1958. AEC Report HW-58491,* 29 pages; $1.00.

"Analysis for Neptunium by Controlled Potential Coulometry," Feb. 1959. AEC Report HW-59447,* 20 pages; 75 cents.

"Evaluation of Materials for Use as Anodes in the Flurex Process," Feb. 1959. AEC Report HW-59780,* 23 pages; 75 cents.

"Thorex Pilot Plant Corrosion Studies: 1. Corrosion of Types 304L and 309SCb Stainless Steel During Production and Development Periods," no date. AEC Report ORNL-2673,* 73 pages; $2.25.

"Corrosion Prevention," Office of the Chief of Civil Engineers, Bureau of Yards and Docks, U. S. Navy, Dec. 1956. Manual PB 151756,* 431 pages; $6.00.

Data are assembled on atmospheric, submerged, and subsurface corrosion, and corrosion on areas alternately wet and dry. What the Navy has found to be the most practicable methods and material for controlling or minimizing corrosion are described in detail.

Among corrosion processes discussed are those caused by use of dissimilar metals, with particular emphasis on the Electromotive Force Series and galvanic corrosion, direct chemical attack, stray currents, microbiological and atmospheric attack, and marine corrosion.

Such methods of corrosion control are outlined as the use of nonmetallic materials and coatings, claddings, and coverings; passivity; change of environment to reduce exposure to corrosion through the use of passivators or inhibitors, underground backfills, and combinations of zinc and iron in hot water facilities.

One section presents a selection of material combinations and a selection of metals with a discussion of polarization; another gives a complete discussion on cathodic protection and electrochemical processes.

* Order from Office of Technical Services, U. S. Dept. of Commerce, Washington 25, D. C.

"Chemistry of Uranium: Collected Papers," edited by J. J. Katz and E. Rabinowitch, Argonne National Lab., U. S. Atomic Energy Commission, 1958. Report TID-5290,* 2 volumes, 769 pages; $7.25.

This is a collection of 81 papers, most of which have not been widely distributed and a few of which recently have been declassified. Those previously published are given in abstract form with a reference to the publication which carried the paper. Such subjects are covered as "Preparation, Purification, and Properties of Anhydrous Uranium Chlorides," "Some Reactions of Uranium Metal," "X-Ray Investigation of the Uranium-Hydrogen System: The Structure of UH_3," "The Uranium-Nitrogen System," "Use of Uranium and Uranium Compounds in Purifying Gases," "Uranium Hydride," "Experiments on the Electrodeposition of Uranium from Aqueous Systems," and "Electrolysis of Uranium Halides."

"English Abstracts of Russian Technical Journals," a listing of abstracted Russian technical journals currently available by subscription from the Office of Technical Services, may be ordered without charge from OTS, U. S. Dept. of Commerce, Washington 25, D. C.

The listing shows some 100 Soviet technical periodicals abstracted regularly by U. S. Government agencies and released to the public through OTS as part of its program of collection and dissemination of translated technical literature.

The periodicals cover such fields of research as aeronautics, astronomy and mathematics, chemistry and chemical engineering, civil and electrical engineering, fuel and power, geography and geology, mechanical engineering, mining and metallurgy, physics, and general science and technology. Included are the physics, chemistry, and biology series of *Referativnyi Zhurnal*, the Russians' central abstract journal.

The new listing supersedes one published in August 1958 at the outset of the OTS translation program. It reflects new periodicals added to the collection during the past year and ones canceled because of limited usefulness or other reasons.

* Order from Office of Technical Services, U. S. Dept. of Commerce, Washington 25, D. C.

Literature from Industry

"Fisher Chemical Index." The new 1959 "Fisher Chemical Index" (Catalog 123) describes 7000-plus chemicals in one easy-to-use alphabetical listing. It gives structural formulas, formula weights, melting and boiling points, color index numbers. All of the American Chemical Society's specified reagents are included here. The Index also contains instructions on how to store chemicals; defines the various purity grades; and reproduces in miniature a chart of emergency treatments for laboratory mishaps. The 365-page book is free to qualified laboratories from Fisher Scientific Co., 310 Fisher Bldg., Pittsburgh 19, Pa.

Dow Products Catalog. The 1959-1960 edition of the Dow Chemical Co.'s general catalog is available. This 44-page compilation, "Products of The Dow Chemical Company," lists the properties and uses of some 375 industrial, pharmaceutical, and agricultural chemicals currently produced. The listing includes established products and developmental items. The new edition features an expanded section on plastics and coatings products. New sections are included on oxazolidinones, automotive chemicals, textile fibers, and the company's Dowell division. Copies are available from the Dow Chemical Co., Midland, Mich., or any Dow sales office.

Advertiser's Index

M. Ames Chemical Works, Inc. 317C
E. I. du Pont de Nemours & Company (Inc.) 306C
Thomas A. Edison Industries 317C
Enthone, Incorporated Cover 4
General Motors Research Laboratories 302C
Great Lakes Carbon Corp., Electrode Division Cover 2
Perkin Engineering Corporation 300C-301C
Reynolds Metals Company 317C
E. H. Sargent & Company 304C
Solvay Process Division, Allied Chemical Corp. 317C
Stackpole Carbon Company 305C

STORAGE BATTERY ENGINEERS

Nationally Known Manufacturer
of
Industrial Type Storage Batteries
needs

ENGINEERING and PRODUCTION PERSONNEL with ten or more years' experience in the production of lead acid storage batteries of the motive power type.

College graduates preferred—Age 35 to 55. Salary Open. Send complete resume to:

Technical Employment Supervisor
THOMAS A. EDISON INDUSTRIES
McGRAW-EDISON COMPANY
West Orange, New Jersey

All replies held strictly confidential.

ELECTRO-CHEMIST–RESEARCH

Outstanding research opportunity in metal finishing for physical chemist with advanced degree. Good academic background in kinetics and thermodynamics as well as physical and electro-chemistry preferred for research in aluminum oxidation, electro-chemical processes, and anodizing, plating, and bonderizing metal. Direct replies indicating education, experience, and salary requirements to

General Employment Manager
REYNOLDS METALS COMPANY
Richmond, Virginia

ELECTROPLATING RESEARCH SUPERVISOR

Chemist or chemical engineer to set up and take charge of newly established electroplating laboratory. Challenging opportunity to apply theoretical training and practical background in pioneering research on applications of chemicals in electroplating, on development of new and improved plating procedures, and in solving important customer problems including some contacts with customers.

Applicant should have at least a Bachelor's degree and at least 5 years' experience in the plating field. He must be capable of planning and undertaking experimental electroplating programs.

Complete benefit plans. Location in Central New York near the attractive Finger Lakes Area, the Adirondack Mountains, and the Thousand Islands.

Send detailed resume indicating salary requirements to:

Director of Research
Solvay Process Division
Allied Chemical Corporation
Syracuse 1, New York

Since 1861
AMES has been making these
SILVER SALTS
to YOUR specifications

Silver Nitrate **Silver Cyanide**
Silver Chloride **Silver Sulfate**
Monovalent Silver Oxide
Divalent Silver Oxide

And now for your Battery
Silver Flour
and
for powder metallurgy
Nodular Silver

M. AMES CHEMICAL WORKS, INC.
17-19 Rogers Street
Glen Falls, New York
Phone 2-4394

The Electrochemical Society

Patron Members

Aluminum Co. of Canada, Ltd.,
Montreal, Que., Canada
International Nickel Co., Inc.,
New York, N. Y.
Olin Mathieson Chemical Corp.,
Niagara Falls, N. Y.
Industrial Chemicals Div., Research
and Development Dept.
Union Carbide Corp.
Divisions:
Union Carbide Metals Co.,
New York, N. Y.
National Carbon Co., New York, N. Y.
Westinghouse Electric Corp., Pittsburgh, Pa.

Sustaining Members

Air Reduction Co., Inc.,
New York, N. Y.
Ajax Electro Metallurgical Corp.,
Philadelphia, Pa.
Allen-Bradley Co., Milwaukee, Wis.
Allied Chemical & Dye Corp.
General Chemical Div., Morristown, N. J.
Solvay Process Div., Syracuse, N. Y.
(3 memberships)
Allied Research Products, Inc.,
Detroit, Mich.
Alloy Steel Products Co., Inc., Linden, N. J.
Aluminum Co. of America,
New Kensington, Pa.
American Machine & Foundry Co.,
Raleigh, N. C.
American Metal Climax, Inc.,
New York, N. Y.
American Potash & Chemical Corp.,
Los Angeles, Calif. (2 memberships)
American Zinc Co. of Illinois,
East St. Louis, Ill.
American Zinc, Lead & Smelting Co.,
St. Louis, Mo.
American Zinc Oxide Co., Columbus, Ohio
M. Ames Chemical Works, Inc.,
Glens Falls, N. Y.
Auto City Plating Company Foundation,
Detroit, Mich.
Basic Inc., Maple Grove, Ohio
Bell Telephone Laboratories, Inc.,
New York, N. Y. (2 memberships)
Bethlehem Steel Co., Bethlehem, Pa.
(2 memberships)
Boeing Airplane Co., Seattle, Wash.
Burgess Battery Co., Freeport, Ill.
(4 memberships)
C & D Batteries, Inc., Conshohocken, Pa.
Canadian Industries Ltd., Montreal, Que.,
Canada
Carborundum Co., Niagara Falls, N. Y.
Catalyst Research Corp., Baltimore, Md.
Chrysler Corp., Detroit, Mich.
Ciba Pharmaceutical Products, Inc., Summit,
N. J.
Columbian Carbon Co., New York, N. Y.
Columbia-Southern Chemical Corp.,
Pittsburgh, Pa.
Consolidated Mining & Smelting Co. of
Canada, Ltd., Trail, B. C., Canada
(2 memberships)
Continental Can Co., Inc., Chicago, Ill.
Cooper Metallurgical Associates, Cleveland,
Ohio
Corning Glass Works, Corning, N. Y.
Crane Co., Chicago, Ill.
Diamond Alkali Co., Painesville, Ohio
(2 memberships)
Dow Chemical Co., Midland, Mich.
Wilbur B. Driver Co., Newark, N. J.
(2 memberships)
E. I. du Pont de Nemours & Co., Inc.,
Wilmington, Del.
Eagle-Picher Co., Chemical Div., Joplin, Mo.
Eastman Kodak Co., Rochester, N. Y.
Electric Auto-Lite Co., Toledo, Ohio
Electric Storage Battery Co.,
Philadelphia, Pa.
Englehard Industries, Inc., Newark, N. J.
(2 memberships)
The Eppley Laboratory, Inc., Newport, R. I.
(2 memberships)
Erie Resistor Corp., Erie, Pa.
Exmet Corp., Tuckahoe, N.Y.
Fairchild Semiconductor Corp., Palo Alto,
Calif.
Federal Telecommunication Laboratories,
Nutley, N. J.
Food Machinery & Chemical Corp.
Becco Chemical Div., Buffalo, N. Y.
Westvaco Chlor-Alkali Div., South
Charleston, W. Va.
Foote Mineral Co., Paoli, Pa.
Ford Motor Co., Dearborn, Mich.
General Electric Co., Schenectady, N. Y.
Chemistry & Chemical Engineering
Component, General Engineering
Laboratory
Chemistry Research Dept.
General Physics Research Dept.
Metallurgy & Ceramics Research Dept.
General Instrument Corp., Newark, N. J.

(Sustaining Members cont'd)

General Motors Corp.
Brown-Lipe-Chapin Div., Syracuse, N. Y. (2 memberships)
Guide Lamp Div., Anderson, Ind.
Research Laboratories Div., Detroit, Mich.
General Transistor Corp., Jamaica, N. Y.
Gillette Safety Razor Co., Boston, Mass.
Gould-National Batteries, Inc., Depew, N. Y.
Grace Electronic Chemicals, Inc., Baltimore, Md.
Great Lakes Carbon Corp., New York, N. Y.
Hanson-Van Winkle-Munning Co., Matawan, N. J. (3 memberships)
Harshaw Chemical Co., Cleveland, Ohio (2 memberships)
Hercules Powder Co., Wilmington, Del.
Hill Cross Co., Inc., New York, N. Y.
Hoffman Electronics Corp., Evanston, Ill.
Hooker Chemical Corp., Niagara Falls, N. Y. (3 memberships)
Houdaille Industries, Inc., Detroit, Mich.
Hughes Aircraft Co., Culver City Calif.
International Business Machines Corp., Poughkeepsie, N. Y.
International Minerals & Chemical Corp., Chicago, Ill.
Jones & Laughlin Steel Corp., Pittsburgh, Pa.
K. W. Battery Co., Skokie, Ill.
Kaiser Aluminum & Chemical Corp.
Chemical Research Dept., Permanente, Calif.
Div. of Metallurgical Research, Spokane, Wash.
Kennecott Copper Corp., New York, N. Y.
Keokuk Electro-Metals Co., Keokuk, Iowa
Libbey-Owens-Ford Glass Co., Toledo, Ohio
P. R. Mallory & Co., Indianapolis, Ind.
McGean Chemical Co., Cleveland, Ohio
Merck & Co., Inc., Rahway, N. J.
Metal & Thermit Corp., Detroit, Mich.
Minnesota Mining & Manufacturing Co., St. Paul, Minn.
Monsanto Chemical Co., St. Louis, Mo.
Motorola, Inc., Chicago, Ill.
National Cash Register Co., Dayton, Ohio
National Lead Co., New York, N. Y.
National Research Corp., Cambridge, Mass.
National Steel Corp., Weirton, W. Va.
New York Air Brake Co., Vacuum Equipment Div., Camden, N. J.
Northern Electric Co., Montreal, Que., Canada
Norton Co., Worcester, Mass.
Olin Mathieson Chemical Corp., Niagara Falls, N. Y.
High Energy Fuels Organization (2 memberships)
Peerless Roll Leaf Co., Inc., Union City, N. J.
Pennsalt Chemicals Corp., Philadelphia, Pa.
Phelps Dodge Refining Corp., Maspeth, N. Y.
Philco Corp., Philadelphia, Pa.
Philips Laboratories, Inc., Irvington-on-Hudson, N. Y.
Pittsburgh Metallurgical Co., Inc., Niagara Falls, N. Y.
Poor & Co., Promat Div., Waukegan, Ill.
Potash Co. of America, Carlsbad, N. Mex.
Radio Corp. of America, Harrison, N. J.
Ray-O-Vac Co., Madison, Wis.
Raytheon Manufacturing Co., Waltham, Mass.
Reynolds Metals Co., Richmond, Va. (2 memberships)
Rheem Semiconductor Corp., Mountain View, Calif.
Schering Corporation, Bloomfield, N. J.
Shawinigan Chemicals Ltd., Montreal, Que., Canada
Speer Carbon Co.
International Graphite & Electrode Div., St. Marys, Pa. (2 memberships)
Sprague Electric Co., North Adams, Mass.
Stackpole Carbon Co., St. Marys, Pa.
Stauffer Chemical Co., New York, N. Y.
Sumner Chemical Co., Div. of Miles Laboratories, Inc., Elkhart, Ind.
Sylvania Electric Products Inc., Bayside, N. Y. (2 memberships)
Tennessee Products & Chemical Corp., Nashville, Tenn.
Texas Instruments, Inc., Dallas, Texas
Metals & Controls Div., Attleboro, Mass.
Three Point Four Corp., Yonkers, N. Y.
Titanium Metals Corp. of America, Henderson, Nev.
Tung-Sol Electric Inc., Newark, N. J.
Udylite Corp., Detroit, Mich. (4 memberships)
Universal-Cyclops Steel Corp., Bridgeville, Pa.
Upjohn Co., Kalamazoo, Mich.
Victor Chemical Works, Chicago, Ill.
Western Electric Co., Inc., Chicago, Ill.
Wyandotte Chemicals Corp., Wyandotte, Mich.
Yardney Electric Corp., New York, N. Y.

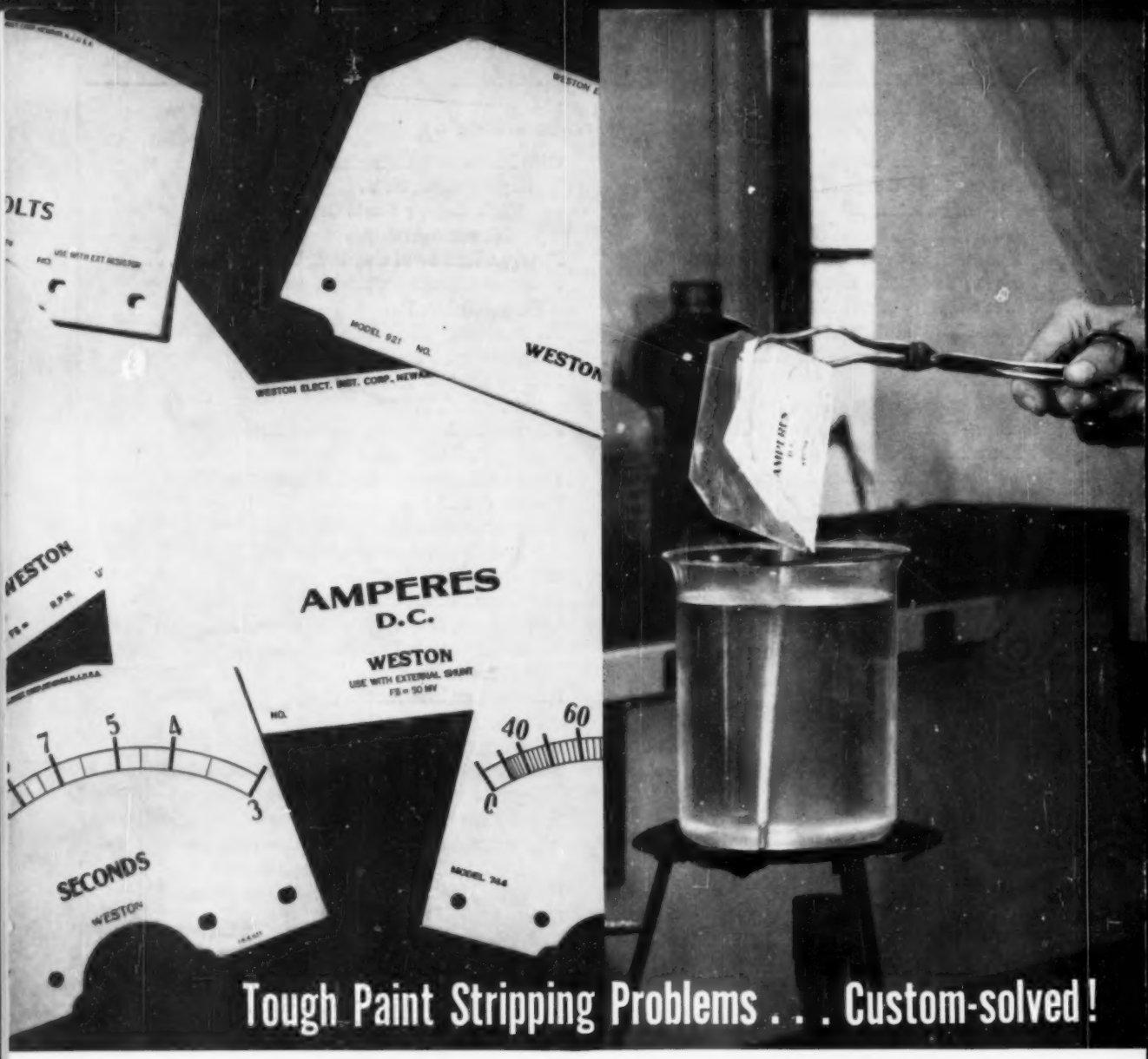

Tough Paint Stripping Problems . . . Custom-solved!

Problem: To remove two coats of specially formulated non-yellowing white baked synthetic enamel, printing, and clear baked enamel top-coat from these Weston Scale plates.

Enthone Stripper Q-561 (specifically developed for Weston Instrument Division of Daystrom, Inc.) breaks the bond between the coatings and the brass or nickel plated brass basis metal.

The many factors that affect paint stripping—type of paint, condition of the metal surface, presence or absence of conversion coatings, method of paint application, baking cycle—make every stripping job unique in itself. In most cases, only laboratory tests on your parts or test panels, and proper evaluation of all the factors involved, can produce the most economical and efficient stripper for your application. Only Enthonics can do this custom research and development job in depth. Write for brochure describing our paint stripping laboratory service. Enthone, Incorporated, 442 Elm Street, New Haven, Connecticut.

ASARCO

ANOTHER PRODUCT OF *Enthonics* RESEARCH

ENTHONE

A Subsidiary of American Smelting and Refining Company